



저작자표시-비영리-변경금지 2.0 대한민국

이용자는 아래의 조건을 따르는 경우에 한하여 자유롭게

- 이 저작물을 복제, 배포, 전송, 전시, 공연 및 방송할 수 있습니다.

다음과 같은 조건을 따라야 합니다:



저작자표시. 귀하는 원저작자를 표시하여야 합니다.



비영리. 귀하는 이 저작물을 영리 목적으로 이용할 수 없습니다.



변경금지. 귀하는 이 저작물을 개작, 변형 또는 가공할 수 없습니다.

- 귀하는, 이 저작물의 재이용이나 배포의 경우, 이 저작물에 적용된 이용허락조건을 명확하게 나타내어야 합니다.
- 저작권자로부터 별도의 허가를 받으면 이러한 조건들은 적용되지 않습니다.

저작권법에 따른 이용자의 권리는 위의 내용에 의하여 영향을 받지 않습니다.

이것은 [이용허락규약\(Legal Code\)](#)을 이해하기 쉽게 요약한 것입니다.

[Disclaimer](#)

공학박사학위논문

**Study on the chain orientation and
interdiffusion of polyimide affected by
drying and curing processes**

건조 및 경화 공정에 따른
폴리이미드 배향과 상호확산에 관한 연구

2016 년 2 월

서울대학교 대학원

화학생물공학부

조 병 욱

Abstract

Study on the chain orientation and interdiffusion of polyimide affected by drying and curing processes

Byoungwook Jo

School of Chemical and Biological Engineering

Seoul National University

Chain orientation in polyimide (PI) film and its interdiffusional behavior influenced by the process conditions were investigated. The amount of residual solvent and the degree of imidization were proved to be the key factors that determine the final chain orientation and interdiffusion width of PIs.

To observe the effect of film thickness, the films made by poly(amic acids) or PAA, the precursor of polyimide, having different thicknesses were prepared. During the drying and curing processes, the depth-wise distribution of residual solvent and imidization rate were observed. For thick PI, it showed a lower degree of in-plane chain orientation, particularly near the substrate. This non-uniform distribution of chain orientation was similar to that of a dried PAA. Fast imidization with higher solvent content for thick PI retarded the formation of a well-ordered structure and resulted in a lower degree of in-plane orientation. Chain orientation of a PI can also be changed by thermal histories. PAA began to imidize

quickly with retaining more solvent as the initial drying temperature increased. The fully imidized PI showed the lowest degree of in-plane chain orientation when it was processed by the protocol of the highest drying temperature. It influenced the in-plane thermal expansion coefficient most significantly, while no significant change in crystallinity or glass transition temperature was observed.

In multi-layer PI film, controlling the interdiffusion and chain orientation is essential to achieve a good adhesion performance. In the present study, bilayer PI films were made by two different drying methods, direct multi-layer (DML) and layer-by-layer (LBL). The extent of interdiffusion between two PAAs was affected by both the amount of solvent and contact time. As a result, the interdiffusion width of the cured PI made by DML was larger than that made by LBL. The chain orientation of the bottom layer, which consists of more rigid chain structure, was observed to be varied more significantly according to the drying conditions. In the bilayer PI film made by LBL method, the degree of in-plane orientation of the bottom layer became reduced compared to the single-layer when it was dried at lower temperature. The result originates from the fast diffusion of solvent in the top layer into the bottom layer.

Keywords: polyimide, residual solvent, degree of imidization, chain orientation, interdiffusion, Raman spectroscopy

Student Number: 2011-30281

Contents

Abstract.....	i
List of Contents	iii
List of Figures.....	vi
List of Tables	xii
Chapter 1. Introduction.....	1
1.1. General introduction.....	2
1.2. Outline of the thesis.....	7
Chapter 2. Background.....	9
2.1. Manufacturing processes of polyimide film.....	10
2.1.1. Poly(amic acid) preparation	12
2.1.2. Thermal imidization of PAA.....	14
2.2. Drying behavior of polymer solutions.....	17
2.2.1. Two drying regimes of polymer solution	18
2.2.2. Stress development in polymer films	21
2.2.3. Stress development in polyimide film.....	22
2.3. Chain orientation of rod-shaped polymers	23
2.3.1. General introduction of polymer chain orientation	23
2.3.2. Chain orientation measurement using polarized Raman spectroscopy	24
2.4. Interdiffusion between two different polymers	30
2.4.1. Polymer/polymer interfaces	30

2.4.2. Interdiffusion at polymer interfaces	34
2.4.3. Interdiffusion between partially miscible polymers	36
2.4.4. Polymer interface and adhesion	37
2.5. Confocal Raman spectroscopy	41
2.5.1. Principles of Raman scattering	41
2.5.2. Principles of confocal Raman spectroscopy	41
Chapter 3. Experimental methods	49
3.1. Sample preparation and characterization	50
3.2. Measurement of residual solvent concentration and the degree of imidization	62
3.3. Measurement of chain orientation of polyimide	68
3.4. Experiments of polyimide interdiffusion.....	73
3.4.1. Measurement of PAA-PAA interdiffusion.....	77
3.4.2. Measurement of solvent diffusion into dried PAA film	78
3.4.3. Measurement of interdiffusion width of cured polyimide films	79
3.5. Characterization of the cured polyimide film.....	81
3.5.1. X-ray diffraction pattern.....	81
3.5.2. Glass transition temperature	81
3.5.3. Thermal expansion coefficient	81
Chapter 4. Results and discussion	83
4.1. Effect of film thickness on the polyimide chain orientation	84
4.1.1. Depth-wise residual solvent content of dried film	84
4.1.2. Depth-wise imidization degree during the curing process	87

4.1.3. Depth-wise chain orientation after curing	90
4.2. Effect of thermal history on the polyimide chain orientation.....	98
4.2.1. Residual solvent and imidization degree during drying	98
4.2.2. Process path and degree of in-plane orientation.....	103
4.2.3. Properties of cured film.....	107
4.3. Interdiffusion and chain orientation in the drying of bilayer polyimide film.....	112
4.3.1. Interdiffusion between PAA solutions having different solvent contents.....	112
4.3.2. Interdiffusion width of cured polyimide film	116
4.3.3. Solvent diffusion into dried PAA films	118
4.3.4. In-plane chain orientation of cured polyimide films	121
Chapter 5. Summary	125
References	131
국문 초록	141
Curriculum Vitae.....	143

List of Figures

Figure 2.1. Schematic diagram of PI manufacturing process.....	11
Figure 2.2. Mechanism of PAA and PI formation	13
Figure 2.3. Schematic diagram of hypothetical potential energy during imidization. The left peak corresponds to the depolymerization energy and the right peak corresponds to the imidization energy	15
Figure 2.4. Drying mechanism. (a) three characteristic periods of drying, (b) two characteristic resistance of drying	19
Figure 2.5. Schematic diagram of main components in polarized Raman spectrometer	26
Figure 2.6. Main directions of film extension, light source excitation, and light scattering	28
Figure 2.7. Cross-sectional image of a bilayer PI film (Left) and its Raman mapping image (Right).....	32
Figure 2.8. Graphical representation of interdiffusion width (w) defined by maximal volume fraction change at the interface.....	39
Figure 2.9. Schematic representation of the strain energy release rate depending on the molecular weight of a polymer	40
Figure 2.10. Schematic diagram of energy level before and after the light excitation	43
Figure 2.11. Schematic diagram of confocal Raman spectrometer	44
Figure 2.12. Depth of focus depending on the refractive index difference. Marginal lights are focused deeper position	47

Figure 3.1. The molecular structure of poly(amic acid) and polyimide composed of BPDA and PDA.....	51
Figure 3.2. Raman intensity calibration graph plotted by solvent concentration against Raman intensity ratio between DMAc and PAA	52
Figure 3.3. Thermal histories for the different drying and curing protocols. The drying process is characterized by constant temperature and the curing is characterized by constant rate of elevating temperature.....	57
Figure 3.4. Molecular structures of PAAs and the corresponding PIs composed of BPDA-PDA (bottom layer) and BPDA-ODA (top layer). PAA is converted to PI by a dehydration cyclization called imidization reaction	59
Figure 3.5. Design scheme for manufacturing four different bilayer polyimide films.....	61
Figure 3.6. Raman spectrum of PAA solution in the spectral range of 600-1200 cm^{-1} . The peaks appeared at 745 cm^{-1} and 1180 cm^{-1} indicate the N-CH ₃ stretching mode of DMAc and the C-N stretching mode of PAA, respectively.....	63
Figure 3.7. Raman spectra of PAA, partially cured PAA-PI and fully cured PI in the spectral range of 1040 -1220 cm^{-1} . The peaks at 1108 cm^{-1} and 1180 cm^{-1} indicate the C-N-C stretching mode of PI and the C6H2 stretching mode of PAA, respectively	65
Figure 3.8. Raman spectra of the PAA solution. The peak appeared at 742 cm^{-1} corresponds to the DMAc activated by N-CH ₃ stretching mode, and	

1608 cm^{-1} corresponds to the PAA activated by aromatic ring stretching mode	67
Figure 3.9. Confocal microscopic image of the PI cross-section and its contour: (a) 10 μm thick PI (left) and 30 μm thick PI (right), and (b) 3D image of white rectangle designated in (a).....	70
Figure 3.10. Schematic diagram of measuring depth-wise profile of PI chain orientation by detecting: (a) in-plane Raman intensity (I_{xx}), and (b) out-of-plane Raman intensity (I_{zz}).....	72
Figure 3.11. Rate dependent shear viscosities for PAA solutions having different solvent contents. Filled symbols represent PAA-1 (BPDA-PDA) and open symbols PAA-2 (BPDA-ODA).....	74
Figure 3.12. Raman spectra of PAA-1, PAA-2 and their 1:1 mixture	75
Figure 3.13. Schematic diagram for the Raman experiments of (a) PAA-1 and PAA-2 interdiffusion, and (b) solvent diffusion into the dried PAA-1 film	77
Figure 3.14. The measurement of interdiffusion width using X-Z mapping of Raman spectroscopy. (a) Raman spectra of PI-1, PI-2 and their 1:1 mixture. (b) Cross-sectional images of a PI bilayer captured by a microscope and its X-Z Raman mapping result. Blue and red colors in the mapping image are distinguished by different Raman peaks appeared at 735 and 695 cm^{-1} respectively.....	80
Figure 4.1. Depth-wise residual solvent profiles of the PAA film at different drying times for the film of thickness (a) 10 μm and (b) 30 μm	86

Figure 4.2. Depth-wise DOI profiles at different curing temperatures: (●) 150 °C; (▼) 170 °C; (■) 200 °C; and (◆) 350 °C, when the thickness of the final PI film is (a) 10 μm, and (b) 30 μm. The right side of the curve corresponds to the air side	89
Figure 4.3. Polar plots of Raman intensities for the (a) uniaxially extended PI film, and (b) intact PI film.	91
Figure 4.4. In-plane and out-of-plane polarized Raman spectra measured at both air and substrate side of (a) PI 10um, (b) PI 30 μm, and mapping image of Raman anisotropy(I_{xx}/I_{zz}) of (c) PI 10 μm, (d) PI 30 μm. x-axis is longitudinal direction of film in picture (c) and (d)	94
Figure 4.5. (a) Depth-wise Fraser fraction (f) profile of two different PI films, and (b) schematic diagram of depth-wise chain orientation	96
Figure 4.6. Depth-wise residual solvent contents (Left) and DOI (Right) during the drying process through (a) protocol A (120 °C drying), (b) protocol B (140 °C drying), and (c) protocol C (160 °C drying)	99
Figure 4.7. Depth-wise residual solvent content (Left) and DOI (Right) during the curing process through (a) protocol A, (b) protocol B, and (c) protocol C. H is a distance from the substrate and H ₀ is the film thickness, thus H/H ₀ =0 and 1 corresponds to the substrate side and air side, respectively.....	101
Figure 4.8. Degree of imidization during the drying and curing processes through different protocols	104
Figure 4.9. (a) Raman spectra of in-plane and out-of-plane polarization appearing at 1610 cm ⁻¹ for PIs made by different protocols. The spectra were	

obtained in the middle part of the PI cross-section. (b) Fraser distribution function (f) along the film thickness direction. In the graph, $H/H_0=0$ and 1 corresponds to the substrate side and air side, respectively..... 106

Figure 4.10. WAXD reflection patterns of the PI films depending on different protocols 109

Figure 4.11. Temperature dependence of $\tan \delta$ measured by DMA for the PI films depending on different protocols..... 110

Figure 4.12. Temperature dependence of sample length measured by TMA for the PI films depending on different protocols 111

Figure 4.13. Depth-wise volume fraction of PAA-2 (Φ_{PAA2}) measured at different times after a contact with PAA-1. Different pairs of PAA-1 and 2 have different solvent concentrations of (a) 88 wt%, (b) 90 wt%, (c) 91.5 wt%, and (d) 93 wt%. Abscissa was shifted by z_0 that is the depth below which the volume fraction of PAA-2 increases 113

Figure 4.14. Log-log plots of the interdiffusion width $w(t)$ between PAA-1 and PAA-2 at different contact time (t). Different symbols represent PAA-1/PAA-2 pairs having different solvent contents which are indicated in the graph..... 115

Figure 4.15. Interdiffusion data of the cured PI bilayers made by the DML and LBL methods. (a) Variation of PI-2 volume fraction (Φ_{PI2}) measured at different positions on the cross section of the cured PI. Abscissa was shifted by Z_0 where the volume of two PIs is equal (i.e. $\Phi_{PI2}= 0.5$). (b)

The interdiffusion width $w(t)$ of the PI bilayers according to the drying temperature of the bottom layer (T_b) 117

Figure 4.16. Depth-wise solvent content (X) measured at different times after a contact between the dried PAA-1 and 2 solutions. The dried PAA-1 was prepared by drying at different temperatures (T_b) of (a) 100 °C, (b) 130 °C, and (c) 160 °C respectively. Dashed line shows the calculated initial solvent content (i.e. $X=7.3$) of PAA-2 solution, which corresponds to 12 wt% 119

Figure 4.17. Degree of in-plane chain orientation of single and bilayer PI films represented by the Fraser distribution function. PI films were made by (a) DML drying($T_b=100$ °C), (b) LBL drying($T_b=100$ °C), (c) LBL drying($T_b=130$ °C), (d) LBL drying($T_b=160$ °C) 122

List of Tables

Table 3.1. Drying and curing conditions for the different protocols. Sampling time indicates the measurement time during drying and sampling temperature indicates the measurement temperature during curing.....	56
--	----

Chapter 1.

Introduction

1.1. General introduction

Polyimide (PI) has high glass transition temperature, good thermal and mechanical strength, relatively low dielectric constant and thermal expansion coefficient due to the stable chemical structure of imide rings. These properties make polyimide a suitable dielectric for flexible printed circuit boards (FPCBs), alignment layers for liquid crystal displays (LCDs), photoresist, and so on. PI has attracted attention as a transparent substrate or transparent cover for flexible displays or interlayer dielectrics for semiconducting memory devices. [1-7] These new applications require PI films with better thermal, electrical and optical properties. Many studies have focused on overcoming the limitations of conventional PI films by employing new monomers or developing PI nanocomposites with inorganic materials. [8-10] However, processing conditions can also affect the final properties of PI films even with the same chemical structure because different microstructures represented by different degree of in-plane chain orientation are developed when the PI films have different thickness, undergo different thermal histories, or show different behavior of interdiffusion between different layers. Thus, in addition to selecting the appropriate monomers, it is important to understand how the different processing conditions such as film thickness, thermal history, and interdiffusion influences the final microstructure of PI.

Thermally cured PI films are manufactured by drying poly(amic acid) (PAA) solution on a substrate and curing it. During the drying process, PAA is solidified at a temperature usually of less than 130 °C and then imidized to PI by further increasing the temperature up to 350 °C or higher. The polymer chains confined by a substrate are biaxially stretched during solvent evaporation, which preferentially aligns the

chains to the in-plane direction.[11-15] Many studies on the degree of chain orientation in PI films have been conducted using birefringence, [13-18, 42-44] X-ray diffraction [12-15, 29, 30, 45, 46] and polarized ATR/FT-IR.[19-22] In these experiments, the chain orientation of PI was associated with the physical and optical properties of a film such as CTE, elastic modulus, and refractive index. [11, 19, 23-25, 40, 41] Among these, CTE was found to be more affected by the variation of chain orientation such that the lateral CTE decreased considerably when the degree of in-plane chain orientation increased. This is because a strong intramolecular force (i.e., covalent bonds) allows little dimensional change of polymer chains along the chain axis in response to the temperature change, whereas a weak intermolecular (i.e., van der Waals) force makes dimensional change easier in the direction perpendicular to the chain axis. As a result, the lateral CTE decreases when more polymer chains are aligned to the in-plane direction of the film. [23, 26, 27]

The degree of chain orientation that influences the properties of a film can be affected by film thickness. Liou et al. [16] observed that the lateral CTE increased while the vertical CTE decreased when the film thickness was increased from 2.5 μm to 20 μm . The fraction of PI chains aligned to the in-plane direction also decreased with increasing film thickness.[15] Jou et al. [26] compared X-ray diffraction patterns between the in-plane and out-of-plane directions and observed the change in the degree of chain orientation when the film thickness increased. In addition, Hasegawa et al. [11] added perylenebismide dye into a PI film and measured the dichroic absorption of dye molecules according to the film thickness to predict the degree of in-plane chain orientation of PIs composed of different monomers. The results prove that an increased film thickness lowers the degree of in-plane chain orientation, which

affects the physical properties of the PI film. Nevertheless questions remain regarding the depth-wise distribution of chain orientation.

The degree of in-plane chain orientation is also affected by thermal history during the drying and curing processes. Johnson and Wunder [28] measured the imidization degree at different curing rates and temperatures. Nomura and Asano [19] reported that the PI chains were randomly oriented near the substrate when heating was fast, but highly oriented to the in-plane direction when heating was slow. Takahashi et al. [29] observed the variation of chain orientation during the curing process by comparing the reflected patterns of wide angle X-ray diffraction with the transmitted patterns. However, these studies are limited to investigating the effect of the curing conditions, mainly curing rate and final temperature, on the chain orientation of PI and its physical properties. [11, 20, 24, 30] However, they do not consider in the respect of thermal history including drying process and do not address how the microstructure developed during the drying process affects the overall microstructure of the cured PI. In addition, due to the difficulties in characterizing the properties in the film depth direction, only the average properties of bulk film or film surface were investigated. These approaches yield an incomplete depiction of the physical properties given that there is an inhomogeneous distribution of chain orientation along the film thickness.

In order to control the film flatness or to give additional functions to PI film, two or more PIs having different molecular structures are stacked together to make a multi-layer film. Unlike a single layer, the adhesion at the interface becomes a crucial factor in manufacturing multi-layer PI film because poor adhesion can cause partial or complete de-adhesion problems due to the interfacial stress generated at high

temperature processing. The interdiffusion between different layers composed of immiscible or partially miscible polymers is essential to get a good adhesion property, and the difference in CTE of each layer must be minimized to reduce the interfacial stress. [31] Especially in the case of multilayer PI, the amount of solvent diffusion from or toward the other layer in contact is another important factor as it can change the residual solvent content of the layer during the processing. Recently, the direct multi-layer (DML) method that dries several layers of polymer solutions at once has been introduced to make multilayer polymer films in a variety of coating industries, replacing the conventional layer-by-layer (LBL) method in which each layer is dried individually in a consecutive manner. [31-33] When the LBL method is applied to make a PI bilayer film, the interdiffusion width at the interface was reported to decrease as a large fraction of PAA in the bottom layer is imidized to PI before the top layer is coated on it. [34-36] It is because the swelling of the bottom layer by the solvent is hindered as PAA in the bottom layer is converted to PI which is insoluble to the solvent. However, these studies only focused on the submicron-sized thin layers of PI, and the different behaviors of interdiffusion when the DML method is applied have not been explored yet. The most significant difference between the DML and LBL methods is the phase of each layer when they contact. For the DML method, both layers are liquid phase containing relatively larger amount of solvent, while one is solid and the other is liquid for the LBL method. When the two different drying methods are used to make multilayer PI films, this difference can influence the extent of interdiffusion and chain orientation of PIs because both translational and rotational mobilities of polymer chains are directly affected by the amount of solvent. Therefore, it is necessary to understand how different drying methods affect the final

interdiffusion width and the chain orientation of PIs in order to provide a proper functionality to the multilayer PI films without any interfacial failure.

In this thesis, chain orientation of PI and its interdiffusional behavior is introduced. Firstly, the in-plane orientation of cured PI films with different thicknesses is quantified. Residual solvent concentration of PAA during the drying process is measured in the film depth direction with confocal Raman spectroscopy, and observed how the residual solvent affects the subsequent curing process. Polarized Raman spectroscopy is used to quantify the degree of chain orientation in the film thickness direction, and the relationship between the chain orientation of PI and that of PAA is examined. Secondly, the variation of chain orientation is investigated for PI films manufactured by different process protocols, i.e. different drying and curing conditions. The final microstructures of the cured PI films are predicted from the process path designed with two parameters, residual solvent concentration and imidization degree, and they were compared to the degree of in-plane chain orientation. The effect of PI microstructure on the film properties is also examined by comparing the degree of in-plane chain orientation with crystallinity, glass transition temperature (T_g), and TEC. Finally, bilayer PI films having similar molecular structure are manufactured using two drying methods, DML and LBL methods. Different aspects of interdiffusional behavior for different drying methods are explained by the role of solvent. At the same time, the chain orientation of PI bilayer is compared with that of a single layer PI film and the difference is explained in terms of the amount of solvent remaining in each layer after the drying process.

1.2. Outline of the thesis

The thesis consists of background, experimental methods, results and discussion, and summary chapters.

Chapter 2 describes the background of the thesis which is divided into manufacturing process of polyimide, chain orientation, polymer interdiffusion and the confocal Raman spectroscopy. First, the manufacturing process of polyimide film is briefly introduced regarding the precursor preparation and thermal imidization of the precursor, and the drying process of general polymer solution is given a more focus. General theories of polymer chain orientation and its interdiffusional behavior are explained to provide a more clear understanding of the results, and the chapter finishes with introducing the key analytical method employed in this study, the confocal Raman spectroscopy.

Chapter 3 deals with experimental methods used in this study starting with the sample preparation and its characterization. Several experimental methods used to analyze the depth-wise properties of polyimide film are introduced in the sequence of measuring the residual solvent concentration, degree of imidization, and chain orientation. In the last part of the chapter, a novel and simple method employed to observe the polymer-polymer interdiffusion is explained, and general characterization methods of the cured polyimide film is also introduced.

In chapter 4, experimental results are divided into three main parts. The first is to show how the film thickness affects the final chain orientation of polyimide films. Comparing the experimental result with that of previous studies, it is proved how well the new analytical approaches used in this study explain the relatively well-known

phenomena. Second part of the chapter explains the effect of thermal history on the polyimide chain orientation. The results show the final microstructure of the polyimide film can be significantly affected by the processing condition except for the chemical structure. Finally, the interdiffusional behavior between two similar but different polyimides, as well as the chain orientation, is examined in bilayer polyimide system.

Chapter 5 summarizes the results on the works about the chain orientation of polyimide and its interdiffusional behavior affected by drying and curing processes.

Chapter 2.

Background

2.1. Manufacturing processes of polyimide film

A general method of making PI film is mainly composed of 3 processes : preparing a precursor polymer solution, coating and drying, curing processes. When making a precursor solution, the solid content of polymer solution or the molecular weight of precursor should be adjusted to be appropriate to process the coating. During the drying process, a certain amount of solvent in the precursor solution evaporates and the film is solidified with a certain critical percent imidization. Afterwards, the solidified film is passed into the curing process where the film is biaxially fixed by a substrate or a tenter and the precursor is converted to PI. The latent heat of evaporation and heat of the imidization reaction are supplied by hot air, radiation from an electrical heater, or infrared (IR) heater. The final curing temperature is typically greater than 350 °C. In the entire drying and curing process, the area of the film is held almost constant by adhesion to the substrate or by in-plane restraint in the tenter. Because the stress-free state shrinks in-plane, this restraint aligns the chain axes in-plane, which increases the tensile strength and modulus of the film. A schematic diagram of the processes is shown in Figure 2.1.

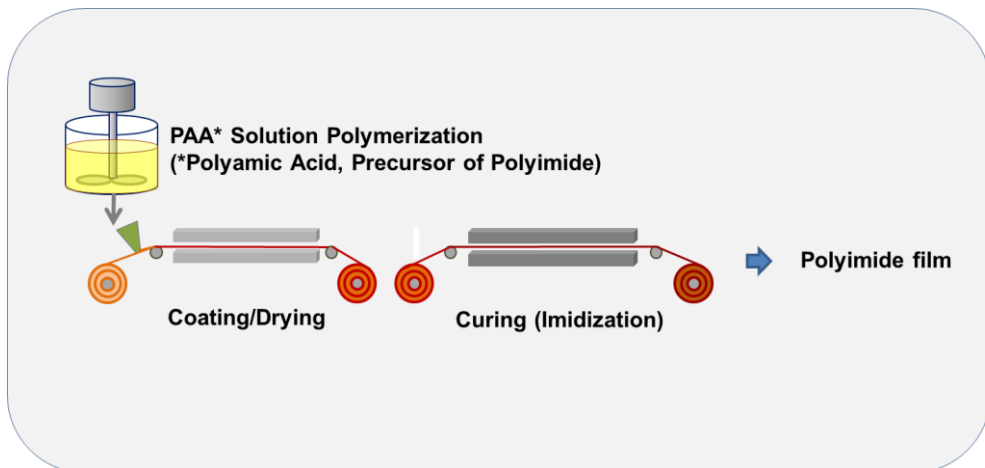


Figure 2.1. Schematic diagram of PI manufacturing process.

2.1.1. Poly(amic acid) preparation

In the general method of polyimide manufacturing, a dianhydride is added to a solution of diamine in a polar aprotic solvents such as N,N-dimethylformamide (DMF), N-methylpyrrolidone and N,N-dimethylacetamide. When a diamine and a dianhydride are mixed in the dipolar aprotic solvent poly(amic acid) (PAA), the precursor of polyimide, is formed as shown in Figure 2.2. The generated PAA is then cyclodehydrated to make a polyimide by thermal heating at elevated temperature or by using chemical dehydrating agents. As the polyimide is usually insoluble, it is processed in the form of PAA accompanied by a solvent. The reaction mechanism of PAA polymerization can be explained by the nucleophilic attack of the amino group on the carbonyl carbon of the anhydride group, followed by the opening of the anhydride ring to form amic acid group. [37] The most important aspect of this process is that it is an equilibrium reaction. It appears to be an irreversible reaction because a high molecular weight PAA is readily formed as long as pure reagents are used. It is because the forward reaction is much faster than the reverse reaction, usually by several orders of magnitude. If the large reaction rate difference is not met, the high molecular weight PAA is not formed. Hence, it is important to examine the driving forces that favor the forward reaction over the reverse reaction. It should also be noted that the acylation reaction of amines is an exothermic reaction and that the equilibrium is favored at lower temperatures.

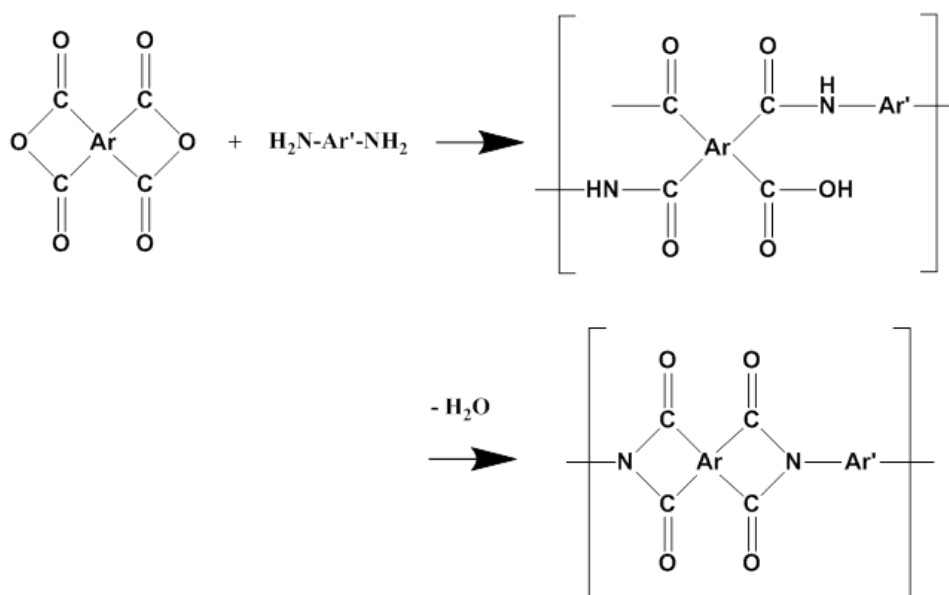


Figure 2.2. Mechanism of PAA and PI formation.

2.1.2. Thermal imidization of PAA

Thermally cured PI films are manufactured by drying PAA solution on a substrate and curing it. During the drying process, PAA is solidified at a temperature usually of less than 130°C and then imidized to PI by further increasing the temperature up to 350°C or higher. The polymer chains confined by a substrate are biaxially stretched during solvent evaporation, which preferentially aligns the chains to the in-plane direction.

Kinetics of imidization

A potential energy diagram for the reactions is shown in Figure 2.3. [37] By reverse reaction, a small portion of the o-carboxycarboxamide can revert to amines and anhydrides. As the temperature increases up to near 250 °C, the anhydride and amine contents drop to almost zero and the majority of o-carboxycarboxamides are converted to imide. It is proved in many studies that the PAA heated to near 300 °C achieves more than 95% imidization. Heating at temperatures above 350 °C for extended periods of time can result in crosslinking. In this condition, polyimides become insoluble to solvents even though it is not clear whether this is due to crosslinking or close chain packing. Crosslinking at this temperature most likely proceeds by a free radical mechanism.

Imidization reaction is known to proceed in two stages under isothermal conditions. [37] At temperatures above 150 °C, imidization proceeds rapidly and is characterized by an initial fast cyclization step that changes into a second, slower cyclization step. The rate constant was found to be constant only in the initial step, and it decreases continuously in the second step until it drops to almost zero. As the imidization

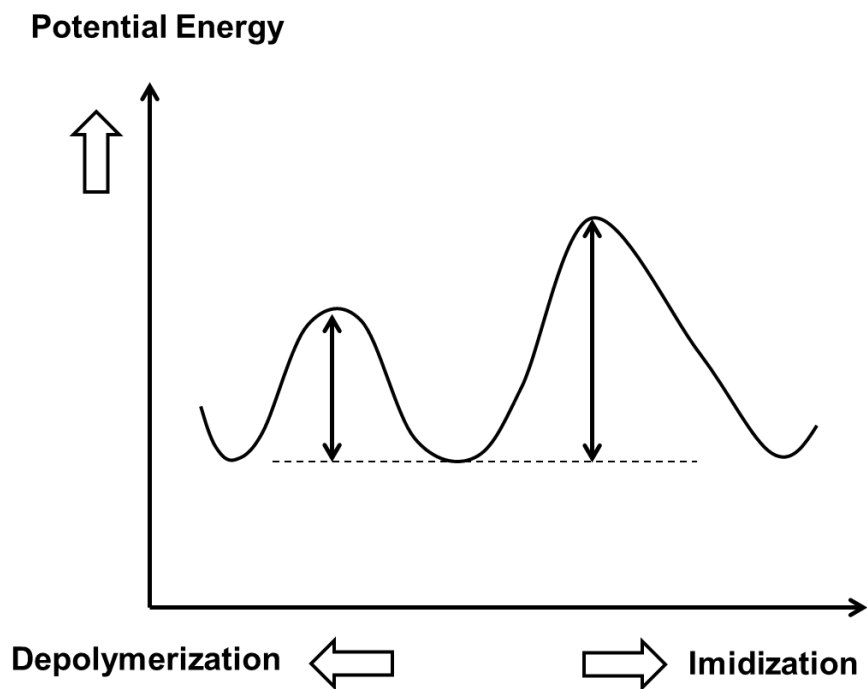


Figure 2.3. Schematic diagram of hypothetical potential energy during imidization. The left peak corresponds to the depolymerization energy and the right peak corresponds to the imidization energy.

temperature increases, the contribution of first step increases, so the degree of imidization becomes higher. And imidization is accompanied by chain scission to anhydride and amine moieties. As a result, these groups are excluded from the cyclization process for a given time. However, as the process proceeds, these groups again react to form amic acid linkages that undergo cyclization again. A drastic change in the slope of cyclization isotherms occurs because the rate at which the amic acid linkages are regenerated in the solid state is slower than the cyclization rate. As the imidization process continues, T_g of the polymer increases so that the polymer changes from a rubbery to a glassy state. This results in the decrease of imidization rate due to the decrease of molecular mobility in the glassy state.

Role of solvents

Imidization reaction can proceed faster in the presence of amide solvents. [19, 36, 38, 39, 47] It is because the solvent molecules allow the reacting groups to attain favorable conformations for imidization and to assist in the loss of the carboxyl proton. Amide solvents are known to form strong hydrogen-bonds with the carboxyl group. As a result, the transfer of a proton to the basic solvent under the imidization conditions seems quite likely. When manufacturing the PI film, different amounts of solvent according to the types of solvent usually remain in the film even after the drying process. And this residual solvent can behave as a plasticizer until the unbound solvent molecules evaporate during the curing process. Thus, the types of solvent used in PAA solution can play an important role in determining the imidization speed, degree of imidization, and even the final chain orientation. And for thicker film, the

solvent molecules stay in the film for a longer time and this also affects these properties.

Role of heating rate

When manufacturing a PI film, heating rate is closely related with the final chain orientation. [11, 20, 24, 27, 48] While the degree of molecular packing of PI chains is increased with the local motion of molecules, high degree of in-plane orientation is achieved by long distance translational diffusion. It means that PI chain should have enough time for rearrangement with a sufficient mobility to get high degree of in-plane orientation. In this regard, faster heating rate of PI can result in lower degree of in-plane orientation because the mobility of PI chain decreases due to the faster evaporation of solvent. At the same time, increasing number of imide rings along the main chain stiffens the backbone and has the effect of slowing the reaction by reducing the availability of suitable conformations for imidization. Especially when the film is thick, it becomes more significant that faster heating rate lowers the degree of in-plane orientation, while there is no difference when the film is thin. However, this is different from the point of local ordering of PI chains in that molecular packing degree is more enhanced by intensive thermal conditions. As a result, it is important to find out the optimized heating rate to avoid unwanted chain orientation which would result in film defects such as a CTE mismatch in multilayer film.

2.2. Drying behavior of polymer solution

Drying of polymer solution basically involves two steps : (a) Diffusion of the solvent towards the film surface, (b) removal of the solvent from the film surface. The resistance to drying related with the diffusion of solvent in the coating is called internal resistance, and the resistance to solvent evaporation at the film surface is called external resistance. Internal resistance generally determines the final residual solvent content after drying.

2.2.1. Two drying regimes of polymer solution

There are two periods of drying that control the speed and amount of solvent evaporation as shown in Figure 2.4. [57-60] The first one is the *constant rate period* and the other is *falling rate period*. The first period is determined by the difference between the partial pressure of the solvent at the surface of the coating. Most of the solvent in the coating is removed during this period. In early stage of the first period, the surface temperature may drop because the latent heat of solvent evaporation has to arrive by heat transfer. And then the coating temperature becomes a steady state, thus the rate of heat supplied from the hot air becomes equal to the rate of heat disappeared by evaporation. During this equilibrium state of heat transfer, the drying rate is constant. This constant rate of drying is the period where the rate of solvent that diffuses from the solution to the film surface is sufficiently faster than the rate of solvent evaporation. This means the slower evaporation rate is the rate determining step, and it is controlled by many factors such as drying temperature, air velocity, solvent concentration, and so on. This constant rate period finishes when the solvent concentration drops so that the solvent diffusion inside becomes slower than the

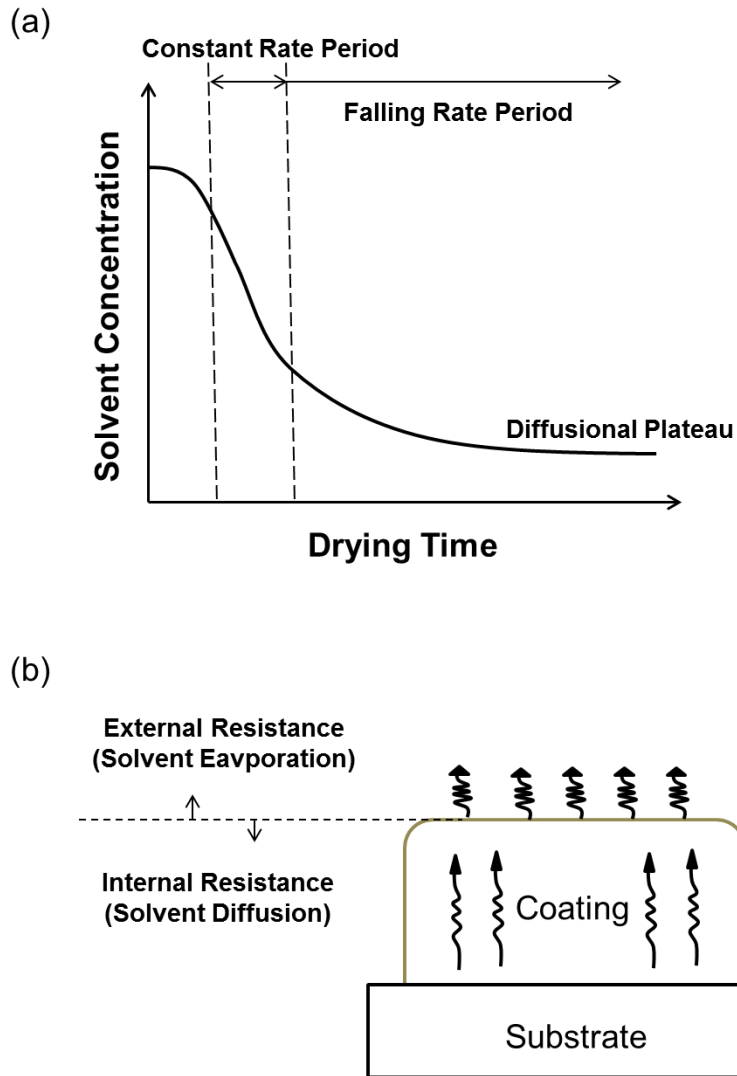


Figure 2.4. Drying mechanism. (a) three characteristic periods of drying, (b) two characteristic resistance of drying.

solvent evaporation at the film surface. The next step is falling rate period. Films are solidified and the rate of solvent diffusion becomes a rate determining step. When internal diffusion controls the solvent evaporation, coating thickness and drying times are important factors which determine the residual solvent amount after drying. As the rate of diffusion is a function of solvent concentration and drying temperature, the rate of drying continuously decreases in this period regarding the constant temperature. At long time of drying afterwards, the rate of solvent evaporation becomes negligible to reach a diffusional plateau.

2.2.2. Stress development in polymer films

Polymeric films as well as most other materials tend to shrink as they dry. [23, 54-56] This is true whether the coating dries due to chemical transformation or purely solvent evaporation. The area of a coating is constrained to remain at its original wet size by adhesion to a normally rigid substrate so volume changes are accommodated by a change in thickness accompanied by fluid flow. After the coating solidifies and can no longer flow, subsequent solvent loss produces an internal strain in the coatings as it proceeds to its final dry state. Even if the viscous component of a film is present, not all this stress relaxes and the remaining residual stresses can affect the final properties of product. This may lead to undesirable defects such as delamination in the region of the coating boundary, cracking on the surface, and in the case of a flexible substrate, wrinkling of the entire system. Additional strains developing in this process of additional mechanical deformation are usually very large, and the associated additional stresses are superposed on the residual stress field developed earlier in the process of drying.

As the concentration gradient is the highest at the top of a drying coating, the stress level is highest there, apart from near the outer edges and any inner edges. The top of the coating is thus where cracks are most likely to initiate and cause defects such as crazing, which is a layer on the surface that is filled with curled pieces separated by small cracks. As the coating dries, it tends to shrink in all directions if it were allowed to do so. However, adhesion of the coating to the substrate is enforced at the substrate, especially at the edges, where the tendency to detach is the highest. Therefore the edge is another site for initiation of cracks. If the bond strength between the coating and the substrate is weak, then crack initiates and propagates between the layers. This is delamination. Even without these cracking failures, the presence of in-plane tensile stress can cause curling of the substrate, which makes it jeopardize the handling of the products in the subsequent processes. Stress gradient through the width of the coating can cause uneven surface and nonuniform coating properties as well.

2.2.3. Stress development in polyimide film

If the PI is deposited on a planar substrate and the coating is constrained by the substrate, the development of biaxial stress is dominated by the mismatch between the CTE of the film and the substrate. [23, 48-53] As the excessive residual stress can result in cracking or delamination of the PI film or film curling, it is important to minimize the CTE mismatch between the film and substrate or between different PI layers. Especially when copper or aluminum metal which has relatively lower CTE than typical PI films is used as a substrate, it is necessary to lower the CTE of the PI film in order to reduce the stress development. At the same time, it has to be considered that relatively flexible and soluble PAA is converted to more rigid PI

during the curing process. In this case, the development of residual stress is also affected by curing process in which solvent evaporates and by-product water is removed. Solvent loss as well as the conversion of flexible PAA to rigid PI critically hinders the polymer molecule to relax. These origins of stress development are integrated in concept of intrinsic stress and thermal stress. The intrinsic stress is related to the volume shrinkage by solvent evaporation while the thermal stress is related to the CTE mismatch between the film and the substrate during the cooling process from the final curing temperature. If the thickness of the film is negligible to the substrate thickness, the thermal stress between two different temperatures can be expressed by [23] :

$$\sigma_f = \int_{T_1}^{T_2} \frac{E}{(1-\nu_f)} (\alpha_s - \alpha_f) dT \quad (2.1)$$

where σ_f is the film stress, T_c is the final curing temperature, E_f is the Young's modulus of the film, α_s and α_f are the CTEs of the substrate and the film, and ν_f is the Poisson's ratio of the film. Here, the T_1 becomes T_g , the glass transition temperature when T_1 is small than T_g .

2.3. Chain orientation of rod-shaped polymers

2.3.1. General introduction of polymer chain orientation

Macroscopic properties of materials are closely related to their microstructures. For semicrystalline polymers, the ratio of crystalline and amorphous phases and chain orientation are considered to be critical factors in understanding the macroscopic properties. [61] Among these, Chain orientation is a unique phenomenon to polymer system. The linear chain makes it possible to obtain strongly anisotropic properties. The anisotropy arises when molecules are aligned to a specific direction and the intrinsic properties of a polymer chain strongly depend on its orientation. The strong covalent bonds along the chain axis and the weaker bonds in perpendicular directions result in a significant anisotropy such as birefringence and anisotropic tensile strength. In semicrystalline polymers, the crystalline and amorphous parts show different degree of orientation. Several techniques of chain orientation measurement exist such as birefringence, wide-angle X-ray diffraction (WAXD), nuclear magnetic resonance (NMR), fluorescence measurements, and vibrational spectroscopic measurements such as polarized FT-IR and polarized Raman spectroscopy. [11, 14, 21, 22, 29, 40, 42, 62]

Each technique has its advantages and disadvantages. Birefringence measurements are simple and reasonable but give information only about the distributions averaged over the sample, while NMR is very costly. Molecular orientation distributions in the crystalline phases only are obtained by WAXD, although this is only the technique allowing the precise distribution to be obtained, since all coefficients in the orientation distribution functions can be determined. For spectroscopic techniques, fluorescence

spectroscopy gives information about the molecular orientation distribution in phases only where fluorescent probes can migrate. Infrared (IR) dichroism measurements are capable of evaluating the molecular orientation distribution in both the crystalline and amorphous phase. However, the distributions obtained by IR spectroscopy lack accuracy because only one coefficient for the distribution functions can be determined. [21, 40] At the same time, the sample is required to be highly transparent and thin for the absorbance measurements. In this regard, polarized Raman spectroscopy can be a powerful tool to obtain information about chain orientation. [62-66] Similar to IR dichroism measurements, it is possible to analyze the distributions in both the crystalline and amorphous phases. Since this technique is compatible with optical microscopy, it is also suitable for study of chain orientation in the material at the micron size scale or in a micron region in the material. Furthermore, this technique has considerable potential for depth-wise profiling of film cross-section owing to its non-destructive nature.

2.3.2. Chain orientation measurement using polarized Raman spectroscopy

Polarized Raman spectroscopy is a vibrational technique that is widely used for the directional study of polymer chains. [62-69] When a laser beam with electric vector E is incident on a molecule, an electric dipole P is induced according to the relation,

$$P = \alpha E \quad (2.2)$$

Where α is the polarizability of the molecule. In general, the induced polarizability is not in the direction of the incident beam, thus it is expressed by a tensor quantity.

$$\begin{aligned}
 P_x &= \alpha_{xx}E_x + \alpha_{xy}E_y + \alpha_{xz}E_z \\
 P_y &= \alpha_{yx}E_x + \alpha_{yy}E_y + \alpha_{yz}E_z \\
 P_z &= \alpha_{zx}E_x + \alpha_{zy}E_y + \alpha_{zz}E_z
 \end{aligned}
 \tag{2.3}$$

Where the quantities α_{FF} are independent of the components of the electric vector but are dependent on the orientation of the molecule relative to the space fixed axes, X, Y, Z. The intensity of the Raman scattered light is proportional to the square of the magnitude of P.

In general, the light from a radiation source involves waves with no preferential direction of the electric field vector. When it encounters a substance, the light interferes with the atoms and induces a dipole moment in the material. The degree of the interference depends on the angle and the magnitude of the polarizability. So, it contains directional information about the orientation of the differential polarizability. The directional information can be obtained if polarized light with a specific electric vector is used as the incident beam. In polarized Raman, the Raman scattering is observed as a result of the interference of the polarized light with the vibrating molecules. Furthermore, by means of an analyzer, which is another polarizer before the detector, the precise directional information about the differential polarizability of the molecules can be obtained. In Figure 2.5, general components for the polarized Raman measurements are represented.

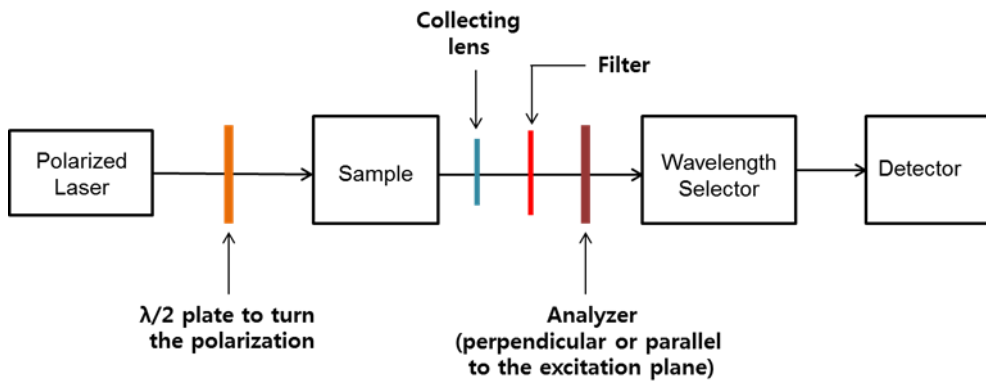


Figure 2.5. Schematic diagram of main components in polarized Raman spectrometer.

Assume that the excitation is done by light propagating in the X direction as shown in Figure 2.6. The scattered light is measured in the Y direction and the optical axis of the sample at which molecules are oriented is parallel to the Z direction. Excitation can be done with light polarized either in the Y or Z direction. The scattered light is measured with Z or X polarization. Four different combinations of polarization can be applied to the geometry of the sample like :

Polarization direction		Notation
Excitation	Scattering	
Z	Z	ZZ
Z	X	ZX
Y	Z	YZ
Y	X	YX

The intensities of Raman spectrum measured in each of these spectra are proportional to the squares of the components of the tensor $\alpha(F)$ defined in the space fixed coordinate system F. in order to express the measured elements $\alpha_{FF'}^2$ in terms of the elements of the tensor $\alpha(g)$ defined in the molecular coordinate system g, the transformation matrix $\Phi(F,g)$ is used and averaged over all the space like :

$$I_{ff'} \sim \alpha_{FF'}^2 = (\sum_{gg'} \Phi_{Fg} \Phi_{F'g'} \alpha_{gg'})^2 \quad (2.3)$$

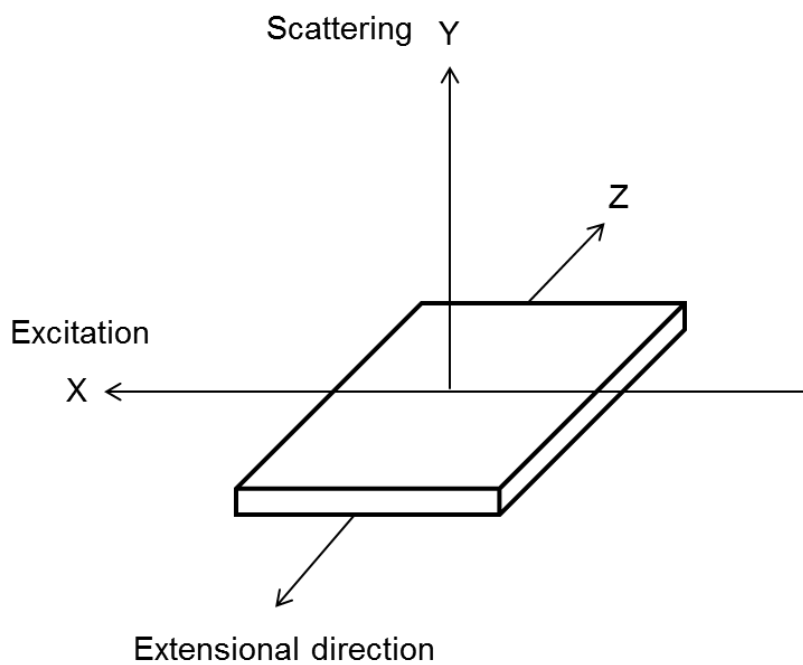


Figure 2.6. Main directions of film extension, light source excitation, and light scattering.

Perfect uniaxial orientation

The longitudinal axis z is put fixed parallel to the stretching direction Z , while the x and y axes are isotropically distributed around this direction. In this case the transformation matrix has the simple form like :

$$\emptyset(F, g) = \begin{pmatrix} \cos \emptyset & -\sin \emptyset & 0 \\ \sin \emptyset & \cos \emptyset & 0 \\ 0 & 0 & 1 \end{pmatrix} \quad (2.4)$$

Applying Equation 2.3, the following expressions are obtained for the intensities measured in the different polarized spectra :

$$I_{ZZ} \sim \alpha_{zz}^2$$

$$I_{ZX} \sim \frac{1}{2}(\alpha_{zx}^2 + \alpha_{zy}^2)$$

$$I_{YZ} \sim \frac{1}{2}(\alpha_{xz}^2 + \alpha_{yx}^2)$$

$$I_{YX} \sim \frac{1}{8}[(\alpha_{xx} - \alpha_{yy})^2 + (\alpha_{xy} - \alpha_{yx})^2 + 2(\alpha_{xy}^2 + \alpha_{yx}^2)] \quad (2.5)$$

Random orientation

Applying of Equation 2.3 to random orientation case, the meaningful intensity detected in Z direction is obtained like :

$$I_{ZZ} \sim \frac{1}{45}(45\alpha^2 + 4\gamma^2 - 5\delta^2) \quad (2.6)$$

Where α^2 , γ^2 , and δ^2 are three invariants of the scattering tensor, called isotropy, anisotropy and asymmetry invariants. Full expressions of each invariant are described in Chapter 4.3.3.

Partial orientation

In case of polymer drying, polymer chains tend to partially orient to the in-plane direction. It can be described as that a fraction f of the molecules is oriented with the longitudinal axes of the molecules in the direction of film plane, whereas the fraction $1-f$ is randomly oriented. [62, 69] Therefore, the meaningful intensity detected in Z direction can now be expressed by :

$$I_{ZZ} \sim f\alpha_{zz}^2 + \frac{1}{45}(1-f)(45\alpha^2 + 4\gamma^2 - 5\delta^2) \quad (2.7)$$

2.4. Interdiffusion between two different polymers

2.4.1. Polymer/polymer interfaces

Polymer interface is important as it significantly affects adhesion property in multilayer film. Figure 2.7 shows an interfacial region between two different polyimides measured by Raman spectroscopy. The change in interface structure is related with the diffusion of polymer chains through the contact area between two polymer components. The mixing behavior at the interface between two dissimilar

polymers, polymer A and B, can be explained by Flory-Huggins theory. [61, 70, 71] It provides an expression for the change in Gibbs free energy on mixing as :

$$\frac{\Delta G_m}{RT} = \frac{\phi_A}{M_A} \ln \phi_A + \frac{\phi_B}{M_B} \ln \phi_B + \chi \phi_A \phi_B \quad (2.8)$$

Where Φ_A , Φ_B are volume fractions, M_A , M_B are degree of polymerization of polymer A, B, respectively and χ is the Flory interaction parameter. The first two terms in the right part of the equation are configurational entropy of mixing. They are negative and usually very small because M_A and M_B are very larger for polymers. On the other hand, χ is negative so that most polymers are immiscible. The lack of miscibility between polymers limits the interdiffusion of polymer chains across the interface. This limitation results in a narrow overlap between two polymer layers. The length scale of transition zone between two polymer layers is usually referred to as the polymer interdiffusion width. This interdiffusion width play a critical role in many polymer industries as it directly affects the bonding properties.

For many industrial applications, there is always needs for good adhesion strength and strong interactions between different polymer layers. Therefore it is necessary to predict and measure the concentration variation of different polymers near the polymer interface. Helfand and Tagami firstly predicted the characteristics of the interface between two immiscible polymers using a self-consistent field theory. [72] They derived analytical expressions for the interdiffusion width, w_h , between two homopolymers as :

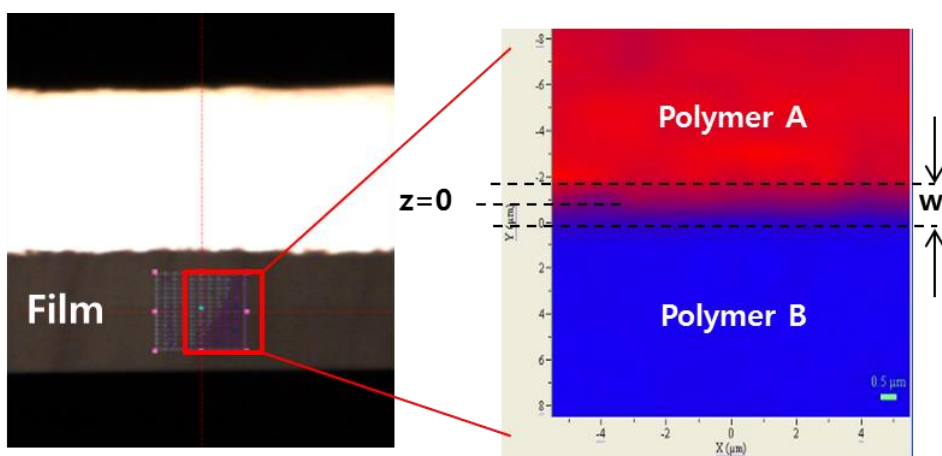


Figure 2.7. Cross-sectional image of a bilayer PI film (Left) and its Raman mapping image (Right).

$$w_h = \frac{2b}{(6\chi)^{0.5}}$$

$$b = \sqrt{\frac{b_1^2 + b_2^2}{2}} \quad (2.9)$$

where b_1 and b_2 are the statistical lengths for the two homopolymers. The polymer volume fraction profile at the interface can be given by :

$$\phi(z) = \frac{1}{2} \left(1 - \tanh \left(\frac{2z}{w_h} \right) \right) \quad (2.10)$$

where z is a coordinate normal to the interface. The general volume fraction profile for one composition along the z -axis near the interface is shown in Figure 2. 8. This simple equation relates the interfacial width to the interaction parameter χ . The interdiffusion width used here equals the full width at half maximum (FWHM). The FWHM value of a one-dimensional interface profile can be calculated also from the root mean square (RMS) roughness, σ_R , of a locally sharp interface as :

$$w = \sqrt{2\pi} \sigma_R \quad (2.11)$$

when considering the finite molecular weight effect, this w can be correlated as :

$$w = w_h \left[1 + \ln 2 \left(\frac{1}{\chi N_A} + \frac{1}{\chi N_B} \right) \right] \quad (2.12)$$

where N_A and N_B are chain lengths of two polymers. This equation is valid for strongly immiscible polymer systems where the interdiffusion width is smaller than the chain radius of gyration. If χ is large, the contribution of chain length becomes smaller. Based on this theory, χ plays a crucial role in determining the extent of interdiffusion width.

2.4.2. Interdiffusion at Polymer interfaces

Interdiffusion of polymer chains is related with the molecular motion. Edwards and de Gennes first developed the reptation model to describe the diffusion of polymer chains in an entangled system. [32, 70] This model looks an individual chain as diffusion freely under the assumption that each chain is located in a tube generated by chain entanglements. Time scales regarding the reptation model can be divided into 3 : the Rouse entanglement time (t_e), the Rouse relaxation time (t_r), and the reptation time (t_d). t_e shows the segmental diffusion for distances corresponding to the diameter of the tube. For a diffusion time smaller than t_e , the movement of the segments is not constrained by the virtual tub and the mean square displacement of a chain segment, $\langle r^2 \rangle$, is proportional to $t^{1/2}$. At t_e , the displacement is approximately decided by tube diameter. The Rouse relaxation time, t_r , is the time over which the motion of a segment becomes affected by the connection in an entire chain. For $t_e < t < t_r$, the movement is hindered by entanglements and $\langle r^2 \rangle$ becomes proportional to $t^{1/4}$. The reptation time, t_d , is the time required for a chain to escape from its original tube, it is expressed by :

$$t_d = \frac{R_g^2}{3\pi^2 D_s} \quad (2.13)$$

Where D_s is the self-diffusion coefficient. For $t_r < t < t_d$, chains move by reptation and $\langle r^2 \rangle$ is proportional to $t^{1/2}$. For $t > t_d$, chains are diffused by normal Fickian diffusion by which $\langle r^2 \rangle$ is proportional to t . The time dependence of the interface broadening $w(t)$ to $\langle r^2 \rangle$ can be expressed by :

$$w(t) = \sqrt{\frac{\langle r^2 \rangle}{3}} \quad (2.14)$$

The factor $1/3$ is due to the fact that only the movement of molecules is seen in one dimension.

Different from freely moving polymer chains, the interdiffusion between two immiscible polymers shows different aspect of diffusional behavior. The interdiffusion rate can be expressed by the mutual diffusion coefficient, D . Generally, two models, the fast and the slow theory, are used to explain this movement. In fast theory, D is given by :

$$D = (\phi_B D_A N_A + \phi_A D_B N_B) \cdot \left[\frac{\phi_A}{N_B} + \frac{\phi_B}{N_A} - 2\chi \phi_A \phi_B \right] \quad (2.15)$$

Where N_A and N_B are degrees of polymerization, D_A and D_B are the tracer diffusion coefficient of polymer A and B. If one polymer diffuses much faster than the other, the faster polymer determines the interdiffusion coefficient D in this case.

For the slow theory, on the other hand, shows :

$$D = \left(\frac{1}{\frac{\phi_B}{D_A N_A} + \frac{\phi_A}{D_B N_B}} \right) \cdot \left[\frac{\phi_A}{N_B} + \frac{\phi_B}{N_A} - 2\chi\phi_A\phi_B \right] \quad (2.16)$$

This equation implies that the diffusion of faster moving polymer is slowed down by the other component. If the two polymers are same (i.e. $N_A=N_B$, $D_A=D_B$), the two theories become the same. However, these theories assume that polymer chains are flexible and the diffusion is isotropic, but chain orientation can affect the diffusivity of polymer chains reducing the movement perpendicular to the direction of orientation. It was reported that rod-like polymer chains require deeper interpenetration to achieve sufficient adhesion compared with flexible polymers in multi layer system.

2.4.3. Interdiffusion between partially miscible polymers

Mutual diffusion between miscible polymers is well studied and understood, but little is known about the kinetics of interdiffusion between immiscible or partially miscible polymers. This is important because most binary polymer pairs show little compatibility at accessible temperature. When two different polymers contact, if polymers A and B are compatible, the initial sharp interface will be broadened as a result of Fickian diffusion. But two different polymers in contact do not interdiffuses freely, and an interfacial zone of finite width separates them at equilibrium. Interdiffusion across an interface between two polymers which are not fully miscible is limited to a region of finite width (i.e. interdiffusion width) at long times. [73-75] This immiscibility arises from a low combintional entropy of mixing which scales inversely with the polymerization degree, N , with interactions between two polymers.

If the interdiffusion width, w , is defined by the reciprocal of the maximal concentration gradient across the polymer A and B interface, the width w increases with time slower than that of typical Fickian type diffusion of $w(t) \sim t^\alpha$. Different from phase separation, interfacial mixing occurs by interdiffusion which is driven by thermodynamic forces. This interdiffusion is dependent on thermodynamic conditions such as molecular weight, temperature, and interaction parameter between two polymers. [76-79] A mean-field approach shows that the exponent α in a scaling law, $w(t) \sim t^\alpha$ is ranged between 1/4 and 1/2 near the critical temperature of the phase separation. And it also depends strongly on the definition of interdiffusion width as well.

2.4.4. Polymer interface and adhesion

Molecular interactions at the interface make adhesion. [70, 71] There are three ways to provide adhesion between two different polymers. They are (a) van der Waals force or hydrogen bonding, (b) chain entanglements, and (c) chemical bonding. Among these, chemical bonding is not often encountered as it needs chemical reaction between two polymers. For polymer pairs having large value of χ , the interdiffusion width is narrow and chains are hard to interpenetrate to the other polymer matrix. Thus, only overcoming a weak van der Waals force is sufficient to detach the two polymers in contact. A simple calculation based on van der Waals force between two polymers showed that the adhesion strength is on the order of mJ/m. But the actually measured level of adhesion was on the order of J/m. This shows the meaningful contribution of polymer entanglement. It is widely proved that the adhesion between two polymers is controlled by the degree of entanglement between them.

In order to explain how the entanglements can enhance the adhesion strength, three active adhesive failure mechanisms were proposed. They are (a) chain scission, (b) chain pullout, and (c) crazing. The maximum value of G_c , the energy necessary to make a crack, that can be obtained by chain scission or chain pullout is relatively low. As shown in Figure 2.9, the region in which each failure mechanism dominated is closely related with the interdiffusion width. The crazing mechanism corresponds to a relatively strong adhesion. At a weak interface, the adhesion failure is mostly come through chain scission or chain pullout, and crazing becomes dominant as the interdiffusion width increases. Once after this transition is passed, G_c comes to a plateau and becomes independent of the interdiffusion width because the failure stress can be maintained by the fibrils in the crazing zone. This increase arises from the onset of sufficient entanglements to raise the stability of the fibrils of an interfacial craze to the level of a craze occurring in the bulk homopolymer.

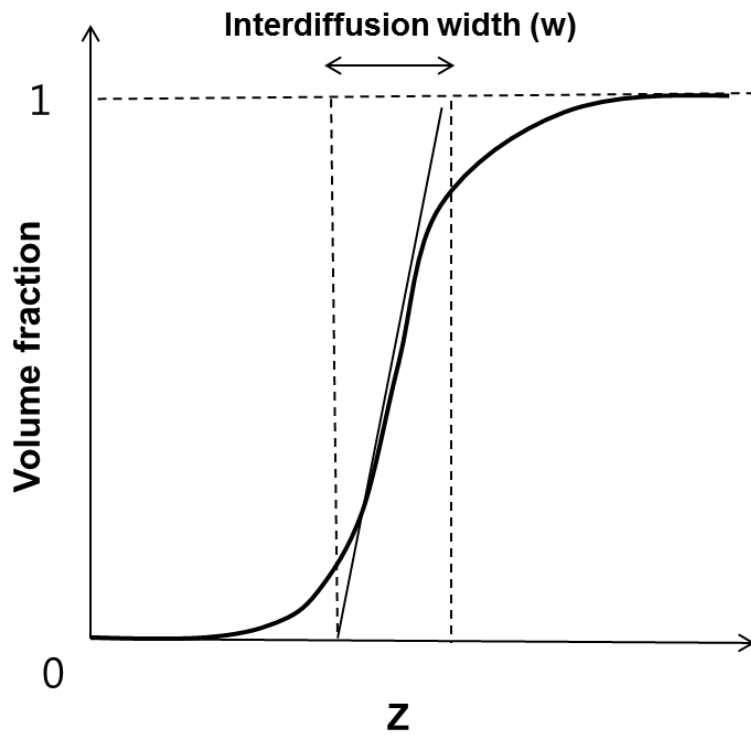


Figure 2.8. Graphical representation of interdiffusion width (w) defined by maximal volume fraction change at the interface.

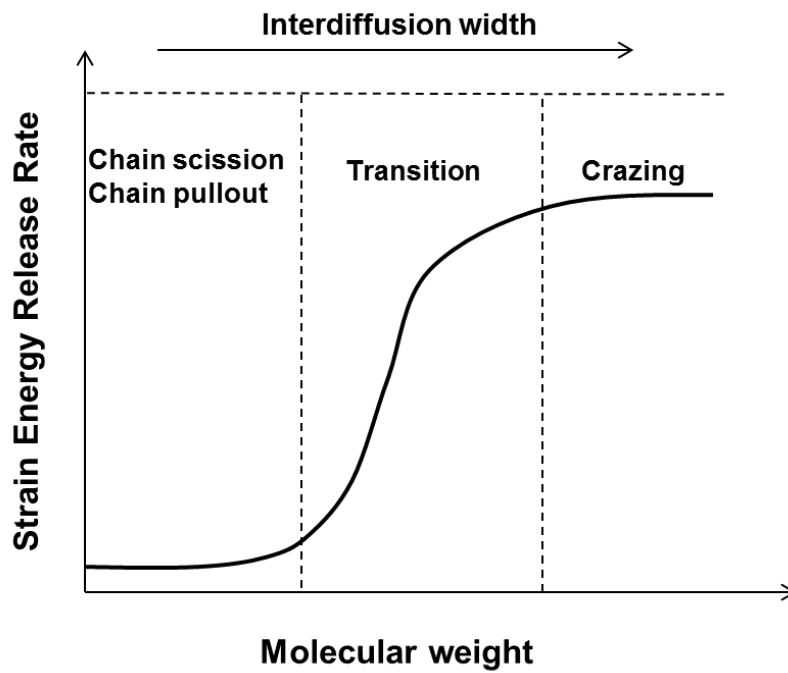


Figure 2.9. Schematic representation of the strain energy release rate depending on the molecular weight of a polymer.

2.5. Confocal Raman spectroscopy

2.5.1. Principle of Raman scattering

Raman scattering is considered as the inelastic scattering of light interacting with molecules. [68] When incident light encounters a molecule, the electric field of the light induces a dipole moment in the molecule due to its polarizability. The amount of the induced moment is proportional to the polarizability of the molecule. The excited molecule, then, relaxes to a higher level and the emitted photon has lower energy than the exciting laser light. Usually the Stokes region of the Raman spectrum is more intense than the anti-Stokes region as most of molecules are on the ground vibrational level at room temperature. [80] The energy of a vibrational mode depends on the molecular structure and environment. Atomic mass, bond order, molecular substituents, molecular geometry and hydrogen bonding all affect the vibrational force constant which, in turn dictates the vibrational energy. Vibrational Raman spectroscopy is not limited to intramolecular vibrations. Crystal lattice vibrations and other motions of extended solids are Raman-active.

2.5.2. Principle of confocal Raman spectroscopy

The confocal Raman spectroscopy consists of Raman spectroscopy and microscopy. [80, 81] After observing the specimen with microscopy, the point observed is then measured with Raman spectroscopy. The confocal Raman microscope focuses a laser beam down to a small volume and is operated readily in a confocal mode by placing an aperture at a back focal plane of the microscope. The aperture improves the lateral and axial spatial resolution of the microscope, allowing nondestructive depth profiling

by acquiring spectra as the laser focus is moved incrementally deeper into a transparent sample. This approach often is termed “optical sectioning,” as opposed to mechanically cutting a cross-section and scanning the laser beam laterally across the section. Confocal Raman microscopy can be applied in two ways. The first involves plotting the intensity of a component specific band as a function of the distance from the sample surface. This reveals compositional or structural gradients as a depth profile. The second approach is to attempt to acquire a pure spectrum of a buried structure for identification purposes. Both of these applications require knowledge of the exact size and position of the microscope focal volume as it moves deeper into the sample.

With these advantages, a few studies have been conducted using confocal Raman spectroscopy to observe the depth-wise solvent concentration of dried films. [82-85] Confocal Raman spectroscopy is an effective method of measuring the solvent concentration in a film because it enables depth-wise profiling of film composition with non-contact and non-destructive manner as mentioned above.

Intensity of Raman scattering

The intensity of Raman scattering is described by the following equation. [82]

$$I \sim N \cdot I_0 \cdot \left(\frac{d\sigma}{d\theta} \right) \quad (2.17)$$

where N is the number of scattering molecules per unit volume, I₀ is the intensity of the laser, and (dσ/dθ) is the differential scattering cross-section. If the intensity of the incident laser is constant the intensity of the scattered light is proportional to the

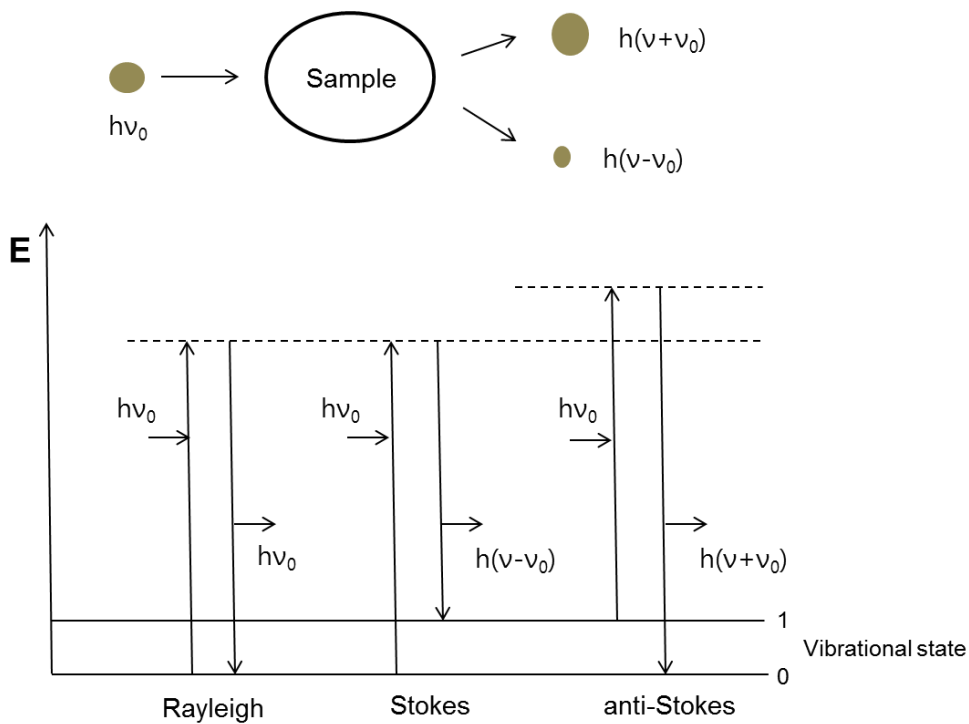


Figure 2.10. Schematic diagram of energy level before and after the light excitation.

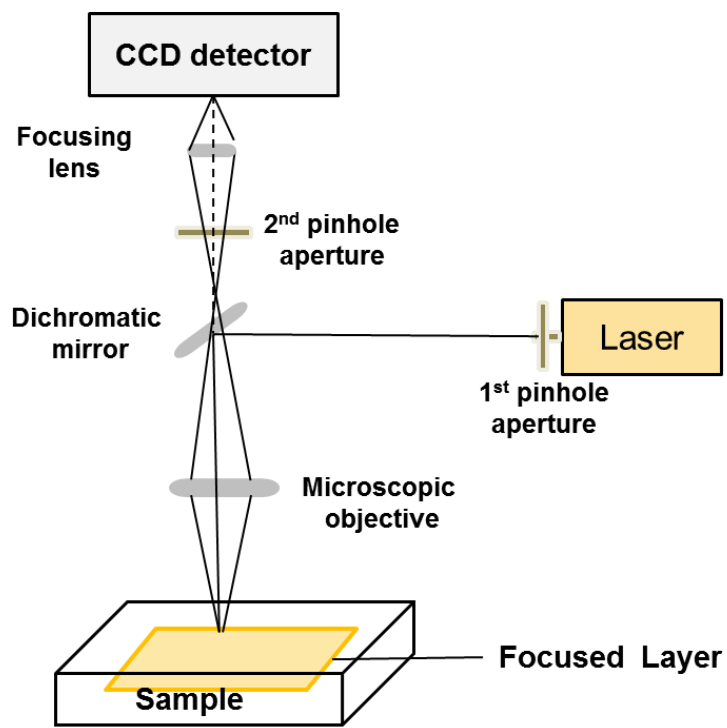


Figure 2.11. Schematic diagram of confocal Raman spectrometer.

number of scattering molecules activated. Raman calibration makes it possible to quantitatively analyze the chemical compositions using the linear relationship between the number of scattering molecules and the measured intensity. The detailed procedure of Raman calibration is shown in Chapter 3.1.

Depth resolution of confocal Raman spectroscopy

Figure 2.12 shows the simple representation of dispersive Raman spectroscopy combined with CCD (charge coupled device) detector. A sample is firstly put on the sample holder and a specific point is focused by observing with microscope. The laser beam encounters the point and only the scattered light from the sample that passes through a small pinhole is come into the CCD detector to generate the Raman spectrum. The first pinhole in Figure 2.12 reduces the amount of scattered light and the second pinhole is contributed to eliminate the scattered light that is out-of-focus.

To understand the intrinsic and variable depth resolution of Raman spectroscopy is important in Depth-profiling of chemical composition. Depth resolution mainly depends on two factors. The one is the volume of the laser focus and the other is how the scattered light is come back into the detector through the pinhole aperture. The limiting depth of focus (DOF) can be expressed by [81] :

$$\text{DOF} = \frac{2.2 n \lambda}{(NA)^2} \quad (2.18)$$

where n is refractive index of the objective lens or immersion medium, λ is the light wavelength, and NA is the numerical aperture of the focusing lens. NA can be expressed by $n \sin \theta$ where the θ is depicted in Figure 2.12. This equation shows that

the depth resolution is improved proportional to the NA. For example, a depth resolution of nearly 3 μm is achieved when using the He-Ne laser with 633nm wavelength, $n=1.4$ (glass), and $NA=0.75$. However, this concept of intrinsic depth resolution is incomplete to explain the varied depth resolution often encountered in depth-profiling of chemical composition. Expressing the focusing depth from the sample surface with z , $z=0$ when the laser beam is focused on the sample surface and d becomes positive when the focusing position goes down into sample. If z is positive and a sample with $n>1$, the lights are refracted and the measured laser intensity distribution becomes distorted. (Figure 2.12) Any light that passes into a sample in air suffers this refraction problem following Snell's law (i.e. $n = \sin\theta_i / \sin\theta_t$), where θ_i and θ_t are the angles of incidence and transmission with respect to the surface normal as shown in Figure 2.12. When $n>1$, the focal point lies deeper at z' . The ratio of refracted and nonrefracted position can be expressed by :

$$\frac{z'}{z} = \frac{\tan\theta_i}{\tan\theta_t} \quad (2.19)$$

In the equation, z'/z has a minimum value of n as it approaches to n when θ_i tends to zero, and increases as θ_i becomes larger.

To calculate the varying DOF in more detail, it is necessary to calculate the focal depth as a function of the radial coordinate of each ray leaving the objective. If the diffraction is negligible, focal depth has a simple solution as :

$$z' = z \times \left(\frac{r^2 NA^2 (n^2-1)}{R^2(1-NA^2)} + n^2 \right)^{0.5} = z \times \left(k^2 \times \frac{NA^2 (n^2-1)}{(1-NA^2)} + n^2 \right)^{0.5} \quad (2.20)$$

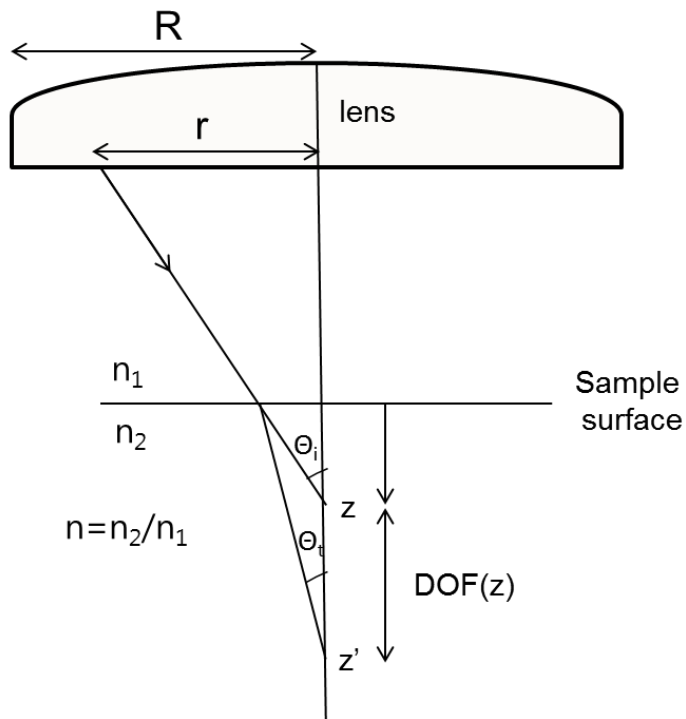


Figure 2.12. Depth of focus depending on the refractive index difference. Marginal lights are focused deeper position.

where r is the radius of a specific ray passing the lens, R is the maximum radius of lens, and k is defined by r/R . This equation shows the true point of focus (z'). It is obvious that lights that originate at different radii on the objective are focused to a different depth. The ratio of the refracted and non-refracted focal depth increases with both m and NA . Now, the varying depth of focus (DOF) can be defined as the difference between the maximum and minimum depths of focus.

$$DOF(z) = z_{k=1} - z_{k=0} = z \times \left\{ \left(\frac{r^2 NA^2 (n^2 - 1)}{R^2 (1 - NA^2)} + n^2 \right)^{0.5} - n \right\} \quad (2.21)$$

This implies that the depth resolution diminishes linearly as measuring position becomes deeper and increasing the aperture makes a worse depth resolution. This works the opposite way to the effect of diffraction, and if the NA is reduced too much the broadening due to diffraction will dominate.

Chapter 3.

Experimental methods

3.1. Sample preparation and characterization

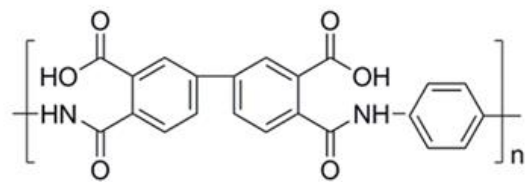
For Chapter 4.1

PAA preparation

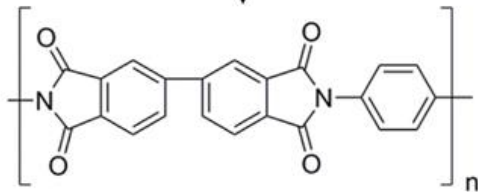
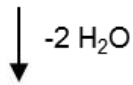
The starting materials used in this study were 3,3',4,4'-biphenyltetracarboxylic acid (BPDA, Ube Industries) and p-phenylene diamine (PDA, DuPont). N, N-dimethylacetamide (DMAc, Sigma-Aldrich) was used as a solvent. 2.0 g of PDA (0.02 mol) was put in a sealed flask containing 55 g of DMAc. After PDA was dissolved in DMAc, 5.5 g of BPDA (0.02 mol) was added to the flask and mixed overnight at room temperature. The viscosity of the prepared PAA solution was about 20 Pa·s at the shear rate of 1 s^{-1} , and the intrinsic viscosity was 1.9 (dl/g). The molecular structures of PAA and the corresponding PI are shown in Figure 3.1.

Calibration of Raman intensity

A calibration needs to be conducted in advance to relate the Raman intensity with the solvent concentration before measuring the residual solvent in depth direction. For this purpose, five PAA solutions having different concentrations were made by diluting the original PAA solution, and the Raman spectra were measured for each solution. In the measured spectra, the N-CH₃ stretching mode which appears at 745 cm^{-1} was used for a characteristic peak of DMAc, and the C-N stretching mode at 1180 cm^{-1} was used for PAA. As the intensity of each Raman peak is proportional to the amount of the corresponding component in the polymer solution, the solvent concentration can be obtained from the following relationship [82] :



Poly(amic acid)



Polyimide

Figure 3.1. The molecular structure of poly(amic acid) and polyimide composed of BPDA and PDA.

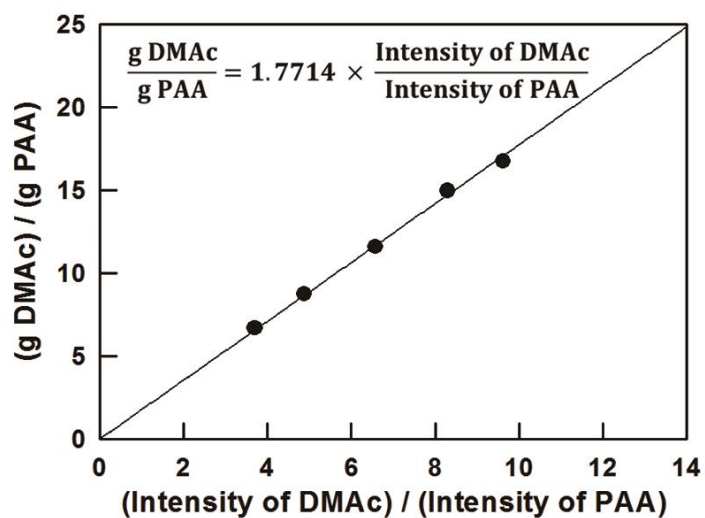


Figure 3.2. Raman intensity calibration graph plotted by solvent concentration against Raman intensity ratio between DMAc and PAA.

$$\frac{I_s}{I_p} = \left(\frac{\partial \sigma_s / \partial \theta}{\partial \sigma_p / \partial \theta} \frac{M_s}{M_p} \right) (X_s) \quad (3.1)$$

Here, I is the intensity of the Raman peak, σ the scattering cross section, θ the spatial angle, M the molar mass, X the concentration, and subscript s means solvent and p means polymer. The intensity ratio of the two characteristic peaks of DMAc at 745 cm^{-1} and PAA at 1180 cm^{-1} is plotted against the solvent concentration in Figure 3.2. In the figure, the slope of the linearly fitted line which corresponds to the constant in Equation 3.1 was measured to be about 1.77.

Drying and curing procedures

To see the effect of film thickness on the chain orientation of PI, PAA was coated on a PAA was coated on a clean glass substrate with two different wet thicknesses, $80 \text{ }\mu\text{m}$ and $250 \text{ }\mu\text{m}$, using a micrometer-adjustable film applicator. The coated PAA solutions were dried at $120 \text{ }^\circ\text{C}$ in a home-made convection oven, while the sample was removed from the oven after 3, 5, 7, and 10 min of drying and the film was depth-profiled to trace the evolution of the solvent concentration. The samples were sufficiently solidified to get a clear Raman spectrum even at shortest drying time, 3 min, and a considerable amount of residual solvent remained inside the film even at the longest drying time, 10 min. The thickness of the dried PAA film after 10 min was measured to be about $13 \text{ }\mu\text{m}$ and $42 \text{ }\mu\text{m}$, respectively.

Four samples of PAA films with two different film thicknesses were prepared by drying the PAA solution at $120 \text{ }^\circ\text{C}$ for 10 min. They were cured one by one in a heating chamber attached to a rheometer (RMS 800, Rheometrics) by elevating the

temperature from 120 °C to the final temperatures of 150 °C, 170 °C, 200 °C, and 350 °C at the rate of 5 °C/min. For each experiment, depth-wise DOI was measured by taking out of the sample from the heating chamber when it reached the final temperature.

For Chapter 4.2

PAA preparation

3,3',4,4'-biphenyltetracarboxylic acid (s-BPDA, 99.5% purity) purchased from Mitsubishi Chemical Co. Ltd. was used as dianhydride and p-phenylene diamine (PDA, 99.9% purity) purchased from DuPont was used as diamine to make a PAA solution. The solid concentration of the solution was 12 % in dimethylacetamide (DMAc, Sigma-Aldrich). The PAA solution was synthesized through the following steps. 5.50 g of PDA (0.019 mol) was put in a glass flask containing 55.1 g of DMAc and was stirred at 25 °C for 30 minutes to completely dissolve PDA. 2.01 g of s-BPDA (0.019 mol) was added into the PDA solution and mixed at 25 °C by an overhead mixer for more than 24 hours to make a viscous PAA solution. The viscosity of the PAA solution was measured about 18 Pa·s at the shear rate 1 s^{-1} . The chemical compositions of the PAA and its corresponding PI are given in Figure 3.1.

Drying and curing procedures

The coated PAA solution was imidized by three different drying and curing protocols in order to see the effect of thermal history on the final microstructure of PI

film. The thermal and temporal conditions for each protocol are shown in Table 3.1, and the temperature change according to the process time is shown in Figure 3.3. Here, the drying process is characterized by the pre-baking step that evaporates considerable amounts of solvent at the constant temperature, and the curing process by the main imidization step in which the temperature increases up to 350 °C at the constant rate. Drying was conducted at three different temperatures, 120, 140, and 160 °C in a home-made oven in which the temperature and flow rate of the supplying hot air were controlled. The drying times were decided 20, 8, and 4 minutes respectively to keep the amount of solvent remaining in the film after the drying process to be similar between the different protocols. The variation of the residual solvent contents and DOI during the drying process was measured by taking out the sample from the oven when it reached specific sampling times shown in Table 3.1. Each measurement took about 15 minutes; a period of time short enough to ignore the solvent evaporation or diffusion in the film during the measurement as the solvent concentration was sufficiently low.

Curing was conducted in a heating chamber attached to the rheometer (RMS 800, Rheometrics). The starting temperature of curing was the same as the drying temperature and was elevated to 350 °C at the rate of 10 °C/min to achieve a full imidization of PI. The same measurements were performed during the curing process by detecting the residual solvent concentration and DOI when the sample reached specific temperatures. Sampling temperatures are also shown in Table 3.1.

Protocol	Drying Condition	Sampling Time	Curing Condition	Sampling Temperature
A	120°C, 20 min	5, 10, 20 min	120°C → 350°C, 10°C/min	160, 180, 200, 350°C
B	140°C, 8 min	4, 6, 8 min	140°C → 350°C, 10°C/min	170, 200, 250, 350°C
C	160°C, 5 min	3, 4, 5 min	160°C → 350°C, 10°C/min	170, 200, 250, 350°C

Table 3.1. Drying and curing conditions for the different protocols. Sampling time indicates the measurement time during drying and sampling temperature indicates the measurement temperature during curing.

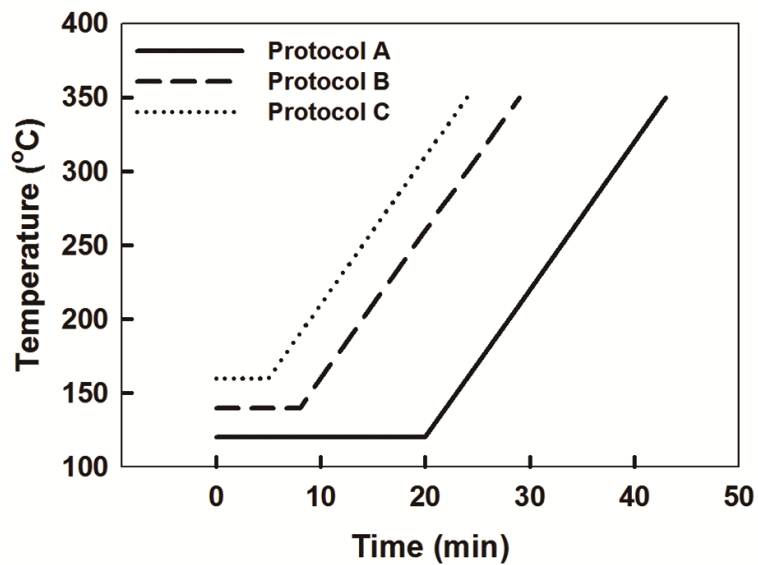


Figure 3.3. Thermal histories for the different drying and curing protocols. The drying process is characterized by constant temperature and the curing is characterized by constant rate of elevating temperature.

For Chapter 4.3.

Sample preparation

Two PAA solutions were made using 3,3',4,4'-biphenyltetracarboxylic acid (s-BPDA, Ube industries) as a dianhydride and two kinds of diamine, 1,4-phenylene diamine (PDA, DuPont) and 4,4'-oxydianiline (ODA, Wakayama). Dimethylacetamide (DMAc, Sigma-Aldrich) was used as a solvent and the solid concentration of PAA solutions was set to 12 wt%. First, 2.38 g (1.000 mol) of PDA was totally dissolved in 65.1 g of DMAc by mixing for 30 minutes at 25 °C. Additional mixing was done for 24 hours after 6.5 g (1.005 mol) of BPDA was added to the solution and PAA-1 composed of BPDA-PDA was prepared. The viscosity of the solution was about 30 Pa·s at the shear rate of 1 s^{-1} . In the same way, 3.56 g (1.000 mol) of ODA and 5.33 g (1.017 mol) of BPDA were mixed in DMAc to make PAA-2 composed of BPDA-ODA. The viscosity was about 28 Pa·s. Molecular structures of the PAA pairs and their corresponding PIs are shown in Figure 3.4.

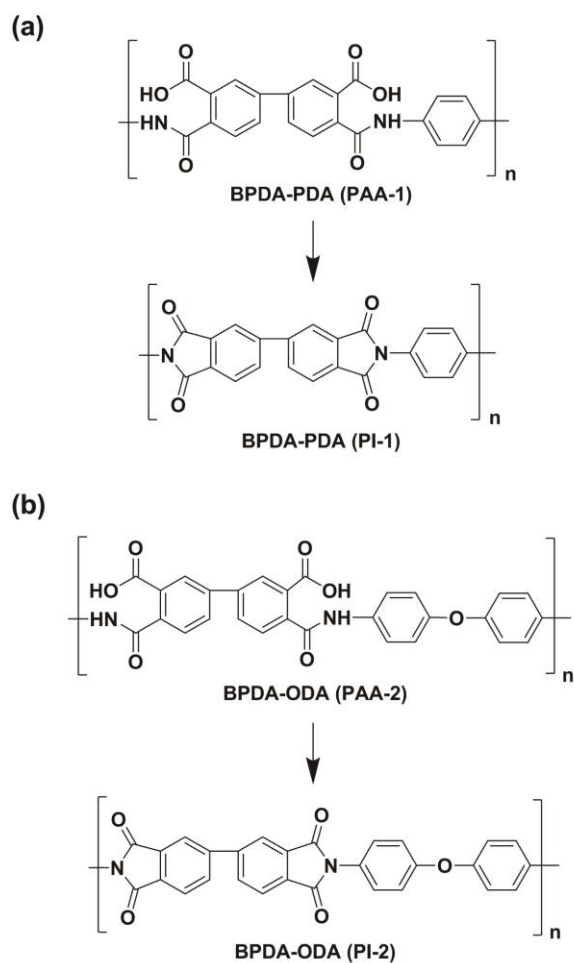


Figure 3.4. Molecular structures of PAAs and the corresponding PIs composed of BPDA-PDA (bottom layer) and BPDA-ODA (top layer). PAA is converted to PI by a dehydration cyclization called imidization reaction.

Drying and curing procedures

Bilayer PI films were constructed starting from the two PAA solutions through the DML and LBL methods as shown in Figure 3.5. For DML drying, PAA-1 and PAA-2 were continuously coated on a clean glass substrate using a micrometer-adjustable film applicator and dried in a convection oven at 100 °C for 10 minutes to get a solidified film. To apply the LBL method, PAA-1 was coated on three different glass substrates and dried at 100, 130, and 160 °C respectively for 5 minutes. The drying temperature of PAA-1, the bottom layer, was denoted as T_b . PAA-2 was then coated on the dried PAA-1 layer and they were dried at 100 °C for another 5 minutes to make three different dried films. Total drying time of the bottom layer was maintained at 10 minutes, same for all the samples regardless of the drying method. The dried PAA films were cured in a heating chamber attached to a rheometer (RMS 800, Rheometrics) by heating from 100 °C to 350 °C at the rate of 10 °C/min. After cooling to room temperature, four different bilayer PI films composed of PI-1 and PI-2 layer with 20 μm thick each were finally obtained.

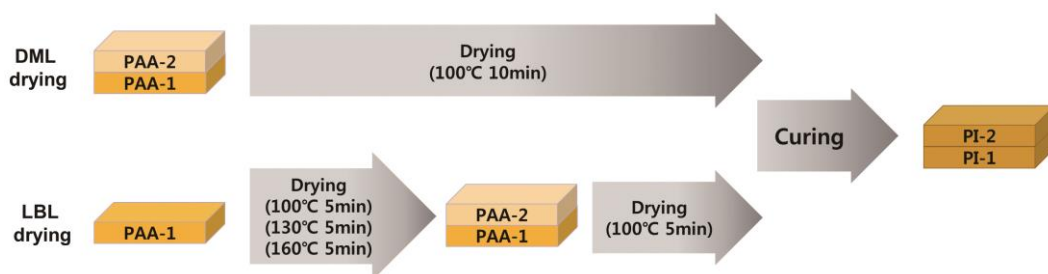


Figure 3.5. Design scheme for manufacturing four different bilayer polyimide films.

3.2. Measurement of residual solvent concentration and the degree of imidization (DOI)

For Chapter 4.1

Measurement of residual solvent concentration in dried PAA films

Confocal Raman spectrometer (LabRAM HR800, Horiba Jobin Yvon) was used to measure the distribution of residual solvent in the dried PAA films. The spectrometer was equipped with an LN₂ cooled charge coupled device (CCD) detector, a holographic grating (1800 grooves/mm), and a Raman holographic edge filter. 632.8 nm line of He-Ne laser was used as an excitation source. Each data acquisition comprised three seconds of exposure time and five times of data accumulation in order to get a sufficient level of signal to noise (S/N) ratio.

Depth profiling of the residual solvent took about 10 minutes for each sample, during which the variation of the sample weight due to solvent evaporation was assured to be less than 3 % of the total film weight. A depth profile of dried PAA film was obtained by moving the focus of the microscope from the film surface to the bottom at intervals of 3 μm or 4 μm, and a depth resolution of 3 μm was secured by using x100 lens for each measurement.

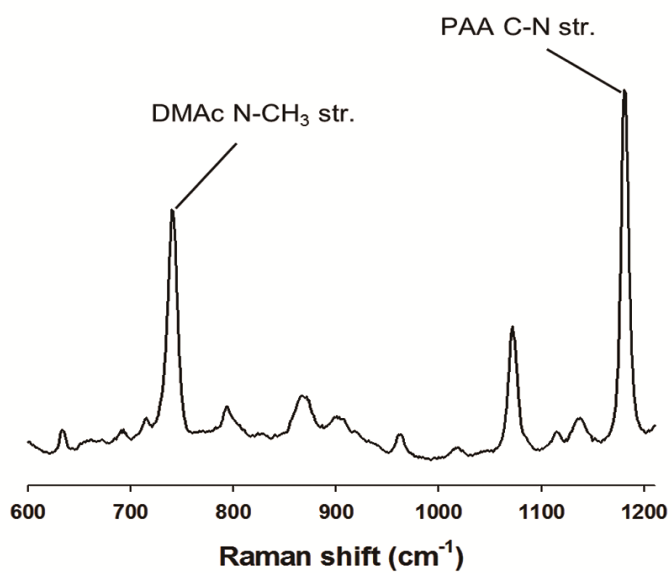


Figure 3.6. Raman spectrum of PAA solution in the spectral range of 600-1200 cm^{-1} . The peaks at 745 cm^{-1} and 1180 cm^{-1} indicate the N-CH₃ stretching mode of DMAc and the C-N stretching mode of PAA, respectively.

Measurement of the degree of imidization (DOI)

Confocal Raman spectroscopy was also used to measure DOI in the thickness direction when the dried PAA was cured. First, we compared the Raman spectra of non-imidized PAA, partially imidized PAA-PI, and fully imidized PI that was made by curing the film at 400 °C for 30 min (Figure 3.7). In Figure 3.7, the peak at 1180 cm^{-1} (i.e., the C-X stretching mode of C_6H_2 ring) disappeared as PAA was imidized, while the peak at 1108 cm^{-1} (i.e., the C-N-C transverse stretching mode) became more distinct. This proves that the peaks at 1180 cm^{-1} and 1108 cm^{-1} can be used as characteristic peaks of PAA and PI, respectively, when measuring the relative extent of imidization. Using the ratio of two characteristic peaks, the DOI was defined by

$$\text{DOI} = \frac{I(\text{PI})}{I(\text{PAA})+I(\text{PI})} = \frac{I(1108 \text{ cm}^{-1})}{I(1180 \text{ cm}^{-1})+I(1108 \text{ cm}^{-1})} \quad (3.2)$$

where I is the intensity of the characteristic Raman peaks. In Equation 3.2, the DOI becomes zero when there exists only PAA, and it becomes one when all the PAA is converted to PI.

Similar to the measurement of residual solvent, the depth profiling of each sample was conducted by moving the focus of the microscope from surface to bottom at intervals of 3 μm .

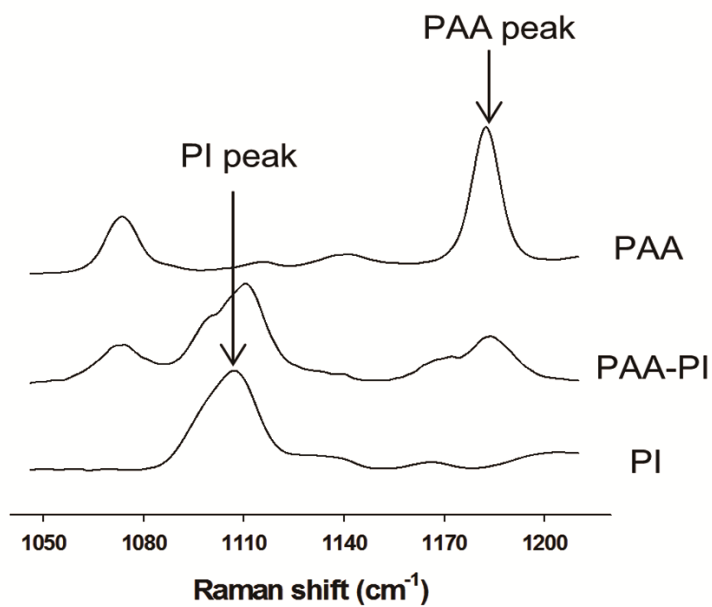


Figure 3.7. Raman spectra of PAA, partially cured PAA-PI and fully cured PI in the spectral range of 1040 -1220 cm⁻¹. The peaks at 1108 cm⁻¹ and 1180 cm⁻¹ indicate the C-N-C stretching mode of PI and the C₆H₂ stretching mode of PAA, respectively.

For Chapter 4.2

Measurements of residual solvent and degree of imidization (DOI)

The residual solvent concentration and DOI were measured when the PAA was imidized during the drying and curing processes using confocal Raman spectrometer. (LabRAM, Horiba Jobin Yvon) The exposure time to the laser was set to 3 seconds, and 5 scans per spectrum were averaged to obtain an adequate signal to noise ratio. A calibration experiment was first conducted to get the relationship between Raman intensity and solvent concentration in PAA solutions. The peak at 742 cm^{-1} (i.e., N-CH₃ stretching mode) was used as a characteristic peak of DMAc and the peak at 1608 cm^{-1} (i.e., aromatic ring stretching mode) as a characteristic peak of PAA. (Figure 3.8) The reason that the peak at 1608 cm^{-1} , instead of 1180 cm^{-1} , is used as a characteristic peak of PAA is that the peak is not affected by the imidization reaction, thus it can be used as characteristic peak of PAA not only during drying but also the curing process. The proportional constant in Equation 3.1 obtained from this Raman calibration experiment was about 3.57. A depth-wise profile was obtained by moving the laser focus stepwise ($3\text{ }\mu\text{m}$ or $4\text{ }\mu\text{m}$ intervals) from the film surface to the bottom. The depth resolution of the measurement was about $3\text{ }\mu\text{m}$ when using the x100 objective lens.

The same instrument was used to measure the DOI in the film depth direction. Also using the ratio of two characteristic peaks, 1180 cm^{-1} (i.e., C-X stretching mode of C₆H₂) could be used as the characteristic peak of PAA, and the peak at 1108 cm^{-1} (i.e., C-N-C transverse stretching mode), the DOI was measured. Again, a depth-wise

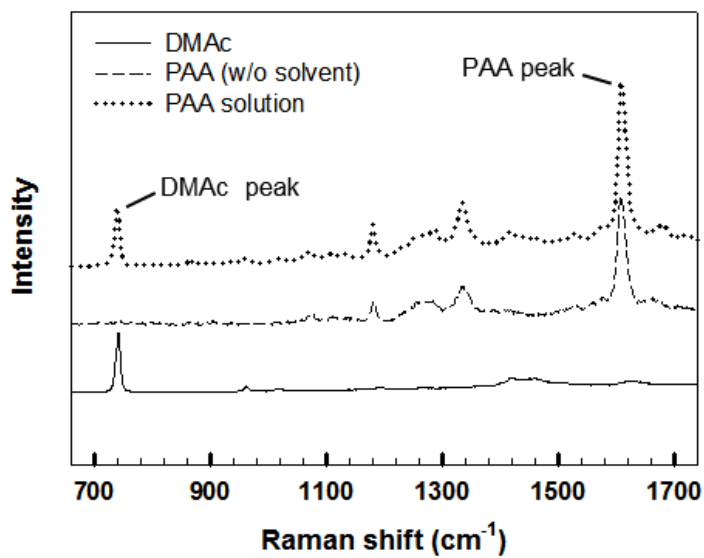


Figure 3.8. Raman spectra of the PAA solution. The peak at 742 cm^{-1} corresponds to the DMAC activated by N-CH₃ stretching, and 1608 cm^{-1} corresponds to the PAA activated by aromatic ring stretching.

profile of each sample was obtained by moving the laser focus by 3 μm interval from the surface to the bottom.

3.3. Measurement of chain orientation of polyimide

Chain orientation of extended polyimide film

Polarized Raman spectroscopy was used to analyze the chain orientation of PI. The polarized direction of the incident laser was controlled by installing the rotating half wave plate on the confocal Raman spectrometer, and an additional analyzer was equipped before the CCD detector to determine the polarization direction of diffracted lights from the sample.

Before measuring the degree of depth-wise chain orientation, the availability of polarized Raman spectroscopy was confirmed by checking the existence of a stretching mode in the BPDA-PDA PI chain which vibrates parallel to the chain axis. First, PAA film dried at 120 $^{\circ}\text{C}$ for 5 min was biaxially extended using UTM (3300 series, Instron) and cured from 120 $^{\circ}\text{C}$ to 350 $^{\circ}\text{C}$ at the rate of 5 $^{\circ}\text{C}/\text{min}$. The elongation ratio of the film was measured as 50 %. The cured PI film was fixed on a rotatable stage of the Raman microscope, and the polarization of incident laser was set parallel to the direction of film extension, which was defined as 0 $^{\circ}$. Then, the film was rotated by an angle of 15 $^{\circ}$ and the variation of the Raman spectrum was observed. If there is a stretching mode in PI molecules that vibrates parallel to the chain axis, the Raman intensity of the peak will be maximum at 0 $^{\circ}$ and minimum at 90 $^{\circ}$, and this mode can be used to quantify the orientation of the PI chains.

Depth-wise measurement of polyimide chain orientation

To obtain the information on depth-wise degree of chain orientation, the cross-section of the PI film was analyzed using polarized Raman spectroscopy. The finally cured PI film was stripped off the glass substrate and cut using a focused ion beam (Helios650, FEI) to get a sharp cross-section. The PI film was separated from the substrate at this stage in order to remove the alteration of the Raman intensity influenced by residual stress at the film interface [20] which could be generated by the CTE difference between PI and the glass substrate during the cooling process. In addition, the intensity of the Raman spectrum could be subtly affected by defects generated during the ion beam milling. It is therefore necessary to inspect the condition of the cross-section before the measurement. As the confocal microscope (OLS3000, Olympus) image shows in Figure 3.9(a), the grain was developed on the cross-section of both films along the film thickness direction (i.e., the z-axis). At the same time, the difference of height in the y-axis between the two sides that face the substrate and the air was observed in Figure 3.9(b). Hereafter, the sides of the film facing the substrate and facing the air are referred to as ‘substrate side’ and ‘air side,’ respectively. The difference in height mainly arises from the accumulated contact of ion beams with the film at the incident side during the milling process, and this effect becomes more pronounced for the thicker film. The difference in height measured from the 3D image of the 30 μm thick PI film was about 4 μm as shown in Figure 3.9(b), which is much larger than the scale of grain roughness. Considering the surface roughness, every measurement of polarized Raman spectroscopy on the film cross-section was conducted by locating the focus of the Raman microscope at a depth of 10 μm from the surface of the cross-section to exclude the effect of possible surface defect.

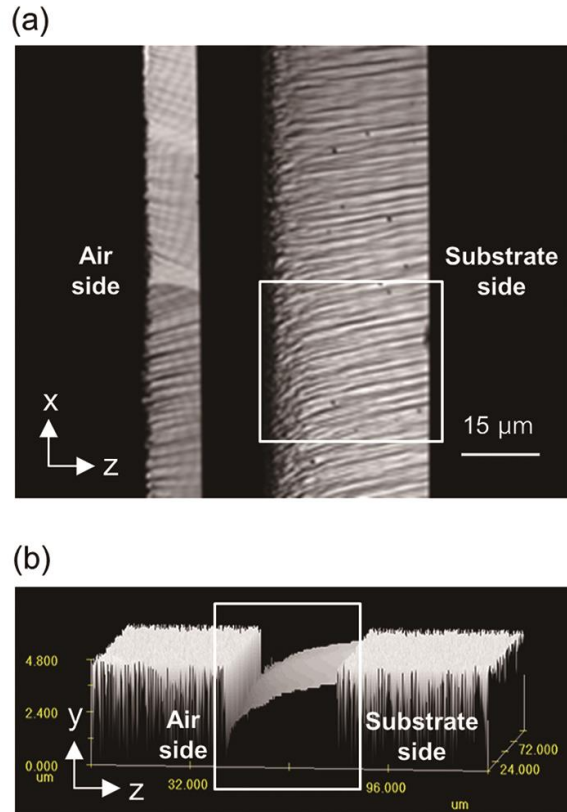


Figure 3.9. Confocal microscopic image of the PI cross-section and its contour: (a) 10 μm thick PI (left) and 30 μm thick PI (right), and (b) 3D image of white rectangle designated in (a).

In order to quantify the depth-wise degree of in-plane (i.e. x-direction in Figure 3.10(a)) chain orientation, two Raman intensity components, I_{xx} and I_{zz} , were measured on a film cross-section using polarized Raman spectroscopy in depth direction (i.e. z-direction in Figure 3.10(a)). The ratio of two components is so-called Raman anisotropy [63] which is analogous to the dichroic ratio in polarized IR measurement. This Raman anisotropy is used to obtain the Fraser distribution function [69], f , which is a fraction of perfectly oriented molecules in the direction of the x-axis. The detailed procedure for the analysis is as follows. An incident laser beam polarized in the x-axis is imposed on a point of interest and the Raman intensity of diffracted lights polarized in the same direction is detected, which becomes I_{xx} (Figure 3.10(a)). Again, a laser beam polarized in the z-axis is imposed and detected to get I_{zz} at the same point (Figure 3.10(b)). The Fraser distribution function is obtained from the ratio of these two Raman intensities (i.e. Raman anisotropy). By mapping Raman anisotropy on the cross-section of the PI film, the Fraser distribution function from the air to the substrate side can be obtained. The spatial resolution of the measurement on the x-z plane was about 1 μm when using x100 lens.

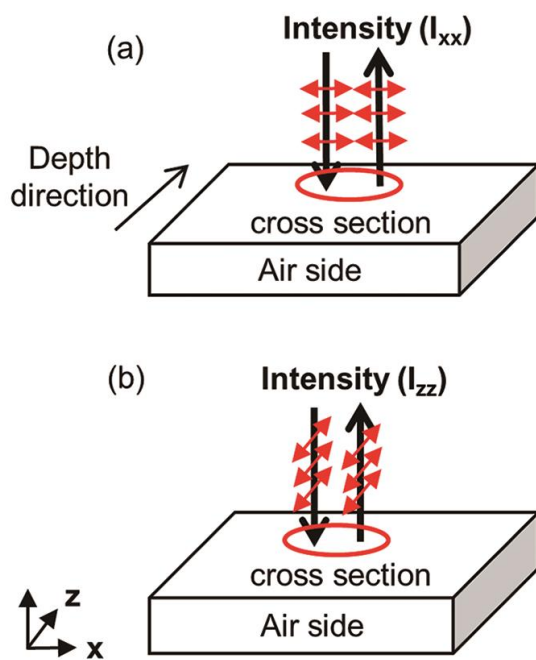


Figure 3.10. Schematic diagram of measuring depth-wise profile of PI chain orientation by detecting: (a) in-plane Raman intensity (I_{xx}), and (b) out-of-plane Raman intensity (I_{zz}).

3.4. Experiments of polyimide interdiffusion

3.4.1. Measurement of PAA-PAA interdiffusion

The prepared PAA solutions were diluted to make four different PAA-1 and 2 pairs having solvent concentrations of 88, 90, 91.5, and 93 wt% to see the effect of solvent content on the interdiffusion between PAA chains. The viscosities measured by a rheometer (DHR-3, TA instruments) were almost same between the PAA pairs that had the same solvent concentration as can be seen in Figure 3.11.

Confocal Raman spectrometer (LabRAM HR800, Horiba Jobin Yvon) was used to observe a compositional change of PAA at the interface where the two PAAs contact and interdiffuse. Raman spectra of PAA-1 and 2 are shown in Figure 3.12. In the figure, the peak at 1180 cm^{-1} was used as a characteristic peak of PAA-1 and 1160 cm^{-1} as that of PAA-2. By calibrating the Raman intensities with PAA compositions, the relationship between the volume fraction of PAA-2 and its peak intensity ratio was obtained as below.

$$\begin{aligned}\phi_{\text{PAA2}} &= \frac{w_{\text{PAA2}}}{w_{\text{PAA1}} + w_{\text{PAA2}}} \\ &= \alpha \times \frac{I_{\text{PAA2}}(1160\text{cm}^{-1})}{I_{\text{PAA1}}(1180\text{cm}^{-1}) + I_{\text{PAA2}}(1160\text{cm}^{-1})}\end{aligned}\quad (3.3)$$

Here, ϕ is the volume fraction, w is the weight, I is the intensity of Raman peak, and α is the proportional constant that was fitted to be 0.86 from the calibration

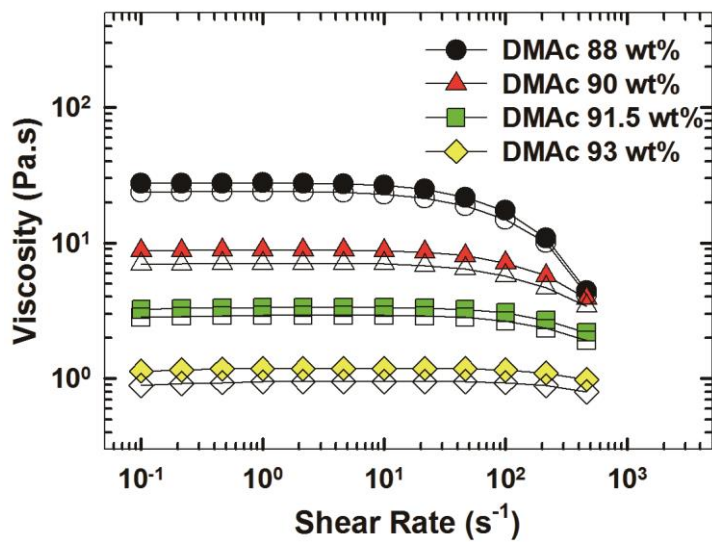


Figure 3.11. Rate dependent shear viscosities for PAA solutions having different solvent contents. Filled symbols represent PAA-1 (BPDA-PDA) and open symbols PAA-2 (BPDA-ODA).

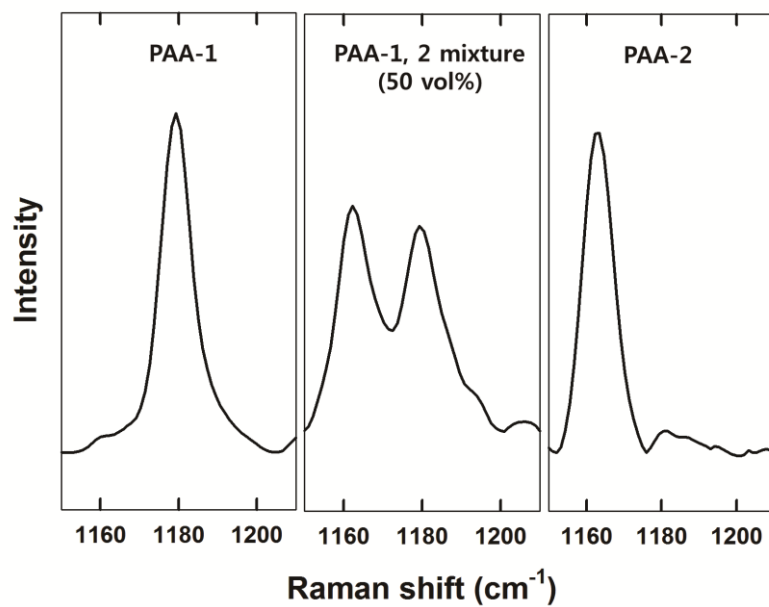


Figure 3.12. Raman spectra of PAA-1, PAA-2 and their 1:1 mixture.

result. The density and molecular weight of PAA-1 and 2 were assumed to be the same.

In order to observe the interdiffusion behavior between PAA-1 and 2, 50 μm -thick PAA-1 was coated on a 150 μm -thick cover glass using a film applicator, and it was placed on PAA-2 drop to make a bilayer structure as shown in Figure 3.13(a). The time when the two PAAs contact was set to 0 and the compositional change at the interface was measured by depth profiling the Raman spectrum from $z=0$ μm at the interval of 3 to 5 μm at different times, 10, 20, 30, and 40 min. All the Raman experiments were conducted at room temperature, and the x100 objective lens (numerical aperture, $\text{NA}=0.9$) equipped with 632.8 nm line of He-Ne laser was used. In this experiment, 1800 grooves/mm of a holographic grating was adopted and data acquisition comprised 3 s of laser exposure time and two times of repeated scan. A whole depth profiling time was about two minutes. The refractive index (n) of PAA solution was measured to be 1.47~1.49 by a prism coupler (Metricon 2010), which is similar to DMAc ($n_{\text{DMAc}}=1.44$). To match the refractive index, borosilicate ($n_{\text{glass}}=1.48$) was used as the cover glass and glycerol ($n_{\text{oil}}=1.47$) was used as the immersion oil.

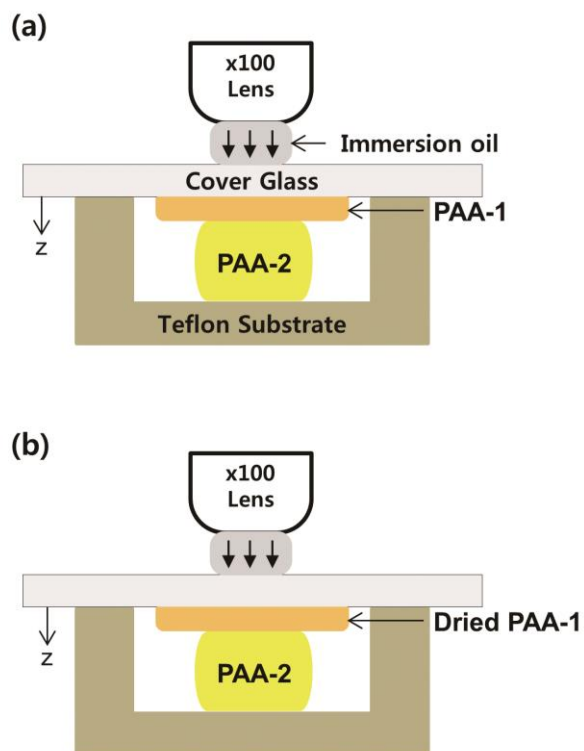


Figure 3.13. Schematic diagram for the Raman experiments of (a) PAA-1 and 2 interdiffusion, and (b) solvent diffusion into the dried PAA-1 film.

3.4.2. Measurement of solvent diffusion into dried PAA film

When a PI bilayer is made by LBL drying, the solvent in the top PAA-2 layer can diffuse down into the dried PAA-1. The diffusion of solvent can affect chain orientation of the cured PI as well as PAA interdiffusion, thus the extent of solvent diffusion according to the T_b was investigated. First, the PAA-1 was coated on a cover glass using a film applicator to make the wet thickness 330 μm and dried at three different temperatures, 100, 130, and 160 $^{\circ}\text{C}$ for 5 minutes. The film thickness was about 40 μm after drying, still containing more than 20 wt% of solvent in the film. After the dried PAA-1 made a contact with the PAA-2 solution (i.e. $t=0$ min) as shown in Fig 3.13(b), the solvent distribution in the film was depth profiled using the Raman spectroscopy from $z=0$ μm at the interval of 5 μm at different times, 1, 5, 10, and 15 min. Solvent content in a dried film or PAA solution was defined as previously :

$$X = \frac{w_{\text{solvent}}}{w_{\text{PAA}}} = \alpha' \times \frac{I_{\text{solvent}} (742 \text{ cm}^{-1})}{I_{\text{PAA}} (1608 \text{ cm}^{-1})} \quad (3.4)$$

where X is the solvent concentration, w the weight, I the intensity of Raman peak, and α' the proportional constant which was measured to be 10.9 by fitting the calibration result. 300 grooves/mm of holographic gratings was used, and a whole depth profiling took 20 s by applying 1 s of laser exposure and one scan at a time. The refractive index of dried PAAs (n_{PAA}) was ranged 1.75~1.80, and borosilicate ($n_{\text{glass}}=1.48$) and glycerol ($n_{\text{oil}}=1.47$) were also used as the cover glass and immersion oil respectively. Due to the mismatch of refractive index between the sample and immersing oil, about 24 μm of instrumental broadening can occur at $z=40$ μm , which corresponds to the depth of focus (DOF) as calculated in Equation. 3.5.

$$\text{DOF}(z) = z \times \left[\left\{ \frac{\text{NA}^2(n^2-1)}{(1-\text{NA}^2)} + n^2 \right\}^2 - n \right] \sim 24 \mu\text{m} \quad (z = 40\mu\text{m}) \quad (3.5)$$

In the equation, n means $n_{\text{PAA}}/n_{\text{oil}}$, the ratio of refractive indices.

3.4.3. Measurement of interdiffusion width of cured polyimide films

Bilayer PI films made by the DML and LBL methods were peeled off from the glass substrate and cut by cryo-ultramicrotome (PT/PC Ultramicrotome, Boeckeler Instruments) to measure the interdiffusion width. After the cross-section of the cut film was exposed to Raman spectrometer, the compositional change between PI-1 and 2 at the interface was detected by X-Z mapping method as shown in Figure 3.14(b). Here, the peak at 735 cm^{-1} was used as the characteristic peak of PI-1 and 695 cm^{-1} as that of PI-2. (Figure 3.14(a)) Volume fraction of PI-2 was measured in the same way with PAA-2 and the proportional constant α'' in Equation 3.6 was calibrated to be 0.71.

$$\phi_{\text{PI2}} = \frac{w_{\text{PI2}}}{w_{\text{PI1}} + w_{\text{PI2}}} = \alpha'' \times \frac{I_{\text{PI2}}(695\text{cm}^{-1})}{I_{\text{PI1,2}}(735\text{cm}^{-1}) + I_{\text{PI2}}(695\text{cm}^{-1})} \quad (3.6)$$

Each measurement in the Z axis in Figure 3.14(b) was spaced $0.3 \mu\text{m}$ apart and 1,800 grooves/mm of grating was used. The laser exposure time and scan times for every measurement were set 5 s and 5 times respectively to minimize the signal to noise (S/N) ratio of the spectrum.

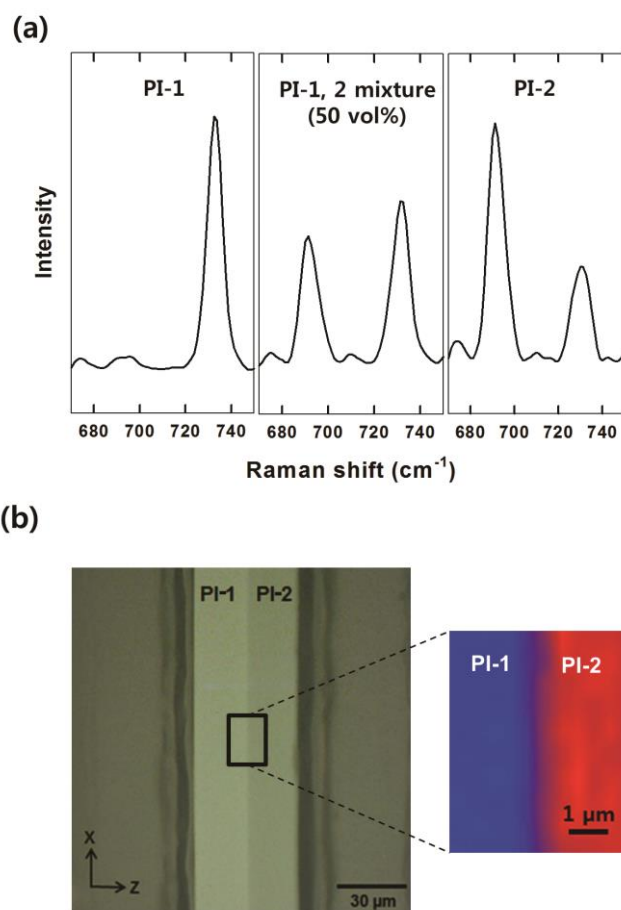


Figure 3.14. The measurement of interdiffusion width using X-Z mapping of Raman spectroscopy. (a) Raman spectra of PI-1, PI-2 and their 1:1 mixture. (b) Cross-sectional images of a PI bilayer captured by a microscope and its X-Z Raman mapping result. Blue and red colors in the mapping image are distinguished by different Raman peaks appeared at 735 and 695 cm^{-1} respectively.

3.5. Characterization of the cured polyimide film

3.5.1. X-ray diffraction pattern

Wide angle x-ray diffractometer (D8 ADVANCE with DAVINCI, Bruker) equipped with LYNXEYE XE detector was used for the characterization of molecular order and crystallinity of PI films. Wide angle X-ray diffraction (WAXD) patterns were collected in the reflection mode over $2\theta = 2^\circ \sim 40^\circ$. Scan step was 0.02° with the speed of 0.5 sec/step. The X-ray generator was run at 40kV, 40mA.

3.5.2. Glass transition temperature (T_g)

A dynamic mechanical thermal analyzer (SDTA861e, Mettler Toledo) was used to measure the loss factor ($\tan \delta$) as a function of temperature for the cured PI films. Specimens were prepared 5 mm in width and 40 mm in length. The measurement was conducted in oscillation mode, in which the displacement amplitude was set 10 μm at a frequency of 1 hz. The loss factor was obtained from 150 $^\circ\text{C}$ to 450 $^\circ\text{C}$, and T_g was measured by observing the temperature at which the peak of loss factor appeared.

3.5.3. Thermal expansion coefficient (TEC)

Thermal mechanical analysis (TMA) of PI films was conducted with a Hitachi DMA 7100 analyzer. The width of the specimen was 5 mm and length was 15 mm, and the tensile load during the experiment was set to 50 mN. The specimen was heated to 150 $^\circ\text{C}$ at the rate of 20 $^\circ\text{C}/\text{min}$ and was retained for 20 minutes to remove absorbed water in PI films. After cooling again to the room temperature, the changes in the film length were detected by heating the specimen to 250 $^\circ\text{C}$ at the rate of

5 °C/min. The average value of thermal expansion coefficient (TEC) between 100 °C and 200 °C was used as a representative value.

Chapter 4.

Results and discussion

4.1. Effect of film thickness on the polyimide chain orientation

4.1.1. Depth-wise residual solvent content of dried film

Drying induces chain alignment on the film plane in the presence of a substrate. [13, 14, 19, 23] This is due to the tensile stress developed on polymer chains by solvent evaporation during which the relaxation time of the polymer becomes larger than the time scale of volume shrinkage. This means that the degree of in-plane chain orientation can be predicted if the extent of volume shrinkage is known during the drying process. When a considerable amount of solvent remains in the film after drying as is the case with the PAA film, the amount of residual solvent can indicate how much polymer chains are well aligned to the in-plane direction. It also provides information on the degree of chain orientation in the film thickness direction when there is a depth-wise distribution of residual solvent profile.

Based on the calibration result, the depth-wise residual solvent profile was tracked for two PAA films of different thicknesses at different drying times (Figure 4.1). Hereafter, the thickness of these two films is referred to as '10 μm ' and '30 μm ' based on the thickness of the final cured PI film. The result in Figure 4.1 was confirmed to be reproducible by repeating the experiments three times. For 10 μm thick PI film in Figure 4.1(a), the residual solvent concentration of about 0.6 ($\text{g}_{\text{solvent}}/\text{g}_{\text{solid}}$) when dried for 3 min at 120 $^{\circ}\text{C}$ was reduced to 0.4 (g/g) after 10 min. The solvent concentration at both sides was evenly reduced to make a uniform profile of residual solvent along the film thickness. That is, a depth-wise homogeneous PAA film was obtained after drying when the film was thin. On the other hand, the 30 μm thick PI film exhibited a significant amount of solvent remaining in the film after the drying process compared

to the 10 μm film (Fig. 4.1(b)). The final residual solvent concentration after 10 min showed a significant difference between the two sides of about 0.8 (g/g) at the substrate side and 0.4 (g/g) at the air side, compared to a uniform value of around 1.1 (g/g) at 3 min of drying. This side-to-side difference of residual solvent concentration resulted from the hindered diffusion of solvent molecules for the thick film. [57, 86-88] The increased film thickness increased the time for the solvent molecules to reach the surface, and the diffusional resistance increased sharply at the film surface due to the low solvent concentration. Thus, the rate of solvent diffusion near the substrate was decreased and the solvent became trapped inside the film.

The aforementioned difference between the two PAA films could be related to the extent of chain alignment and its depth-wise uniformity. PAA chains composed of BPDA-PDA are known to have a fully extended structure in DMAc. [29] With less residual solvent remaining after drying, the stronger biaxial tensile stress is exerted and more polymer chains align to the in-plane direction by packing themselves closely with a well-ordered structure. Therefore, the 10 μm thick PI is expected to have a relatively high degree of in-plane orientation with a uniform distribution, while the 30 μm thick PI has an inhomogeneous and lower degree of in-plane orientation so that the chains are more randomly oriented at the substrate side than the air side. The effect of these differences on the imidization rate and the depth-wise chain orientation of the finally cured PI is investigated in the following sections.

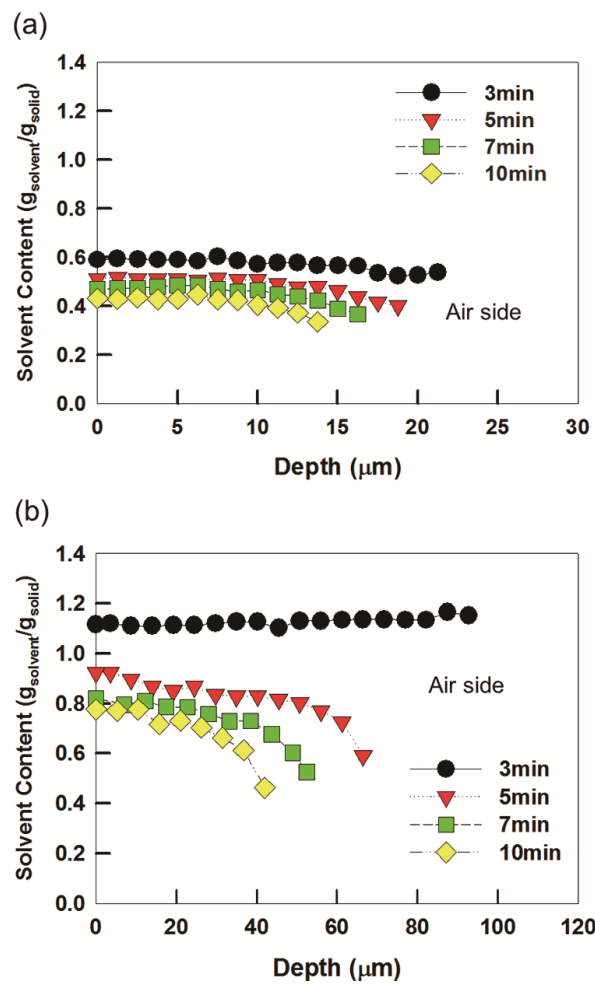


Figure 4.1. Depth-wise residual solvent profiles of the PAA film at different drying times for the film of thickness (a) 10 μm and (b) 30 μm .

4.1.2. Depth-wise imidization degree during curing

Imidization reaction starts at about 130 °C, after which PAA is converted to PI. [39] The rate of imidization or its starting temperature, however, depends on many factors such as the molecular structure of PAA, temperature profile, and affinity with solvent. In addition, imidization rate can also be accelerated when more solvents remain in the film because free solvent molecules around PAA chains can increase the mobility of carboxyl and amino groups. In a few studies, the role of the solvent in enhancing the imidization reaction was clearly established by using Raman and FTIR spectroscopy, but they could not provide depth-wise information, i.e., the difference in the rate of imidization according to the distribution of residual solvent in the depth direction. For this purpose, PAA films dried at 120 °C for 10 min were placed in a heating chamber and the temperature was raised from 120 °C to the following final temperatures: 150 °C, 170 °C, 200 °C, and 350 °C. The depth-wise DOI was measured when they reached the above temperatures and the results are shown in Figure 4.2. In the figure, the film depth shown in the x-axis was normalized by the total thickness of the film to focus on the depth-wise distribution of the extent of imidization. DOI in the y-axis was derived from Equation 4.1 using the two characteristic peaks of PAA and PI in Figure 3.7.

$$\begin{aligned} \text{DOI (\%)} &= \frac{I(\text{PI})}{I(\text{PAA})+I(\text{PI})} \times 100 \\ &= \frac{I(1108 \text{ cm}^{-1})}{I(1180 \text{ cm}^{-1})+I(1108 \text{ cm}^{-1})} \times 100 \end{aligned} \quad (4.1)$$

When PI was 10 μm thick, DOI was about 20 % at 150 $^{\circ}\text{C}$, 60 % at 170 $^{\circ}\text{C}$ and higher than 90 % at 200 $^{\circ}\text{C}$, which implies that most of the PAA was imidized to PI in the vicinity of 200 $^{\circ}\text{C}$. (Figure 4.2(a)) In addition, the distribution of DOI in the film thickness direction was uniform similar to the result of residual solvent profile for the thin PI film. On the other hand, a different result at the initial stage of curing was obtained for the 30 μm thick PI as can be seen in Figure 4.2(b). The DOI was already higher than 50% when the curing temperature reached 150 $^{\circ}\text{C}$, and DOI near the substrate side was 20% larger than the air side. This side-to-side difference of DOI decreased when the curing temperature was further increased to 170 $^{\circ}\text{C}$ and higher. Again, more than 90 % of the PAA chains were converted to PI when the temperature was 200 $^{\circ}\text{C}$ as in the case of the 10 μm thick PI. At the final curing temperature of 350 $^{\circ}\text{C}$, the 30 μm thick PI has 3~4 % higher DOI than the thin PI had.

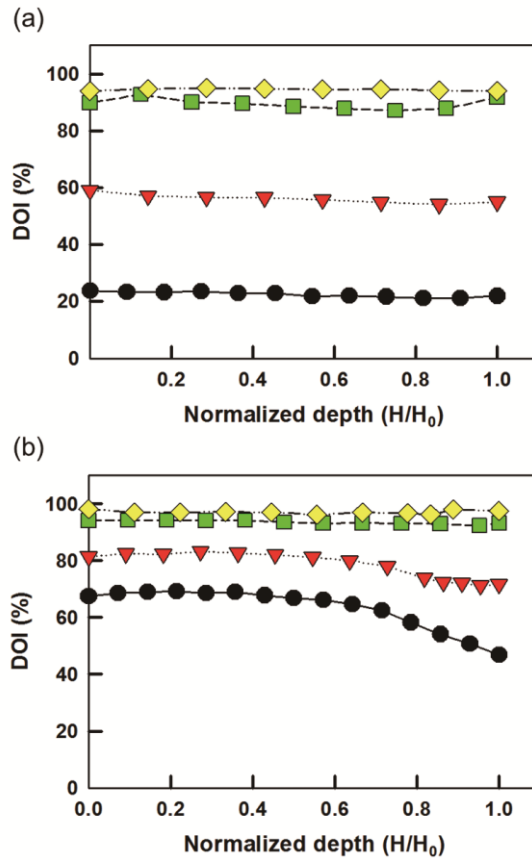


Figure 4.2. Depth-wise DOI profiles at different curing temperatures: (●) 150 °C; (▼) 170 °C; (■) 200 °C; and (◆) 350 °C, when the thickness of the final PI film is (a) 10 μm, and (b) 30 μm. The right side of the curve corresponds to the air side.

4.3.3. Depth-wise chain orientation after curing

In order to determine the vibration mode of PI molecules that vibrates parallel to the chain axis, the angular variation of the Raman spectrum was observed by rotating the extended PI film as explained in the experimental section. In the measured Raman spectrum, the Raman intensities originating from the benzene ring stretching mode which appears at 1610 cm^{-1} were plotted at different angles in Figure 4.3(a). The same measurement was conducted for a pristine PI and compared in Figure 4.3(b). The figure does not exhibit any significant variation of Raman intensity at different angles in the case of pristine PI, but the Raman intensity is maximized at 0° and minimized at 90° when the extended PI film is used. This result proves that the principal vibration axis of the benzene ring stretching mode is coincident with the PI chain axis and this can be used to analyze the chain orientation.

Using the vibration mode at 1610 cm^{-1} , a distribution function proposed by Fraser [63, 69] was used to quantify the degree of in-plane chain orientation. Fraction f , the so-called Fraser distribution function or Fraser fraction, is a value that represents the fraction of perfectly oriented molecules in an extended film and $(1-f)$ is the fraction of randomly oriented molecules. Liem et al. reported that the Fraser distribution function can be expressed by a simple relationship with the measurable Raman intensity ratio, i.e., Raman anisotropy, when a polymer chain has a highly uniaxial Raman tensor and its principal axis is parallel to the chain axis. [63] In their study, if the chains were aligned to the x-axis and their perpendicular direction was fixed to the z-axis, I_{xx} which is diffracted by perfectly oriented polymer chains to the x-axis is expressed by :

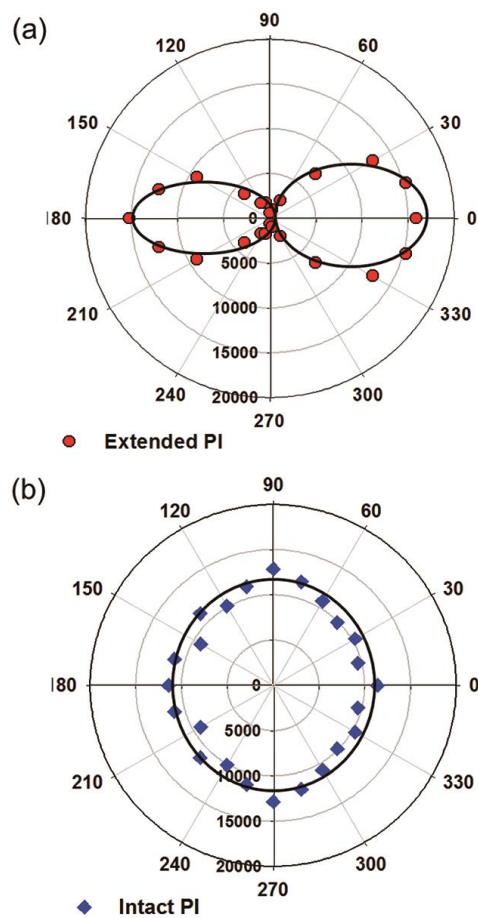


Figure 4.3. Polar plots of Raman intensities for the (a) uniaxially extended PI film, and (b) intact PI film.

$$I_{xx}(\text{perfect}) = f\alpha_{xx}^2 \quad (4.2)$$

where I is the Raman intensity, α_{ij} the component of Raman tensor and the two subscripts mean the polarizing direction of incident laser and diffracted light, respectively. The Raman intensity diffracted from the fraction of randomly oriented molecules (1-f) can be determined by the following equations:

$$I_{xx}(\text{random}) = I_{zz}(\text{random}) = \frac{1}{45}(1-f)(45\check{\alpha}^2 + 4\gamma^2 - 5\delta^2)$$

$$\check{\alpha}^2 = \frac{1}{9}(\alpha_{xx} + \alpha_{yy} + \alpha_{zz})$$

$$\begin{aligned} \gamma^2 = \frac{1}{2} [& (\alpha_{xx} - \alpha_{yy})^2 + (\alpha_{yy} - \alpha_{zz})^2 + (\alpha_{zz} - \alpha_{xx})^2 \\ & + 3(\alpha_{xy}^2 + \alpha_{yx}^2 + \alpha_{yz}^2 + \alpha_{zy}^2 + \alpha_{zx}^2 + \alpha_{xz}^2) + \delta^2] \end{aligned}$$

$$\delta^2 = (\alpha_{xy} - \alpha_{yx})^2 + (\alpha_{yz} - \alpha_{zy})^2 + (\alpha_{zx} - \alpha_{xz})^2 \quad (4.3)$$

In the equation, $\check{\alpha}^2$, γ^2 , and δ^2 correspond to the isotropic, anisotropic and asymmetric invariants of the Raman tensor. It simplifies to $I_{xx}(\text{random})=I_{zz}(\text{random})=1/5\alpha_{xx}$ because every component of the Raman tensor is assumed to be 0 except for α_{xx} when the molecular vibration with highly uniaxial Raman tensor is considered. Thus, the Raman anisotropy which is the ratio of I_{xx} measured by in-plane polarization and I_{zz} measured by out-of-plane polarization can be simply related with Fraser distribution function as follows:

$$R = \frac{I_{xx}}{I_{zz}} = \frac{I_{xx}(perf) + I_{zz}(rand)}{I_{xx}(rand)} = \frac{1+4f}{1-f}$$

$$f = \frac{R-1}{R+4} \quad (4.4)$$

In this paper, the depth-wise orientation of PI chain was analyzed by measuring the Fraser distribution function on a cross-section of the film along the depth direction. The polarized Raman spectra of the in-plane polarization and out-of-plane polarization for two PIs with different thicknesses are shown in Figures 4.4(a) and (b). The Raman intensity measured by in-plane polarization (I_{xx}) is stronger than that of out-of-plane polarization (I_{zz}), which coincides well with the fact that the polymer chains in a solvent-cast film typically align to the in-plane direction. Using the 1610 cm^{-1} peak assigned to the benzene ring stretching mode which meets the required condition of polarized Raman analysis, the Raman anisotropy, R (I_{xx}/I_{zz}), is mapped throughout the area of interest for two different PIs as shown in Figures 4.4(c) and (d). In the figure, the PI cross-section is shown in red color with the x-axis designating the in-plane direction and the z-axis the film thickness direction. The brightness of the red color corresponds to the value of Raman anisotropy and hence reveals the absence of any notable Raman anisotropy along the longitudinal direction (i.e., the x-axis) for both films, and the distribution is observed only along the depth direction (i.e., the z-axis) for the 30 μm thick PI as shown in Figure 4.4(d). In the case of the 30 μm thick PI, the brightness of the red color is changed when it comes from the air side to the substrate side, and the color near the substrate side is darker than that of the 10 μm thick PI film.

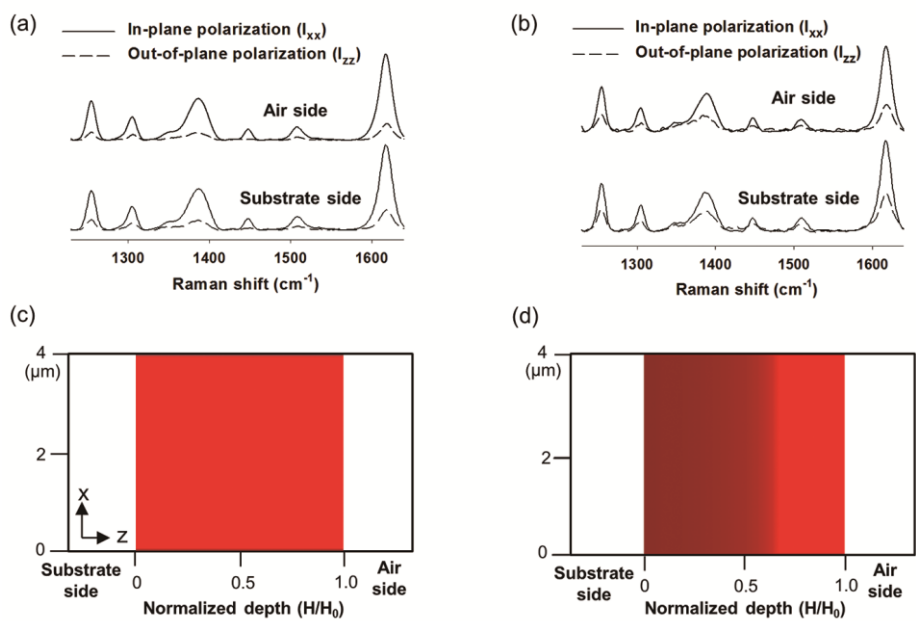


Figure 4.4. In-plane and out-of-plane polarized Raman spectra measured at both air and substrate side of (a) PI 10 μm , (b) PI 30 μm , and mapping image of Raman anisotropy(I_{xx}/I_{zz}) of (c) PI 10 μm , (d) PI 30 μm . x-axis is longitudinal direction of film in picture (c) and (d).

With the measured Raman anisotropy, the Fraser distribution function, f , is plotted along the film depth in Figure 4.5(a). As the orientation function, f , is proportional to Raman anisotropy, it shows similar results to those of the Raman mapping data. In Figure 4.5(a), the value of f is about 0.46 for the 10 μm thick PI and its depth-wise distribution is uniform, whereas the 30 μm thick PI exhibits an inhomogeneous distribution with f value of about 0.19 at the substrate side and about 0.35 at the air side. This indicates that overall degree of in-plane orientation decreases as the film thickness increases, especially near the substrate than near the air side, resulting in depth-wise inhomogeneity. This result explains the curling of the PI film when it is detached from the glass substrate as remarked by Nomura and Asano. [19, 20] During the experiment no curling was observed when the 10 μm thick PI was detached from the substrate, whereas the film was curved for the 30 μm thick PI. This curling originates from the side-to-side difference of CTE which is inversely proportional to the degree of in-plane orientation of PI in general. Therefore, the 30 μm thick PI film has higher CTE at the substrate side than at the air side, which makes the film shrink more at the substrate side during the cooling process after curing. The curling originating from the side-to-side difference of chain orientation is not revealed under the constraint of a substrate, and it appears when the film is separated from the substrate.

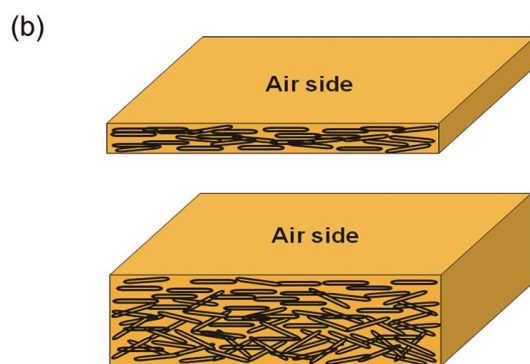
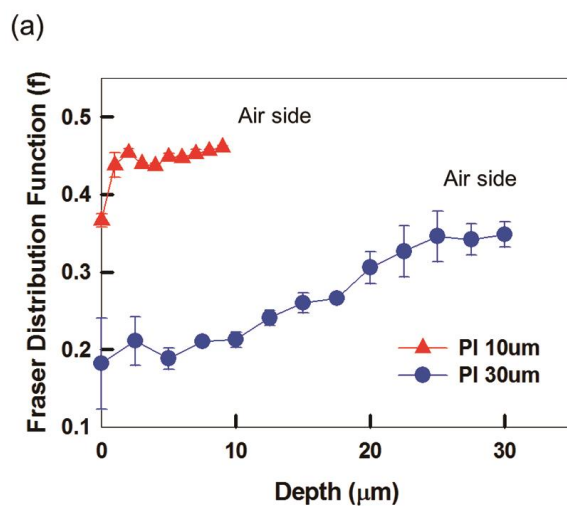


Figure 4.5. (a) Depth-wise Fraser fraction (f) profile of two different PI films, and (b) schematic diagram of depth-wise chain orientation.

The measured depth-wise distribution of the PI orientation is analogous to the estimated distribution of PAA chain orientation after drying. As aforementioned, more solvent remains after drying for thick PI, especially near the substrate side, which means that the biaxial tensile stress due to solvent evaporation is developed less on PAA chains. In other words, the degree of in-plane orientation of PAA chains near the substrate side is lower than that near the air side in the dried film. As curing progresses, more solvent inside the thick film accelerates the imidization rate, and the relatively flexible PAA chains can be changed more rapidly to stiff PIs that can no longer easily form a highly ordered structure. Therefore, even though the tensile stress is additionally generated through the subsequent solvent evaporation during the curing process, the depth-wise chain orientation of the cured PI can hardly deviate from that of the dried PAA.

4.2. Effect of thermal history on the polyimide chain orientation

4.2.1. Residual solvent and imidization degree during drying

In general, biaxial tensile stress is exerted on the polymeric film when a polymer solution is dried under the constraint of a substrate. [13, 14, 19] A polymeric chain backbone that is randomly oriented in a large amount of solvent at the initial state becomes aligned in the plane of the film during solvent evaporation due to this biaxial stress. This means that the amount of evaporated solvent or remaining solvent during the drying process can reflect the extent of in-plane orientation of polymer chains. In addition, the rigidity of polymer chain affects the degree of in-plane chain orientation after drying as it influences the packing ability of polymer chains when the film is densified by solvent evaporation.

The rigidity of the polymer chain increases when the PAA composed of BPDA-PDA is converted to PI as evidenced by an increase of the Kuhn length from 43 Å to 78 Å . [27] As the PI manufacturing process involves both solvent evaporation and increase in chain rigidity, it is necessary to examine the variation of the amount of solvent evaporation and the imidization degree at the same time during the drying and curing processes in order to predict the final microstructure of PI. For this purpose, the residual solvent concentration and DOI was measured during the drying process first. (Figure 4.6)

In figure 4.6, the residual solvent concentration decreases and DOI increases as drying proceeds. According to the depth profile, the solvent concentration is lower near the air side regardless of drying temperature. It was reported that the side-to-side

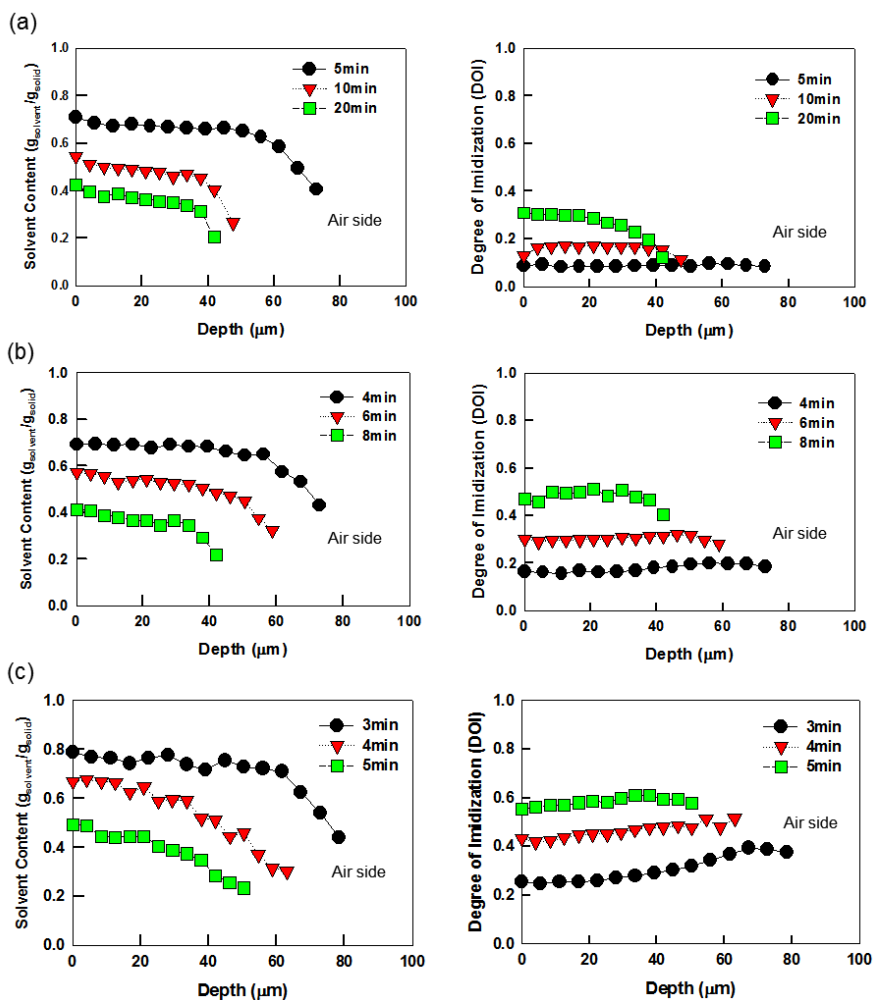


Figure 4.6. Depth-wise residual solvent contents (Left) and DOI (Right) during the drying process through (a) protocol A (120 °C drying), (b) protocol B (140 °C drying), and (c) protocol C (160 °C drying).

difference of residual solvent content was enhanced when the film thickness increased. This is attributed to the increased diffusional resistance of solvent with the increase of film thickness, while the solvent evaporation rate at the film surface remains the same. [46] Different drying temperature, on the other hand, does not affect depth-wise inhomogeneity because higher temperature increases the evaporation rate at the film surface as well as the diffusion rate of solvent in the bulk. So, changing the temperature has little effect on the distribution of residual solvent concentration in the film depth direction during the drying process.

In contrast to the residual solvent concentration, the rate of imidization and its distribution along the film thickness show significant differences. (Figure 4.6) The DOI at the final state of drying is about 0.3, 0.5, and 0.6 when drying temperatures are 120 °C, 140 °C and 160 °C, respectively. The DOI increases with drying temperature even though the amount of residual solvent is almost the same at the final state. This suggests that an increment in imidization rate exceeds the rate of solvent evaporation when the drying temperature increases. The DOI at the air side is found to be lower than the substrate side after 20 min of drying when the drying temperature is 120 °C. (Figure 4.6(a)) It is because the solvent can act as a plasticizer that promotes the imidization reaction. [28, 47] Because the solvent concentration is higher near the substrate during the drying process, imidization occurs faster closer to the substrate. When the drying temperature increases to 140 °C and 160 °C, the side-to-side difference of DOI becomes smaller at the final state even though there still exists a depth-wise inhomogeneous distribution in residual solvent concentration. (Figures 4.6(b), (c)) This can be ascribed to the role of high thermal energy which provides sufficient mobility to the PAA chains, diminishing the capacity of the solvent to act as

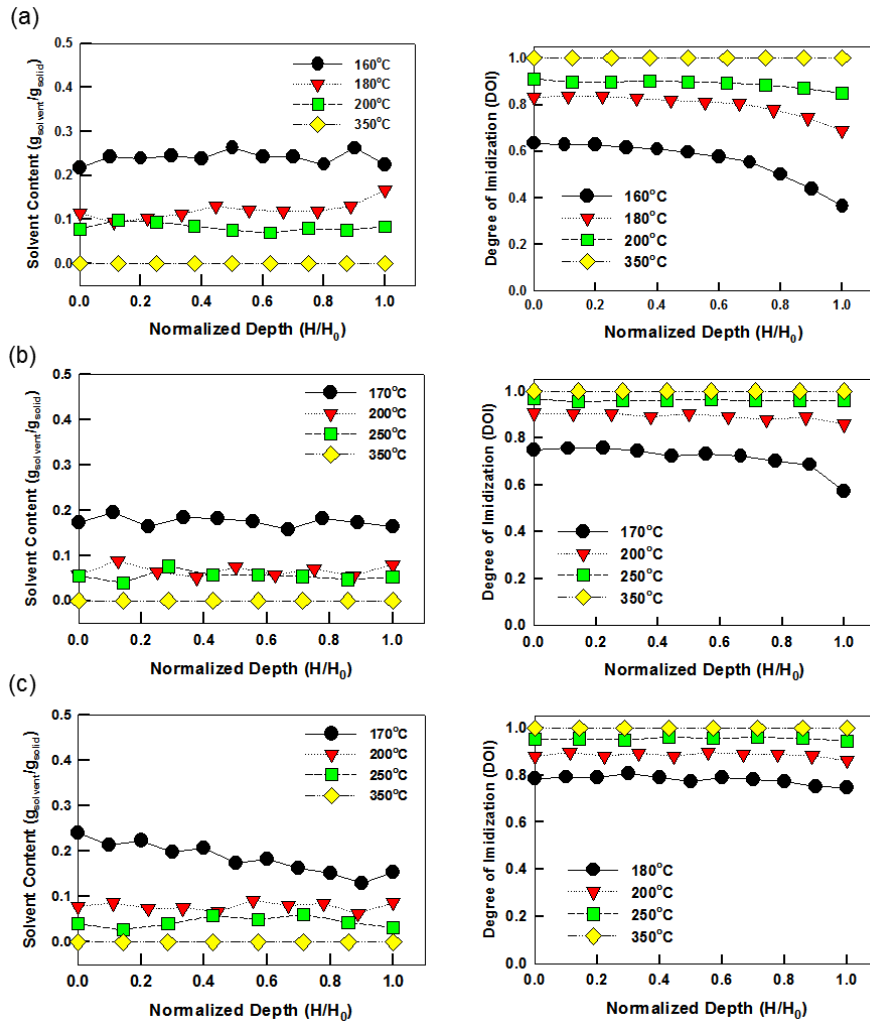


Figure 4.7. Depth-wise residual solvent content (Left) and DOI (Right) during the curing process through (a) protocol A, (b) protocol B, and (c) protocol C. H is a distance from the substrate and H_0 is the film thickness, thus $H/H_0=0$ and 1 corresponds to the substrate side and air side, respectively.

a plasticizer at temperatures higher than 140 °C.

The residual solvent concentration and DOI were measured at different temperatures during the curing process and the results are shown in Figure 4.7. In the figure, the amount of residual solvent decreases while the DOI increases on the way of complete imidization (i.e., DOI=1). The residual solvent concentration and DOI are about 0.1 (g/g) and 0.9, similar to each other regardless of process protocol when the temperature reaches 200 °C. Considering the actual stay time in the curing chamber of protocol A to be 30% longer than protocol C, the result suggests that the temperature, rather than the stay time, is more crucial to the amount of residual solvent and DOI during the curing process. Thus, it can be expected that the change in the residual solvent concentration and DOI will show similar trends after 200 °C independent of the protocols. In addition, the depth-wise inhomogeneity of the residual solvent concentration and DOI which was clearly observed in the drying process disappears after 200 °C due to the high thermal energy provided uniformly along the film thickness direction.

4.2.2. Process path and degree of in-plane chain orientation

The process path was defined in terms of the residual solvent concentration and DOI for different process protocols. (Figure 4.8) Here, the solvent concentration (C_s) was replaced by solid volume fraction using Equation 4.5.

$$\phi = \frac{1}{1 + \rho_r \cdot C_s}, \quad \rho_r = \frac{\rho_p}{\rho_s} \quad (4.5)$$

In the equation, ϕ is the volume fraction of polymer, ρ_p and ρ_s are the density of polymer and solvent, respectively. The density of polymer changes from 1.30 g/cm³ to 1.44 g/cm³ when the PAA is converted to PI [27], but the average value, 1.37 g/cm³ was used as the density of polymer as the difference is not significant. In Fig 7, both the solid volume fraction and DOI increase through different paths as drying and curing proceed, finally reaching 1.0 for every protocol. Compared at the same solid volume fraction, the DOI of protocol A is the lowest while the protocol C the highest. This means that PAA starts to imidize at lower solid content in the case of protocol C, retaining more solvents. As polymer chains are more randomly oriented when there are more solvents in the film and it becomes difficult for stiffer PI chains to be packed closely under biaxial tensile stress, the final degree of in-plane chain orientation of PI made by protocol C can be expected to be lower than the others. And the difference in their paths in different protocols is reduced as the process approaches full imidization. Thus, the process condition during the drying process and at the initial stage of curing process, when there still remains a considerable amount of residual solvent, is considered to act an important role in determining the final microstructure of PI.

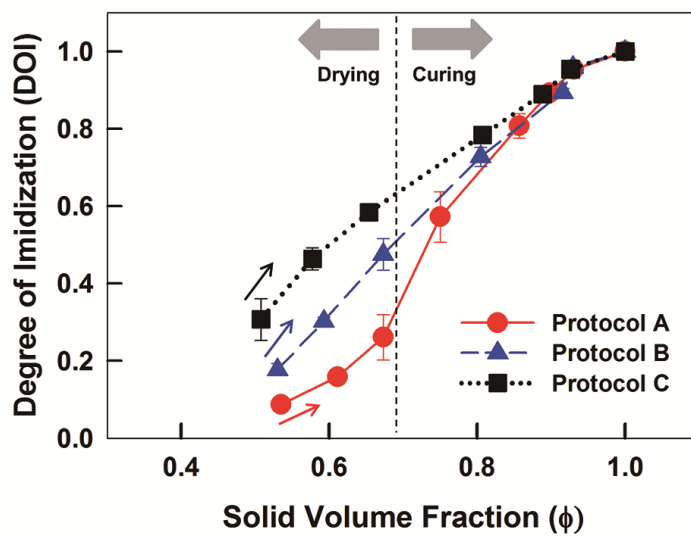


Figure 4.8. Degree of imidization during the drying and curing processes through different protocols.

The degree of in-plane chain orientation of PI films made by different protocols was compared using polarized Raman spectroscopy. (Figure 4.9) In Figure 4.9(a), the Raman intensity of in-plane polarization (I_{xx}) is higher than that of out-of-plane polarization (I_{zz}). It proves that PI chains are preferentially oriented to the in-plane direction due to biaxial tensile stress caused by solvent evaporation. In Figure 4.9(b), a depth-wise profile of the Fraser distribution function, f , is uniform except for protocol A where the f value at the air side is about 0.1 higher than the substrate side. This means that more PI chains orient to the in-plane direction near the film surface in the case of protocol A. This inhomogeneity comes from the lower solvent concentration and imidization rate at the air side, which enables polymer chains to be more densely packed. On the other hand, this side-to-side difference of chain orientation is not observed for protocol B and C because imidization rate along the film thickness is more uniform in these cases. To compare the average value for each protocol, the f of protocol A is about 0.5, while those of protocol B and C are about 0.35 and 0.25, respectively. This indicates that the degree of in-plane chain orientation made by protocol C is the lowest, and the trend coincides well with the result of chain orientation predicted by the process path. It is demonstrated from these results that the process path expressed by the solid volume fraction and DOI can be an effective tool in predicting the final degree of in-plane chain orientation of PI.

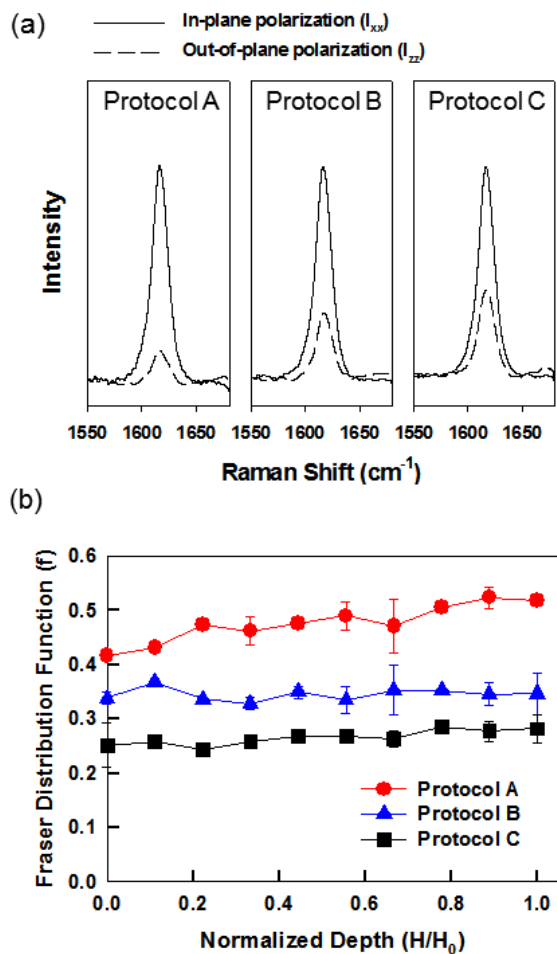


Figure 4.9. (a) Raman spectra of in-plane and out-of-plane polarization appearing at 1610 cm^{-1} for PIs made by different protocols. The spectra were obtained in the middle part of the PI cross-section. (b) Fraser distribution function (f) along the film thickness direction. In the graph, $H/H_0=0$ and 1 corresponds to the substrate side and air side, respectively.

4.2.3. Properties of the cured film

The properties of PI film made by different protocols were examined to observe the effect of different degree of in-plane chain orientation. As shown in Figure 4.10, the structural information of different PI film was first investigated by reflection patterns in WAXD. In all cases the (200) and (210) peaks, normally attributed to the intermolecular packing density and the order of PI crystalline phase, are clearly observed. In a number of studies using WAXD, it was reported that the curing rate or maximum curing temperature affects the chain ordering of PI, resulting in the intensity change or position shift of diffraction peaks. [46, 48] In Figure 4.10, however, the intensity and the position of diffraction peaks are almost the same for PI films made by different protocols, suggesting that the crystallinity and molecular order of the crystalline phase are not much different. Instead, the intensity of the (210) peak relative to the (200) peak is slightly decreased for protocol C, which means that the stacking order of planar units composed of dianhydride, diamine and phenyl ring is weak for PI made by protocol C, and this can be related to the lowest degree of in-plane chain orientation. Because the decrease of peak intensity is so small, however, the difference in chain orientation evidenced by different value of Fraser distribution function has little influence on the degree of crystalline order. This is confirmed by dynamic mechanical analysis (DMA) measurement in Figure 4.11. In the figure, T_g corresponds to the temperature at the maximum peak of $\tan \delta$, thus T_g of different PIs is observed almost the same near 350 °C. It also supports that the crystallinity or molecular packing density is similar for different PIs, otherwise a change in T_g would be observed. This is possible because the measurement of crystallinity or T_g does not necessarily include the information of chain orientation.

In-plane TEC, which represents the dimensional stability of the film, was measured by TMA for different PI films. (Figure 4.12) It was widely reported that TEC of rod-shaped PI is directly related with the chain orientation such that TEC decreases when the PI has higher degree of in-plane chain orientation as it is hard to expand or shrink along the polymer chain axis. [23] In Figure 4.12, the value of TEC increases from 9 ppm/°C to 23 ppm/°C when it goes from protocol A to C. This coincides with the results of in-plane chain orientation indicated by Fraser distribution function. The TEC of the PI made by protocol C is the highest as it shows the lowest value of Fraser distribution function (i.e., the lowest degree of in-plane chain orientation). From the results, it is expected that the PIs made by different protocols have similar crystallinity and stacking order in the crystalline phase, while the orientation of the crystalline phase composed of rod-shaped PI chains is different from each other. In addition, the difference of chain orientation influences more critically on the in-plane TEC than the other physical properties of PI investigated in this study.

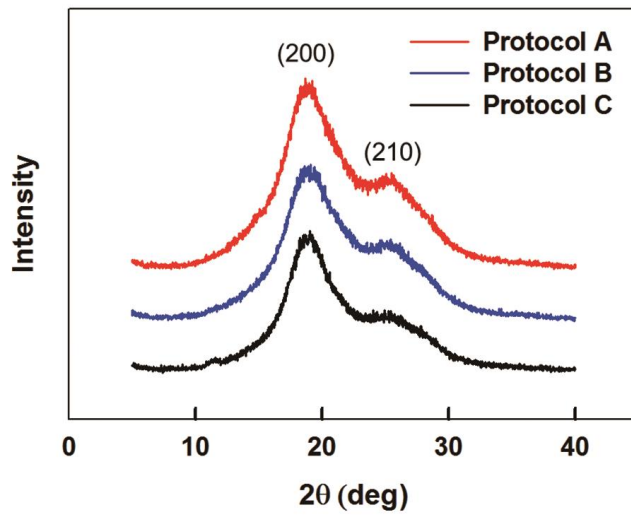


Figure 4.10. WAXD reflection patterns of the PI films depending on different protocols.

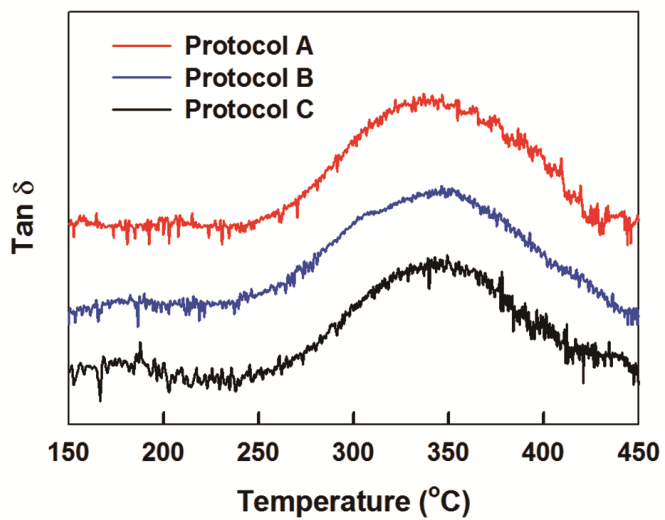


Figure 4.11. Temperature dependence of $\tan \delta$ measured by DMA for the PI films depending on different protocols.

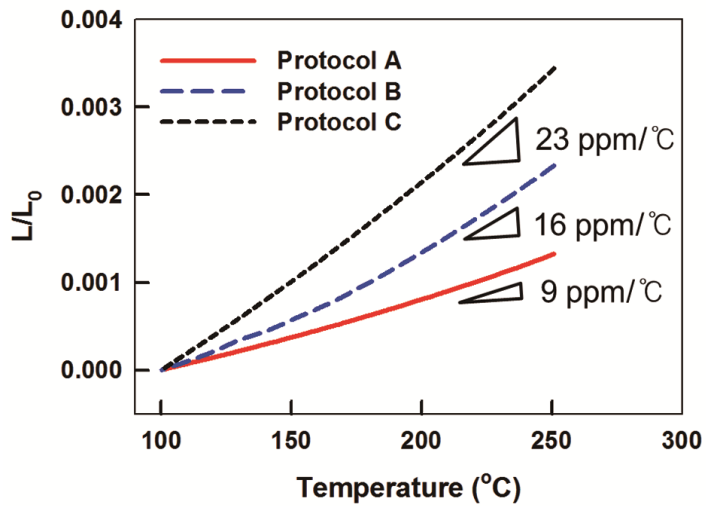


Figure 4.12. Temperature dependence of sample length measured by TMA for the PI films depending on different protocols.

4.3. Interdiffusion and chain orientation in the drying of bilayer polyimide film

4.3.1. Interdiffusion of PAAs having different solvent contents

Different from polymer melts, the solvent can play a crucial role when considering the interdiffusion between different polymer solutions. It is because the mobility of the polymer chain is mainly affected by the amount of solvent that acts as a plasticizer. If a PI bilayer is made by DML drying, total solvent amount included in the top and bottom layer is larger than that in the case of LBL drying at the contact of two layers. Thus, the effect of solvent content in PAA solutions on the interdiffusion speed is investigated first to comprehend the difference in the interdiffusion width of the final cured PI film.

In Figure 4.13, the slope of a compositional change in depth direction becomes less steep as the contact time of two PAAs increases. In addition, the slope is more gradual when the solvent concentration is higher when compared at the same contact time, which means a broader interdiffusion zone. To quantify this, the interdiffusion width (w) is defined by the reciprocal of the maximal slope (w_{app}) where the compositional change occurs most rapidly. [76] :

$$w(t) = w_{app}(t) - w(0), \quad w_{app}(t) = \max[(d\phi/dz)^{-1}] \quad (4.6)$$

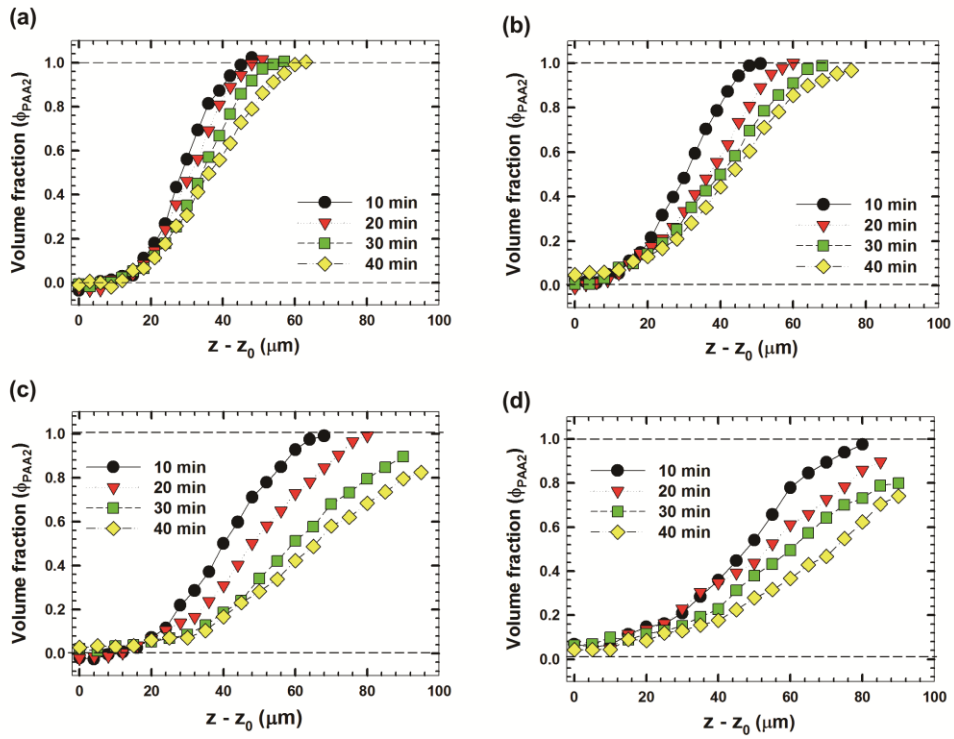


Figure 4.13. Depth-wise volume fraction of PAA-2 (Φ_{PAA2}) measured at different times after a contact with PAA-1. Different pairs of PAA-1 and 2 have different solvent concentrations of (a) 88 wt%, (b) 90 wt%, (c) 91.5 wt%, and (d) 93 wt%. Abscissa was shifted by z_0 that is the depth below which the volume fraction of PAA-2 increases.

In Equation 4.6, $w(0)$ means the instrumental broadening decided by the DOF of Raman spectrometer. The DOF generally depends on the depth (z) in Raman experiments [81], but it was disregarded in this experiment as the refractive indices between the immersing medium and samples were matched almost the same. Instead, the intrinsic DOF was decided by the wavelength of the laser ($\lambda=633\text{nm}$) and the optical numerical aperture ($\text{NA}=0.9$) as shown in Equation 4.7.

$$w(0) = \frac{2.2 \times \lambda}{(\text{NA})^2} = 1.7 \quad (4.7)$$

Figure 4.14 shows the log-log plot of contact time and $w(t)$ for PAA pairs having different solvent contents. The linear fit in the graph shows the development of $w(t)$ with time can be expressed by a power law $w(t) \propto t^\beta$. The exponent β are 0.12, 0.29, 0.39, and 0.43 for solvent contents, 88, 90, 91.5, and 93 wt%, respectively; it is approaching to the Fickian exponent of 0.5 as the solvent content increases. This behavior is similar to that of polymer melts in that the interdiffusion width increases with time slower than a Fickian diffusion of $w(t) \propto t^{0.5}$, but the speed is critically affected by the amount of solvent in this case. Thus, the interdiffusion between PAAs can be faster when they are processed by the DML method as they contain more solvents than LBL even when the same PAA pairs are used. In addition, it is expected for a PI bilayer made by DML to have a longer interdiffusion width because the contact time is 10 min during the drying process, twice the LBL drying in this experiment.

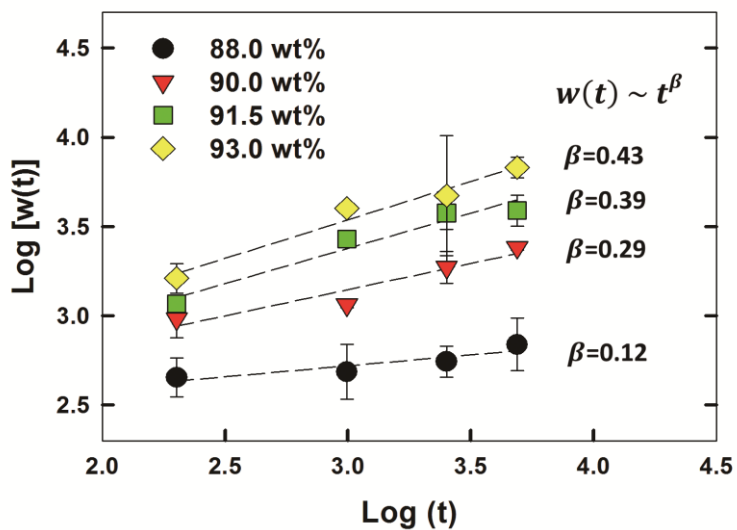


Figure 4.14. Log-log plot of the interdiffusion width $w(t)$ between PAA-1 and 2 at different contact time (t). Different symbols represent PAA-1/PAA-2 pairs having different solvent contents which are indicated in the graph.

4.3.2. Interdiffusion width of cured PI

Raman spectroscopy was used to detect the actual interdiffusion width of bilayer PI films made by the DML and LBL methods. Instead of depth profiling the film, a lateral profiling method was used to enhance the spatial resolution of the measurements and the compositional changes at the film interface are plotted in Figure 4.15(a). To compare the interdiffusion width, the same definition of interdiffusion width as used in Equation 4.6 was employed. Here, $w(0)$ was replaced by the laser focus waist diameter as in Equation 4.8. [89]

$$w(0) = \frac{1.22 \times \lambda}{NA} = 0.86 \mu m \quad (4.8)$$

Comparing the interdiffusion width of PI bilayers made by the LBL method in Figure 4.15(b), the width decreases as the drying temperature of the bottom layer (T_b) increases. It is because larger fraction of PAA chains in the bottom layer is converted to PI at the elevated temperature, which results in an increase of the Flory interaction parameter for the upper PAA layer. [36] At the same time, the swelling of the bottom layer due to the solvent inclusion is hindered as PI is insoluble to DMAc. [33, 34, 35, 90] The extent of solvent diffusion depending on the imidization degree will be discussed in the following section. However, the decrease in the interdiffusion width according to T_b is slight in Figure 4.15(b). This can be ascribed to the spatial resolution of the Raman spectrometer which is about $0.86 \mu m$, not high enough to precisely detect the small width when T_b is high. On the other hand, the interdiffusion width of PI made by DML drying is about $1.1 \mu m$ which is clearly larger than that made by LBL drying. This difference can be explained by the faster interdiffusion

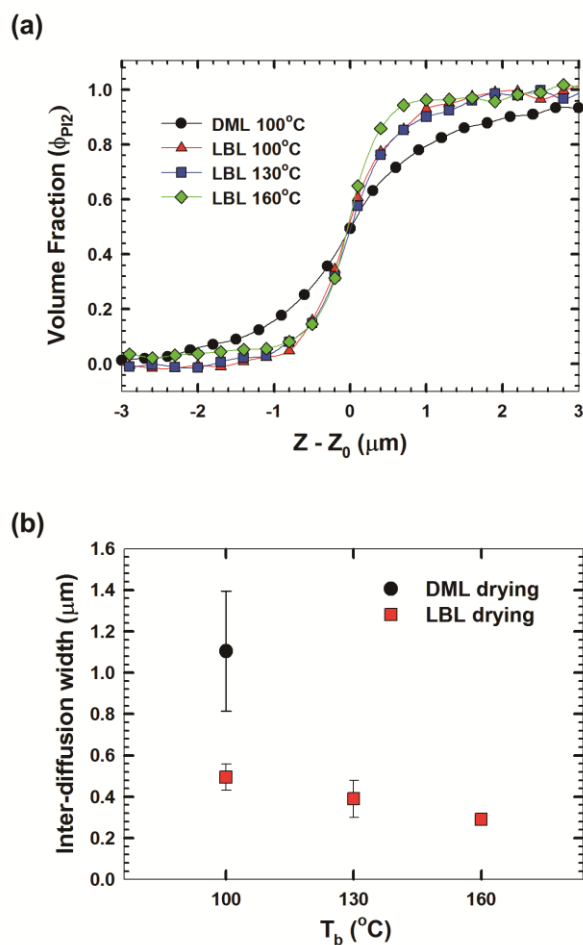


Figure 4.15. Interdiffusion data of the cured PI bilayers made by the DML and LBL methods. (a) Variation of PI-2 volume fraction (ϕ_{PI2}) measured at different positions on the cross section of the cured PI. Abscissa was shifted by Z_0 where the volume of two PIs is equal (i.e. $\phi_{PI2} = 0.5$). (b) The interdiffusion width $w(t)$ of the PI bilayers according to the drying temperature of the bottom layer (T_b).

between PAAs in the case of DML drying as discussed in the previous section. Two PAAs interdiffuse faster and the contact between two layers is longer for DML drying. As the interdiffusion during the curing process that involves only a small amount of solvent can be neglected, [35] the difference in their speed of interdiffusion during the drying process plays a crucial role in determining the interdiffusion width of the final PI bilayers. Considering the adhesion property between immiscible or partially miscible polymers is strengthened by the wider interdiffusion layer, the DML method is regarded to be more beneficial in making multilayer polymer films with a reliable interfacial strength compared to the conventional LBL method.

4.3.3. Solvent diffusion into dried PAA films

The DOI of the bottom layer is varied according to the drying temperature when the bilayer PI film is made by the LBL method. This results in the change in its interaction with the top layer. Among them, the extent of solvent diffusion into the bottom layer can directly affect the chain orientation of the cured PI film as well as the interdiffusion width. DOI can be defined as in Equation 4.9 using the ratio of two characteristic peaks of PAA and PI appeared in the Raman spectrum.

$$\text{DOI} = \frac{I(\text{PI})}{I(\text{PAA})+I(\text{PI})} = \frac{I(1108 \text{ cm}^{-1})}{I(1180 \text{ cm}^{-1})+I(1108 \text{ cm}^{-1})} \quad (4.9)$$

From this definition, DOI=1.0 means that all the PAA chains are imidized to PI. Actual DOI of PAA-1 dried at 100, 130, and 160 °C for 5 min was measured to be 0.03, 0.25, and 0.75 respectively, showing that the increase of DOI at higher

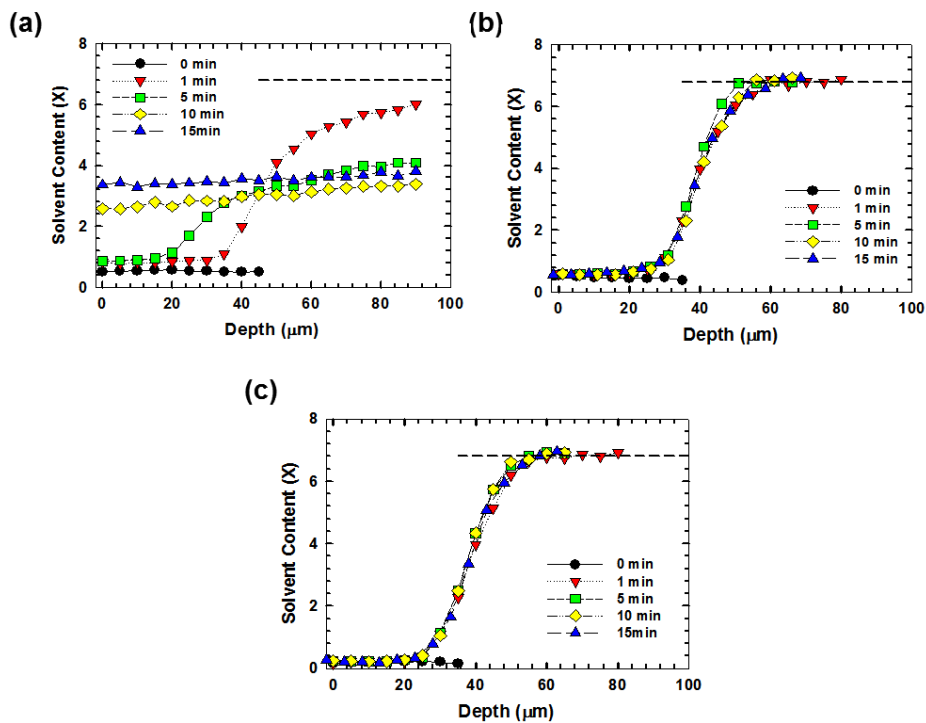


Figure 4.16. Depth-wise solvent content (X) measured at different times after a contact between the dried PAA-1 and 2 solutions. The dried PAA-1 was prepared by drying at different temperatures (T_b) of (a) 100 °C, (b) 130 °C, and (c) 160 °C respectively. Dashed line shows the calculated initial solvent content (i.e. $X=7.3$) of PAA-2 solution, which corresponds to 12 wt%.

temperature was very significant. After the PAA-1 films which were dried at these temperatures were put on the PAA-2 solution as can be seen in Figure 3.13(b), the distribution of solvent content (X) in both layers was depth profiled at different times. (Figure 4.16) Figure 4.16(a) shows how the solvent in PAA-2 diffuses into PAA-1, and the solvent content in PAA-1 increases rapidly from the interface when $T_b=100$ °C. When $t=10$ min, the distribution of solvent concentration becomes almost constant in depth direction, reaching to a nearly equilibrium state. As this experiment is conducted at room temperature, it is expected that the solvent diffusion will be much faster when it is assumed that the two layers are dried at 100 °C which is the temperature actually used to make a bilayer PI film. In the cases of $T_b=130, 160$ °C, a gradual increase of solvent content is observed at the interface from $t=1$ min. (Figure 4.16(b), (c)) Considering the DOF caused by the refractive index mismatch is about 24 μm , this gradual change in solvent content distribution is more reasonably ascribed to the instrumental broadening, not to the actual solvent diffusion. Furthermore, the distribution of solvent content at $t=15$ min shows no difference with $t=1$ min, all of which leads to the conclusion that the solvent in PAA-2 can hardly diffuse into PAA-1 when T_b is higher than 130 °C. This marked difference results from the increased DOI of PAA-1 that impedes the inclusion of solvent as explained earlier. It is worth noting that the amount of solvent diffusion into PAA-1 is drastically reduced at $T_b=130$ °C compared with $T_b=100$ °C even though the DOI is as small as 0.25. The difference in the extent of solvent diffusion can affect the chain orientation of PAA in the bottom layer after the drying process and finally changes the chain orientation of the cured PI film.

4.3.4. In-plane chain orientation of cured PIs

Except for the molecular structure of PI chain, the degree of in-plane chain orientation of a cured PI is influenced by the process path that consists of two parameters, the residual solvent content and the DOI during drying and curing. PAA chains are more randomly oriented when there is a larger amount of solvent remaining in a dried film. Faster imidization at this state lowers the final degree of in-plane chain orientation as it becomes difficult for polymer chains to make a well-ordered structure after the PAA imidizes to more rigid PI. This implies that the lower degree of in-plane chain orientation of a single layer PI results when the film thickness or drying temperature increases. In order to see how the chain orientation of a multilayer PI film is different from that of a single layer, the degree of in-plane chain orientation was measured on the cross-section of bilayer PI films made by the DML and LBL method as shown in Figure 3.10, and the results are compared with the 20 μm -thick PI-1 single layer. (Figure 4.17)

In Figure 4.17, the Fraser distribution function of all the PI-2 layers on top is smaller than the PI-1 layers. This is because the PI-2 chain that has ether linkage is structurally more flexible than PI-1, resulting in the lower degree of in-plane orientation. Here, the abscissa was shifted by the interface (Z_0) between PI-1 and 2. Comparing the chain orientation of PI-2 in Figure 4.17(e), the f values of PI-2 are almost same regardless of drying method or drying temperature of the bottom layer. In Figure 4.17, the Fraser distribution function of all the PI-2 layers on top is smaller than the PI-1 layers. This is because the PI-2 chain that has ether linkage is structurally more flexible than PI-1, resulting in the lower degree of in-plane orientation. Here, the abscissa was shifted by

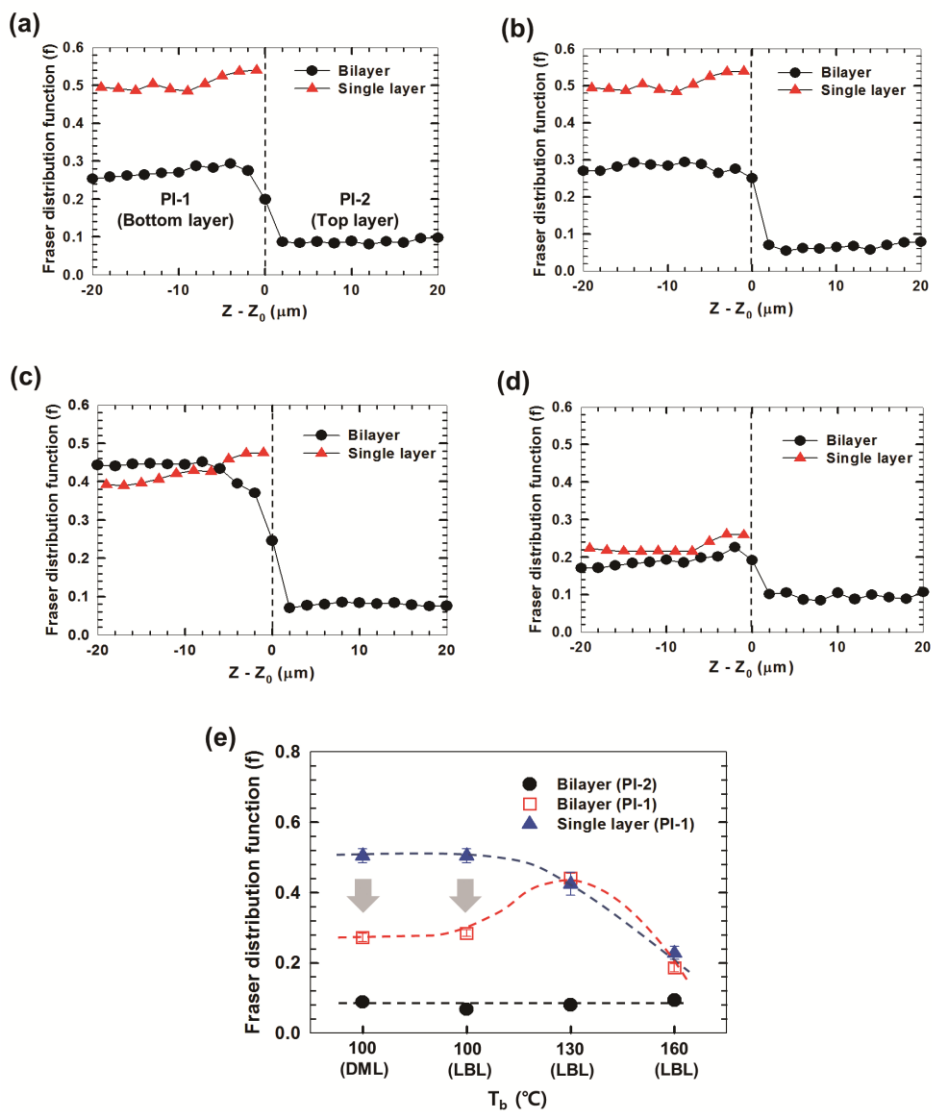


Figure 4.17. Degree of in-plane chain orientation of single and bilayer PI films represented by the Fraser distribution function. PI films were made by (a) DML drying ($T_b = 100^\circ\text{C}$), (b) LBL drying ($T_b = 100^\circ\text{C}$), (c) LBL drying ($T_b = 130^\circ\text{C}$), (d) LBL drying ($T_b = 160^\circ\text{C}$).

the interface (Z_0) between PI-1 and 2. Comparing the chain orientation of PI-2 in Figure 4.17(e), the f values of PI-2 are almost same regardless of drying method or drying temperature of the bottom layer. This seems to be related with a high flexibility of PI-2 that makes the chain orientation less dependent on the processing conditions than PI-1 which has a more rigid structure. Besides, maintaining the drying temperature of the top layer at 100 °C can be another reason for the similar f between PI-2 layers. In Figure 4.17(a), the f value of PI-1 in bilayer film made by the DML is about 0.3, almost half of the PI-1 single layer. The degree of in-plane chain orientation of a single layer PI decreases when the film thickness increases as mentioned before, and this explanation can be applied to the lower degree of in-plane chain orientation of PI-1 in a PI bilayer. From the view point of PI-1, the structuring of PI-1 and 2 layers having 20 μm for each by the DML experiences the same process path with the structuring of 40 μm -thick PI-1 single layer at a time. Likewise, the f of PI-1 in a bilayer that was made by the LBL method at $T_b=100$ °C is much smaller than that of the PI-1 single layer as in Figure 4.17(b). It is because the solvent in the top layer can diffuse easily into the bottom layer when $T_b=100$ °C as shown in Figure 4.16(a). PAA-1 chain highly ordered to the in-plane direction after drying of the bottom layer can lose its alignment due to the inclusion of solvent when the top layer is coated. As the imidization proceeds with this weak alignment of PAA chains during the curing process, the final degree of in-plane orientation of PI-1 becomes lower than that of a single layer. On the other hand, the f of PI-1 makes no difference between single and bilayer films at $T_b=130, 160$ °C as shown in Figures 4.17(c), (d). This is caused by the imidization of the bottom layer during drying that hinders the solvent in the top layer from diffusing into the bottom layer as described in Figures 4.17(b), (c). If there is no

additional inclusion of solvent into the bottom layer, the final chain orientation of PI-1 in bilayer film is simply decided by the same process path with manufacturing a 20 μm -thick PI-1 single layer. To summarize, the degree of in-plane chain orientation of a PI-1 single layer decreases at higher drying temperature and it corresponds well with the result of previous study. When an additional layer is structured by the LBL method, the chain orientation of the bottom layer shows different aspects from a single layer depending on the extent of solvent inflow from the top layer. If the solvent in the top layer can easily diffuse into the bottom layer (i.e. $T_b=100\text{ }^\circ\text{C}$), the degree of in-plane chain orientation becomes lower than that of a single layer and it is comparable with the chain orientation of PI-1 in a bilayer film made by the DML method.

Chapter 5. Summary

In this thesis, the effect of film thickness and processing conditions on the chain orientation of PI film was investigated using confocal Raman spectroscopy. In addition, the interdiffusional behavior between two different PIs was observed in bilayer PI film and how the two different drying methods affect the final width of interdiffusion and chain orientation.

Firstly, the effect of film thickness on the final chain orientation was examined. As the thickness of the BPDA-PDA PI film increased, the amount of residual solvent after drying was increased, and more solvent remained near the substrate side than near the air side leading to an inhomogeneous depth-wise distribution. This is because it takes longer for solvent molecules to diffuse out to a film surface as the film thickness increases, and the diffusional resistance increases near the film surface due to solvent evaporation. As a result, the tensile stress that induces an in-plane chain orientation was reduced for a thick PI film with an inhomogeneous depth-wise profile. In other words, the thicker film had a lower degree of in-plane chain orientation, especially near the substrate than near the surface. In addition, the beginning of imidization reaction in the curing process followed by drying was faster for thick PI as it retained more residual solvent inside. It is because the solvent molecules that were unbound to polymer chains could promote the imidization reaction by acting as a plasticizer. Once the chain rigidity of the polymer was enhanced by the imidization reaction, the chains were hardly packed densely to give a highly ordered structure in which the polymer chains were preferentially aligned to the in-plane direction. Therefore, both the degree and uniformity of the chain orientation of the dried PAA film in the thickness direction could considerably affect those of the PI film. The thick PI exhibited a lower average degree of in-plane orientation after curing than that of the

thin film and an inhomogeneous distribution with much lower degree of in-plane orientation near the substrate side than near the air side.

To see the effect of thermal history, BPDA-PDA PI films were manufactured by three different process protocols, and the degree of in-plane chain orientation of the fully imidized PI was investigated. The process path was defined according to the residual solvent concentration and DOI which were measured during the process of drying and curing. These variables explain the difference in chain orientation of the fully imidized PIs. For the protocol starting at higher temperature, the PAA was converted to PI with larger amount of solvent in the film. Because biaxial tensile stress caused by solvent evaporation makes PAA chains align to the in-plane direction, more residual solvent means less fraction of polymer chains orient to the in-plane direction. As a result, the protocol with a higher drying temperature made the PAA imidized to the stiffer PI at a more randomly oriented state. This feature was observed to lower the degree of in-plane chain orientation of the fully imidized PI. It could be due to an increase of chain rigidity which retards close packing of polymer chains during the subsequent solvent evaporation. The difference in chain orientation influenced the in-plane TEC. The TEC can be considered as an important parameter representing the dimensional stability of the film at high temperature processing. The TEC changed from 9 ppm/°C to more than 20 ppm/°C when manufactured by different protocols. In spite of the difference in TEC, the crystallinity and T_g did not change much, suggesting that the in-plane TEC was more significantly affected by the thermal history among the other film properties when manufacturing rod-shaped PI films.

Finally, the interdiffusion width and chain orientation of PI bilayer film was investigated when the film was made by both DML and LBL drying methods. The interdiffusion occurs during the drying process of PAA bilayer composed of BPDA-PDA and BPDA-ODA. The measurement of interdiffusion speed showed the broadening of interdiffusion width with a power law behavior with time and the exponent increased if there remained a larger amount of solvent in PAA solution. It means that the mobility of PAA chains which is most significantly affected by the solvent content, and the contact time of two layers can be crucial factors in determining the final interdiffusion width. As the bilayer film made by the DML method undergoes a longer contact time containing more solvent during the drying process, the interdiffusion width of the cured PI bilayer was observed larger than that made by the LBL method.

The chain orientation that directly affects the thermal expansivity of PI film is influenced by the variation of residual solvent content and imidization degree during the manufacturing process. The degree of in-plane orientation of the bottom layer which had a more rigid structure was observed to be vulnerable to the processing conditions. The degree of in-plane chain orientation of the bottom layer was smaller than that of a 20 μm -thick single layer film when the bilayer PI film consisting of two 20 μm -thick layers was made by the DML method. This was because the bilayer PI film made by DML drying experienced the same thermal history with a 40 μm -thick single layer, which generally lowers the degree of in-plane chain orientation. In case of LBL drying, the chain orientation of the bottom layer was mainly affected by the extent of solvent intrusion from the top layer. The solvent in the top layer diffused into the bottom layer easily when the bottom layer was dried at 100 $^{\circ}\text{C}$ and this made the

final degree of in-plane chain orientation of the bottom layer lower than that of a single layer. On the other hand, no significant difference in the degree of in-plane chain orientation was observed when the drying temperature of the bottom layer exceeded 130 °C. It was ascribed to the restrained solvent diffusion from the top layer as a larger fraction of PAA in the bottom layer was converted to PI at such a high drying temperature, becoming less soluble to the solvent.

References

1. G. Zhao, T. Ishizaka, H. Kasai, M. Hasegawa, T. Furukawa, H. Nakanishi, H. Oikawa, Ultralow-dielectric-constant films prepared from hollow polyimide nanoparticles possessing controllable core sizes, *Chem. Mater.* **2009**, 21, 419-424.
2. T. Kurosawa, T. Higashihara, M. Ueda, Polyimide memory: a pithy guideline for future applications, *Polym. Chem.* **2013**, 4, 16-30.
3. K. Xi, Z. Meng, L. Heng, R. Ge, H. He, X. Yu, X. Jia, Polyimide-polydimethylsiloxane copolymers for low dielectric constant and moisture resistance applications, *J. of Appl. Polym. Sci.* **2009**, 113, 1633-1641.
4. J.-S. Park, T.-W. Kim, D. Stryakhilev, J.-S. Lee, S.-G. An, Y.-S. Pyo, D.-B. Lee, Y. G. Mo, D.-U. Jin, H. K. Chung, Flexible full color organic light-emitting diode display on polyimide plastic substrate driven by amorphous indium gallium zinc oxide thin-film transistors, *Appl. Phys. Lett.* **2009**, 95, 013503.
5. B.-S. Park, W. Y. Kim, K.-B. Yoon, Luminous polyimide bearing the coumarin 6 chromophore in the side group: synthesis and fluorescence image patterning, *Korean J. Chem. Eng.* **2014**, 31, 172-177.
6. I.-H. Tseng, M.-H. Tsai, C.-W. Chung, Flexible and transparent polyimide films containing two-dimensional alumina nanosheets templated by graphene oxide for improved barrier property, *Appl. Mater. Interfaces* **2014**, 6, 13098-13105.
7. Y. Momoi, O. Sato, T. Koda, A. Nishioka, O. Haba, K. Yonetake, Surface rheology of rubbed polyimide film in liquid crystal display, *Optical Material Express* **2014**, 4, 1057-1066.

8. Y. Tsuda, Y. Matsuda, T. Matsuda, Soluble polyimides bearing long-chain alkyl groups on their side chain via polymer reaction, *Int. J. of Polym. Sci.* **2012**, 1-10.
9. Y. Mansoori, S. S. Sanaei, M.-R. Zamanloo, G. Imanzadeh, S. V. Atghia, Synthesis and properties of new polyimide/clay nanocomposite films, *Bull. Mater. Sci.* **2013**, 36, 789-798.
10. E. Hamciuc, C. Hamciuc, V. E. Musteata, Y. Kalvachev, A. Wolinska-Grabczyk, Preparation and characterization of new polyimide films containing zeolite L and/or silica, *High Performance Polymers*, **2013**, 1-13.
11. M. Hasegawa, T. Matano, Y. Shindo, T. Sugimura, Spontaneous molecular orientation of polyimides induced by thermal imidization. 2. In-plane orientation, *Macromolecules* **1996**, 29, 7897-7909.
12. H. M. Tong, K. D. Hsuen, K. L. Saenger, G. W. Su, Thickness-direction coefficient of thermal expansion measurement of thin polymer films, *Rev. Sci. Instrum.* **1991**, 62, 422-430.
13. W. M. Prest, D. J. Luca, The origin of the optical anisotropy of solvent cast polymeric films, *J. Appl. Phys.* **1979**, 50, 6067-6071.
14. W. M. Prest, D. J. Luca, The alignment of polymers during the solvent-coating process, *J. Appl. Phys.* **1980**, 51, 5170-5174.
15. F. Li, K.-H. Kim, E. P. Savitski, J.-C. Chen, F. W. Harris, S. Z. D. Cheng, Molecular weight and film thickness effects on linear optical anisotropy of 6FDA-PFMB polyimides, *Polymer* **1997**, 38, 3223-3227.

16. H.-C. Liou, P. S. Ho, R. Stierman, Thickness dependence of the anisotropy in thermal expansion of PMDA-ODA and BPDA-PDA thin films, *Thin Solid films* **1999**, 339, 68-73.
17. J.-S. King, W. Lee, Li, Chang, W. Whang, Structural effect on stretch-induced birefringence in polyimide films *Jpn., J. Appl. Phys.* **2007**, 46, 6801-6806.
18. S. C. Noe, J. Y. Pan, S. D. Senturia, Optical waveguide as a method for characterizing the effect of extended cure and moisture on polyimide films, *Polym. Eng. Sci.* **1992**, 32, 1015-1020.
19. H. Nomura, M. Asano, *Jpn. J. Appl. Phys. Part1* **1993**, 32, 3933-3937.
20. H. Nomura, M. Asano, *Jpn. J. Appl. Phys. Part1* **1996**, 11, 5825-5830.
21. Y. Terui, S.-I. Matsuda, S. Ando, Molecular structure and thickness dependence of chain orientation in aromatic polyimide films, *J. Polym. Sci., Part B: Polym. Phys.* **2005**, 43, 2109-2120.
22. S.-I. Matsuda, S. Ando, Molecular orientation of rigid-rod polyimide films characterized by polarized attenuated total reflection/Fourier transform infrared spectroscopy, *J. Polym. Sci., Part B: Polym. Phys.* **2003**, 41, 418-428.
23. J. C. Coburn, M. T. Pottiger, S. C. Noe, S. D. Senturia, Stress in polyimide coatings, *J. Polym. Sci., Part B: Polym. Phys.* **1994**, 32, 1271-1283.
24. T. Miwa, Y. Okabe, M. Ishida, Effects of precursor structure and imidization process on thermal expansion coefficient of polyimide (BPDA/PDA), *Polymer* **1997**, 38, 4945-4949.
25. H.-C. Liou, R. Willecke, P. S. Ho, Study of out-of-plane elastic properties of PMDA-ODA and BPDA-PDA polyimide thin films, *Thin Solid Films* **1998**, 323, 203-208.

26. J.-H. Jou, P.-T. Huang, H.-C. Chen, C.-N. Liao, Coating thickness effect on the orientation and thermal expansion coefficient of polyimide films, *Polymer* **1992**, 33, 967-974.
27. M. Dabral, S. Xia, W. W. Gerberich, L. F. Francis, L. E. Scriven, Near-surface structure formation in chemically imidized polyimide films, *J. Polym. Sci., Part B: Polym. Phys.* **2001**, 39, 1824-1838.
28. C. Johnson, S. L. Wunder, FT-Raman investigation of the thermal curing of PMDA/ODA polyamic acids, *J. Polym. Sci., Part B: Polym. Phys.* **1993**, 31, 677-682.
29. N. Takahashi, D. Y. Yoon, W. Parrish, molecular order in condensed states of semiflexible poly(amic acid) and polyimide, *Macromolecules* **1984**, 17, 2583-2588.
30. Y. Zhai, Q. Yang, R. Zhu, Y. Gu, The study on imidization degree of polyamic acid in solution and ordering degree of its polyimide film, *J. Mater. Sci.* **2008**, 43, 338-344.
31. L. Leger, C. Creton, Adhesion mechanisms at soft polymer interfaces, *Phil. Trans. R. Soc.* **2008**, 366, 1425-1442.
32. P. G. de Gennes, Reptation of a polymer chain in the presence of fixed obstacles, *J. Chem. Phys.* **1971**, 55, 572.
33. S. F. Tead, E. J. Kramer, T. P. Russell, W. Volksen, Interdiffusion at polyimide interfaces, *Polymer* **1992**, 33, 3382-3387.
34. H. R. Brown, A. C. M. Yang, T. P. Russell, W. Volksen, Diffusion and self-adhesion of the polyimide PMDA-ODA, *Polymer* **1988**, 29, 1807-1811.

35. N. C. Stoffel, E. J. Kramer, W. Volksen, T. P. Russell, Imidization and interdiffusion of poly(amic ethyl ester) precursors of PMDA/3,4'-ODA, *J. Polym. Sci., Part B: Polym. Phys.* **1998**, 36, 2247-2258.
36. S. F. Tead, E. J. Kramer, T. P. Russell, W. Volksen, Solvent and curing effects on diffusion at polyimide interfaces, *W. Mater. Res. Soc. Symp. Proc.* **1989**, 154.
37. D. Wilson, H. D. Stenzenberger, P. M. Hergenrother, *Polyimides*, Blackie & Son Ltd, **1990**, Chapter 1.
38. N. C. Stoffel, E. J. Kramer, W. Volksen, T. P. Russell, Solvent and isomer effects on the imidization of pyromellitic dianhydride-oxydianiline-based poly(amic ethyl ester)s, *Polymer* **1993**, 34, 4524-4530.
39. S. I. Kim, S. M. Pyo, M. Ree, Investigation of glass transition behaviors in poly(amic acid) precursors of semiflexible polyimides by oscillating differential scanning calorimetry, *Macromolecules* **1997**, 30, 7890-7897.
40. Y. Terui, S. Ando, Coefficient of molecular packing and intrinsic birefringence of aromatic polyimides estimated using refractive indices and molecular polarizabilities, *J. Polym. Sci., Part B: Polym. Phys.* **2004**, 42, 2354-2366.
41. M. Hasegawa, N. Sensui, Y. Shindo, R. Yokota, Structure and properties of novel asymmetric biphenyl type polyimides. Homo- and copolymers and blends, *Macromolecules* **1999**, 32, 387-396.
42. L. Lin, S. A. Bidstrup, Effect of molecular orientation on the dielectric properties of spin-coated polyimide films, *J. Appl. Polym. Sci.* **1994**, 54, 553-560.

43. S. C. Noe, J. Y. Pan, S. D. Senturia, Optical waveguiding as a method for characterizing the effect of extended cure and moisture on polyimide films, *Polym. Eng. Sci.* **1992**, 32, 1015-1020.
44. H.-C. Liou, P. S. Ho, R. Stierman, Thickness dependence of the anisotropy in thermal expansion of PMDA-ODA and BPDA-PDA thin films, *Thin Solid Films* **1999**, 339, 68-73.
45. K. Sekiguchi, K. Takizawa, S. Ando, Thermal expansion behavior of the ordered domain in polyimide films investigated by variable temperature WAXD measurements, *J. Photopolym. Sci. Tech.* **2013**, 26, 327-332.
46. P. S. Ho, T. W. Poon, J. Leu, Molecular structure and thermal /mechanical properties of polymer thin films, *J. Phys. Chem. Solids* **1994**, 55, 1115-1124.
47. Y.-K. Xu, M.-S. Zhan, K. Wang, Structure and properties of polyimide films during a far-infrared-induced imidization process, *J. Polym. Sci., Part B: Polym. Phys.* **2004**, 42, 2490-2501.
48. H. Chung, Y. Joe, H. Han, The effect of curing history on the residual stress behavior of polyimide thin films, *J. Appl. Polym. Sci.* **1999**, 74, 3287-3298.
49. H. Chung, J. Lee, W. Jang, Stress behaviors and thermal properties of polyimide thin films depending on the different curing process, *J. Polym. Sci., Part B: Polym. Phys.* **2000**, 38, 2879-2890.
50. M. Ree, T. J. Shin, Y.-H. Park, S. I. Kim, S. H. Woo, C. K. Cho, C. E. Park, Residual stress and optical properties of fully rod-like poly(p-phenylene pyromellitimide) in thin films: Effects of soft-bake and thermal imidization history, *J. Polym. Sci., Part B: Polym. Phys.* **1998**, 36, 1261-1273.

51. S. H. Lee, Y. C. Bae, Thermal stress analysis for polyimide thin films and a substrate layer system, *Macromol. Chem. Phys.* **2000**, 201, 1286-1291.
52. T. Nishino, M. Kotera, N. Inayoshi, N. Miki, K. Nakamae, Residual stress and microstructures of aromatic polyimide with different imidization processes, *Polymer* **2000**, 41, 6913-6918.
53. H. Chung, C. Lee, H. Han, Moisture-induced stress relaxation of polyimide thin films, *Polymer* **2001**, 42, 319-328.
54. H. Lei, J. A. Payne, A. V. McCormick, L. F. Francis, W. W. Gerberich, L. E. Scriven, Stress development in drying coatings, *J. Appl. Polym. Sci.* **2001**, 81, 1000-1013.
55. J. A. Payne, A. V. McCormick, L. F. Francis, In situ stress measurement apparatus for liquid applied coatings, *Rev. Sci. Instrum.* **1997**, 68, 4564-4568.
56. S.-Y. Tam, Stress effects in drying coating, Thesis, **1997**, 58-05, 2564.
57. R. A. Cairncross, The fate of residual solvent in drying coatings: Can it get trapped and how?, Proceedings of the Pressure Sensitive Tape Council Tech XXV meeting **2002**.
58. E. B. Guttoff, Fundamentals of drying coatings, Proceedings of Tech XXVIII Technical Seminar **2005**.
59. B. Cuerrier, C. Bouchard, C. Allain, C. Bernard, Drying kinetics of polymer films, *AIChE* **1998**, 44, 791-798.
60. A. K. Ghosh, Fundamentals of paper drying – theory and application from industrial perspective, *Intech* **2011**, 25, 535-582.
61. U. W. Gedde, Polymer physics, Kluwer Academic Publishers **2001**, Chapter 9.

62. H.-M. Liem, P. Etchegoin, K. S. Whitehead, D. D. C. Bradley, Raman anisotropy measurement: An effective probe of molecular orientation in conjugated polymer thin films, *Adv. Funct. Mater.* **2003**, 13, 66-72.
63. H.-M. Liem, P. Etchegoin, K. S. Whitehead, D. D. C. Bradley, Raman scattering as a probe of morphology in conjugated polymer thin films, *J. Appl. Phys.* **2002**, 92, 1154-1161.
64. H.-M. Liem, P. Etchegoin, D. D. C. Bradley, Anomalous Raman scattering from the surface of conjugated polymer melts, *Physical Review B* **2001**, 64, 144209.
65. R. G. Snyder, Raman scattering activities for partially oriented molecules, *J. Mol. Spectroscopy* **1971**, 37, 353-365.
66. L. Margulies, M. Stockburger, Polarized resonance Raman spectra of an oriented diphenylpolyene, *J. Raman Spectroscopy* **1979**, 8, 26-31.
67. B. Jasse, J. L. Koenig, Orientational measurements in polymer using vibrational spectroscopy, *J. Macromol. Sci., Part C* **1979**, 17, 61-135.
68. M. Tanaka, R. J. Young, Review: Polarised Raman spectroscopy for the study of molecular orientation distributions in polymers, *J. Mater. Sci.* **2006**, 41, 963-991.
69. R. D. B. Fraser, The interpretation of infrared dichroism in fibrous protein structures, *J. Chem. Phys.* 1953, 21, 1511-1515.
70. W. Yu, Interfacial structure of bilayer compensation films prepared by direct coating process, Thesis **2012**.
71. E. Jabbari, N. A. Peppas, Polymer-polymer interdiffusion and adhesion, *Rev. Macromol. Chem. Phys.* **1994**, C34, 205-241.

72. E. Helfand, Y. Tagami, Theory of the interface between immiscible polymers, *J. Polym. Sci., Part B: Polym. Lett.* **1971**, 9, 741-746.
73. W. C. Kim, H. Pak, Interdiffusion at interfaces of binary polymer mixtures with different molecular weights, *Bull. Korean Chem. Soc.* **1999**, 20, 1323-1328.
74. W. C. Kim, C. J. Lee, H. G. Sim, H. Pak, Interdiffusion at interfaces of polymers with similar physical properties, *Bull. Korean Chem. Soc.* **2000**, 21, 577-582.
75. J.-M. Jung, H. Pak, Interdiffusion at interfaces of polymers with dissimilar physical properties, *Bull. Korean Chem. Soc.* **1997**, 18, 720-729.
76. U. Steiner, g. Krausch, G. Schatz, J. Klein, Dynamics of mixing between partially miscible polymers, *Phy. Rev. Lett.* **1990**, 64, 1119-1121.
77. H. Kim, Interdiffusion at polymer-polymer interfaces, Durham Thesis **2005**.
78. A. Karim, G. P. Felcher, T. P. Russell, Interdiffusion of polymers at short times, *Macromolecules* **1994**, 27, 6973-6979.
79. R. J. Composto, E. J. Kramer, D. M. White, Mutual diffusion in the miscible polymer blend polystyrene/poly(xylynyl ether), *Macromolecules* **1988**, 21, 2580-2588.
80. J. Vyorykka, Confocal Raman microscopy in chemical and physical characterization of coated and printed papers, Thesis, Helsinki university of Tech. **2004**.
81. N. Everall, Depth profiling with confocal Raman microscopy, part 1,2, *Spectroscopy* 2004, 19.

82. W. Schabel, I. Ludwig, M. Kind, Measurements of concentration profiles in polymeric solvent coatings by means of an inverse confocal micro Raman spectrometer-initial results, *Drying Tech.* **2004**, 22, 285-294
83. R. K. Arya, Non-Fickian drying of polymeric coatings, *Int. J. Sci. Tech. Res.* **2012**, 1,
84. I. Ludwig, W. Schabel, M. Kind, J.-C. Castaing, P. Ferlin, Drying and film formation of industrial waterborne latices, *AIChE* **2007**, 53, 549-560.
85. J. Krenn, P. Scharfer, M. Kind, W. Schabel, Drying of solvent-borne coatings with pre-loaded drying gas, *Eur. Phys. J. Special Topics* **2009**, 166, 45-48.
86. M. Vinjamur, R. A. Cairncross, Experimental investigations of trapping skinning, *J. Appl. Polym. Sci.* **2002**, 83, 2269-2273.
87. R. Saure, G. R. Wagner, E.-U. Schlunder, Drying of solvent-borne polymeric coatings: 1. Modeling the drying process, *Surf. Coat. Technol.* **1998**, 99, 253-256.
88. R. Saure, G. R. Wagner, E.-U. Schlunder, Drying of solvent-borne polymeric coatings: 2. Experimental results using FTIR spectroscopy, *Surf. Coat. Technol.* **1998**, 99, 257-265.
89. F. Adar, E. Lee, S. Mamedov, A. Whiteley, Experimental evaluation of the depth resolution of a Raman microscope, *Microsc. Microanal.* **2010**, 16, 360-361.
90. K. L. Saenger, H. M. Tong, Improved polyimide/polyimide adhesion via swelling agent enhanced interdiffusion, *J. Polym. Sci., Part C: Polym. Lett.* **1989**, 27, 235-237.

국문 초록

본 연구에서는 공정조건에 따라 변화하는 폴리이미드 사슬의 배향과 상호확산 현상에 대해 관찰하였다. 이를 통해 폴리이미드 필름 내에 잔류하는 용매량과 이미드화도의 두 가지 인자가 최종 사슬 배향과 상호확산 정도를 결정하는 데 있어 핵심적인 역할을 하게 됨을 알 수 있었다.

먼저, 폴리이미드 필름의 두께가 사슬 배향에 미치는 영향을 확인하기 위해 폴리이미드의 전구체인 폴리아믹산 용액을 이용하여 서로 다른 두께를 갖는 필름을 제조하였다. 그리고 건조와 경화 과정에서 필름 두께 방향으로의 잔류용매량 및 이미드화도 분포를 측정하였다. 필름이 두꺼워질수록 고분자 사슬은 더 낮은 in-plane 배향도를 갖게 되는데 특히 필름 표면보다 기재 쪽의 in-plane 배향도가 더 낮음을 알 수 있었다. 이러한 불균일한 배향 분포는 건조가 끝난 상태에서의 폴리아믹산 배향 분포와 유사하였다. 이는 필름이 두꺼워질 경우, 잔류 용매량이 많은 상태에서 더 빨리 강직한 구조를 갖는 폴리이미드로 변해 충분히 조밀한 구조를 갖지 못하기 때문인 것으로 설명이 가능하였다. 이러한 폴리이미드 사슬의 배향은 열이력 차이에 의해서도 달라질 수 있다. 초기 건조 온도가 높을수록 폴리아믹산 필름은 잔류 용매를 많이 함유한 상태에서 더 빨리 이미드화 반응을 진행하게 된다. 결과적으로 가장 높은 온도에서 건조한 경우에 최종적으로 경화된 폴리이미드 사슬의 in-plane 배향도가 가장 낮음을 알 수 있었다. 이 같은 배향 차이는 폴리이미드 필름의 결정화도나 유리전이온도에는 큰 변화를 주지 못한 반면 필름의 열팽창률을 크게 변화시킬 수 있음을 확인하였다.

다층 구조의 폴리이미드 필름을 제조하는데 있어 고분자 사슬의 배향과 상호확산 정도를 제어하는 것은 층간 접착특성을 확보하는 데 있어서 매우 중요한 인자이다. 본 연구에서는 2 층 구조의 폴리이미드 필름을 제조하는데 있어 direct multi-layer (DML) 건조 방식과 layer-by-layer (LBL) 건조 방식을 적용해 보았다. 두 폴리아믹산 사이에서 발생하는 상호확산의 정도는 함유하고 있는 용매의 양과 두 층이 접촉하는 시간에 영향을 받는다. 이로부터 LBL 건조 방식에 비해 DML 건조 방식으로 제조된 폴리이미드가 더 큰 상호확산 폭을 갖게 됨을 설명할 수 있었다. 사슬 배향에 있어서는 상대적으로 강직한 분자 구조를 갖는 아래층이 건조 방식에 따라 큰 배향 변화를 보였다. 특히 LBL 건조 방식에서는 아래층의 건조 온도가 낮은 경우 이를 단일층으로 제조했을 때보다 더 낮은 in-plane 배향도를 갖는다는 것을 확인하였는데, 이는 건조 온도가 낮을 경우 위층의 용매가 아래층으로 쉽게 확산되는 현상과 밀접한 관련이 있음을 알 수 있었다.

주요어: 폴리이미드, 잔류용매, 이미드화도, 사슬 배향, 상호확산, 라만 분광법

학 번: 2011-30281



저작자표시-비영리-변경금지 2.0 대한민국

이용자는 아래의 조건을 따르는 경우에 한하여 자유롭게

- 이 저작물을 복제, 배포, 전송, 전시, 공연 및 방송할 수 있습니다.

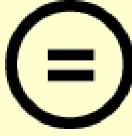
다음과 같은 조건을 따라야 합니다:



저작자표시. 귀하는 원저작자를 표시하여야 합니다.



비영리. 귀하는 이 저작물을 영리 목적으로 이용할 수 없습니다.



변경금지. 귀하는 이 저작물을 개작, 변형 또는 가공할 수 없습니다.

- 귀하는, 이 저작물의 재이용이나 배포의 경우, 이 저작물에 적용된 이용허락조건을 명확하게 나타내어야 합니다.
- 저작권자로부터 별도의 허가를 받으면 이러한 조건들은 적용되지 않습니다.

저작권법에 따른 이용자의 권리는 위의 내용에 의하여 영향을 받지 않습니다.

이것은 [이용허락규약\(Legal Code\)](#)을 이해하기 쉽게 요약한 것입니다.

[Disclaimer](#)

공학박사학위논문

**Study on the chain orientation and
interdiffusion of polyimide affected by
drying and curing processes**

건조 및 경화 공정에 따른
폴리이미드 배향과 상호확산에 관한 연구

2016 년 2 월

서울대학교 대학원

화학생물공학부

조 병 욱

Abstract

Study on the chain orientation and interdiffusion of polyimide affected by drying and curing processes

Byoungwook Jo

School of Chemical and Biological Engineering

Seoul National University

Chain orientation in polyimide (PI) film and its interdiffusional behavior influenced by the process conditions were investigated. The amount of residual solvent and the degree of imidization were proved to be the key factors that determine the final chain orientation and interdiffusion width of PIs.

To observe the effect of film thickness, the films made by poly(amic acids) or PAA, the precursor of polyimide, having different thicknesses were prepared. During the drying and curing processes, the depth-wise distribution of residual solvent and imidization rate were observed. For thick PI, it showed a lower degree of in-plane chain orientation, particularly near the substrate. This non-uniform distribution of chain orientation was similar to that of a dried PAA. Fast imidization with higher solvent content for thick PI retarded the formation of a well-ordered structure and resulted in a lower degree of in-plane orientation. Chain orientation of a PI can also be changed by thermal histories. PAA began to imidize

quickly with retaining more solvent as the initial drying temperature increased. The fully imidized PI showed the lowest degree of in-plane chain orientation when it was processed by the protocol of the highest drying temperature. It influenced the in-plane thermal expansion coefficient most significantly, while no significant change in crystallinity or glass transition temperature was observed.

In multi-layer PI film, controlling the interdiffusion and chain orientation is essential to achieve a good adhesion performance. In the present study, bilayer PI films were made by two different drying methods, direct multi-layer (DML) and layer-by-layer (LBL). The extent of interdiffusion between two PAAs was affected by both the amount of solvent and contact time. As a result, the interdiffusion width of the cured PI made by DML was larger than that made by LBL. The chain orientation of the bottom layer, which consists of more rigid chain structure, was observed to be varied more significantly according to the drying conditions. In the bilayer PI film made by LBL method, the degree of in-plane orientation of the bottom layer became reduced compared to the single-layer when it was dried at lower temperature. The result originates from the fast diffusion of solvent in the top layer into the bottom layer.

Keywords: polyimide, residual solvent, degree of imidization, chain orientation, interdiffusion, Raman spectroscopy

Student Number: 2011-30281

Contents

Abstract.....	i
List of Contents	iii
List of Figures.....	vi
List of Tables	xii
Chapter 1. Introduction.....	1
1.1. General introduction.....	2
1.2. Outline of the thesis.....	7
Chapter 2. Background.....	9
2.1. Manufacturing processes of polyimide film.....	10
2.1.1. Poly(amic acid) preparation	12
2.1.2. Thermal imidization of PAA.....	14
2.2. Drying behavior of polymer solutions.....	17
2.2.1. Two drying regimes of polymer solution	18
2.2.2. Stress development in polymer films	21
2.2.3. Stress development in polyimide film.....	22
2.3. Chain orientation of rod-shaped polymers	23
2.3.1. General introduction of polymer chain orientation	23
2.3.2. Chain orientation measurement using polarized Raman spectroscopy	24
2.4. Interdiffusion between two different polymers	30
2.4.1. Polymer/polymer interfaces	30

2.4.2. Interdiffusion at polymer interfaces	34
2.4.3. Interdiffusion between partially miscible polymers	36
2.4.4. Polymer interface and adhesion	37
2.5. Confocal Raman spectroscopy	41
2.5.1. Principles of Raman scattering	41
2.5.2. Principles of confocal Raman spectroscopy	41
Chapter 3. Experimental methods	49
3.1. Sample preparation and characterization	50
3.2. Measurement of residual solvent concentration and the degree of imidization	62
3.3. Measurement of chain orientation of polyimide	68
3.4. Experiments of polyimide interdiffusion.....	73
3.4.1. Measurement of PAA-PAA interdiffusion.....	77
3.4.2. Measurement of solvent diffusion into dried PAA film	78
3.4.3. Measurement of interdiffusion width of cured polyimide films	79
3.5. Characterization of the cured polyimide film.....	81
3.5.1. X-ray diffraction pattern.....	81
3.5.2. Glass transition temperature	81
3.5.3. Thermal expansion coefficient	81
Chapter 4. Results and discussion	83
4.1. Effect of film thickness on the polyimide chain orientation	84
4.1.1. Depth-wise residual solvent content of dried film	84
4.1.2. Depth-wise imidization degree during the curing process	87

4.1.3. Depth-wise chain orientation after curing	90
4.2. Effect of thermal history on the polyimide chain orientation.....	98
4.2.1. Residual solvent and imidization degree during drying	98
4.2.2. Process path and degree of in-plane orientation.....	103
4.2.3. Properties of cured film.....	107
4.3. Interdiffusion and chain orientation in the drying of bilayer polyimide film.....	112
4.3.1. Interdiffusion between PAA solutions having different solvent contents.....	112
4.3.2. Interdiffusion width of cured polyimide film	116
4.3.3. Solvent diffusion into dried PAA films	118
4.3.4. In-plane chain orientation of cured polyimide films	121
Chapter 5. Summary	125
References	131
국문 초록	141
Curriculum Vitae.....	143

List of Figures

Figure 2.1. Schematic diagram of PI manufacturing process.....	11
Figure 2.2. Mechanism of PAA and PI formation	13
Figure 2.3. Schematic diagram of hypothetical potential energy during imidization. The left peak corresponds to the depolymerization energy and the right peak corresponds to the imidization energy	15
Figure 2.4. Drying mechanism. (a) three characteristic periods of drying, (b) two characteristic resistance of drying	19
Figure 2.5. Schematic diagram of main components in polarized Raman spectrometer	26
Figure 2.6. Main directions of film extension, light source excitation, and light scattering	28
Figure 2.7. Cross-sectional image of a bilayer PI film (Left) and its Raman mapping image (Right).....	32
Figure 2.8. Graphical representation of interdiffusion width (w) defined by maximal volume fraction change at the interface.....	39
Figure 2.9. Schematic representation of the strain energy release rate depending on the molecular weight of a polymer	40
Figure 2.10. Schematic diagram of energy level before and after the light excitation	43
Figure 2.11. Schematic diagram of confocal Raman spectrometer	44
Figure 2.12. Depth of focus depending on the refractive index difference. Marginal lights are focused deeper position	47

Figure 3.1. The molecular structure of poly(amic acid) and polyimide composed of BPDA and PDA.....	51
Figure 3.2. Raman intensity calibration graph plotted by solvent concentration against Raman intensity ratio between DMAc and PAA	52
Figure 3.3. Thermal histories for the different drying and curing protocols. The drying process is characterized by constant temperature and the curing is characterized by constant rate of elevating temperature.....	57
Figure 3.4. Molecular structures of PAAs and the corresponding PIs composed of BPDA-PDA (bottom layer) and BPDA-ODA (top layer). PAA is converted to PI by a dehydration cyclization called imidization reaction	59
Figure 3.5. Design scheme for manufacturing four different bilayer polyimide films.....	61
Figure 3.6. Raman spectrum of PAA solution in the spectral range of 600-1200 cm^{-1} . The peaks appeared at 745 cm^{-1} and 1180 cm^{-1} indicate the N-CH ₃ stretching mode of DMAc and the C-N stretching mode of PAA, respectively.....	63
Figure 3.7. Raman spectra of PAA, partially cured PAA-PI and fully cured PI in the spectral range of 1040 -1220 cm^{-1} . The peaks at 1108 cm^{-1} and 1180 cm^{-1} indicate the C-N-C stretching mode of PI and the C6H2 stretching mode of PAA, respectively	65
Figure 3.8. Raman spectra of the PAA solution. The peak appeared at 742 cm^{-1} corresponds to the DMAc activated by N-CH ₃ stretching mode, and	

1608 cm^{-1} corresponds to the PAA activated by aromatic ring stretching mode	67
Figure 3.9. Confocal microscopic image of the PI cross-section and its contour: (a) 10 μm thick PI (left) and 30 μm thick PI (right), and (b) 3D image of white rectangle designated in (a).....	70
Figure 3.10. Schematic diagram of measuring depth-wise profile of PI chain orientation by detecting: (a) in-plane Raman intensity (I_{xx}), and (b) out-of-plane Raman intensity (I_{zz}).....	72
Figure 3.11. Rate dependent shear viscosities for PAA solutions having different solvent contents. Filled symbols represent PAA-1 (BPDA-PDA) and open symbols PAA-2 (BPDA-ODA).....	74
Figure 3.12. Raman spectra of PAA-1, PAA-2 and their 1:1 mixture	75
Figure 3.13. Schematic diagram for the Raman experiments of (a) PAA-1 and PAA-2 interdiffusion, and (b) solvent diffusion into the dried PAA-1 film	77
Figure 3.14. The measurement of interdiffusion width using X-Z mapping of Raman spectroscopy. (a) Raman spectra of PI-1, PI-2 and their 1:1 mixture. (b) Cross-sectional images of a PI bilayer captured by a microscope and its X-Z Raman mapping result. Blue and red colors in the mapping image are distinguished by different Raman peaks appeared at 735 and 695 cm^{-1} respectively.....	80
Figure 4.1. Depth-wise residual solvent profiles of the PAA film at different drying times for the film of thickness (a) 10 μm and (b) 30 μm	86

Figure 4.2. Depth-wise DOI profiles at different curing temperatures: (●) 150 °C; (▼) 170 °C; (■) 200 °C; and (◆) 350 °C, when the thickness of the final PI film is (a) 10 μm, and (b) 30 μm. The right side of the curve corresponds to the air side	89
Figure 4.3. Polar plots of Raman intensities for the (a) uniaxially extended PI film, and (b) intact PI film.	91
Figure 4.4. In-plane and out-of-plane polarized Raman spectra measured at both air and substrate side of (a) PI 10um, (b) PI 30 μm, and mapping image of Raman anisotropy(I_{xx}/I_{zz}) of (c) PI 10 μm, (d) PI 30 μm. x-axis is longitudinal direction of film in picture (c) and (d)	94
Figure 4.5. (a) Depth-wise Fraser fraction (f) profile of two different PI films, and (b) schematic diagram of depth-wise chain orientation	96
Figure 4.6. Depth-wise residual solvent contents (Left) and DOI (Right) during the drying process through (a) protocol A (120 °C drying), (b) protocol B (140 °C drying), and (c) protocol C (160 °C drying)	99
Figure 4.7. Depth-wise residual solvent content (Left) and DOI (Right) during the curing process through (a) protocol A, (b) protocol B, and (c) protocol C. H is a distance from the substrate and H ₀ is the film thickness, thus H/H ₀ =0 and 1 corresponds to the substrate side and air side, respectively.....	101
Figure 4.8. Degree of imidization during the drying and curing processes through different protocols	104
Figure 4.9. (a) Raman spectra of in-plane and out-of-plane polarization appearing at 1610 cm ⁻¹ for PIs made by different protocols. The spectra were	

obtained in the middle part of the PI cross-section. (b) Fraser distribution function (f) along the film thickness direction. In the graph, $H/H_0=0$ and 1 corresponds to the substrate side and air side, respectively..... 106

Figure 4.10. WAXD reflection patterns of the PI films depending on different protocols 109

Figure 4.11. Temperature dependence of $\tan \delta$ measured by DMA for the PI films depending on different protocols..... 110

Figure 4.12. Temperature dependence of sample length measured by TMA for the PI films depending on different protocols 111

Figure 4.13. Depth-wise volume fraction of PAA-2 (Φ_{PAA2}) measured at different times after a contact with PAA-1. Different pairs of PAA-1 and 2 have different solvent concentrations of (a) 88 wt%, (b) 90 wt%, (c) 91.5 wt%, and (d) 93 wt%. Abscissa was shifted by z_0 that is the depth below which the volume fraction of PAA-2 increases 113

Figure 4.14. Log-log plots of the interdiffusion width $w(t)$ between PAA-1 and PAA-2 at different contact time (t). Different symbols represent PAA-1/PAA-2 pairs having different solvent contents which are indicated in the graph..... 115

Figure 4.15. Interdiffusion data of the cured PI bilayers made by the DML and LBL methods. (a) Variation of PI-2 volume fraction (Φ_{PI2}) measured at different positions on the cross section of the cured PI. Abscissa was shifted by Z_0 where the volume of two PIs is equal (i.e. $\Phi_{PI2}= 0.5$). (b)

The interdiffusion width $w(t)$ of the PI bilayers according to the drying temperature of the bottom layer (T_b) 117

Figure 4.16. Depth-wise solvent content (X) measured at different times after a contact between the dried PAA-1 and 2 solutions. The dried PAA-1 was prepared by drying at different temperatures (T_b) of (a) 100 °C, (b) 130 °C, and (c) 160 °C respectively. Dashed line shows the calculated initial solvent content (i.e. $X=7.3$) of PAA-2 solution, which corresponds to 12 wt% 119

Figure 4.17. Degree of in-plane chain orientation of single and bilayer PI films represented by the Fraser distribution function. PI films were made by (a) DML drying($T_b=100$ °C), (b) LBL drying($T_b=100$ °C), (c) LBL drying($T_b=130$ °C), (d) LBL drying($T_b=160$ °C) 122

List of Tables

Table 3.1. Drying and curing conditions for the different protocols. Sampling time indicates the measurement time during drying and sampling temperature indicates the measurement temperature during curing.....	56
--	----

Chapter 1.

Introduction

1.1. General introduction

Polyimide (PI) has high glass transition temperature, good thermal and mechanical strength, relatively low dielectric constant and thermal expansion coefficient due to the stable chemical structure of imide rings. These properties make polyimide a suitable dielectric for flexible printed circuit boards (FPCBs), alignment layers for liquid crystal displays (LCDs), photoresist, and so on. PI has attracted attention as a transparent substrate or transparent cover for flexible displays or interlayer dielectrics for semiconducting memory devices. [1-7] These new applications require PI films with better thermal, electrical and optical properties. Many studies have focused on overcoming the limitations of conventional PI films by employing new monomers or developing PI nanocomposites with inorganic materials. [8-10] However, processing conditions can also affect the final properties of PI films even with the same chemical structure because different microstructures represented by different degree of in-plane chain orientation are developed when the PI films have different thickness, undergo different thermal histories, or show different behavior of interdiffusion between different layers. Thus, in addition to selecting the appropriate monomers, it is important to understand how the different processing conditions such as film thickness, thermal history, and interdiffusion influences the final microstructure of PI.

Thermally cured PI films are manufactured by drying poly(amic acid) (PAA) solution on a substrate and curing it. During the drying process, PAA is solidified at a temperature usually of less than 130 °C and then imidized to PI by further increasing the temperature up to 350 °C or higher. The polymer chains confined by a substrate are biaxially stretched during solvent evaporation, which preferentially aligns the

chains to the in-plane direction.[11-15] Many studies on the degree of chain orientation in PI films have been conducted using birefringence, [13-18, 42-44] X-ray diffraction [12-15, 29, 30, 45, 46] and polarized ATR/FT-IR.[19-22] In these experiments, the chain orientation of PI was associated with the physical and optical properties of a film such as CTE, elastic modulus, and refractive index. [11, 19, 23-25, 40, 41] Among these, CTE was found to be more affected by the variation of chain orientation such that the lateral CTE decreased considerably when the degree of in-plane chain orientation increased. This is because a strong intramolecular force (i.e., covalent bonds) allows little dimensional change of polymer chains along the chain axis in response to the temperature change, whereas a weak intermolecular (i.e., van der Waals) force makes dimensional change easier in the direction perpendicular to the chain axis. As a result, the lateral CTE decreases when more polymer chains are aligned to the in-plane direction of the film. [23, 26, 27]

The degree of chain orientation that influences the properties of a film can be affected by film thickness. Liou et al. [16] observed that the lateral CTE increased while the vertical CTE decreased when the film thickness was increased from 2.5 μm to 20 μm . The fraction of PI chains aligned to the in-plane direction also decreased with increasing film thickness.[15] Jou et al. [26] compared X-ray diffraction patterns between the in-plane and out-of-plane directions and observed the change in the degree of chain orientation when the film thickness increased. In addition, Hasegawa et al. [11] added perylenebismide dye into a PI film and measured the dichroic absorption of dye molecules according to the film thickness to predict the degree of in-plane chain orientation of PIs composed of different monomers. The results prove that an increased film thickness lowers the degree of in-plane chain orientation, which

affects the physical properties of the PI film. Nevertheless questions remain regarding the depth-wise distribution of chain orientation.

The degree of in-plane chain orientation is also affected by thermal history during the drying and curing processes. Johnson and Wunder [28] measured the imidization degree at different curing rates and temperatures. Nomura and Asano [19] reported that the PI chains were randomly oriented near the substrate when heating was fast, but highly oriented to the in-plane direction when heating was slow. Takahashi et al. [29] observed the variation of chain orientation during the curing process by comparing the reflected patterns of wide angle X-ray diffraction with the transmitted patterns. However, these studies are limited to investigating the effect of the curing conditions, mainly curing rate and final temperature, on the chain orientation of PI and its physical properties. [11, 20, 24, 30] However, they do not consider in the respect of thermal history including drying process and do not address how the microstructure developed during the drying process affects the overall microstructure of the cured PI. In addition, due to the difficulties in characterizing the properties in the film depth direction, only the average properties of bulk film or film surface were investigated. These approaches yield an incomplete depiction of the physical properties given that there is an inhomogeneous distribution of chain orientation along the film thickness.

In order to control the film flatness or to give additional functions to PI film, two or more PIs having different molecular structures are stacked together to make a multi-layer film. Unlike a single layer, the adhesion at the interface becomes a crucial factor in manufacturing multi-layer PI film because poor adhesion can cause partial or complete de-adhesion problems due to the interfacial stress generated at high

temperature processing. The interdiffusion between different layers composed of immiscible or partially miscible polymers is essential to get a good adhesion property, and the difference in CTE of each layer must be minimized to reduce the interfacial stress. [31] Especially in the case of multilayer PI, the amount of solvent diffusion from or toward the other layer in contact is another important factor as it can change the residual solvent content of the layer during the processing. Recently, the direct multi-layer (DML) method that dries several layers of polymer solutions at once has been introduced to make multilayer polymer films in a variety of coating industries, replacing the conventional layer-by-layer (LBL) method in which each layer is dried individually in a consecutive manner. [31-33] When the LBL method is applied to make a PI bilayer film, the interdiffusion width at the interface was reported to decrease as a large fraction of PAA in the bottom layer is imidized to PI before the top layer is coated on it. [34-36] It is because the swelling of the bottom layer by the solvent is hindered as PAA in the bottom layer is converted to PI which is insoluble to the solvent. However, these studies only focused on the submicron-sized thin layers of PI, and the different behaviors of interdiffusion when the DML method is applied have not been explored yet. The most significant difference between the DML and LBL methods is the phase of each layer when they contact. For the DML method, both layers are liquid phase containing relatively larger amount of solvent, while one is solid and the other is liquid for the LBL method. When the two different drying methods are used to make multilayer PI films, this difference can influence the extent of interdiffusion and chain orientation of PIs because both translational and rotational mobilities of polymer chains are directly affected by the amount of solvent. Therefore, it is necessary to understand how different drying methods affect the final

interdiffusion width and the chain orientation of PIs in order to provide a proper functionality to the multilayer PI films without any interfacial failure.

In this thesis, chain orientation of PI and its interdiffusional behavior is introduced. Firstly, the in-plane orientation of cured PI films with different thicknesses is quantified. Residual solvent concentration of PAA during the drying process is measured in the film depth direction with confocal Raman spectroscopy, and observed how the residual solvent affects the subsequent curing process. Polarized Raman spectroscopy is used to quantify the degree of chain orientation in the film thickness direction, and the relationship between the chain orientation of PI and that of PAA is examined. Secondly, the variation of chain orientation is investigated for PI films manufactured by different process protocols, i.e. different drying and curing conditions. The final microstructures of the cured PI films are predicted from the process path designed with two parameters, residual solvent concentration and imidization degree, and they were compared to the degree of in-plane chain orientation. The effect of PI microstructure on the film properties is also examined by comparing the degree of in-plane chain orientation with crystallinity, glass transition temperature (T_g), and TEC. Finally, bilayer PI films having similar molecular structure are manufactured using two drying methods, DML and LBL methods. Different aspects of interdiffusional behavior for different drying methods are explained by the role of solvent. At the same time, the chain orientation of PI bilayer is compared with that of a single layer PI film and the difference is explained in terms of the amount of solvent remaining in each layer after the drying process.

1.2. Outline of the thesis

The thesis consists of background, experimental methods, results and discussion, and summary chapters.

Chapter 2 describes the background of the thesis which is divided into manufacturing process of polyimide, chain orientation, polymer interdiffusion and the confocal Raman spectroscopy. First, the manufacturing process of polyimide film is briefly introduced regarding the precursor preparation and thermal imidization of the precursor, and the drying process of general polymer solution is given a more focus. General theories of polymer chain orientation and its interdiffusional behavior are explained to provide a more clear understanding of the results, and the chapter finishes with introducing the key analytical method employed in this study, the confocal Raman spectroscopy.

Chapter 3 deals with experimental methods used in this study starting with the sample preparation and its characterization. Several experimental methods used to analyze the depth-wise properties of polyimide film are introduced in the sequence of measuring the residual solvent concentration, degree of imidization, and chain orientation. In the last part of the chapter, a novel and simple method employed to observe the polymer-polymer interdiffusion is explained, and general characterization methods of the cured polyimide film is also introduced.

In chapter 4, experimental results are divided into three main parts. The first is to show how the film thickness affects the final chain orientation of polyimide films. Comparing the experimental result with that of previous studies, it is proved how well the new analytical approaches used in this study explain the relatively well-known

phenomena. Second part of the chapter explains the effect of thermal history on the polyimide chain orientation. The results show the final microstructure of the polyimide film can be significantly affected by the processing condition except for the chemical structure. Finally, the interdiffusional behavior between two similar but different polyimides, as well as the chain orientation, is examined in bilayer polyimide system.

Chapter 5 summarizes the results on the works about the chain orientation of polyimide and its interdiffusional behavior affected by drying and curing processes.

Chapter 2.

Background

2.1. Manufacturing processes of polyimide film

A general method of making PI film is mainly composed of 3 processes : preparing a precursor polymer solution, coating and drying, curing processes. When making a precursor solution, the solid content of polymer solution or the molecular weight of precursor should be adjusted to be appropriate to process the coating. During the drying process, a certain amount of solvent in the precursor solution evaporates and the film is solidified with a certain critical percent imidization. Afterwards, the solidified film is passed into the curing process where the film is biaxially fixed by a substrate or a tenter and the precursor is converted to PI. The latent heat of evaporation and heat of the imidization reaction are supplied by hot air, radiation from an electrical heater, or infrared (IR) heater. The final curing temperature is typically greater than 350 °C. In the entire drying and curing process, the area of the film is held almost constant by adhesion to the substrate or by in-plane restraint in the tenter. Because the stress-free state shrinks in-plane, this restraint aligns the chain axes in-plane, which increases the tensile strength and modulus of the film. A schematic diagram of the processes is shown in Figure 2.1.

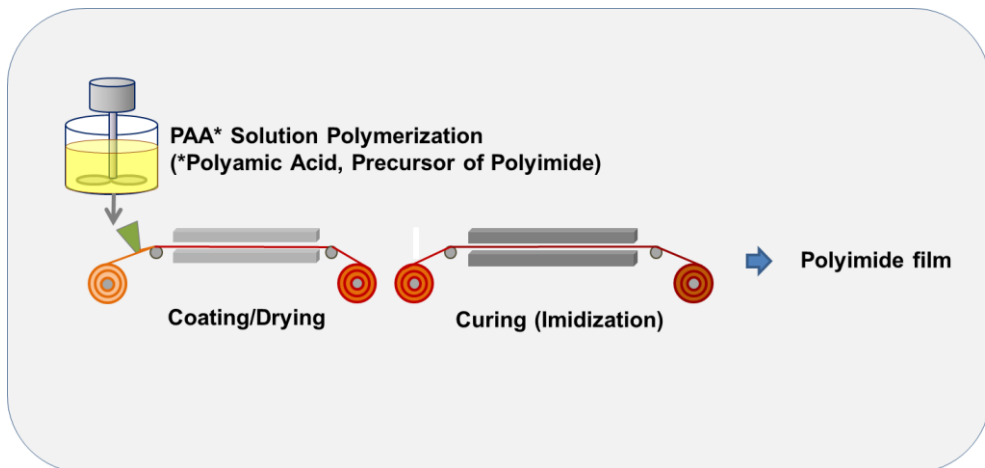


Figure 2.1. Schematic diagram of PI manufacturing process.

2.1.1. Poly(amic acid) preparation

In the general method of polyimide manufacturing, a dianhydride is added to a solution of diamine in a polar aprotic solvents such as N,N-dimethylformamide (DMF), N-methylpyrrolidone and N,N-dimethylacetamide. When a diamine and a dianhydride are mixed in the dipolar aprotic solvent poly(amic acid) (PAA), the precursor of polyimide, is formed as shown in Figure 2.2. The generated PAA is then cyclodehydrated to make a polyimide by thermal heating at elevated temperature or by using chemical dehydrating agents. As the polyimide is usually insoluble, it is processed in the form of PAA accompanied by a solvent. The reaction mechanism of PAA polymerization can be explained by the nucleophilic attack of the amino group on the carbonyl carbon of the anhydride group, followed by the opening of the anhydride ring to form amic acid group. [37] The most important aspect of this process is that it is an equilibrium reaction. It appears to be an irreversible reaction because a high molecular weight PAA is readily formed as long as pure reagents are used. It is because the forward reaction is much faster than the reverse reaction, usually by several orders of magnitude. If the large reaction rate difference is not met, the high molecular weight PAA is not formed. Hence, it is important to examine the driving forces that favor the forward reaction over the reverse reaction. It should also be noted that the acylation reaction of amines is an exothermic reaction and that the equilibrium is favored at lower temperatures.

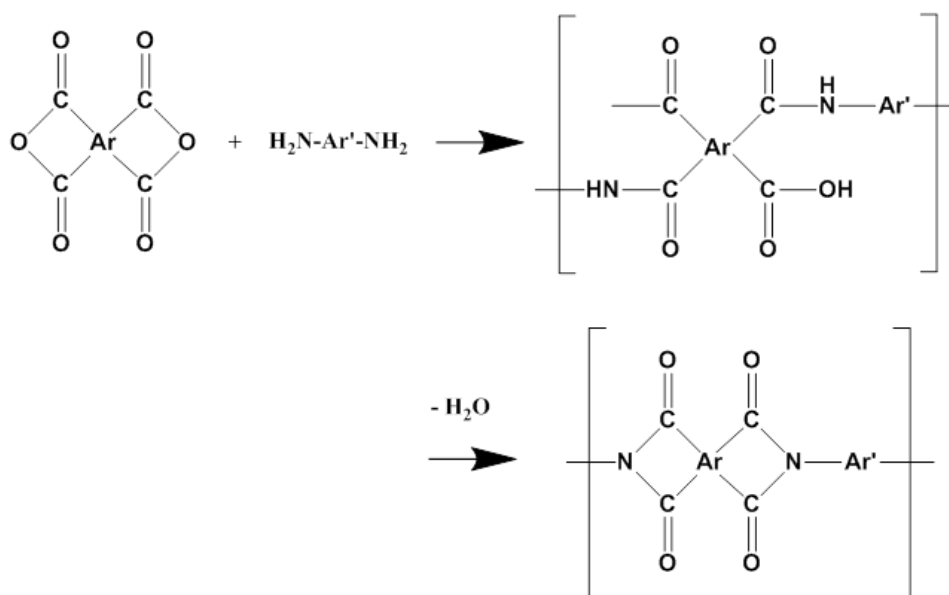


Figure 2.2. Mechanism of PAA and PI formation.

2.1.2. Thermal imidization of PAA

Thermally cured PI films are manufactured by drying PAA solution on a substrate and curing it. During the drying process, PAA is solidified at a temperature usually of less than 130°C and then imidized to PI by further increasing the temperature up to 350°C or higher. The polymer chains confined by a substrate are biaxially stretched during solvent evaporation, which preferentially aligns the chains to the in-plane direction.

Kinetics of imidization

A potential energy diagram for the reactions is shown in Figure 2.3. [37] By reverse reaction, a small portion of the o-carboxycarboxamide can revert to amines and anhydrides. As the temperature increases up to near 250 °C, the anhydride and amine contents drop to almost zero and the majority of o-carboxycarboxamides are converted to imide. It is proved in many studies that the PAA heated to near 300 °C achieves more than 95% imidization. Heating at temperatures above 350 °C for extended periods of time can result in crosslinking. In this condition, polyimides become insoluble to solvents even though it is not clear whether this is due to crosslinking or close chain packing. Crosslinking at this temperature most likely proceeds by a free radical mechanism.

Imidization reaction is known to proceed in two stages under isothermal conditions. [37] At temperatures above 150 °C, imidization proceeds rapidly and is characterized by an initial fast cyclization step that changes into a second, slower cyclization step. The rate constant was found to be constant only in the initial step, and it decreases continuously in the second step until it drops to almost zero. As the imidization

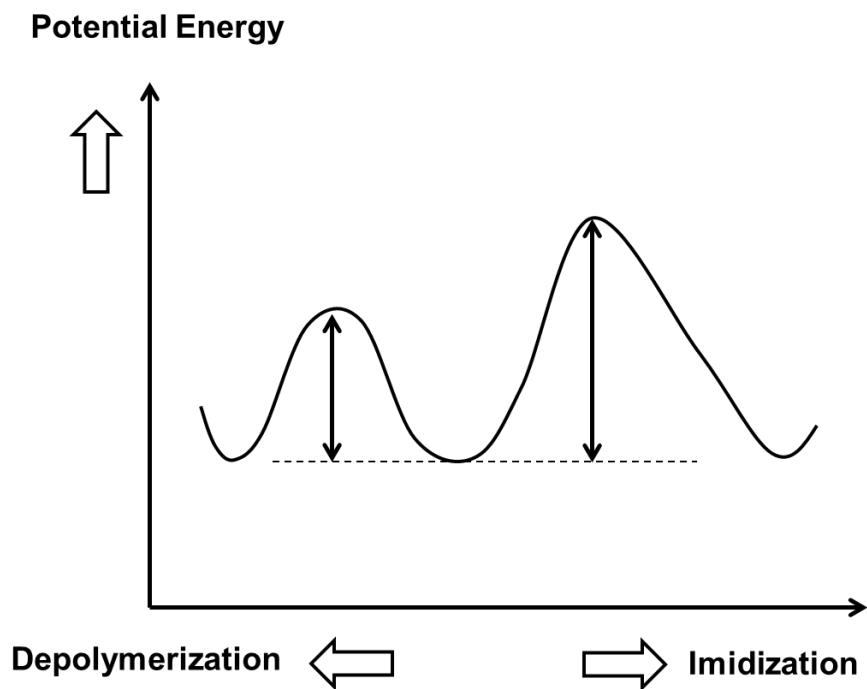


Figure 2.3. Schematic diagram of hypothetical potential energy during imidization. The left peak corresponds to the depolymerization energy and the right peak corresponds to the imidization energy.

temperature increases, the contribution of first step increases, so the degree of imidization becomes higher. And imidization is accompanied by chain scission to anhydride and amine moieties. As a result, these groups are excluded from the cyclization process for a given time. However, as the process proceeds, these groups again react to form amic acid linkages that undergo cyclization again. A drastic change in the slope of cyclization isotherms occurs because the rate at which the amic acid linkages are regenerated in the solid state is slower than the cyclization rate. As the imidization process continues, T_g of the polymer increases so that the polymer changes from a rubbery to a glassy state. This results in the decrease of imidization rate due to the decrease of molecular mobility in the glassy state.

Role of solvents

Imidization reaction can proceed faster in the presence of amide solvents. [19, 36, 38, 39, 47] It is because the solvent molecules allow the reacting groups to attain favorable conformations for imidization and to assist in the loss of the carboxyl proton. Amide solvents are known to form strong hydrogen-bonds with the carboxyl group. As a result, the transfer of a proton to the basic solvent under the imidization conditions seems quite likely. When manufacturing the PI film, different amounts of solvent according to the types of solvent usually remain in the film even after the drying process. And this residual solvent can behave as a plasticizer until the unbound solvent molecules evaporate during the curing process. Thus, the types of solvent used in PAA solution can play an important role in determining the imidization speed, degree of imidization, and even the final chain orientation. And for thicker film, the

solvent molecules stay in the film for a longer time and this also affects these properties.

Role of heating rate

When manufacturing a PI film, heating rate is closely related with the final chain orientation. [11, 20, 24, 27, 48] While the degree of molecular packing of PI chains is increased with the local motion of molecules, high degree of in-plane orientation is achieved by long distance translational diffusion. It means that PI chain should have enough time for rearrangement with a sufficient mobility to get high degree of in-plane orientation. In this regard, faster heating rate of PI can result in lower degree of in-plane orientation because the mobility of PI chain decreases due to the faster evaporation of solvent. At the same time, increasing number of imide rings along the main chain stiffens the backbone and has the effect of slowing the reaction by reducing the availability of suitable conformations for imidization. Especially when the film is thick, it becomes more significant that faster heating rate lowers the degree of in-plane orientation, while there is no difference when the film is thin. However, this is different from the point of local ordering of PI chains in that molecular packing degree is more enhanced by intensive thermal conditions. As a result, it is important to find out the optimized heating rate to avoid unwanted chain orientation which would result in film defects such as a CTE mismatch in multilayer film.

2.2. Drying behavior of polymer solution

Drying of polymer solution basically involves two steps : (a) Diffusion of the solvent towards the film surface, (b) removal of the solvent from the film surface. The resistance to drying related with the diffusion of solvent in the coating is called internal resistance, and the resistance to solvent evaporation at the film surface is called external resistance. Internal resistance generally determines the final residual solvent content after drying.

2.2.1. Two drying regimes of polymer solution

There are two periods of drying that control the speed and amount of solvent evaporation as shown in Figure 2.4. [57-60] The first one is the *constant rate period* and the other is *falling rate period*. The first period is determined by the difference between the partial pressure of the solvent at the surface of the coating. Most of the solvent in the coating is removed during this period. In early stage of the first period, the surface temperature may drop because the latent heat of solvent evaporation has to arrive by heat transfer. And then the coating temperature becomes a steady state, thus the rate of heat supplied from the hot air becomes equal to the rate of heat disappeared by evaporation. During this equilibrium state of heat transfer, the drying rate is constant. This constant rate of drying is the period where the rate of solvent that diffuses from the solution to the film surface is sufficiently faster than the rate of solvent evaporation. This means the slower evaporation rate is the rate determining step, and it is controlled by many factors such as drying temperature, air velocity, solvent concentration, and so on. This constant rate period finishes when the solvent concentration drops so that the solvent diffusion inside becomes slower than the

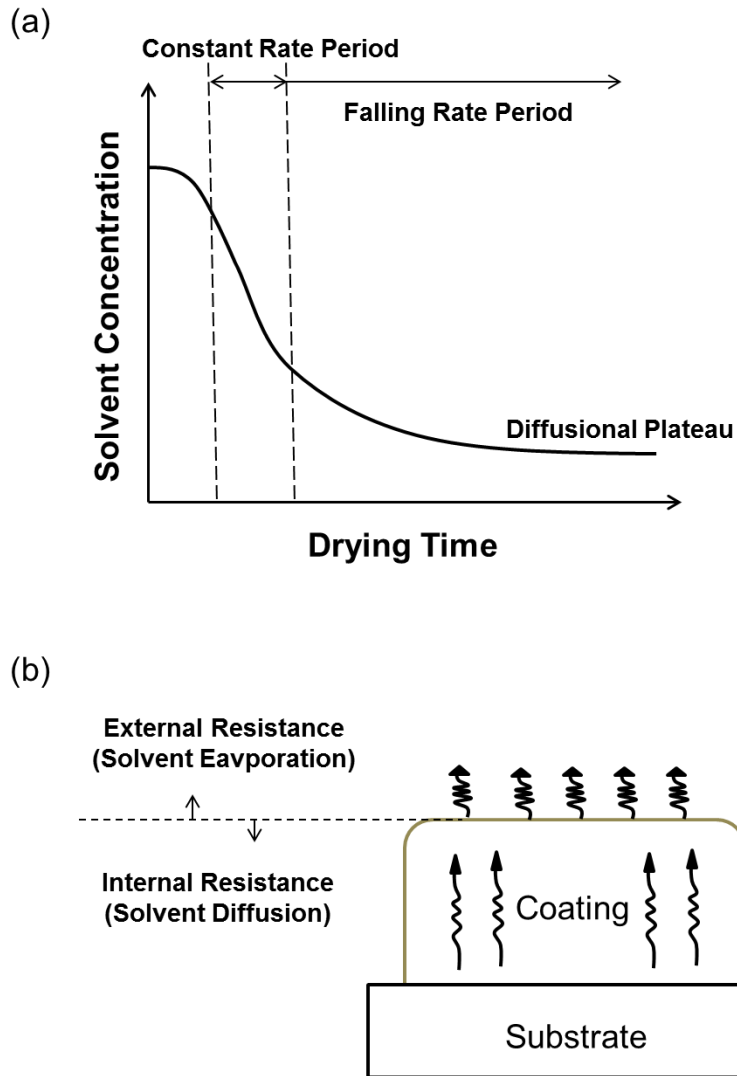


Figure 2.4. Drying mechanism. (a) three characteristic periods of drying, (b) two characteristic resistance of drying.

solvent evaporation at the film surface. The next step is falling rate period. Films are solidified and the rate of solvent diffusion becomes a rate determining step. When internal diffusion controls the solvent evaporation, coating thickness and drying times are important factors which determine the residual solvent amount after drying. As the rate of diffusion is a function of solvent concentration and drying temperature, the rate of drying continuously decreases in this period regarding the constant temperature. At long time of drying afterwards, the rate of solvent evaporation becomes negligible to reach a diffusional plateau.

2.2.2. Stress development in polymer films

Polymeric films as well as most other materials tend to shrink as they dry. [23, 54-56] This is true whether the coating dries due to chemical transformation or purely solvent evaporation. The area of a coating is constrained to remain at its original wet size by adhesion to a normally rigid substrate so volume changes are accommodated by a change in thickness accompanied by fluid flow. After the coating solidifies and can no longer flow, subsequent solvent loss produces an internal strain in the coatings as it proceeds to its final dry state. Even if the viscous component of a film is present, not all this stress relaxes and the remaining residual stresses can affect the final properties of product. This may lead to undesirable defects such as delamination in the region of the coating boundary, cracking on the surface, and in the case of a flexible substrate, wrinkling of the entire system. Additional strains developing in this process of additional mechanical deformation are usually very large, and the associated additional stresses are superposed on the residual stress field developed earlier in the process of drying.

As the concentration gradient is the highest at the top of a drying coating, the stress level is highest there, apart from near the outer edges and any inner edges. The top of the coating is thus where cracks are most likely to initiate and cause defects such as crazing, which is a layer on the surface that is filled with curled pieces separated by small cracks. As the coating dries, it tends to shrink in all directions if it were allowed to do so. However, adhesion of the coating to the substrate is enforced at the substrate, especially at the edges, where the tendency to detach is the highest. Therefore the edge is another site for initiation of cracks. If the bond strength between the coating and the substrate is weak, then crack initiates and propagates between the layers. This is delamination. Even without these cracking failures, the presence of in-plane tensile stress can cause curling of the substrate, which makes it jeopardize the handling of the products in the subsequent processes. Stress gradient through the width of the coating can cause uneven surface and nonuniform coating properties as well.

2.2.3. Stress development in polyimide film

If the PI is deposited on a planar substrate and the coating is constrained by the substrate, the development of biaxial stress is dominated by the mismatch between the CTE of the film and the substrate. [23, 48-53] As the excessive residual stress can result in cracking or delamination of the PI film or film curling, it is important to minimize the CTE mismatch between the film and substrate or between different PI layers. Especially when copper or aluminum metal which has relatively lower CTE than typical PI films is used as a substrate, it is necessary to lower the CTE of the PI film in order to reduce the stress development. At the same time, it has to be considered that relatively flexible and soluble PAA is converted to more rigid PI

during the curing process. In this case, the development of residual stress is also affected by curing process in which solvent evaporates and by-product water is removed. Solvent loss as well as the conversion of flexible PAA to rigid PI critically hinders the polymer molecule to relax. These origins of stress development are integrated in concept of intrinsic stress and thermal stress. The intrinsic stress is related to the volume shrinkage by solvent evaporation while the thermal stress is related to the CTE mismatch between the film and the substrate during the cooling process from the final curing temperature. If the thickness of the film is negligible to the substrate thickness, the thermal stress between two different temperatures can be expressed by [23] :

$$\sigma_f = \int_{T_1}^{T_2} \frac{E}{(1-\nu_f)} (\alpha_s - \alpha_f) dT \quad (2.1)$$

where σ_f is the film stress, T_c is the final curing temperature, E_f is the Young's modulus of the film, α_s and α_f are the CTEs of the substrate and the film, and ν_f is the Poisson's ratio of the film. Here, the T_1 becomes T_g , the glass transition temperature when T_1 is small than T_g .

2.3. Chain orientation of rod-shaped polymers

2.3.1. General introduction of polymer chain orientation

Macroscopic properties of materials are closely related to their microstructures. For semicrystalline polymers, the ratio of crystalline and amorphous phases and chain orientation are considered to be critical factors in understanding the macroscopic properties. [61] Among these, Chain orientation is a unique phenomenon to polymer system. The linear chain makes it possible to obtain strongly anisotropic properties. The anisotropy arises when molecules are aligned to a specific direction and the intrinsic properties of a polymer chain strongly depend on its orientation. The strong covalent bonds along the chain axis and the weaker bonds in perpendicular directions result in a significant anisotropy such as birefringence and anisotropic tensile strength. In semicrystalline polymers, the crystalline and amorphous parts show different degree of orientation. Several techniques of chain orientation measurement exist such as birefringence, wide-angle X-ray diffraction (WAXD), nuclear magnetic resonance (NMR), fluorescence measurements, and vibrational spectroscopic measurements such as polarized FT-IR and polarized Raman spectroscopy. [11, 14, 21, 22, 29, 40, 42, 62]

Each technique has its advantages and disadvantages. Birefringence measurements are simple and reasonable but give information only about the distributions averaged over the sample, while NMR is very costly. Molecular orientation distributions in the crystalline phases only are obtained by WAXD, although this is only the technique allowing the precise distribution to be obtained, since all coefficients in the orientation distribution functions can be determined. For spectroscopic techniques, fluorescence

spectroscopy gives information about the molecular orientation distribution in phases only where fluorescent probes can migrate. Infrared (IR) dichroism measurements are capable of evaluating the molecular orientation distribution in both the crystalline and amorphous phase. However, the distributions obtained by IR spectroscopy lack accuracy because only one coefficient for the distribution functions can be determined. [21, 40] At the same time, the sample is required to be highly transparent and thin for the absorbance measurements. In this regard, polarized Raman spectroscopy can be a powerful tool to obtain information about chain orientation. [62-66] Similar to IR dichroism measurements, it is possible to analyze the distributions in both the crystalline and amorphous phases. Since this technique is compatible with optical microscopy, it is also suitable for study of chain orientation in the material at the micron size scale or in a micron region in the material. Furthermore, this technique has considerable potential for depth-wise profiling of film cross-section owing to its non-destructive nature.

2.3.2. Chain orientation measurement using polarized Raman spectroscopy

Polarized Raman spectroscopy is a vibrational technique that is widely used for the directional study of polymer chains. [62-69] When a laser beam with electric vector E is incident on a molecule, an electric dipole P is induced according to the relation,

$$P = \alpha E \quad (2.2)$$

Where α is the polarizability of the molecule. In general, the induced polarizability is not in the direction of the incident beam, thus it is expressed by a tensor quantity.

$$\begin{aligned}
 P_x &= \alpha_{xx}E_x + \alpha_{xy}E_y + \alpha_{xz}E_z \\
 P_y &= \alpha_{yx}E_x + \alpha_{yy}E_y + \alpha_{yz}E_z \\
 P_z &= \alpha_{zx}E_x + \alpha_{zy}E_y + \alpha_{zz}E_z
 \end{aligned} \tag{2.3}$$

Where the quantities α_{FF} are independent of the components of the electric vector but are dependent on the orientation of the molecule relative to the space fixed axes, X, Y, Z. The intensity of the Raman scattered light is proportional to the square of the magnitude of P.

In general, the light from a radiation source involves waves with no preferential direction of the electric field vector. When it encounters a substance, the light interferes with the atoms and induces a dipole moment in the material. The degree of the interference depends on the angle and the magnitude of the polarizability. So, it contains directional information about the orientation of the differential polarizability. The directional information can be obtained if polarized light with a specific electric vector is used as the incident beam. In polarized Raman, the Raman scattering is observed as a result of the interference of the polarized light with the vibrating molecules. Furthermore, by means of an analyzer, which is another polarizer before the detector, the precise directional information about the differential polarizability of the molecules can be obtained. In Figure 2.5, general components for the polarized Raman measurements are represented.

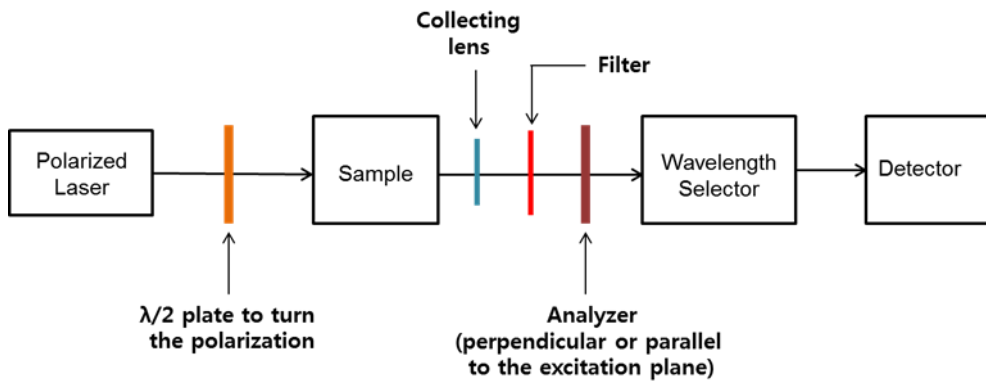


Figure 2.5. Schematic diagram of main components in polarized Raman spectrometer.

Assume that the excitation is done by light propagating in the X direction as shown in Figure 2.6. The scattered light is measured in the Y direction and the optical axis of the sample at which molecules are oriented is parallel to the Z direction. Excitation can be done with light polarized either in the Y or Z direction. The scattered light is measured with Z or X polarization. Four different combinations of polarization can be applied to the geometry of the sample like :

Polarization direction		Notation
Excitation	Scattering	
Z	Z	ZZ
Z	X	ZX
Y	Z	YZ
Y	X	YX

The intensities of Raman spectrum measured in each of these spectra are proportional to the squares of the components of the tensor $\alpha(F)$ defined in the space fixed coordinate system F. in order to express the measured elements $\alpha_{FF'}^2$ in terms of the elements of the tensor $\alpha(g)$ defined in the molecular coordinate system g, the transformation matrix $\Phi(F,g)$ is used and averaged over all the space like :

$$I_{ff'} \sim \alpha_{FF'}^2 = (\sum_{gg'} \Phi_{Fg} \Phi_{F'g'} \alpha_{gg'})^2 \quad (2.3)$$

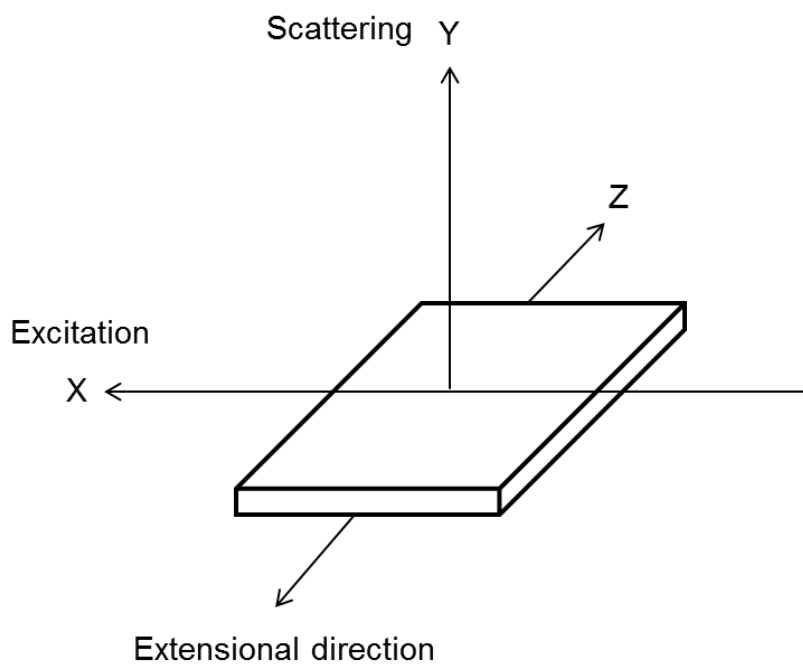


Figure 2.6. Main directions of film extension, light source excitation, and light scattering.

Perfect uniaxial orientation

The longitudinal axis z is put fixed parallel to the stretching direction Z , while the x and y axes are isotropically distributed around this direction. In this case the transformation matrix has the simple form like :

$$\emptyset(F, g) = \begin{pmatrix} \cos \emptyset & -\sin \emptyset & 0 \\ \sin \emptyset & \cos \emptyset & 0 \\ 0 & 0 & 1 \end{pmatrix} \quad (2.4)$$

Applying Equation 2.3, the following expressions are obtained for the intensities measured in the different polarized spectra :

$$I_{ZZ} \sim \alpha_{zz}^2$$

$$I_{ZX} \sim \frac{1}{2}(\alpha_{zx}^2 + \alpha_{zy}^2)$$

$$I_{YZ} \sim \frac{1}{2}(\alpha_{xz}^2 + \alpha_{yx}^2)$$

$$I_{YX} \sim \frac{1}{8}[(\alpha_{xx} - \alpha_{yy})^2 + (\alpha_{xy} - \alpha_{yx})^2 + 2(\alpha_{xy}^2 + \alpha_{yx}^2)] \quad (2.5)$$

Random orientation

Applying of Equation 2.3 to random orientation case, the meaningful intensity detected in Z direction is obtained like :

$$I_{ZZ} \sim \frac{1}{45}(45\alpha^2 + 4\gamma^2 - 5\delta^2) \quad (2.6)$$

Where α^2 , γ^2 , and δ^2 are three invariants of the scattering tensor, called isotropy, anisotropy and asymmetry invariants. Full expressions of each invariant are described in Chapter 4.3.3.

Partial orientation

In case of polymer drying, polymer chains tend to partially orient to the in-plane direction. It can be described as that a fraction f of the molecules is oriented with the longitudinal axes of the molecules in the direction of film plane, whereas the fraction $1-f$ is randomly oriented. [62, 69] Therefore, the meaningful intensity detected in Z direction can now be expressed by :

$$I_{ZZ} \sim f\alpha_{zz}^2 + \frac{1}{45}(1-f)(45\alpha^2 + 4\gamma^2 - 5\delta^2) \quad (2.7)$$

2.4. Interdiffusion between two different polymers

2.4.1. Polymer/polymer interfaces

Polymer interface is important as it significantly affects adhesion property in multilayer film. Figure 2.7 shows an interfacial region between two different polyimides measured by Raman spectroscopy. The change in interface structure is related with the diffusion of polymer chains through the contact area between two polymer components. The mixing behavior at the interface between two dissimilar

polymers, polymer A and B, can be explained by Flory-Huggins theory. [61, 70, 71] It provides an expression for the change in Gibbs free energy on mixing as :

$$\frac{\Delta G_m}{RT} = \frac{\phi_A}{M_A} \ln \phi_A + \frac{\phi_B}{M_B} \ln \phi_B + \chi \phi_A \phi_B \quad (2.8)$$

Where Φ_A , Φ_B are volume fractions, M_A , M_B are degree of polymerization of polymer A, B, respectively and χ is the Flory interaction parameter. The first two terms in the right part of the equation are configurational entropy of mixing. They are negative and usually very small because M_A and M_B are very larger for polymers. On the other hand, χ is negative so that most polymers are immiscible. The lack of miscibility between polymers limits the interdiffusion of polymer chains across the interface. This limitation results in a narrow overlap between two polymer layers. The length scale of transition zone between two polymer layers is usually referred to as the polymer interdiffusion width. This interdiffusion width play a critical role in many polymer industries as it directly affects the bonding properties.

For many industrial applications, there is always needs for good adhesion strength and strong interactions between different polymer layers. Therefore it is necessary to predict and measure the concentration variation of different polymers near the polymer interface. Helfand and Tagami firstly predicted the characteristics of the interface between two immiscible polymers using a self-consistent field theory. [72] They derived analytical expressions for the interdiffusion width, w_h , between two homopolymers as :

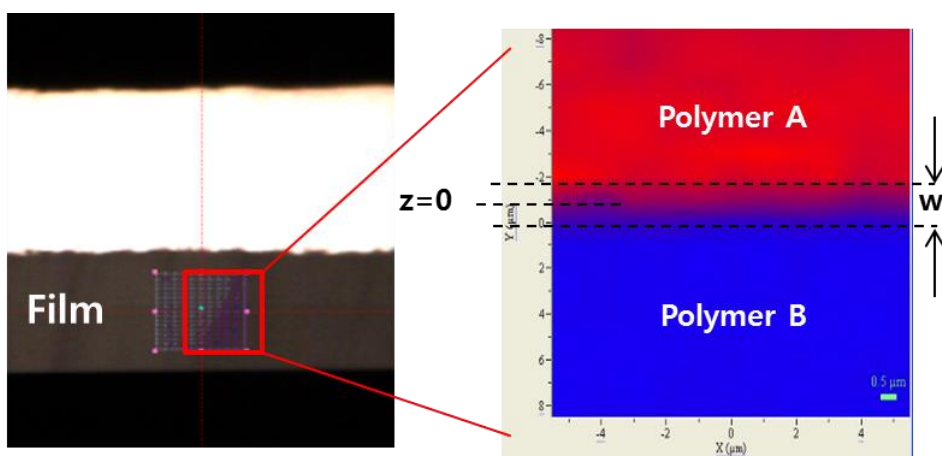


Figure 2.7. Cross-sectional image of a bilayer PI film (Left) and its Raman mapping image (Right).

$$w_h = \frac{2b}{(6\chi)^{0.5}}$$

$$b = \sqrt{\frac{b_1^2 + b_2^2}{2}} \quad (2.9)$$

where b_1 and b_2 are the statistical lengths for the two homopolymers. The polymer volume fraction profile at the interface can be given by :

$$\phi(z) = \frac{1}{2} \left(1 - \tanh \left(\frac{2z}{w_h} \right) \right) \quad (2.10)$$

where z is a coordinate normal to the interface. The general volume fraction profile for one composition along the z -axis near the interface is shown in Figure 2. 8. This simple equation relates the interfacial width to the interaction parameter χ . The interdiffusion width used here equals the full width at half maximum (FWHM). The FWHM value of a one-dimensional interface profile can be calculated also from the root mean square (RMS) roughness, σ_R , of a locally sharp interface as :

$$w = \sqrt{2\pi} \sigma_R \quad (2.11)$$

when considering the finite molecular weight effect, this w can be correlated as :

$$w = w_h \left[1 + \ln 2 \left(\frac{1}{\chi N_A} + \frac{1}{\chi N_B} \right) \right] \quad (2.12)$$

where N_A and N_B are chain lengths of two polymers. This equation is valid for strongly immiscible polymer systems where the interdiffusion width is smaller than the chain radius of gyration. If χ is large, the contribution of chain length becomes smaller. Based on this theory, χ plays a crucial role in determining the extent of interdiffusion width.

2.4.2. Interdiffusion at Polymer interfaces

Interdiffusion of polymer chains is related with the molecular motion. Edwards and de Gennes first developed the reptation model to describe the diffusion of polymer chains in an entangled system. [32, 70] This model looks an individual chain as diffusion freely under the assumption that each chain is located in a tube generated by chain entanglements. Time scales regarding the reptation model can be divided into 3 : the Rouse entanglement time (t_e), the Rouse relaxation time (t_r), and the reptation time (t_d). t_e shows the segmental diffusion for distances corresponding to the diameter of the tube. For a diffusion time smaller than t_e , the movement of the segments is not constrained by the virtual tub and the mean square displacement of a chain segment, $\langle r^2 \rangle$, is proportional to $t^{1/2}$. At t_e , the displacement is approximately decided by tube diameter. The Rouse relaxation time, t_r , is the time over which the motion of a segment becomes affected by the connection in an entire chain. For $t_e < t < t_r$, the movement is hindered by entanglements and $\langle r^2 \rangle$ becomes proportional to $t^{1/4}$. The reptation time, t_d , is the time required for a chain to escape from its original tube, it is expressed by :

$$t_d = \frac{R_g^2}{3\pi^2 D_s} \quad (2.13)$$

Where D_s is the self-diffusion coefficient. For $t_r < t < t_d$, chains move by reptation and $\langle r^2 \rangle$ is proportional to $t^{1/2}$. For $t > t_d$, chains are diffused by normal Fickian diffusion by which $\langle r^2 \rangle$ is proportional to t . The time dependence of the interface broadening $w(t)$ to $\langle r^2 \rangle$ can be expressed by :

$$w(t) = \sqrt{\frac{\langle r^2 \rangle}{3}} \quad (2.14)$$

The factor $1/3$ is due to the fact that only the movement of molecules is seen in one dimension.

Different from freely moving polymer chains, the interdiffusion between two immiscible polymers shows different aspect of diffusional behavior. The interdiffusion rate can be expressed by the mutual diffusion coefficient, D . Generally, two models, the fast and the slow theory, are used to explain this movement. In fast theory, D is given by :

$$D = (\phi_B D_A N_A + \phi_A D_B N_B) \cdot \left[\frac{\phi_A}{N_B} + \frac{\phi_B}{N_A} - 2\chi\phi_A\phi_B \right] \quad (2.15)$$

Where N_A and N_B are degrees of polymerization, D_A and D_B are the tracer diffusion coefficient of polymer A and B. If one polymer diffuses much faster than the other, the faster polymer determines the interdiffusion coefficient D in this case.

For the slow theory, on the other hand, shows :

$$D = \left(\frac{1}{\frac{\phi_B}{D_A N_A} + \frac{\phi_A}{D_B N_B}} \right) \cdot \left[\frac{\phi_A}{N_B} + \frac{\phi_B}{N_A} - 2\chi\phi_A\phi_B \right] \quad (2.16)$$

This equation implies that the diffusion of faster moving polymer is slowed down by the other component. If the two polymers are same (i.e. $N_A=N_B$, $D_A=D_B$), the two theories become the same. However, these theories assume that polymer chains are flexible and the diffusion is isotropic, but chain orientation can affect the diffusivity of polymer chains reducing the movement perpendicular to the direction of orientation. It was reported that rod-like polymer chains require deeper interpenetration to achieve sufficient adhesion compared with flexible polymers in multi layer system.

2.4.3. Interdiffusion between partially miscible polymers

Mutual diffusion between miscible polymers is well studied and understood, but little is known about the kinetics of interdiffusion between immiscible or partially miscible polymers. This is important because most binary polymer pairs show little compatibility at accessible temperature. When two different polymers contact, if polymers A and B are compatible, the initial sharp interface will be broadened as a result of Fickian diffusion. But two different polymers in contact do not interdiffuses freely, and an interfacial zone of finite width separates them at equilibrium. Interdiffusion across an interface between two polymers which are not fully miscible is limited to a region of finite width (i.e. interdiffusion width) at long times. [73-75] This immiscibility arises from a low combintional entropy of mixing which scales inversely with the polymerization degree, N , with interactions between two polymers.

If the interdiffusion width, w , is defined by the reciprocal of the maximal concentration gradient across the polymer A and B interface, the width w increases with time slower than that of typical Fickian type diffusion of $w(t) \sim t^\alpha$. Different from phase separation, interfacial mixing occurs by interdiffusion which is driven by thermodynamic forces. This interdiffusion is dependent on thermodynamic conditions such as molecular weight, temperature, and interaction parameter between two polymers. [76-79] A mean-field approach shows that the exponent α in a scaling law, $w(t) \sim t^\alpha$ is ranged between 1/4 and 1/2 near the critical temperature of the phase separation. And it also depends strongly on the definition of interdiffusion width as well.

2.4.4. Polymer interface and adhesion

Molecular interactions at the interface make adhesion. [70, 71] There are three ways to provide adhesion between two different polymers. They are (a) van der Waals force or hydrogen bonding, (b) chain entanglements, and (c) chemical bonding. Among these, chemical bonding is not often encountered as it needs chemical reaction between two polymers. For polymer pairs having large value of χ , the interdiffusion width is narrow and chains are hard to interpenetrate to the other polymer matrix. Thus, only overcoming a weak van der Waals force is sufficient to detach the two polymers in contact. A simple calculation based on van der Waals force between two polymers showed that the adhesion strength is on the order of mJ/m. But the actually measured level of adhesion was on the order of J/m. This shows the meaningful contribution of polymer entanglement. It is widely proved that the adhesion between two polymers is controlled by the degree of entanglement between them.

In order to explain how the entanglements can enhance the adhesion strength, three active adhesive failure mechanisms were proposed. They are (a) chain scission, (b) chain pullout, and (c) crazing. The maximum value of G_c , the energy necessary to make a crack, that can be obtained by chain scission or chain pullout is relatively low. As shown in Figure 2.9, the region in which each failure mechanism dominated is closely related with the interdiffusion width. The crazing mechanism corresponds to a relatively strong adhesion. At a weak interface, the adhesion failure is mostly come through chain scission or chain pullout, and crazing becomes dominant as the interdiffusion width increases. Once after this transition is passed, G_c comes to a plateau and becomes independent of the interdiffusion width because the failure stress can be maintained by the fibrils in the crazing zone. This increase arises from the onset of sufficient entanglements to raise the stability of the fibrils of an interfacial craze to the level of a craze occurring in the bulk homopolymer.

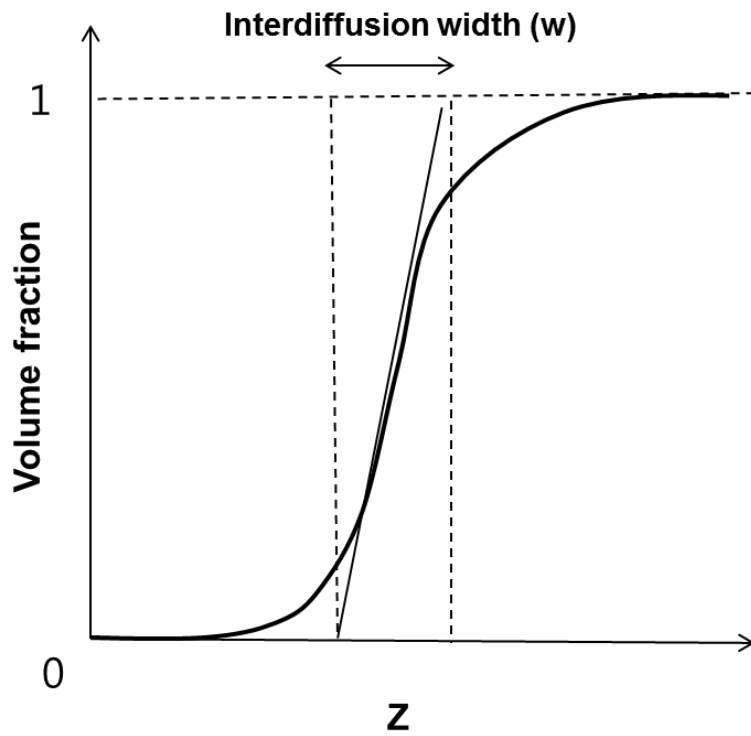


Figure 2.8. Graphical representation of interdiffusion width (w) defined by maximal volume fraction change at the interface.

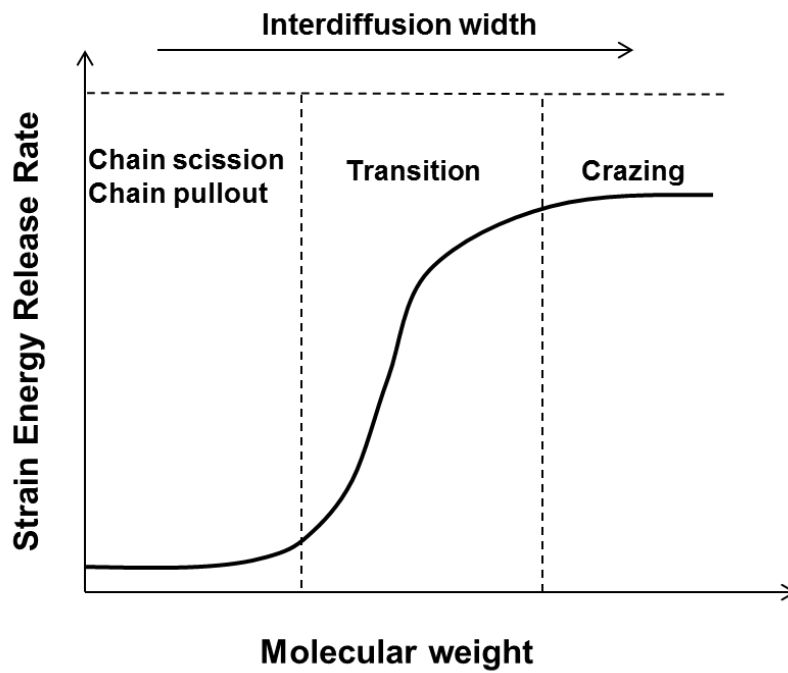


Figure 2.9. Schematic representation of the strain energy release rate depending on the molecular weight of a polymer.

2.5. Confocal Raman spectroscopy

2.5.1. Principle of Raman scattering

Raman scattering is considered as the inelastic scattering of light interacting with molecules. [68] When incident light encounters a molecule, the electric field of the light induces a dipole moment in the molecule due to its polarizability. The amount of the induced moment is proportional to the polarizability of the molecule. The excited molecule, then, relaxes to a higher level and the emitted photon has lower energy than the exciting laser light. Usually the Stokes region of the Raman spectrum is more intense than the anti-Stokes region as most of molecules are on the ground vibrational level at room temperature. [80] The energy of a vibrational mode depends on the molecular structure and environment. Atomic mass, bond order, molecular substituents, molecular geometry and hydrogen bonding all affect the vibrational force constant which, in turn dictates the vibrational energy. Vibrational Raman spectroscopy is not limited to intramolecular vibrations. Crystal lattice vibrations and other motions of extended solids are Raman-active.

2.5.2. Principle of confocal Raman spectroscopy

The confocal Raman spectroscopy consists of Raman spectroscopy and microscopy. [80, 81] After observing the specimen with microscopy, the point observed is then measured with Raman spectroscopy. The confocal Raman microscope focuses a laser beam down to a small volume and is operated readily in a confocal mode by placing an aperture at a back focal plane of the microscope. The aperture improves the lateral and axial spatial resolution of the microscope, allowing nondestructive depth profiling

by acquiring spectra as the laser focus is moved incrementally deeper into a transparent sample. This approach often is termed “optical sectioning,” as opposed to mechanically cutting a cross-section and scanning the laser beam laterally across the section. Confocal Raman microscopy can be applied in two ways. The first involves plotting the intensity of a component specific band as a function of the distance from the sample surface. This reveals compositional or structural gradients as a depth profile. The second approach is to attempt to acquire a pure spectrum of a buried structure for identification purposes. Both of these applications require knowledge of the exact size and position of the microscope focal volume as it moves deeper into the sample.

With these advantages, a few studies have been conducted using confocal Raman spectroscopy to observe the depth-wise solvent concentration of dried films. [82-85] Confocal Raman spectroscopy is an effective method of measuring the solvent concentration in a film because it enables depth-wise profiling of film composition with non-contact and non-destructive manner as mentioned above.

Intensity of Raman scattering

The intensity of Raman scattering is described by the following equation. [82]

$$I \sim N \cdot I_0 \cdot \left(\frac{d\sigma}{d\theta} \right) \quad (2.17)$$

where N is the number of scattering molecules per unit volume, I₀ is the intensity of the laser, and (dσ/dθ) is the differential scattering cross-section. If the intensity of the incident laser is constant the intensity of the scattered light is proportional to the

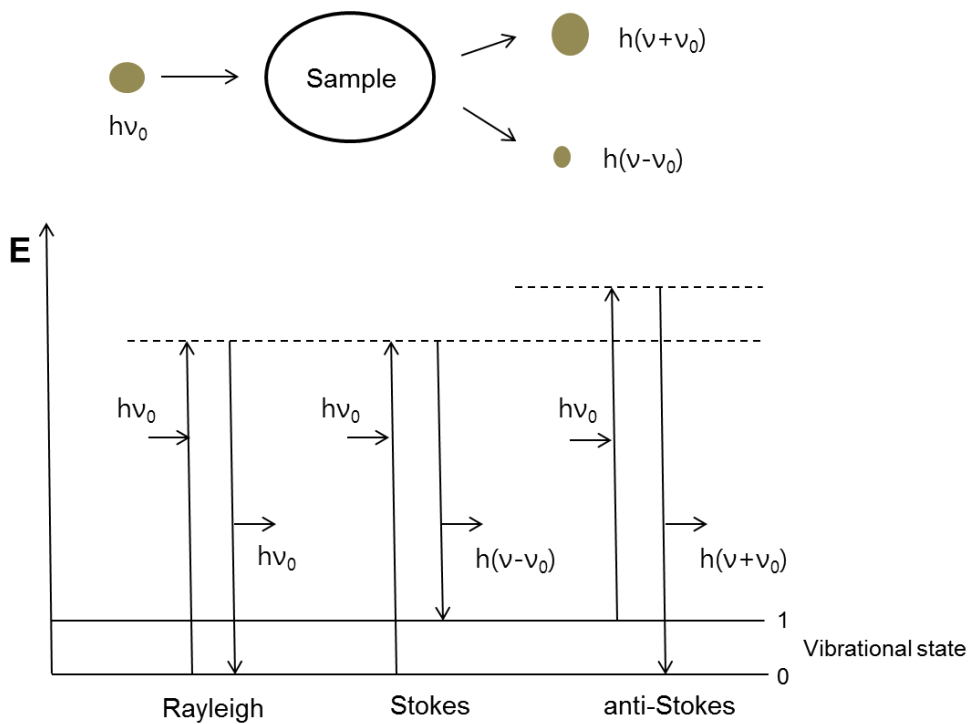


Figure 2.10. Schematic diagram of energy level before and after the light excitation.

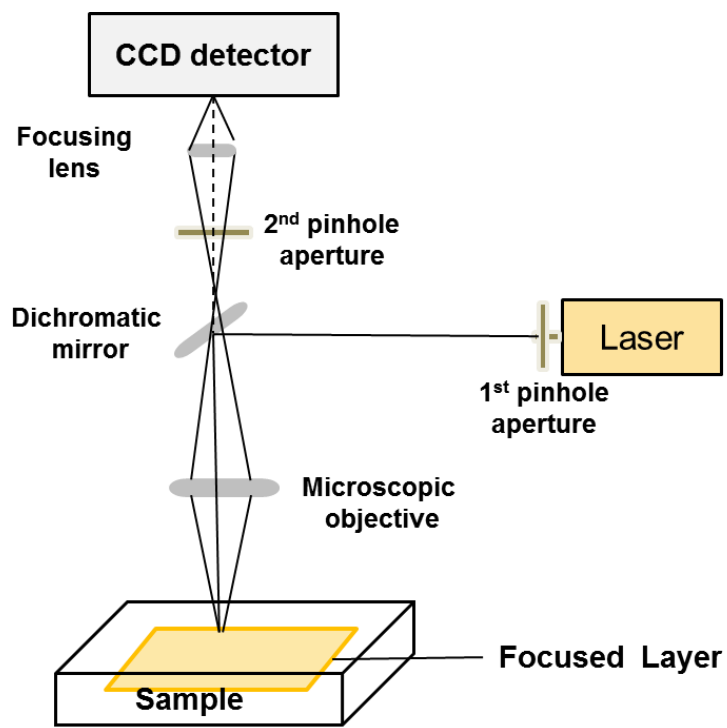


Figure 2.11. Schematic diagram of confocal Raman spectrometer.

number of scattering molecules activated. Raman calibration makes it possible to quantitatively analyze the chemical compositions using the linear relationship between the number of scattering molecules and the measured intensity. The detailed procedure of Raman calibration is shown in Chapter 3.1.

Depth resolution of confocal Raman spectroscopy

Figure 2.12 shows the simple representation of dispersive Raman spectroscopy combined with CCD (charge coupled device) detector. A sample is firstly put on the sample holder and a specific point is focused by observing with microscope. The laser beam encounters the point and only the scattered light from the sample that passes through a small pinhole is come into the CCD detector to generate the Raman spectrum. The first pinhole in Figure 2.12 reduces the amount of scattered light and the second pinhole is contributed to eliminate the scattered light that is out-of-focus.

To understand the intrinsic and variable depth resolution of Raman spectroscopy is important in Depth-profiling of chemical composition. Depth resolution mainly depends on two factors. The one is the volume of the laser focus and the other is how the scattered light is come back into the detector through the pinhole aperture. The limiting depth of focus (DOF) can be expressed by [81] :

$$\text{DOF} = \frac{2.2 n \lambda}{(NA)^2} \quad (2.18)$$

where n is refractive index of the objective lens or immersion medium, λ is the light wavelength, and NA is the numerical aperture of the focusing lens. NA can be expressed by $n \sin \theta$ where the θ is depicted in Figure 2.12. This equation shows that

the depth resolution is improved proportional to the NA. For example, a depth resolution of nearly 3 μm is achieved when using the He-Ne laser with 633nm wavelength, $n=1.4$ (glass), and $NA=0.75$. However, this concept of intrinsic depth resolution is incomplete to explain the varied depth resolution often encountered in depth-profiling of chemical composition. Expressing the focusing depth from the sample surface with z , $z=0$ when the laser beam is focused on the sample surface and d becomes positive when the focusing position goes down into sample. If z is positive and a sample with $n>1$, the lights are refracted and the measured laser intensity distribution becomes distorted. (Figure 2.12) Any light that passes into a sample in air suffers this refraction problem following Snell's law (i.e. $n = \sin\theta_i / \sin\theta_t$), where θ_i and θ_t are the angles of incidence and transmission with respect to the surface normal as shown in Figure 2.12. When $n>1$, the focal point lies deeper at z' . The ratio of refracted and nonrefracted position can be expressed by :

$$\frac{z'}{z} = \frac{\tan\theta_i}{\tan\theta_t} \quad (2.19)$$

In the equation, z'/z has a minimum value of n as it approaches to n when θ_i tends to zero, and increases as θ_i becomes larger.

To calculate the varying DOF in more detail, it is necessary to calculate the focal depth as a function of the radial coordinate of each ray leaving the objective. If the diffraction is negligible, focal depth has a simple solution as :

$$z' = z \times \left(\frac{r^2 NA^2 (n^2-1)}{R^2(1-NA^2)} + n^2 \right)^{0.5} = z \times \left(k^2 \times \frac{NA^2 (n^2-1)}{(1-NA^2)} + n^2 \right)^{0.5} \quad (2.20)$$

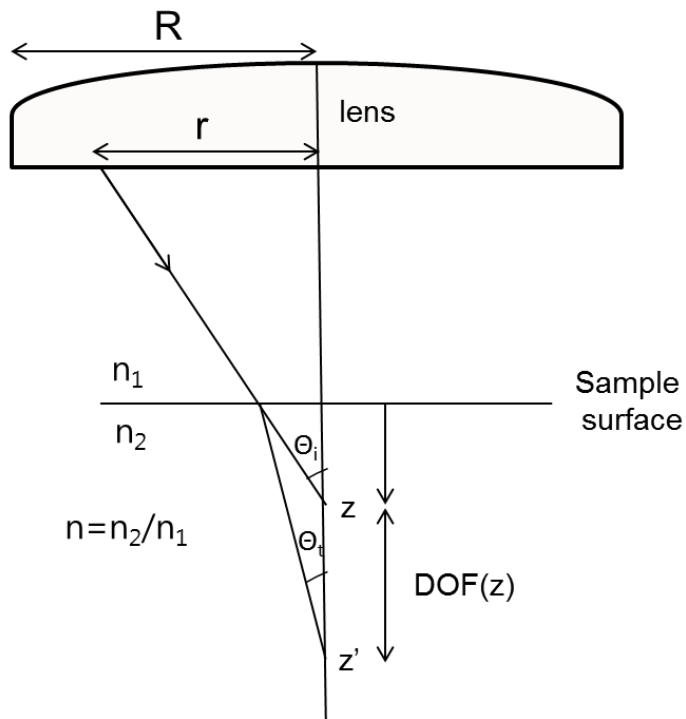


Figure 2.12. Depth of focus depending on the refractive index difference. Marginal lights are focused deeper position.

where r is the radius of a specific ray passing the lens, R is the maximum radius of lens, and k is defined by r/R . This equation shows the true point of focus (z'). It is obvious that lights that originate at different radii on the objective are focused to a different depth. The ratio of the refracted and non-refracted focal depth increases with both m and NA . Now, the varying depth of focus (DOF) can be defined as the difference between the maximum and minimum depths of focus.

$$DOF(z) = z_{k=1} - z_{k=0} = z \times \left\{ \left(\frac{r^2 NA^2 (n^2 - 1)}{R^2 (1 - NA^2)} + n^2 \right)^{0.5} - n \right\} \quad (2.21)$$

This implies that the depth resolution diminishes linearly as measuring position becomes deeper and increasing the aperture makes a worse depth resolution. This works the opposite way to the effect of diffraction, and if the NA is reduced too much the broadening due to diffraction will dominate.

Chapter 3.

Experimental methods

3.1. Sample preparation and characterization

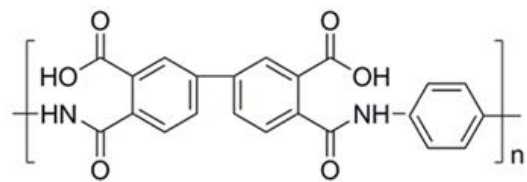
For Chapter 4.1

PAA preparation

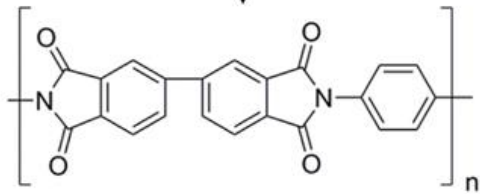
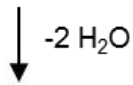
The starting materials used in this study were 3,3',4,4'-biphenyltetracarboxylic acid (BPDA, Ube Industries) and p-phenylene diamine (PDA, DuPont). N, N-dimethylacetamide (DMAc, Sigma-Aldrich) was used as a solvent. 2.0 g of PDA (0.02 mol) was put in a sealed flask containing 55 g of DMAc. After PDA was dissolved in DMAc, 5.5 g of BPDA (0.02 mol) was added to the flask and mixed overnight at room temperature. The viscosity of the prepared PAA solution was about 20 Pa·s at the shear rate of 1 s^{-1} , and the intrinsic viscosity was 1.9 (dl/g). The molecular structures of PAA and the corresponding PI are shown in Figure 3.1.

Calibration of Raman intensity

A calibration needs to be conducted in advance to relate the Raman intensity with the solvent concentration before measuring the residual solvent in depth direction. For this purpose, five PAA solutions having different concentrations were made by diluting the original PAA solution, and the Raman spectra were measured for each solution. In the measured spectra, the N-CH₃ stretching mode which appears at 745 cm^{-1} was used for a characteristic peak of DMAc, and the C-N stretching mode at 1180 cm^{-1} was used for PAA. As the intensity of each Raman peak is proportional to the amount of the corresponding component in the polymer solution, the solvent concentration can be obtained from the following relationship [82] :



Poly(amic acid)



Polyimide

Figure 3.1. The molecular structure of poly(amic acid) and polyimide composed of BPDA and PDA.

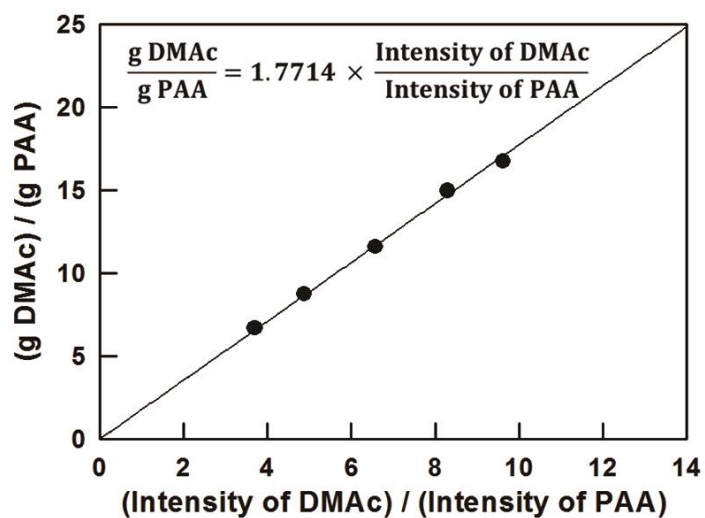


Figure 3.2. Raman intensity calibration graph plotted by solvent concentration against Raman intensity ratio between DMAc and PAA.

$$\frac{I_s}{I_p} = \left(\frac{\partial \sigma_s / \partial \theta}{\partial \sigma_p / \partial \theta} \frac{M_s}{M_p} \right) (X_s) \quad (3.1)$$

Here, I is the intensity of the Raman peak, σ the scattering cross section, θ the spatial angle, M the molar mass, X the concentration, and subscript s means solvent and p means polymer. The intensity ratio of the two characteristic peaks of DMAc at 745 cm^{-1} and PAA at 1180 cm^{-1} is plotted against the solvent concentration in Figure 3.2. In the figure, the slope of the linearly fitted line which corresponds to the constant in Equation 3.1 was measured to be about 1.77.

Drying and curing procedures

To see the effect of film thickness on the chain orientation of PI, PAA was coated on a PAA was coated on a clean glass substrate with two different wet thicknesses, $80 \mu\text{m}$ and $250 \mu\text{m}$, using a micrometer-adjustable film applicator. The coated PAA solutions were dried at $120 \text{ }^\circ\text{C}$ in a home-made convection oven, while the sample was removed from the oven after 3, 5, 7, and 10 min of drying and the film was depth-profiled to trace the evolution of the solvent concentration. The samples were sufficiently solidified to get a clear Raman spectrum even at shortest drying time, 3 min, and a considerable amount of residual solvent remained inside the film even at the longest drying time, 10 min. The thickness of the dried PAA film after 10 min was measured to be about $13 \mu\text{m}$ and $42 \mu\text{m}$, respectively.

Four samples of PAA films with two different film thicknesses were prepared by drying the PAA solution at $120 \text{ }^\circ\text{C}$ for 10 min. They were cured one by one in a heating chamber attached to a rheometer (RMS 800, Rheometrics) by elevating the

temperature from 120 °C to the final temperatures of 150 °C, 170 °C, 200 °C, and 350 °C at the rate of 5 °C/min. For each experiment, depth-wise DOI was measured by taking out of the sample from the heating chamber when it reached the final temperature.

For Chapter 4.2

PAA preparation

3,3',4,4'-biphenyltetracarboxylic acid (s-BPDA, 99.5% purity) purchased from Mitsubishi Chemical Co. Ltd. was used as dianhydride and p-phenylene diamine (PDA, 99.9% purity) purchased from DuPont was used as diamine to make a PAA solution. The solid concentration of the solution was 12 % in dimethylacetamide (DMAc, Sigma-Aldrich). The PAA solution was synthesized through the following steps. 5.50 g of PDA (0.019 mol) was put in a glass flask containing 55.1 g of DMAc and was stirred at 25 °C for 30 minutes to completely dissolve PDA. 2.01 g of s-BPDA (0.019 mol) was added into the PDA solution and mixed at 25 °C by an overhead mixer for more than 24 hours to make a viscous PAA solution. The viscosity of the PAA solution was measured about 18 Pa·s at the shear rate 1 s^{-1} . The chemical compositions of the PAA and its corresponding PI are given in Figure 3.1.

Drying and curing procedures

The coated PAA solution was imidized by three different drying and curing protocols in order to see the effect of thermal history on the final microstructure of PI

film. The thermal and temporal conditions for each protocol are shown in Table 3.1, and the temperature change according to the process time is shown in Figure 3.3. Here, the drying process is characterized by the pre-baking step that evaporates considerable amounts of solvent at the constant temperature, and the curing process by the main imidization step in which the temperature increases up to 350 °C at the constant rate. Drying was conducted at three different temperatures, 120, 140, and 160 °C in a home-made oven in which the temperature and flow rate of the supplying hot air were controlled. The drying times were decided 20, 8, and 4 minutes respectively to keep the amount of solvent remaining in the film after the drying process to be similar between the different protocols. The variation of the residual solvent contents and DOI during the drying process was measured by taking out the sample from the oven when it reached specific sampling times shown in Table 3.1. Each measurement took about 15 minutes; a period of time short enough to ignore the solvent evaporation or diffusion in the film during the measurement as the solvent concentration was sufficiently low.

Curing was conducted in a heating chamber attached to the rheometer (RMS 800, Rheometrics). The starting temperature of curing was the same as the drying temperature and was elevated to 350 °C at the rate of 10 °C/min to achieve a full imidization of PI. The same measurements were performed during the curing process by detecting the residual solvent concentration and DOI when the sample reached specific temperatures. Sampling temperatures are also shown in Table 3.1.

Protocol	Drying Condition	Sampling Time	Curing Condition	Sampling Temperature
A	120°C, 20 min	5, 10, 20 min	120°C → 350°C, 10°C/min	160, 180, 200, 350°C
B	140°C, 8 min	4, 6, 8 min	140°C → 350°C, 10°C/min	170, 200, 250, 350°C
C	160°C, 5 min	3, 4, 5 min	160°C → 350°C, 10°C/min	170, 200, 250, 350°C

Table 3.1. Drying and curing conditions for the different protocols. Sampling time indicates the measurement time during drying and sampling temperature indicates the measurement temperature during curing.

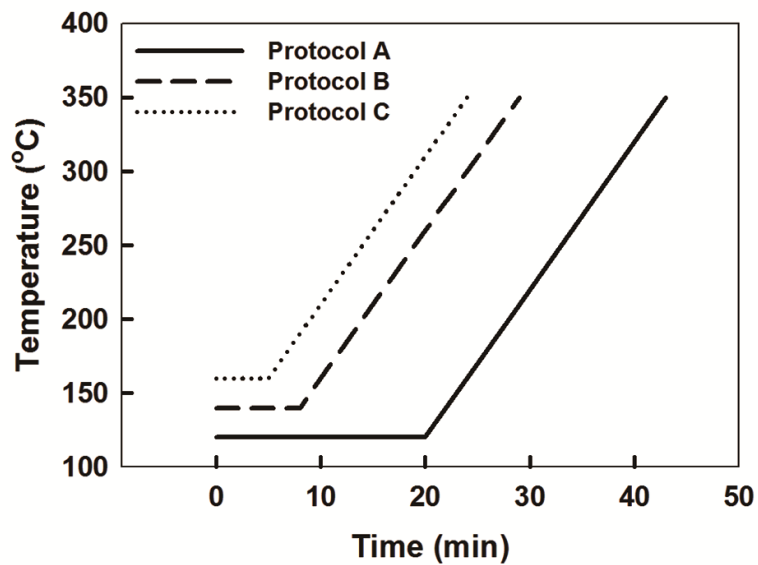


Figure 3.3. Thermal histories for the different drying and curing protocols. The drying process is characterized by constant temperature and the curing is characterized by constant rate of elevating temperature.

For Chapter 4.3.

Sample preparation

Two PAA solutions were made using 3,3',4,4'-biphenyltetracarboxylic acid (s-BPDA, Ube industries) as a dianhydride and two kinds of diamine, 1,4-phenylene diamine (PDA, DuPont) and 4,4'-oxydianiline (ODA, Wakayama). Dimethylacetamide (DMAc, Sigma-Aldrich) was used as a solvent and the solid concentration of PAA solutions was set to 12 wt%. First, 2.38 g (1.000 mol) of PDA was totally dissolved in 65.1 g of DMAc by mixing for 30 minutes at 25 °C. Additional mixing was done for 24 hours after 6.5 g (1.005 mol) of BPDA was added to the solution and PAA-1 composed of BPDA-PDA was prepared. The viscosity of the solution was about 30 Pa·s at the shear rate of 1 s^{-1} . In the same way, 3.56 g (1.000 mol) of ODA and 5.33 g (1.017 mol) of BPDA were mixed in DMAc to make PAA-2 composed of BPDA-ODA. The viscosity was about 28 Pa·s. Molecular structures of the PAA pairs and their corresponding PIs are shown in Figure 3.4.

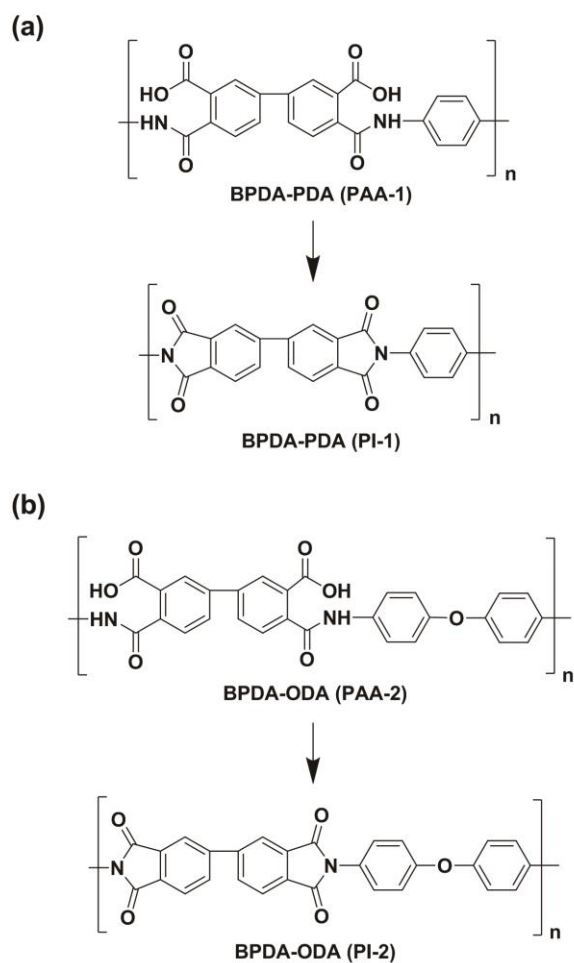


Figure 3.4. Molecular structures of PAAs and the corresponding PIs composed of BPDA-PDA (bottom layer) and BPDA-ODA (top layer). PAA is converted to PI by a dehydration cyclization called imidization reaction.

Drying and curing procedures

Bilayer PI films were constructed starting from the two PAA solutions through the DML and LBL methods as shown in Figure 3.5. For DML drying, PAA-1 and PAA-2 were continuously coated on a clean glass substrate using a micrometer-adjustable film applicator and dried in a convection oven at 100 °C for 10 minutes to get a solidified film. To apply the LBL method, PAA-1 was coated on three different glass substrates and dried at 100, 130, and 160 °C respectively for 5 minutes. The drying temperature of PAA-1, the bottom layer, was denoted as T_b . PAA-2 was then coated on the dried PAA-1 layer and they were dried at 100 °C for another 5 minutes to make three different dried films. Total drying time of the bottom layer was maintained at 10 minutes, same for all the samples regardless of the drying method. The dried PAA films were cured in a heating chamber attached to a rheometer (RMS 800, Rheometrics) by heating from 100 °C to 350 °C at the rate of 10 °C/min. After cooling to room temperature, four different bilayer PI films composed of PI-1 and PI-2 layer with 20 μm thick each were finally obtained.

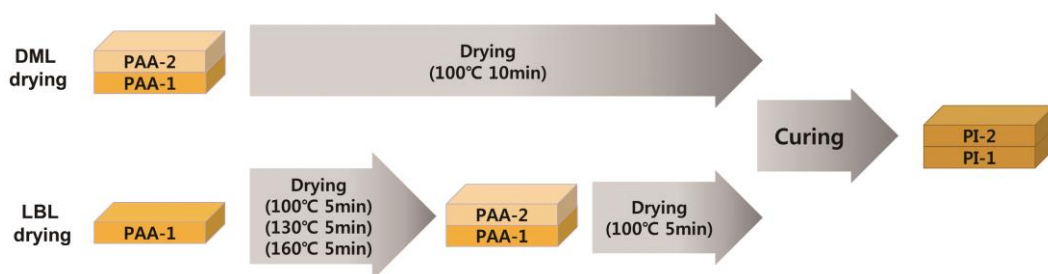


Figure 3.5. Design scheme for manufacturing four different bilayer polyimide films.

3.2. Measurement of residual solvent concentration and the degree of imidization (DOI)

For Chapter 4.1

Measurement of residual solvent concentration in dried PAA films

Confocal Raman spectrometer (LabRAM HR800, Horiba Jobin Yvon) was used to measure the distribution of residual solvent in the dried PAA films. The spectrometer was equipped with an LN₂ cooled charge coupled device (CCD) detector, a holographic grating (1800 grooves/mm), and a Raman holographic edge filter. 632.8 nm line of He-Ne laser was used as an excitation source. Each data acquisition comprised three seconds of exposure time and five times of data accumulation in order to get a sufficient level of signal to noise (S/N) ratio.

Depth profiling of the residual solvent took about 10 minutes for each sample, during which the variation of the sample weight due to solvent evaporation was assured to be less than 3 % of the total film weight. A depth profile of dried PAA film was obtained by moving the focus of the microscope from the film surface to the bottom at intervals of 3 μm or 4 μm, and a depth resolution of 3 μm was secured by using x100 lens for each measurement.

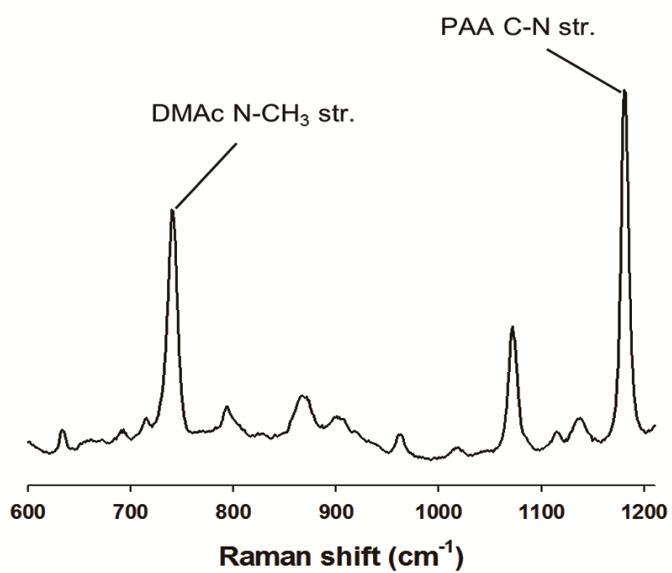


Figure 3.6. Raman spectrum of PAA solution in the spectral range of 600-1200 cm⁻¹. The peaks at 745 cm⁻¹ and 1180 cm⁻¹ indicate the N-CH₃ stretching mode of DMAc and the C-N stretching mode of PAA, respectively.

Measurement of the degree of imidization (DOI)

Confocal Raman spectroscopy was also used to measure DOI in the thickness direction when the dried PAA was cured. First, we compared the Raman spectra of non-imidized PAA, partially imidized PAA-PI, and fully imidized PI that was made by curing the film at 400 °C for 30 min (Figure 3.7). In Figure 3.7, the peak at 1180 cm^{-1} (i.e., the C-X stretching mode of C_6H_2 ring) disappeared as PAA was imidized, while the peak at 1108 cm^{-1} (i.e., the C-N-C transverse stretching mode) became more distinct. This proves that the peaks at 1180 cm^{-1} and 1108 cm^{-1} can be used as characteristic peaks of PAA and PI, respectively, when measuring the relative extent of imidization. Using the ratio of two characteristic peaks, the DOI was defined by

$$\text{DOI} = \frac{I(\text{PI})}{I(\text{PAA})+I(\text{PI})} = \frac{I(1108 \text{ cm}^{-1})}{I(1180 \text{ cm}^{-1})+I(1108 \text{ cm}^{-1})} \quad (3.2)$$

where I is the intensity of the characteristic Raman peaks. In Equation 3.2, the DOI becomes zero when there exists only PAA, and it becomes one when all the PAA is converted to PI.

Similar to the measurement of residual solvent, the depth profiling of each sample was conducted by moving the focus of the microscope from surface to bottom at intervals of 3 μm .

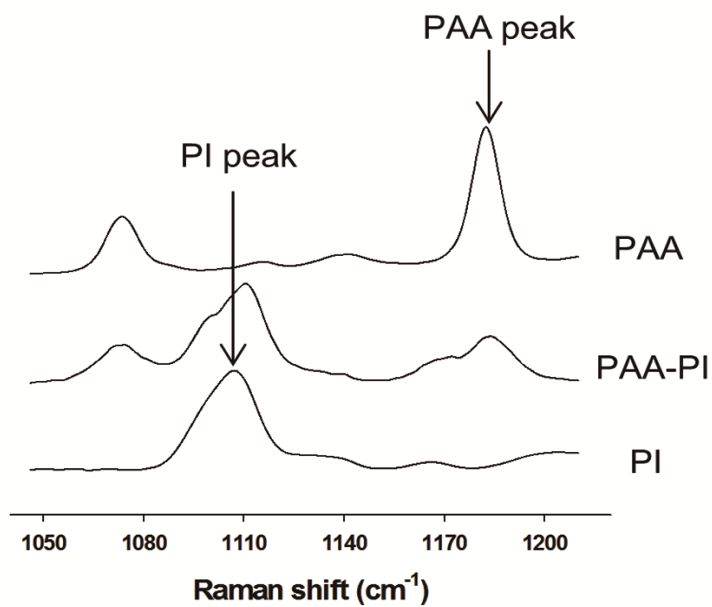


Figure 3.7. Raman spectra of PAA, partially cured PAA-PI and fully cured PI in the spectral range of 1040 -1220 cm⁻¹. The peaks at 1108 cm⁻¹ and 1180 cm⁻¹ indicate the C-N-C stretching mode of PI and the C6H2 stretching mode of PAA, respectively.

For Chapter 4.2

Measurements of residual solvent and degree of imidization (DOI)

The residual solvent concentration and DOI were measured when the PAA was imidized during the drying and curing processes using confocal Raman spectrometer. (LabRAM, Horiba Jobin Yvon) The exposure time to the laser was set to 3 seconds, and 5 scans per spectrum were averaged to obtain an adequate signal to noise ratio. A calibration experiment was first conducted to get the relationship between Raman intensity and solvent concentration in PAA solutions. The peak at 742 cm^{-1} (i.e., N-CH₃ stretching mode) was used as a characteristic peak of DMAc and the peak at 1608 cm^{-1} (i.e., aromatic ring stretching mode) as a characteristic peak of PAA. (Figure 3.8) The reason that the peak at 1608 cm^{-1} , instead of 1180 cm^{-1} , is used as a characteristic peak of PAA is that the peak is not affected by the imidization reaction, thus it can be used as characteristic peak of PAA not only during drying but also the curing process. The proportional constant in Equation 3.1 obtained from this Raman calibration experiment was about 3.57. A depth-wise profile was obtained by moving the laser focus stepwise ($3\text{ }\mu\text{m}$ or $4\text{ }\mu\text{m}$ intervals) from the film surface to the bottom. The depth resolution of the measurement was about $3\text{ }\mu\text{m}$ when using the x100 objective lens.

The same instrument was used to measure the DOI in the film depth direction. Also using the ratio of two characteristic peaks, 1180 cm^{-1} (i.e., C-X stretching mode of C₆H₂) could be used as the characteristic peak of PAA, and the peak at 1108 cm^{-1} (i.e., C-N-C transverse stretching mode), the DOI was measured. Again, a depth-wise

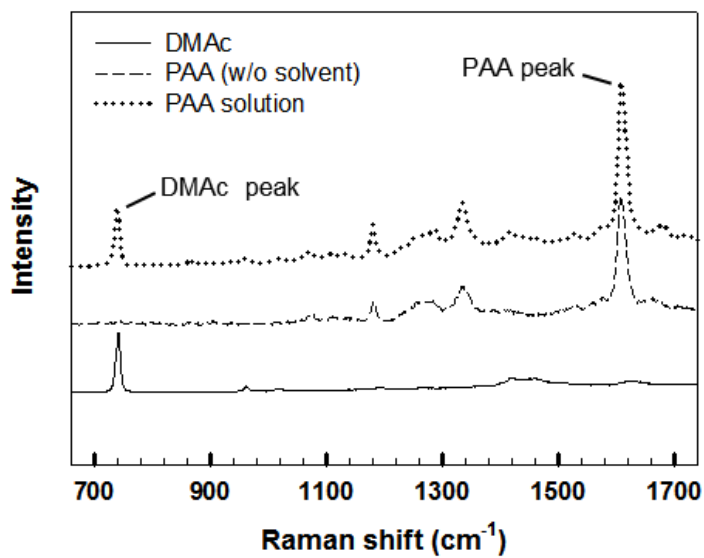


Figure 3.8. Raman spectra of the PAA solution. The peak at 742 cm^{-1} corresponds to the DMAC activated by N-CH₃ stretching, and 1608 cm^{-1} corresponds to the PAA activated by aromatic ring stretching.

profile of each sample was obtained by moving the laser focus by 3 μm interval from the surface to the bottom.

3.3. Measurement of chain orientation of polyimide

Chain orientation of extended polyimide film

Polarized Raman spectroscopy was used to analyze the chain orientation of PI. The polarized direction of the incident laser was controlled by installing the rotating half wave plate on the confocal Raman spectrometer, and an additional analyzer was equipped before the CCD detector to determine the polarization direction of diffracted lights from the sample.

Before measuring the degree of depth-wise chain orientation, the availability of polarized Raman spectroscopy was confirmed by checking the existence of a stretching mode in the BPDA-PDA PI chain which vibrates parallel to the chain axis. First, PAA film dried at 120 $^{\circ}\text{C}$ for 5 min was biaxially extended using UTM (3300 series, Instron) and cured from 120 $^{\circ}\text{C}$ to 350 $^{\circ}\text{C}$ at the rate of 5 $^{\circ}\text{C}/\text{min}$. The elongation ratio of the film was measured as 50 %. The cured PI film was fixed on a rotatable stage of the Raman microscope, and the polarization of incident laser was set parallel to the direction of film extension, which was defined as 0 $^{\circ}$. Then, the film was rotated by an angle of 15 $^{\circ}$ and the variation of the Raman spectrum was observed. If there is a stretching mode in PI molecules that vibrates parallel to the chain axis, the Raman intensity of the peak will be maximum at 0 $^{\circ}$ and minimum at 90 $^{\circ}$, and this mode can be used to quantify the orientation of the PI chains.

Depth-wise measurement of polyimide chain orientation

To obtain the information on depth-wise degree of chain orientation, the cross-section of the PI film was analyzed using polarized Raman spectroscopy. The finally cured PI film was stripped off the glass substrate and cut using a focused ion beam (Helios650, FEI) to get a sharp cross-section. The PI film was separated from the substrate at this stage in order to remove the alteration of the Raman intensity influenced by residual stress at the film interface [20] which could be generated by the CTE difference between PI and the glass substrate during the cooling process. In addition, the intensity of the Raman spectrum could be subtly affected by defects generated during the ion beam milling. It is therefore necessary to inspect the condition of the cross-section before the measurement. As the confocal microscope (OLS3000, Olympus) image shows in Figure 3.9(a), the grain was developed on the cross-section of both films along the film thickness direction (i.e., the z-axis). At the same time, the difference of height in the y-axis between the two sides that face the substrate and the air was observed in Figure 3.9(b). Hereafter, the sides of the film facing the substrate and facing the air are referred to as ‘substrate side’ and ‘air side,’ respectively. The difference in height mainly arises from the accumulated contact of ion beams with the film at the incident side during the milling process, and this effect becomes more pronounced for the thicker film. The difference in height measured from the 3D image of the 30 μm thick PI film was about 4 μm as shown in Figure 3.9(b), which is much larger than the scale of grain roughness. Considering the surface roughness, every measurement of polarized Raman spectroscopy on the film cross-section was conducted by locating the focus of the Raman microscope at a depth of 10 μm from the surface of the cross-section to exclude the effect of possible surface defect.

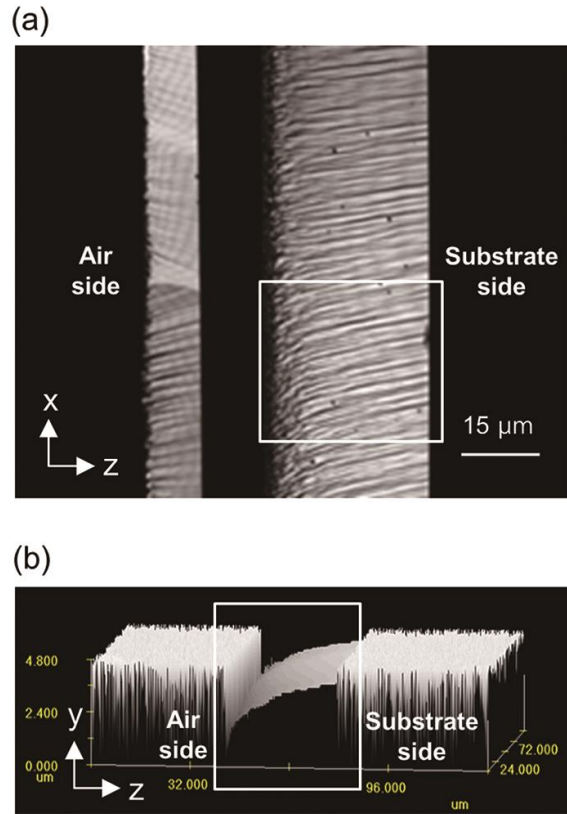


Figure 3.9. Confocal microscopic image of the PI cross-section and its contour: (a) 10 μm thick PI (left) and 30 μm thick PI (right), and (b) 3D image of white rectangle designated in (a).

In order to quantify the depth-wise degree of in-plane (i.e. x-direction in Figure 3.10(a)) chain orientation, two Raman intensity components, I_{xx} and I_{zz} , were measured on a film cross-section using polarized Raman spectroscopy in depth direction (i.e. z-direction in Figure 3.10(a)). The ratio of two components is so-called Raman anisotropy [63] which is analogous to the dichroic ratio in polarized IR measurement. This Raman anisotropy is used to obtain the Fraser distribution function [69], f , which is a fraction of perfectly oriented molecules in the direction of the x-axis. The detailed procedure for the analysis is as follows. An incident laser beam polarized in the x-axis is imposed on a point of interest and the Raman intensity of diffracted lights polarized in the same direction is detected, which becomes I_{xx} (Figure 3.10(a)). Again, a laser beam polarized in the z-axis is imposed and detected to get I_{zz} at the same point (Figure 3.10(b)). The Fraser distribution function is obtained from the ratio of these two Raman intensities (i.e. Raman anisotropy). By mapping Raman anisotropy on the cross-section of the PI film, the Fraser distribution function from the air to the substrate side can be obtained. The spatial resolution of the measurement on the x-z plane was about 1 μm when using x100 lens.

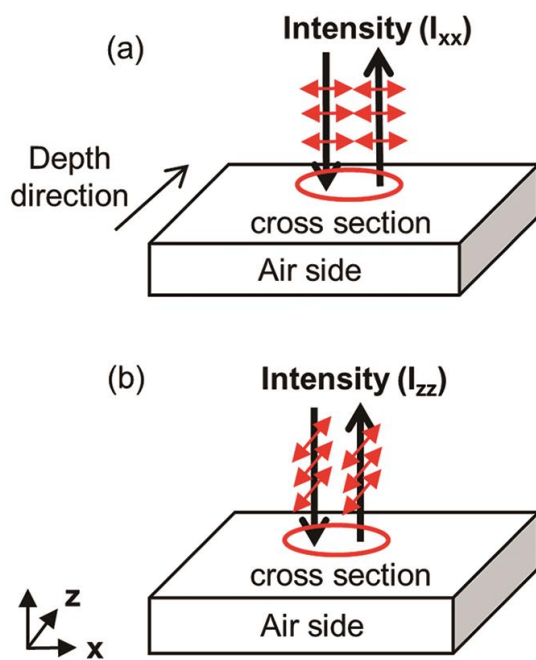


Figure 3.10. Schematic diagram of measuring depth-wise profile of PI chain orientation by detecting: (a) in-plane Raman intensity (I_{xx}), and (b) out-of-plane Raman intensity (I_{zz}).

3.4. Experiments of polyimide interdiffusion

3.4.1. Measurement of PAA-PAA interdiffusion

The prepared PAA solutions were diluted to make four different PAA-1 and 2 pairs having solvent concentrations of 88, 90, 91.5, and 93 wt% to see the effect of solvent content on the interdiffusion between PAA chains. The viscosities measured by a rheometer (DHR-3, TA instruments) were almost same between the PAA pairs that had the same solvent concentration as can be seen in Figure 3.11.

Confocal Raman spectrometer (LabRAM HR800, Horiba Jobin Yvon) was used to observe a compositional change of PAA at the interface where the two PAAs contact and interdiffuse. Raman spectra of PAA-1 and 2 are shown in Figure 3.12. In the figure, the peak at 1180 cm^{-1} was used as a characteristic peak of PAA-1 and 1160 cm^{-1} as that of PAA-2. By calibrating the Raman intensities with PAA compositions, the relationship between the volume fraction of PAA-2 and its peak intensity ratio was obtained as below.

$$\begin{aligned}\phi_{\text{PAA2}} &= \frac{w_{\text{PAA2}}}{w_{\text{PAA1}} + w_{\text{PAA2}}} \\ &= \alpha \times \frac{I_{\text{PAA2}}(1160\text{cm}^{-1})}{I_{\text{PAA1}}(1180\text{cm}^{-1}) + I_{\text{PAA2}}(1160\text{cm}^{-1})}\end{aligned}\quad (3.3)$$

Here, ϕ is the volume fraction, w is the weight, I is the intensity of Raman peak, and α is the proportional constant that was fitted to be 0.86 from the calibration

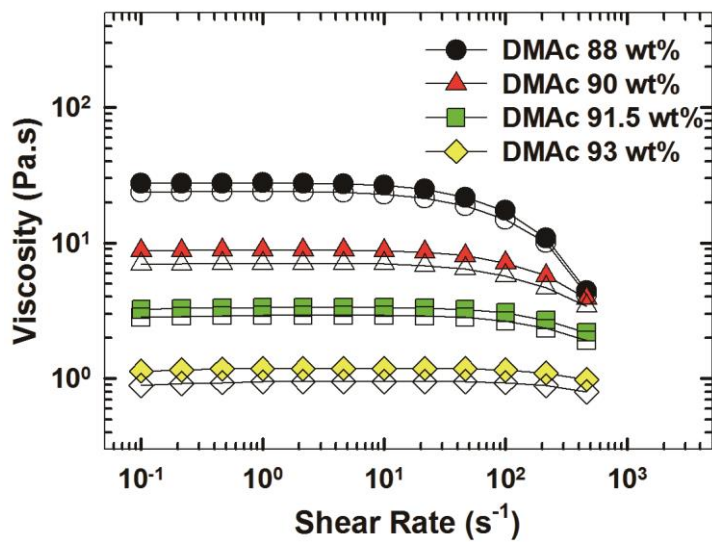


Figure 3.11. Rate dependent shear viscosities for PAA solutions having different solvent contents. Filled symbols represent PAA-1 (BPDA-PDA) and open symbols PAA-2 (BPDA-ODA).

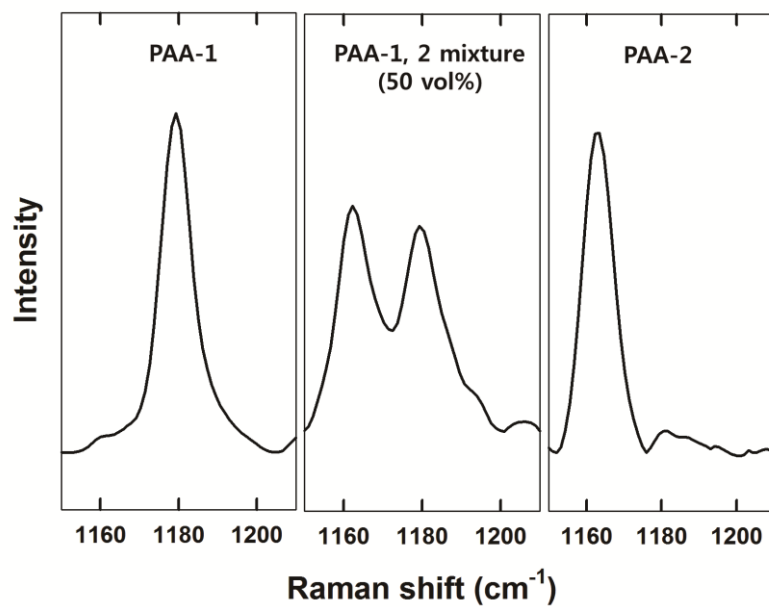


Figure 3.12. Raman spectra of PAA-1, PAA-2 and their 1:1 mixture.

result. The density and molecular weight of PAA-1 and 2 were assumed to be the same.

In order to observe the interdiffusion behavior between PAA-1 and 2, 50 μm -thick PAA-1 was coated on a 150 μm -thick cover glass using a film applicator, and it was placed on PAA-2 drop to make a bilayer structure as shown in Figure 3.13(a). The time when the two PAAs contact was set to 0 and the compositional change at the interface was measured by depth profiling the Raman spectrum from $z=0$ μm at the interval of 3 to 5 μm at different times, 10, 20, 30, and 40 min. All the Raman experiments were conducted at room temperature, and the x100 objective lens (numerical aperture, $\text{NA}=0.9$) equipped with 632.8 nm line of He-Ne laser was used. In this experiment, 1800 grooves/mm of a holographic grating was adopted and data acquisition comprised 3 s of laser exposure time and two times of repeated scan. A whole depth profiling time was about two minutes. The refractive index (n) of PAA solution was measured to be 1.47~1.49 by a prism coupler (Metricon 2010), which is similar to DMAc ($n_{\text{DMAc}}=1.44$). To match the refractive index, borosilicate ($n_{\text{glass}}=1.48$) was used as the cover glass and glycerol ($n_{\text{oil}}=1.47$) was used as the immersion oil.

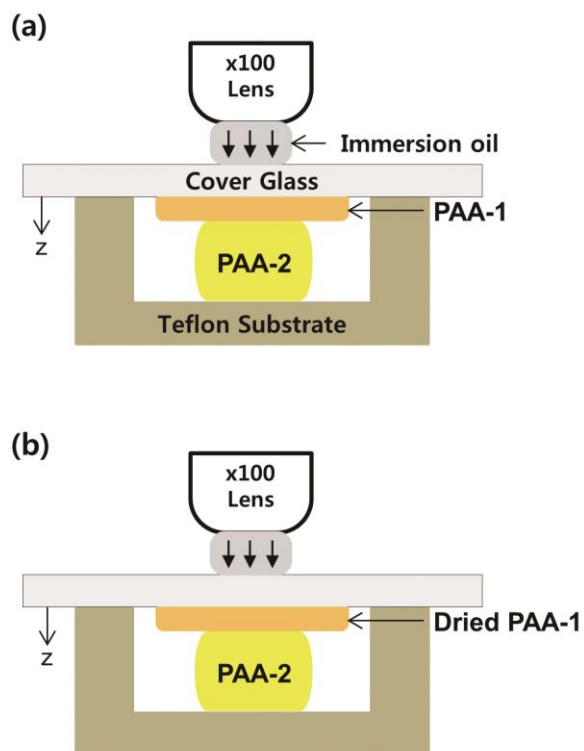


Figure 3.13. Schematic diagram for the Raman experiments of (a) PAA-1 and 2 interdiffusion, and (b) solvent diffusion into the dried PAA-1 film.

3.4.2. Measurement of solvent diffusion into dried PAA film

When a PI bilayer is made by LBL drying, the solvent in the top PAA-2 layer can diffuse down into the dried PAA-1. The diffusion of solvent can affect chain orientation of the cured PI as well as PAA interdiffusion, thus the extent of solvent diffusion according to the T_b was investigated. First, the PAA-1 was coated on a cover glass using a film applicator to make the wet thickness 330 μm and dried at three different temperatures, 100, 130, and 160 $^\circ\text{C}$ for 5 minutes. The film thickness was about 40 μm after drying, still containing more than 20 wt% of solvent in the film. After the dried PAA-1 made a contact with the PAA-2 solution (i.e. $t=0$ min) as shown in Fig 3.13(b), the solvent distribution in the film was depth profiled using the Raman spectroscopy from $z=0$ μm at the interval of 5 μm at different times, 1, 5, 10, and 15 min. Solvent content in a dried film or PAA solution was defined as previously :

$$X = \frac{w_{\text{solvent}}}{w_{\text{PAA}}} = \alpha' \times \frac{I_{\text{solvent}} (742 \text{ cm}^{-1})}{I_{\text{PAA}} (1608 \text{ cm}^{-1})} \quad (3.4)$$

where X is the solvent concentration, w the weight, I the intensity of Raman peak, and α' the proportional constant which was measured to be 10.9 by fitting the calibration result. 300 grooves/mm of holographic gratings was used, and a whole depth profiling took 20 s by applying 1 s of laser exposure and one scan at a time. The refractive index of dried PAAs (n_{PAA}) was ranged 1.75~1.80, and borosilicate ($n_{\text{glass}}=1.48$) and glycerol ($n_{\text{oil}}=1.47$) were also used as the cover glass and immersion oil respectively. Due to the mismatch of refractive index between the sample and immersing oil, about 24 μm of instrumental broadening can occur at $z=40$ μm , which corresponds to the depth of focus (DOF) as calculated in Equation. 3.5.

$$\text{DOF}(z) = z \times \left[\left\{ \frac{\text{NA}^2(n^2-1)}{(1-\text{NA}^2)} + n^2 \right\}^2 - n \right] \sim 24 \mu\text{m} \quad (z = 40\mu\text{m}) \quad (3.5)$$

In the equation, n means $n_{\text{PAA}}/n_{\text{oil}}$, the ratio of refractive indices.

3.4.3. Measurement of interdiffusion width of cured polyimide films

Bilayer PI films made by the DML and LBL methods were peeled off from the glass substrate and cut by cryo-ultramicrotome (PT/PC Ultramicrotome, Boeckeler Instruments) to measure the interdiffusion width. After the cross-section of the cut film was exposed to Raman spectrometer, the compositional change between PI-1 and 2 at the interface was detected by X-Z mapping method as shown in Figure 3.14(b). Here, the peak at 735 cm^{-1} was used as the characteristic peak of PI-1 and 695 cm^{-1} as that of PI-2. (Figure 3.14(a)) Volume fraction of PI-2 was measured in the same way with PAA-2 and the proportional constant α'' in Equation 3.6 was calibrated to be 0.71.

$$\phi_{\text{PI2}} = \frac{w_{\text{PI2}}}{w_{\text{PI1}} + w_{\text{PI2}}} = \alpha'' \times \frac{I_{\text{PI2}}(695\text{cm}^{-1})}{I_{\text{PI1,2}}(735\text{cm}^{-1}) + I_{\text{PI2}}(695\text{cm}^{-1})} \quad (3.6)$$

Each measurement in the Z axis in Figure 3.14(b) was spaced $0.3 \mu\text{m}$ apart and 1,800 grooves/mm of grating was used. The laser exposure time and scan times for every measurement were set 5 s and 5 times respectively to minimize the signal to noise (S/N) ratio of the spectrum.

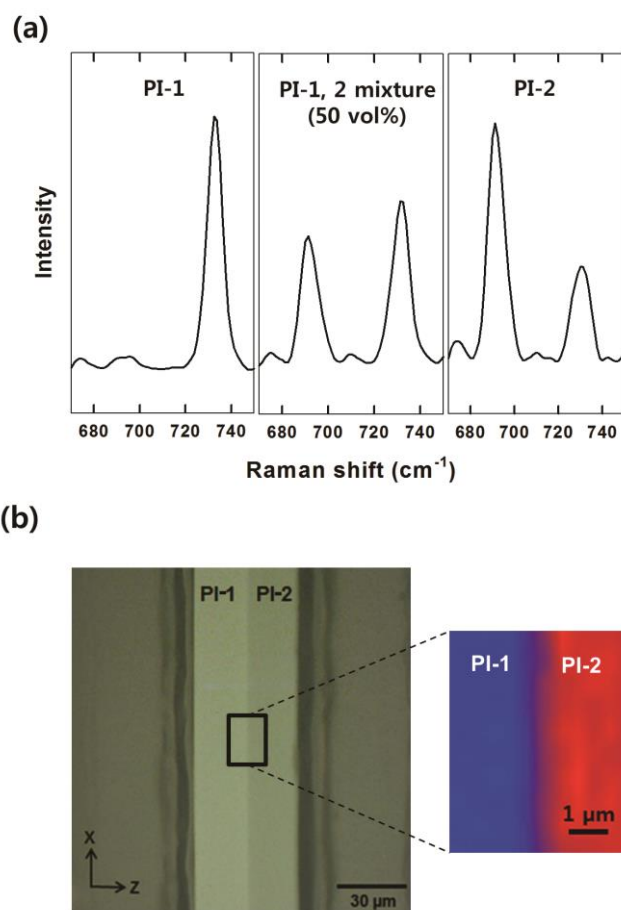


Figure 3.14. The measurement of interdiffusion width using X-Z mapping of Raman spectroscopy. (a) Raman spectra of PI-1, PI-2 and their 1:1 mixture. (b) Cross-sectional images of a PI bilayer captured by a microscope and its X-Z Raman mapping result. Blue and red colors in the mapping image are distinguished by different Raman peaks appeared at 735 and 695 cm^{-1} respectively.

3.5. Characterization of the cured polyimide film

3.5.1. X-ray diffraction pattern

Wide angle x-ray diffractometer (D8 ADVANCE with DAVINCI, Bruker) equipped with LYNXEYE XE detector was used for the characterization of molecular order and crystallinity of PI films. Wide angle X-ray diffraction (WAXD) patterns were collected in the reflection mode over $2\theta = 2^\circ \sim 40^\circ$. Scan step was 0.02° with the speed of 0.5 sec/step. The X-ray generator was run at 40kV, 40mA.

3.5.2. Glass transition temperature (T_g)

A dynamic mechanical thermal analyzer (SDTA861e, Mettler Toledo) was used to measure the loss factor ($\tan \delta$) as a function of temperature for the cured PI films. Specimens were prepared 5 mm in width and 40 mm in length. The measurement was conducted in oscillation mode, in which the displacement amplitude was set 10 μm at a frequency of 1 hz. The loss factor was obtained from 150 $^\circ\text{C}$ to 450 $^\circ\text{C}$, and T_g was measured by observing the temperature at which the peak of loss factor appeared.

3.5.3. Thermal expansion coefficient (TEC)

Thermal mechanical analysis (TMA) of PI films was conducted with a Hitachi DMA 7100 analyzer. The width of the specimen was 5 mm and length was 15 mm, and the tensile load during the experiment was set to 50 mN. The specimen was heated to 150 $^\circ\text{C}$ at the rate of 20 $^\circ\text{C}/\text{min}$ and was retained for 20 minutes to remove absorbed water in PI films. After cooling again to the room temperature, the changes in the film length were detected by heating the specimen to 250 $^\circ\text{C}$ at the rate of

5 °C/min. The average value of thermal expansion coefficient (TEC) between 100 °C and 200 °C was used as a representative value.

Chapter 4.

Results and discussion

4.1. Effect of film thickness on the polyimide chain orientation

4.1.1. Depth-wise residual solvent content of dried film

Drying induces chain alignment on the film plane in the presence of a substrate. [13, 14, 19, 23] This is due to the tensile stress developed on polymer chains by solvent evaporation during which the relaxation time of the polymer becomes larger than the time scale of volume shrinkage. This means that the degree of in-plane chain orientation can be predicted if the extent of volume shrinkage is known during the drying process. When a considerable amount of solvent remains in the film after drying as is the case with the PAA film, the amount of residual solvent can indicate how much polymer chains are well aligned to the in-plane direction. It also provides information on the degree of chain orientation in the film thickness direction when there is a depth-wise distribution of residual solvent profile.

Based on the calibration result, the depth-wise residual solvent profile was tracked for two PAA films of different thicknesses at different drying times (Figure 4.1). Hereafter, the thickness of these two films is referred to as '10 μm ' and '30 μm ' based on the thickness of the final cured PI film. The result in Figure 4.1 was confirmed to be reproducible by repeating the experiments three times. For 10 μm thick PI film in Figure 4.1(a), the residual solvent concentration of about 0.6 ($\text{g}_{\text{solvent}}/\text{g}_{\text{solid}}$) when dried for 3 min at 120 $^{\circ}\text{C}$ was reduced to 0.4 (g/g) after 10 min. The solvent concentration at both sides was evenly reduced to make a uniform profile of residual solvent along the film thickness. That is, a depth-wise homogeneous PAA film was obtained after drying when the film was thin. On the other hand, the 30 μm thick PI film exhibited a significant amount of solvent remaining in the film after the drying process compared

to the 10 μm film (Fig. 4.1(b)). The final residual solvent concentration after 10 min showed a significant difference between the two sides of about 0.8 (g/g) at the substrate side and 0.4 (g/g) at the air side, compared to a uniform value of around 1.1 (g/g) at 3 min of drying. This side-to-side difference of residual solvent concentration resulted from the hindered diffusion of solvent molecules for the thick film. [57, 86-88] The increased film thickness increased the time for the solvent molecules to reach the surface, and the diffusional resistance increased sharply at the film surface due to the low solvent concentration. Thus, the rate of solvent diffusion near the substrate was decreased and the solvent became trapped inside the film.

The aforementioned difference between the two PAA films could be related to the extent of chain alignment and its depth-wise uniformity. PAA chains composed of BPDA-PDA are known to have a fully extended structure in DMAc. [29] With less residual solvent remaining after drying, the stronger biaxial tensile stress is exerted and more polymer chains align to the in-plane direction by packing themselves closely with a well-ordered structure. Therefore, the 10 μm thick PI is expected to have a relatively high degree of in-plane orientation with a uniform distribution, while the 30 μm thick PI has an inhomogeneous and lower degree of in-plane orientation so that the chains are more randomly oriented at the substrate side than the air side. The effect of these differences on the imidization rate and the depth-wise chain orientation of the finally cured PI is investigated in the following sections.

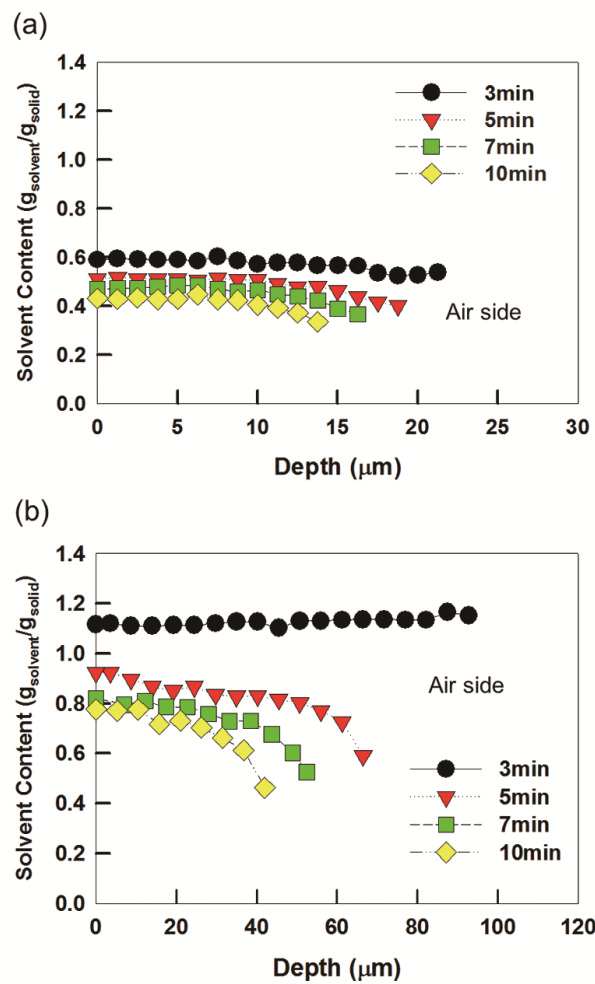


Figure 4.1. Depth-wise residual solvent profiles of the PAA film at different drying times for the film of thickness (a) 10 μm and (b) 30 μm.

4.1.2. Depth-wise imidization degree during curing

Imidization reaction starts at about 130 °C, after which PAA is converted to PI. [39] The rate of imidization or its starting temperature, however, depends on many factors such as the molecular structure of PAA, temperature profile, and affinity with solvent. In addition, imidization rate can also be accelerated when more solvents remain in the film because free solvent molecules around PAA chains can increase the mobility of carboxyl and amino groups. In a few studies, the role of the solvent in enhancing the imidization reaction was clearly established by using Raman and FTIR spectroscopy, but they could not provide depth-wise information, i.e., the difference in the rate of imidization according to the distribution of residual solvent in the depth direction. For this purpose, PAA films dried at 120 °C for 10 min were placed in a heating chamber and the temperature was raised from 120 °C to the following final temperatures: 150 °C, 170 °C, 200 °C, and 350 °C. The depth-wise DOI was measured when they reached the above temperatures and the results are shown in Figure 4.2. In the figure, the film depth shown in the x-axis was normalized by the total thickness of the film to focus on the depth-wise distribution of the extent of imidization. DOI in the y-axis was derived from Equation 4.1 using the two characteristic peaks of PAA and PI in Figure 3.7.

$$\begin{aligned} \text{DOI (\%)} &= \frac{I(\text{PI})}{I(\text{PAA})+I(\text{PI})} \times 100 \\ &= \frac{I(1108 \text{ cm}^{-1})}{I(1180 \text{ cm}^{-1})+I(1108 \text{ cm}^{-1})} \times 100 \end{aligned} \quad (4.1)$$

When PI was 10 μm thick, DOI was about 20 % at 150 $^{\circ}\text{C}$, 60 % at 170 $^{\circ}\text{C}$ and higher than 90 % at 200 $^{\circ}\text{C}$, which implies that most of the PAA was imidized to PI in the vicinity of 200 $^{\circ}\text{C}$. (Figure 4.2(a)) In addition, the distribution of DOI in the film thickness direction was uniform similar to the result of residual solvent profile for the thin PI film. On the other hand, a different result at the initial stage of curing was obtained for the 30 μm thick PI as can be seen in Figure 4.2(b). The DOI was already higher than 50% when the curing temperature reached 150 $^{\circ}\text{C}$, and DOI near the substrate side was 20% larger than the air side. This side-to-side difference of DOI decreased when the curing temperature was further increased to 170 $^{\circ}\text{C}$ and higher. Again, more than 90 % of the PAA chains were converted to PI when the temperature was 200 $^{\circ}\text{C}$ as in the case of the 10 μm thick PI. At the final curing temperature of 350 $^{\circ}\text{C}$, the 30 μm thick PI has 3~4 % higher DOI than the thin PI had.

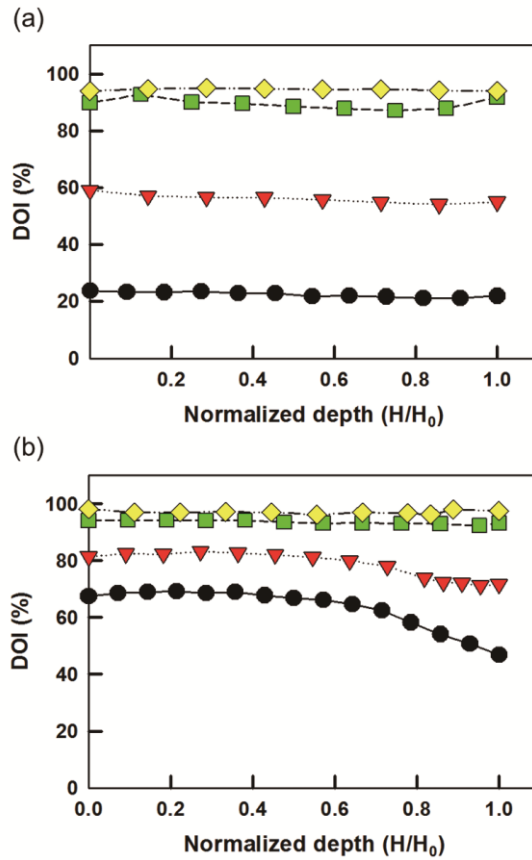


Figure 4.2. Depth-wise DOI profiles at different curing temperatures: (●) 150 °C; (▼) 170 °C; (■) 200 °C; and (◆) 350 °C, when the thickness of the final PI film is (a) 10 μm, and (b) 30 μm. The right side of the curve corresponds to the air side.

4.3.3. Depth-wise chain orientation after curing

In order to determine the vibration mode of PI molecules that vibrates parallel to the chain axis, the angular variation of the Raman spectrum was observed by rotating the extended PI film as explained in the experimental section. In the measured Raman spectrum, the Raman intensities originating from the benzene ring stretching mode which appears at 1610 cm^{-1} were plotted at different angles in Figure 4.3(a). The same measurement was conducted for a pristine PI and compared in Figure 4.3(b). The figure does not exhibit any significant variation of Raman intensity at different angles in the case of pristine PI, but the Raman intensity is maximized at 0° and minimized at 90° when the extended PI film is used. This result proves that the principal vibration axis of the benzene ring stretching mode is coincident with the PI chain axis and this can be used to analyze the chain orientation.

Using the vibration mode at 1610 cm^{-1} , a distribution function proposed by Fraser [63, 69] was used to quantify the degree of in-plane chain orientation. Fraction f , the so-called Fraser distribution function or Fraser fraction, is a value that represents the fraction of perfectly oriented molecules in an extended film and $(1-f)$ is the fraction of randomly oriented molecules. Liem et al. reported that the Fraser distribution function can be expressed by a simple relationship with the measurable Raman intensity ratio, i.e., Raman anisotropy, when a polymer chain has a highly uniaxial Raman tensor and its principal axis is parallel to the chain axis. [63] In their study, if the chains were aligned to the x-axis and their perpendicular direction was fixed to the z-axis, I_{xx} which is diffracted by perfectly oriented polymer chains to the x-axis is expressed by :

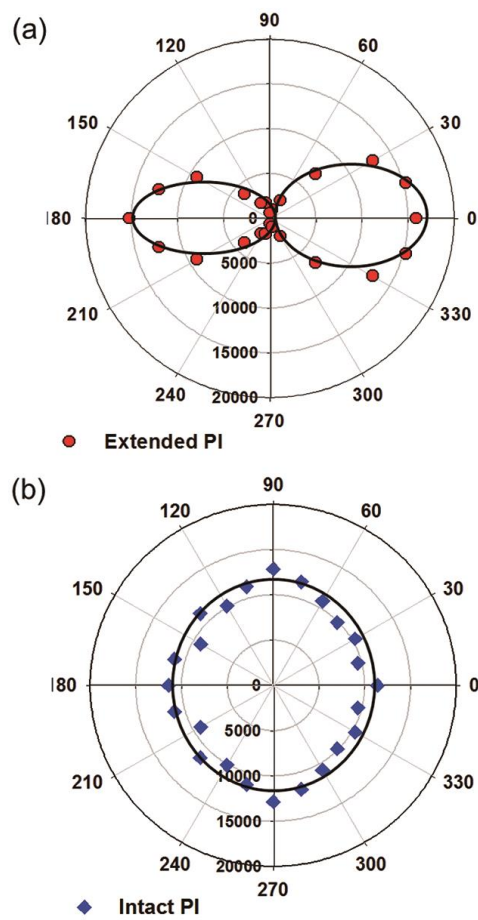


Figure 4.3. Polar plots of Raman intensities for the (a) uniaxially extended PI film, and (b) intact PI film.

$$I_{xx}(\text{perfect}) = f\alpha_{xx}^2 \quad (4.2)$$

where I is the Raman intensity, α_{ij} the component of Raman tensor and the two subscripts mean the polarizing direction of incident laser and diffracted light, respectively. The Raman intensity diffracted from the fraction of randomly oriented molecules (1-f) can be determined by the following equations:

$$I_{xx}(\text{random}) = I_{zz}(\text{random}) = \frac{1}{45}(1-f)(45\check{\alpha}^2 + 4\gamma^2 - 5\delta^2)$$

$$\check{\alpha}^2 = \frac{1}{9}(\alpha_{xx} + \alpha_{yy} + \alpha_{zz})$$

$$\begin{aligned} \gamma^2 = \frac{1}{2} [& (\alpha_{xx} - \alpha_{yy})^2 + (\alpha_{yy} - \alpha_{zz})^2 + (\alpha_{zz} - \alpha_{xx})^2 \\ & + 3(\alpha_{xy}^2 + \alpha_{yx}^2 + \alpha_{yz}^2 + \alpha_{zy}^2 + \alpha_{zx}^2 + \alpha_{xz}^2) + \delta^2] \end{aligned}$$

$$\delta^2 = (\alpha_{xy} - \alpha_{yx})^2 + (\alpha_{yz} - \alpha_{zy})^2 + (\alpha_{zx} - \alpha_{xz})^2 \quad (4.3)$$

In the equation, $\check{\alpha}^2$, γ^2 , and δ^2 correspond to the isotropic, anisotropic and asymmetric invariants of the Raman tensor. It simplifies to $I_{xx}(\text{random})=I_{zz}(\text{random})=1/5\alpha_{xx}$ because every component of the Raman tensor is assumed to be 0 except for α_{xx} when the molecular vibration with highly uniaxial Raman tensor is considered. Thus, the Raman anisotropy which is the ratio of I_{xx} measured by in-plane polarization and I_{zz} measured by out-of-plane polarization can be simply related with Fraser distribution function as follows:

$$R = \frac{I_{xx}}{I_{zz}} = \frac{I_{xx}(perf) + I_{zz}(rand)}{I_{xx}(rand)} = \frac{1+4f}{1-f}$$

$$f = \frac{R-1}{R+4} \quad (4.4)$$

In this paper, the depth-wise orientation of PI chain was analyzed by measuring the Fraser distribution function on a cross-section of the film along the depth direction. The polarized Raman spectra of the in-plane polarization and out-of-plane polarization for two PIs with different thicknesses are shown in Figures 4.4(a) and (b). The Raman intensity measured by in-plane polarization (I_{xx}) is stronger than that of out-of-plane polarization (I_{zz}), which coincides well with the fact that the polymer chains in a solvent-cast film typically align to the in-plane direction. Using the 1610 cm^{-1} peak assigned to the benzene ring stretching mode which meets the required condition of polarized Raman analysis, the Raman anisotropy, R (I_{xx}/I_{zz}), is mapped throughout the area of interest for two different PIs as shown in Figures 4.4(c) and (d). In the figure, the PI cross-section is shown in red color with the x-axis designating the in-plane direction and the z-axis the film thickness direction. The brightness of the red color corresponds to the value of Raman anisotropy and hence reveals the absence of any notable Raman anisotropy along the longitudinal direction (i.e., the x-axis) for both films, and the distribution is observed only along the depth direction (i.e., the z-axis) for the 30 μm thick PI as shown in Figure 4.4(d). In the case of the 30 μm thick PI, the brightness of the red color is changed when it comes from the air side to the substrate side, and the color near the substrate side is darker than that of the 10 μm thick PI film.

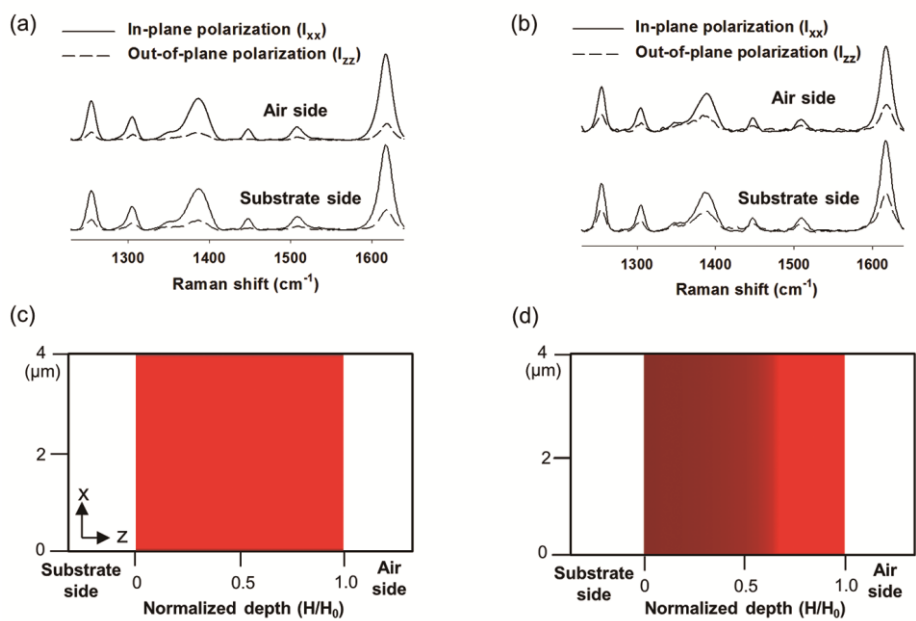


Figure 4.4. In-plane and out-of-plane polarized Raman spectra measured at both air and substrate side of (a) PI 10μm, (b) PI 30 μm, and mapping image of Raman anisotropy(I_{xx}/I_{zz}) of (c) PI 10 μm, (d) PI 30 μm. x-axis is longitudinal direction of film in picture (c) and (d).

With the measured Raman anisotropy, the Fraser distribution function, f , is plotted along the film depth in Figure 4.5(a). As the orientation function, f , is proportional to Raman anisotropy, it shows similar results to those of the Raman mapping data. In Figure 4.5(a), the value of f is about 0.46 for the 10 μm thick PI and its depth-wise distribution is uniform, whereas the 30 μm thick PI exhibits an inhomogeneous distribution with f value of about 0.19 at the substrate side and about 0.35 at the air side. This indicates that overall degree of in-plane orientation decreases as the film thickness increases, especially near the substrate than near the air side, resulting in depth-wise inhomogeneity. This result explains the curling of the PI film when it is detached from the glass substrate as remarked by Nomura and Asano. [19, 20] During the experiment no curling was observed when the 10 μm thick PI was detached from the substrate, whereas the film was curved for the 30 μm thick PI. This curling originates from the side-to-side difference of CTE which is inversely proportional to the degree of in-plane orientation of PI in general. Therefore, the 30 μm thick PI film has higher CTE at the substrate side than at the air side, which makes the film shrink more at the substrate side during the cooling process after curing. The curling originating from the side-to-side difference of chain orientation is not revealed under the constraint of a substrate, and it appears when the film is separated from the substrate.

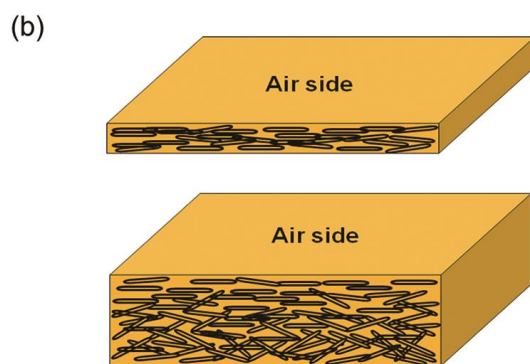
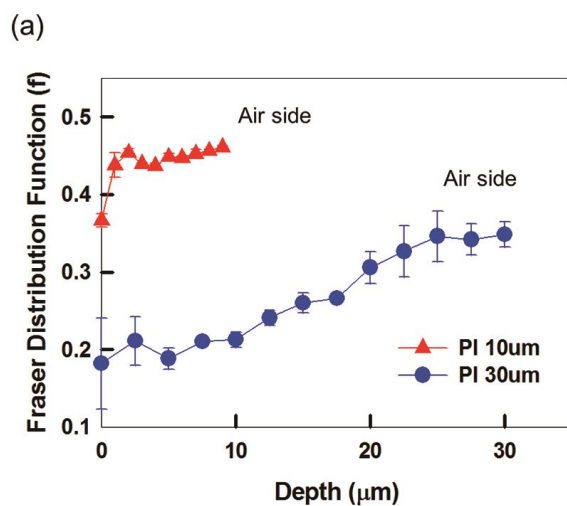


Figure 4.5. (a) Depth-wise Fraser fraction (f) profile of two different PI films, and (b) schematic diagram of depth-wise chain orientation.

The measured depth-wise distribution of the PI orientation is analogous to the estimated distribution of PAA chain orientation after drying. As aforementioned, more solvent remains after drying for thick PI, especially near the substrate side, which means that the biaxial tensile stress due to solvent evaporation is developed less on PAA chains. In other words, the degree of in-plane orientation of PAA chains near the substrate side is lower than that near the air side in the dried film. As curing progresses, more solvent inside the thick film accelerates the imidization rate, and the relatively flexible PAA chains can be changed more rapidly to stiff PIs that can no longer easily form a highly ordered structure. Therefore, even though the tensile stress is additionally generated through the subsequent solvent evaporation during the curing process, the depth-wise chain orientation of the cured PI can hardly deviate from that of the dried PAA.

4.2. Effect of thermal history on the polyimide chain orientation

4.2.1. Residual solvent and imidization degree during drying

In general, biaxial tensile stress is exerted on the polymeric film when a polymer solution is dried under the constraint of a substrate. [13, 14, 19] A polymeric chain backbone that is randomly oriented in a large amount of solvent at the initial state becomes aligned in the plane of the film during solvent evaporation due to this biaxial stress. This means that the amount of evaporated solvent or remaining solvent during the drying process can reflect the extent of in-plane orientation of polymer chains. In addition, the rigidity of polymer chain affects the degree of in-plane chain orientation after drying as it influences the packing ability of polymer chains when the film is densified by solvent evaporation.

The rigidity of the polymer chain increases when the PAA composed of BPDA-PDA is converted to PI as evidenced by an increase of the Kuhn length from 43 Å to 78 Å . [27] As the PI manufacturing process involves both solvent evaporation and increase in chain rigidity, it is necessary to examine the variation of the amount of solvent evaporation and the imidization degree at the same time during the drying and curing processes in order to predict the final microstructure of PI. For this purpose, the residual solvent concentration and DOI was measured during the drying process first. (Figure 4.6)

In figure 4.6, the residual solvent concentration decreases and DOI increases as drying proceeds. According to the depth profile, the solvent concentration is lower near the air side regardless of drying temperature. It was reported that the side-to-side

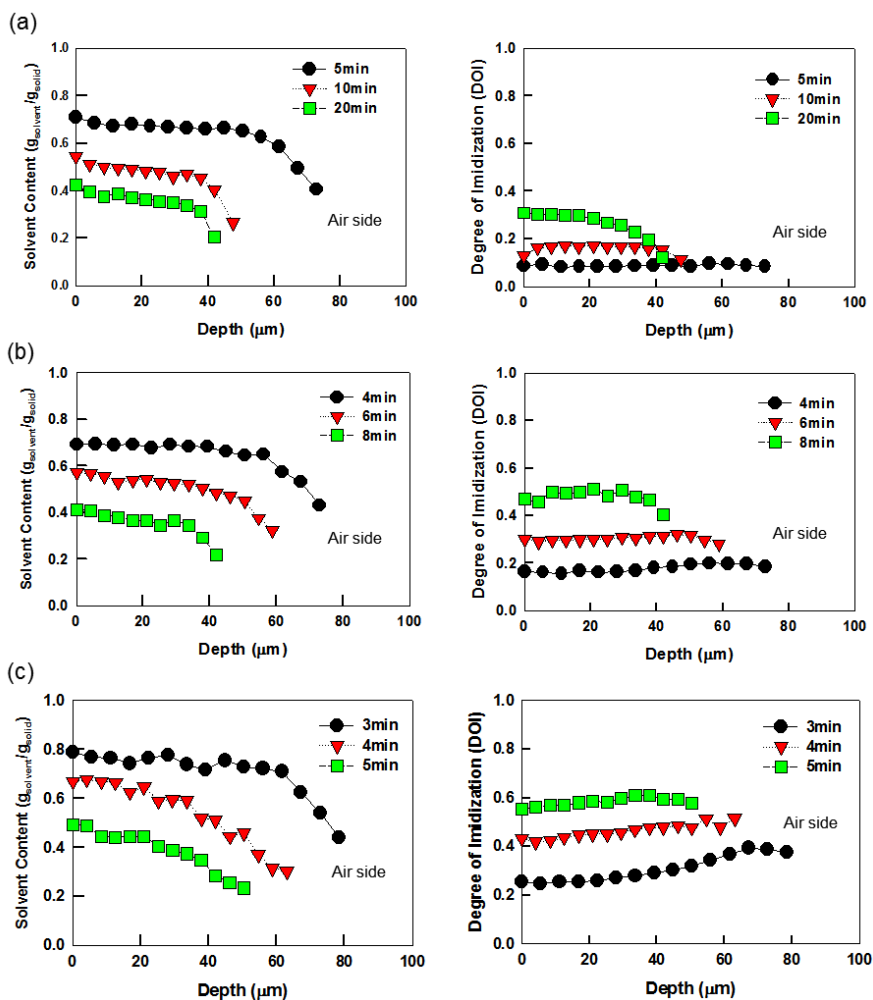


Figure 4.6. Depth-wise residual solvent contents (Left) and DOI (Right) during the drying process through (a) protocol A (120 °C drying), (b) protocol B (140 °C drying), and (c) protocol C (160 °C drying).

difference of residual solvent content was enhanced when the film thickness increased. This is attributed to the increased diffusional resistance of solvent with the increase of film thickness, while the solvent evaporation rate at the film surface remains the same. [46] Different drying temperature, on the other hand, does not affect depth-wise inhomogeneity because higher temperature increases the evaporation rate at the film surface as well as the diffusion rate of solvent in the bulk. So, changing the temperature has little effect on the distribution of residual solvent concentration in the film depth direction during the drying process.

In contrast to the residual solvent concentration, the rate of imidization and its distribution along the film thickness show significant differences. (Figure 4.6) The DOI at the final state of drying is about 0.3, 0.5, and 0.6 when drying temperatures are 120 °C, 140 °C and 160 °C, respectively. The DOI increases with drying temperature even though the amount of residual solvent is almost the same at the final state. This suggests that an increment in imidization rate exceeds the rate of solvent evaporation when the drying temperature increases. The DOI at the air side is found to be lower than the substrate side after 20 min of drying when the drying temperature is 120 °C. (Figure 4.6(a)) It is because the solvent can act as a plasticizer that promotes the imidization reaction. [28, 47] Because the solvent concentration is higher near the substrate during the drying process, imidization occurs faster closer to the substrate. When the drying temperature increases to 140 °C and 160 °C, the side-to-side difference of DOI becomes smaller at the final state even though there still exists a depth-wise inhomogeneous distribution in residual solvent concentration. (Figures 4.6(b), (c)) This can be ascribed to the role of high thermal energy which provides sufficient mobility to the PAA chains, diminishing the capacity of the solvent to act as

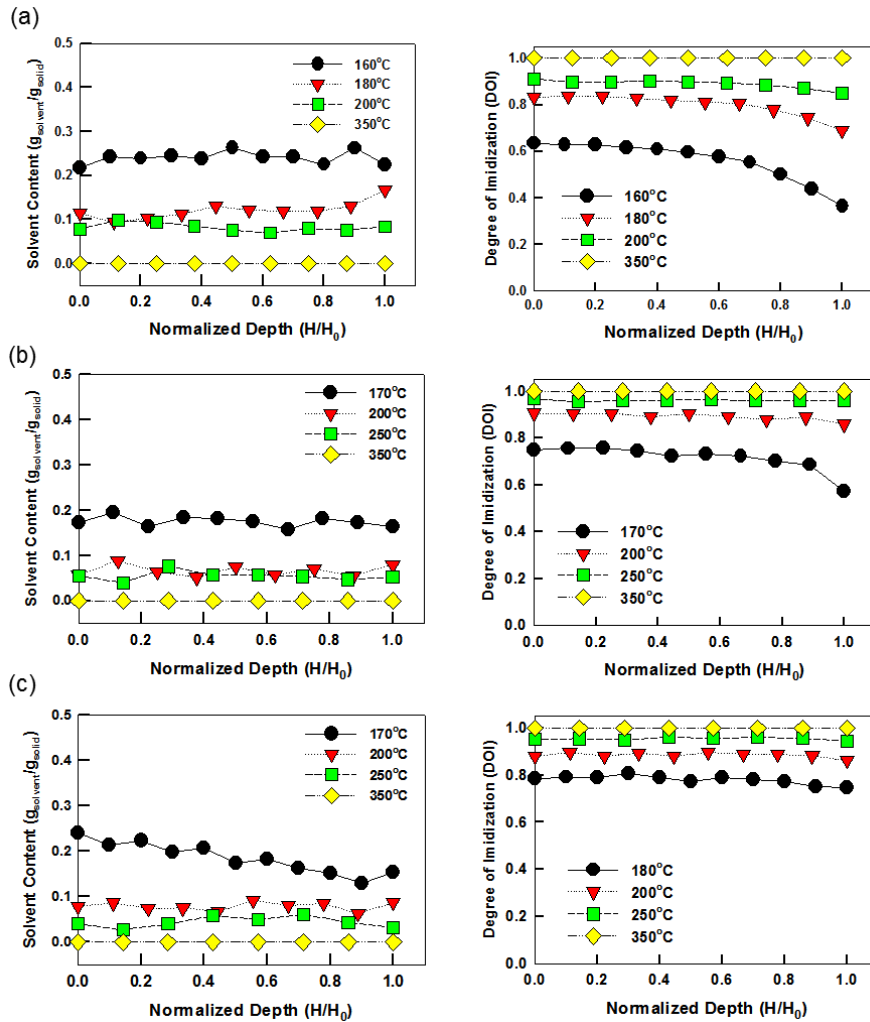


Figure 4.7. Depth-wise residual solvent content (Left) and DOI (Right) during the curing process through (a) protocol A, (b) protocol B, and (c) protocol C. H is a distance from the substrate and H_0 is the film thickness, thus $H/H_0=0$ and 1 corresponds to the substrate side and air side, respectively.

a plasticizer at temperatures higher than 140 °C.

The residual solvent concentration and DOI were measured at different temperatures during the curing process and the results are shown in Figure 4.7. In the figure, the amount of residual solvent decreases while the DOI increases on the way of complete imidization (i.e., DOI=1). The residual solvent concentration and DOI are about 0.1 (g/g) and 0.9, similar to each other regardless of process protocol when the temperature reaches 200 °C. Considering the actual stay time in the curing chamber of protocol A to be 30% longer than protocol C, the result suggests that the temperature, rather than the stay time, is more crucial to the amount of residual solvent and DOI during the curing process. Thus, it can be expected that the change in the residual solvent concentration and DOI will show similar trends after 200 °C independent of the protocols. In addition, the depth-wise inhomogeneity of the residual solvent concentration and DOI which was clearly observed in the drying process disappears after 200 °C due to the high thermal energy provided uniformly along the film thickness direction.

4.2.2. Process path and degree of in-plane chain orientation

The process path was defined in terms of the residual solvent concentration and DOI for different process protocols. (Figure 4.8) Here, the solvent concentration (C_s) was replaced by solid volume fraction using Equation 4.5.

$$\phi = \frac{1}{1 + \rho_r \cdot C_s}, \quad \rho_r = \frac{\rho_p}{\rho_s} \quad (4.5)$$

In the equation, ϕ is the volume fraction of polymer, ρ_p and ρ_s are the density of polymer and solvent, respectively. The density of polymer changes from 1.30 g/cm³ to 1.44 g/cm³ when the PAA is converted to PI [27], but the average value, 1.37 g/cm³ was used as the density of polymer as the difference is not significant. In Fig 7, both the solid volume fraction and DOI increase through different paths as drying and curing proceed, finally reaching 1.0 for every protocol. Compared at the same solid volume fraction, the DOI of protocol A is the lowest while the protocol C the highest. This means that PAA starts to imidize at lower solid content in the case of protocol C, retaining more solvents. As polymer chains are more randomly oriented when there are more solvents in the film and it becomes difficult for stiffer PI chains to be packed closely under biaxial tensile stress, the final degree of in-plane chain orientation of PI made by protocol C can be expected to be lower than the others. And the difference in their paths in different protocols is reduced as the process approaches full imidization. Thus, the process condition during the drying process and at the initial stage of curing process, when there still remains a considerable amount of residual solvent, is considered to act an important role in determining the final microstructure of PI.

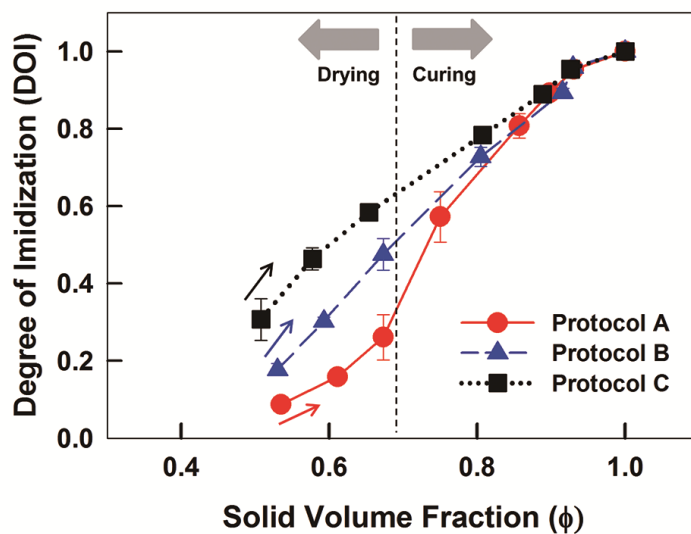


Figure 4.8. Degree of imidization during the drying and curing processes through different protocols.

The degree of in-plane chain orientation of PI films made by different protocols was compared using polarized Raman spectroscopy. (Figure 4.9) In Figure 4.9(a), the Raman intensity of in-plane polarization (I_{xx}) is higher than that of out-of-plane polarization (I_{zz}). It proves that PI chains are preferentially oriented to the in-plane direction due to biaxial tensile stress caused by solvent evaporation. In Figure 4.9(b), a depth-wise profile of the Fraser distribution function, f , is uniform except for protocol A where the f value at the air side is about 0.1 higher than the substrate side. This means that more PI chains orient to the in-plane direction near the film surface in the case of protocol A. This inhomogeneity comes from the lower solvent concentration and imidization rate at the air side, which enables polymer chains to be more densely packed. On the other hand, this side-to-side difference of chain orientation is not observed for protocol B and C because imidization rate along the film thickness is more uniform in these cases. To compare the average value for each protocol, the f of protocol A is about 0.5, while those of protocol B and C are about 0.35 and 0.25, respectively. This indicates that the degree of in-plane chain orientation made by protocol C is the lowest, and the trend coincides well with the result of chain orientation predicted by the process path. It is demonstrated from these results that the process path expressed by the solid volume fraction and DOI can be an effective tool in predicting the final degree of in-plane chain orientation of PI.

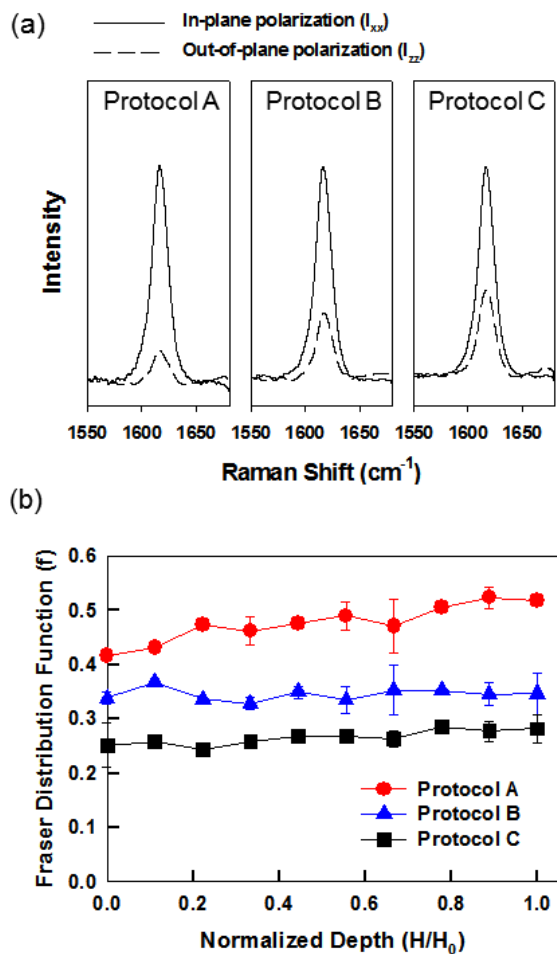


Figure 4.9. (a) Raman spectra of in-plane and out-of-plane polarization appearing at 1610 cm^{-1} for PIs made by different protocols. The spectra were obtained in the middle part of the PI cross-section. (b) Fraser distribution function (f) along the film thickness direction. In the graph, $H/H_0=0$ and 1 corresponds to the substrate side and air side, respectively.

4.2.3. Properties of the cured film

The properties of PI film made by different protocols were examined to observe the effect of different degree of in-plane chain orientation. As shown in Figure 4.10, the structural information of different PI film was first investigated by reflection patterns in WAXD. In all cases the (200) and (210) peaks, normally attributed to the intermolecular packing density and the order of PI crystalline phase, are clearly observed. In a number of studies using WAXD, it was reported that the curing rate or maximum curing temperature affects the chain ordering of PI, resulting in the intensity change or position shift of diffraction peaks. [46, 48] In Figure 4.10, however, the intensity and the position of diffraction peaks are almost the same for PI films made by different protocols, suggesting that the crystallinity and molecular order of the crystalline phase are not much different. Instead, the intensity of the (210) peak relative to the (200) peak is slightly decreased for protocol C, which means that the stacking order of planar units composed of dianhydride, diamine and phenyl ring is weak for PI made by protocol C, and this can be related to the lowest degree of in-plane chain orientation. Because the decrease of peak intensity is so small, however, the difference in chain orientation evidenced by different value of Fraser distribution function has little influence on the degree of crystalline order. This is confirmed by dynamic mechanical analysis (DMA) measurement in Figure 4.11. In the figure, T_g corresponds to the temperature at the maximum peak of $\tan \delta$, thus T_g of different PIs is observed almost the same near 350 °C. It also supports that the crystallinity or molecular packing density is similar for different PIs, otherwise a change in T_g would be observed. This is possible because the measurement of crystallinity or T_g does not necessarily include the information of chain orientation.

In-plane TEC, which represents the dimensional stability of the film, was measured by TMA for different PI films. (Figure 4.12) It was widely reported that TEC of rod-shaped PI is directly related with the chain orientation such that TEC decreases when the PI has higher degree of in-plane chain orientation as it is hard to expand or shrink along the polymer chain axis. [23] In Figure 4.12, the value of TEC increases from 9 ppm/°C to 23 ppm/°C when it goes from protocol A to C. This coincides with the results of in-plane chain orientation indicated by Fraser distribution function. The TEC of the PI made by protocol C is the highest as it shows the lowest value of Fraser distribution function (i.e., the lowest degree of in-plane chain orientation). From the results, it is expected that the PIs made by different protocols have similar crystallinity and stacking order in the crystalline phase, while the orientation of the crystalline phase composed of rod-shaped PI chains is different from each other. In addition, the difference of chain orientation influences more critically on the in-plane TEC than the other physical properties of PI investigated in this study.

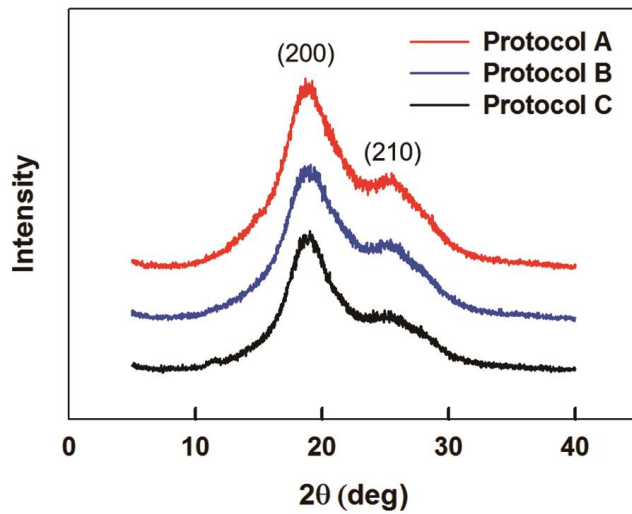


Figure 4.10. WAXD reflection patterns of the PI films depending on different protocols.

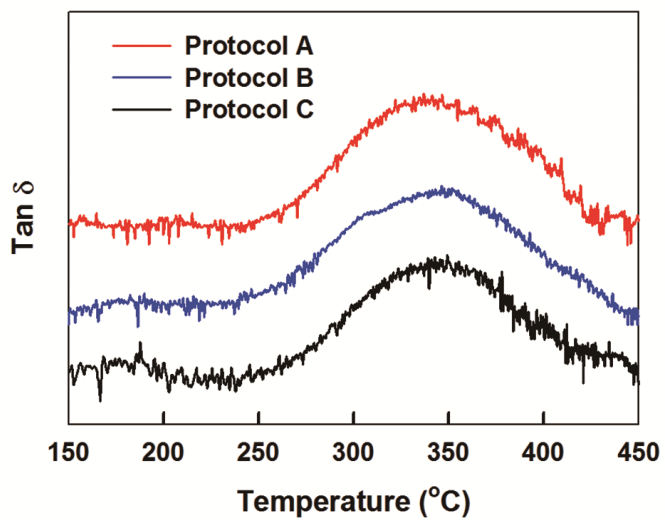


Figure 4.11. Temperature dependence of $\tan \delta$ measured by DMA for the PI films depending on different protocols.

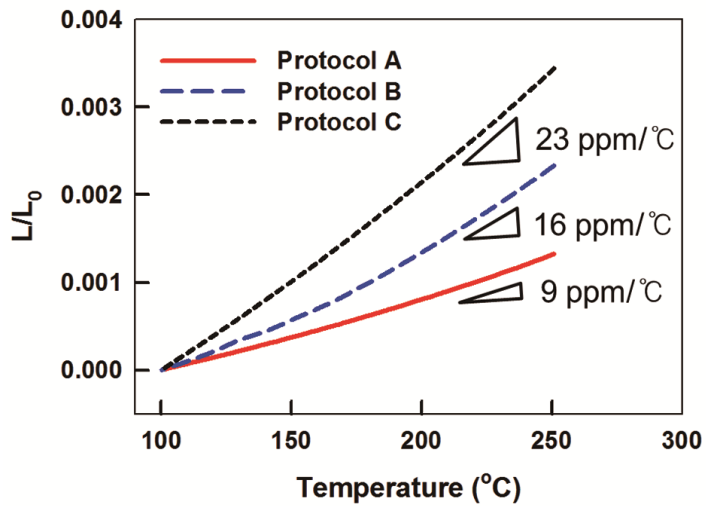


Figure 4.12. Temperature dependence of sample length measured by TMA for the PI films depending on different protocols.

4.3. Interdiffusion and chain orientation in the drying of bilayer polyimide film

4.3.1. Interdiffusion of PAAs having different solvent contents

Different from polymer melts, the solvent can play a crucial role when considering the interdiffusion between different polymer solutions. It is because the mobility of the polymer chain is mainly affected by the amount of solvent that acts as a plasticizer. If a PI bilayer is made by DML drying, total solvent amount included in the top and bottom layer is larger than that in the case of LBL drying at the contact of two layers. Thus, the effect of solvent content in PAA solutions on the interdiffusion speed is investigated first to comprehend the difference in the interdiffusion width of the final cured PI film.

In Figure 4.13, the slope of a compositional change in depth direction becomes less steep as the contact time of two PAAs increases. In addition, the slope is more gradual when the solvent concentration is higher when compared at the same contact time, which means a broader interdiffusion zone. To quantify this, the interdiffusion width (w) is defined by the reciprocal of the maximal slope (w_{app}) where the compositional change occurs most rapidly. [76] :

$$w(t) = w_{app}(t) - w(0), \quad w_{app}(t) = \max[(d\phi/dz)^{-1}] \quad (4.6)$$

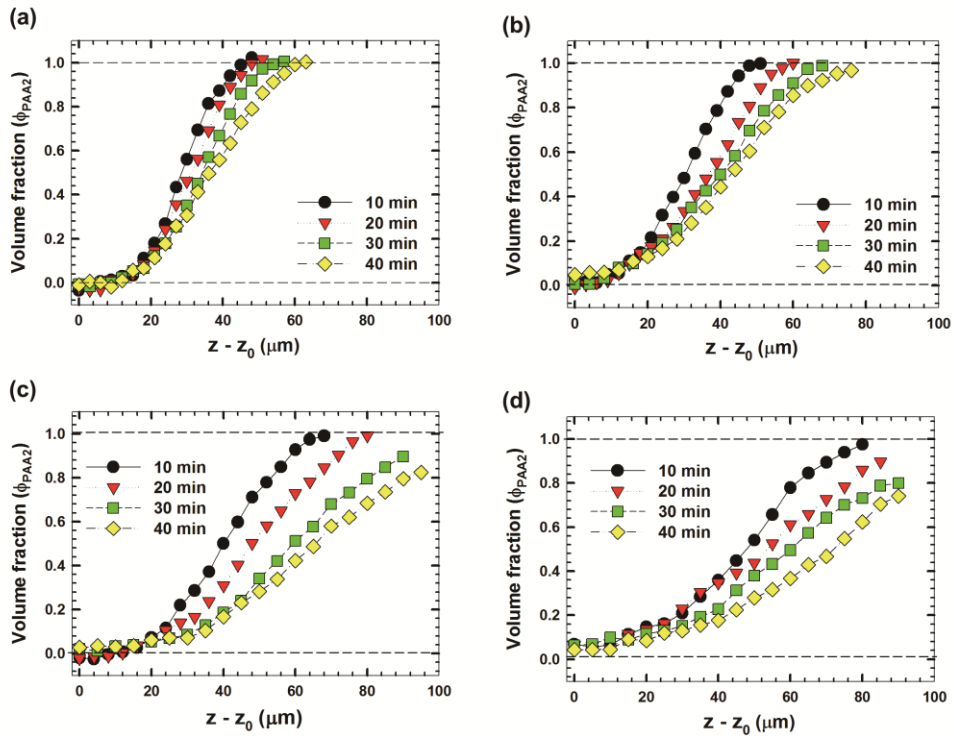


Figure 4.13. Depth-wise volume fraction of PAA-2 ($\Phi_{\text{PAA}2}$) measured at different times after a contact with PAA-1. Different pairs of PAA-1 and 2 have different solvent concentrations of (a) 88 wt%, (b) 90 wt%, (c) 91.5 wt%, and (d) 93 wt%. Abscissa was shifted by z_0 that is the depth below which the volume fraction of PAA-2 increases.

In Equation 4.6, $w(0)$ means the instrumental broadening decided by the DOF of Raman spectrometer. The DOF generally depends on the depth (z) in Raman experiments [81], but it was disregarded in this experiment as the refractive indices between the immersing medium and samples were matched almost the same. Instead, the intrinsic DOF was decided by the wavelength of the laser ($\lambda=633\text{nm}$) and the optical numerical aperture ($\text{NA}=0.9$) as shown in Equation 4.7.

$$w(0) = \frac{2.2 \times \lambda}{(\text{NA})^2} = 1.7 \quad (4.7)$$

Figure 4.14 shows the log-log plot of contact time and $w(t)$ for PAA pairs having different solvent contents. The linear fit in the graph shows the development of $w(t)$ with time can be expressed by a power law $w(t) \propto t^\beta$. The exponent β are 0.12, 0.29, 0.39, and 0.43 for solvent contents, 88, 90, 91.5, and 93 wt%, respectively; it is approaching to the Fickian exponent of 0.5 as the solvent content increases. This behavior is similar to that of polymer melts in that the interdiffusion width increases with time slower than a Fickian diffusion of $w(t) \propto t^{0.5}$, but the speed is critically affected by the amount of solvent in this case. Thus, the interdiffusion between PAAs can be faster when they are processed by the DML method as they contain more solvents than LBL even when the same PAA pairs are used. In addition, it is expected for a PI bilayer made by DML to have a longer interdiffusion width because the contact time is 10 min during the drying process, twice the LBL drying in this experiment.

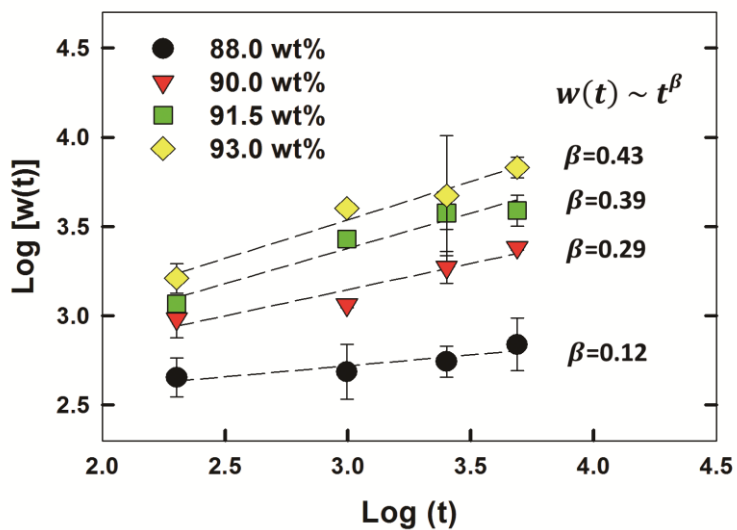


Figure 4.14. Log-log plot of the interdiffusion width $w(t)$ between PAA-1 and 2 at different contact time (t). Different symbols represent PAA-1/PAA-2 pairs having different solvent contents which are indicated in the graph.

4.3.2. Interdiffusion width of cured PI

Raman spectroscopy was used to detect the actual interdiffusion width of bilayer PI films made by the DML and LBL methods. Instead of depth profiling the film, a lateral profiling method was used to enhance the spatial resolution of the measurements and the compositional changes at the film interface are plotted in Figure 4.15(a). To compare the interdiffusion width, the same definition of interdiffusion width as used in Equation 4.6 was employed. Here, $w(0)$ was replaced by the laser focus waist diameter as in Equation 4.8. [89]

$$w(0) = \frac{1.22 \times \lambda}{NA} = 0.86 \mu m \quad (4.8)$$

Comparing the interdiffusion width of PI bilayers made by the LBL method in Figure 4.15(b), the width decreases as the drying temperature of the bottom layer (T_b) increases. It is because larger fraction of PAA chains in the bottom layer is converted to PI at the elevated temperature, which results in an increase of the Flory interaction parameter for the upper PAA layer. [36] At the same time, the swelling of the bottom layer due to the solvent inclusion is hindered as PI is insoluble to DMAc. [33, 34, 35, 90] The extent of solvent diffusion depending on the imidization degree will be discussed in the following section. However, the decrease in the interdiffusion width according to T_b is slight in Figure 4.15(b). This can be ascribed to the spatial resolution of the Raman spectrometer which is about $0.86 \mu m$, not high enough to precisely detect the small width when T_b is high. On the other hand, the interdiffusion width of PI made by DML drying is about $1.1 \mu m$ which is clearly larger than that made by LBL drying. This difference can be explained by the faster interdiffusion

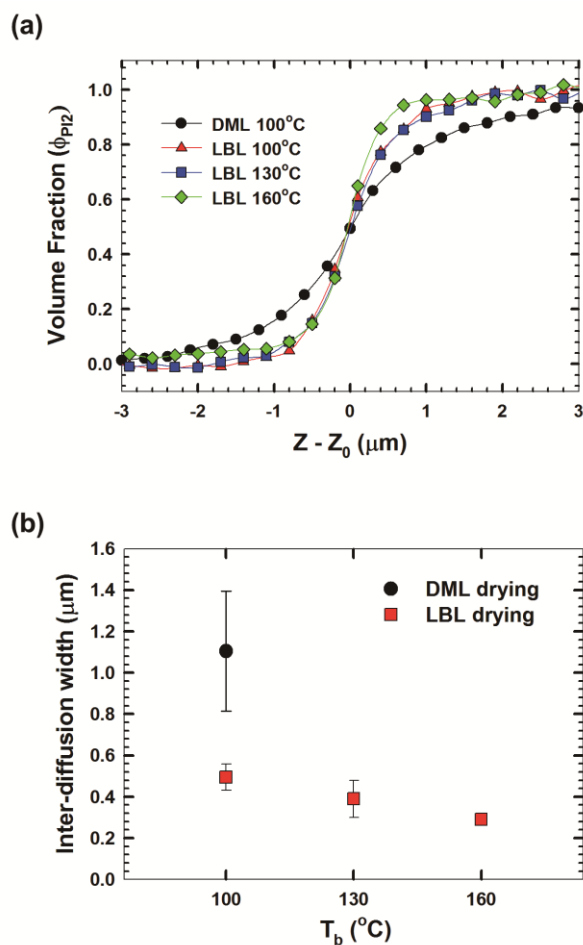


Figure 4.15. Interdiffusion data of the cured PI bilayers made by the DML and LBL methods. (a) Variation of PI-2 volume fraction (ϕ_{PI2}) measured at different positions on the cross section of the cured PI. Abscissa was shifted by Z_0 where the volume of two PIs is equal (i.e. $\phi_{PI2} = 0.5$). (b) The interdiffusion width $w(t)$ of the PI bilayers according to the drying temperature of the bottom layer (T_b).

between PAAs in the case of DML drying as discussed in the previous section. Two PAAs interdiffuse faster and the contact between two layers is longer for DML drying. As the interdiffusion during the curing process that involves only a small amount of solvent can be neglected, [35] the difference in their speed of interdiffusion during the drying process plays a crucial role in determining the interdiffusion width of the final PI bilayers. Considering the adhesion property between immiscible or partially miscible polymers is strengthened by the wider interdiffusion layer, the DML method is regarded to be more beneficial in making multilayer polymer films with a reliable interfacial strength compared to the conventional LBL method.

4.3.3. Solvent diffusion into dried PAA films

The DOI of the bottom layer is varied according to the drying temperature when the bilayer PI film is made by the LBL method. This results in the change in its interaction with the top layer. Among them, the extent of solvent diffusion into the bottom layer can directly affect the chain orientation of the cured PI film as well as the interdiffusion width. DOI can be defined as in Equation 4.9 using the ratio of two characteristic peaks of PAA and PI appeared in the Raman spectrum.

$$\text{DOI} = \frac{I(\text{PI})}{I(\text{PAA})+I(\text{PI})} = \frac{I(1108 \text{ cm}^{-1})}{I(1180 \text{ cm}^{-1})+I(1108 \text{ cm}^{-1})} \quad (4.9)$$

From this definition, DOI=1.0 means that all the PAA chains are imidized to PI. Actual DOI of PAA-1 dried at 100, 130, and 160 °C for 5 min was measured to be 0.03, 0.25, and 0.75 respectively, showing that the increase of DOI at higher

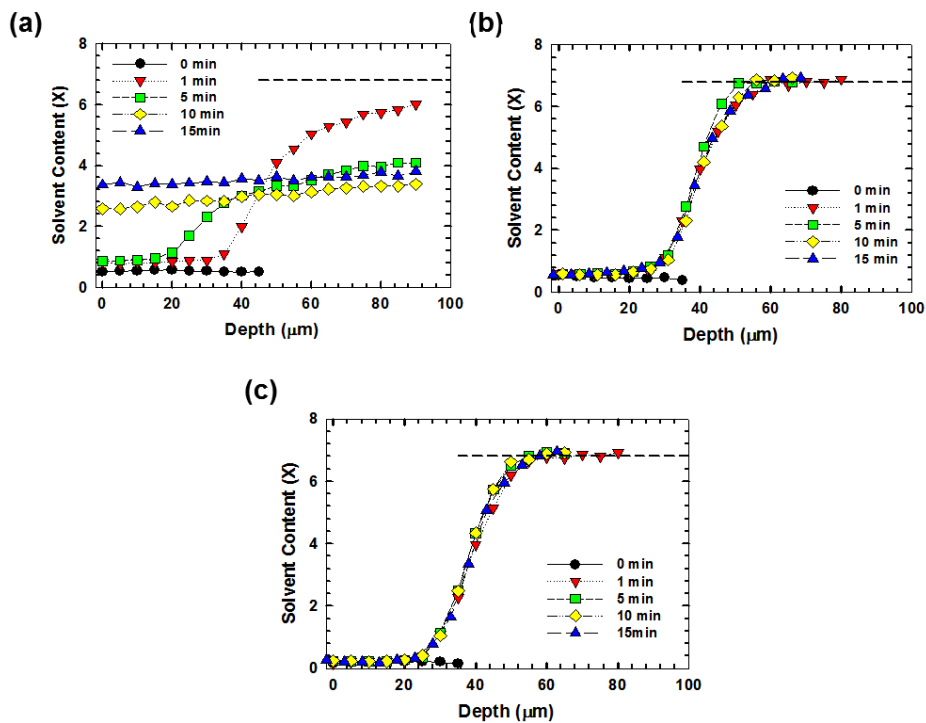


Figure 4.16. Depth-wise solvent content (X) measured at different times after a contact between the dried PAA-1 and 2 solutions. The dried PAA-1 was prepared by drying at different temperatures (T_b) of (a) 100 °C, (b) 130 °C, and (c) 160 °C respectively. Dashed line shows the calculated initial solvent content (i.e. $X=7.3$) of PAA-2 solution, which corresponds to 12 wt%.

temperature was very significant. After the PAA-1 films which were dried at these temperatures were put on the PAA-2 solution as can be seen in Figure 3.13(b), the distribution of solvent content (X) in both layers was depth profiled at different times. (Figure 4.16) Figure 4.16(a) shows how the solvent in PAA-2 diffuses into PAA-1, and the solvent content in PAA-1 increases rapidly from the interface when $T_b=100$ °C. When $t=10$ min, the distribution of solvent concentration becomes almost constant in depth direction, reaching to a nearly equilibrium state. As this experiment is conducted at room temperature, it is expected that the solvent diffusion will be much faster when it is assumed that the two layers are dried at 100 °C which is the temperature actually used to make a bilayer PI film. In the cases of $T_b=130, 160$ °C, a gradual increase of solvent content is observed at the interface from $t=1$ min. (Figure 4.16(b), (c)) Considering the DOF caused by the refractive index mismatch is about 24 μm , this gradual change in solvent content distribution is more reasonably ascribed to the instrumental broadening, not to the actual solvent diffusion. Furthermore, the distribution of solvent content at $t=15$ min shows no difference with $t=1$ min, all of which leads to the conclusion that the solvent in PAA-2 can hardly diffuse into PAA-1 when T_b is higher than 130 °C. This marked difference results from the increased DOI of PAA-1 that impedes the inclusion of solvent as explained earlier. It is worth noting that the amount of solvent diffusion into PAA-1 is drastically reduced at $T_b=130$ °C compared with $T_b=100$ °C even though the DOI is as small as 0.25. The difference in the extent of solvent diffusion can affect the chain orientation of PAA in the bottom layer after the drying process and finally changes the chain orientation of the cured PI film.

4.3.4. In-plane chain orientation of cured PIs

Except for the molecular structure of PI chain, the degree of in-plane chain orientation of a cured PI is influenced by the process path that consists of two parameters, the residual solvent content and the DOI during drying and curing. PAA chains are more randomly oriented when there is a larger amount of solvent remaining in a dried film. Faster imidization at this state lowers the final degree of in-plane chain orientation as it becomes difficult for polymer chains to make a well-ordered structure after the PAA imidizes to more rigid PI. This implies that the lower degree of in-plane chain orientation of a single layer PI results when the film thickness or drying temperature increases. In order to see how the chain orientation of a multilayer PI film is different from that of a single layer, the degree of in-plane chain orientation was measured on the cross-section of bilayer PI films made by the DML and LBL method as shown in Figure 3.10, and the results are compared with the 20 μm -thick PI-1 single layer. (Figure 4.17)

In Figure 4.17, the Fraser distribution function of all the PI-2 layers on top is smaller than the PI-1 layers. This is because the PI-2 chain that has ether linkage is structurally more flexible than PI-1, resulting in the lower degree of in-plane orientation. Here, the abscissa was shifted by the interface (Z_0) between PI-1 and 2. Comparing the chain orientation of PI-2 in Figure 4.17(e), the f values of PI-2 are almost same regardless of drying method or drying temperature of the bottom layer. In Figure 4.17, the Fraser distribution function of all the PI-2 layers on top is smaller than the PI-1 layers. This is because the PI-2 chain that has ether linkage is structurally more flexible than PI-1, resulting in the lower degree of in-plane orientation. Here, the abscissa was shifted by

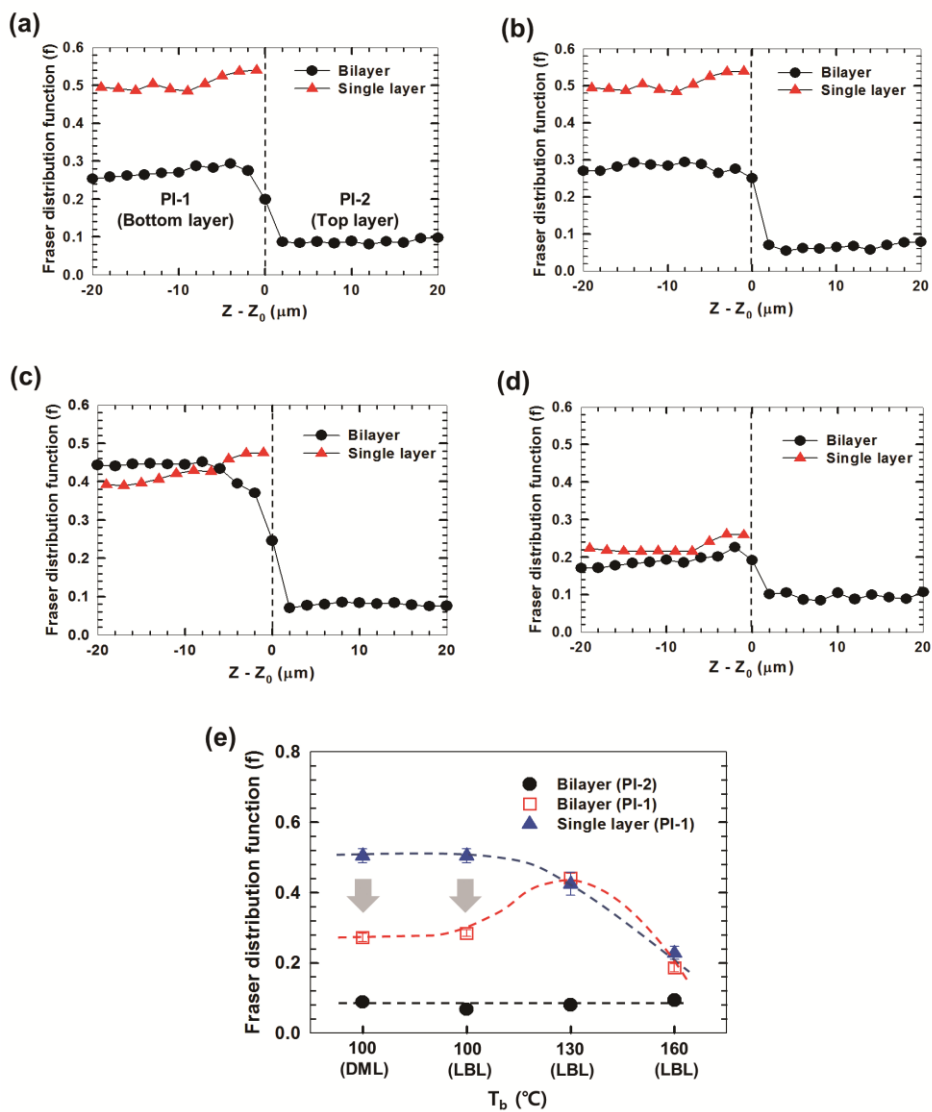


Figure 4.17. Degree of in-plane chain orientation of single and bilayer PI films represented by the Fraser distribution function. PI films were made by (a) DML drying ($T_b = 100^\circ\text{C}$), (b) LBL drying ($T_b = 100^\circ\text{C}$), (c) LBL drying ($T_b = 130^\circ\text{C}$), (d) LBL drying ($T_b = 160^\circ\text{C}$).

the interface (Z_0) between PI-1 and 2. Comparing the chain orientation of PI-2 in Figure 4.17(e), the f values of PI-2 are almost same regardless of drying method or drying temperature of the bottom layer. This seems to be related with a high flexibility of PI-2 that makes the chain orientation less dependent on the processing conditions than PI-1 which has a more rigid structure. Besides, maintaining the drying temperature of the top layer at 100 °C can be another reason for the similar f between PI-2 layers. In Figure 4.17(a), the f value of PI-1 in bilayer film made by the DML is about 0.3, almost half of the PI-1 single layer. The degree of in-plane chain orientation of a single layer PI decreases when the film thickness increases as mentioned before, and this explanation can be applied to the lower degree of in-plane chain orientation of PI-1 in a PI bilayer. From the view point of PI-1, the structuring of PI-1 and 2 layers having 20 μm for each by the DML experiences the same process path with the structuring of 40 μm -thick PI-1 single layer at a time. Likewise, the f of PI-1 in a bilayer that was made by the LBL method at $T_b=100$ °C is much smaller than that of the PI-1 single layer as in Figure 4.17(b). It is because the solvent in the top layer can diffuse easily into the bottom layer when $T_b=100$ °C as shown in Figure 4.16(a). PAA-1 chain highly ordered to the in-plane direction after drying of the bottom layer can lose its alignment due to the inclusion of solvent when the top layer is coated. As the imidization proceeds with this weak alignment of PAA chains during the curing process, the final degree of in-plane orientation of PI-1 becomes lower than that of a single layer. On the other hand, the f of PI-1 makes no difference between single and bilayer films at $T_b=130, 160$ °C as shown in Figures 4.17(c), (d). This is caused by the imidization of the bottom layer during drying that hinders the solvent in the top layer from diffusing into the bottom layer as described in Figures 4.17(b), (c). If there is no

additional inclusion of solvent into the bottom layer, the final chain orientation of PI-1 in bilayer film is simply decided by the same process path with manufacturing a 20 μm -thick PI-1 single layer. To summarize, the degree of in-plane chain orientation of a PI-1 single layer decreases at higher drying temperature and it corresponds well with the result of previous study. When an additional layer is structured by the LBL method, the chain orientation of the bottom layer shows different aspects from a single layer depending on the extent of solvent inflow from the top layer. If the solvent in the top layer can easily diffuse into the bottom layer (i.e. $T_b=100\text{ }^\circ\text{C}$), the degree of in-plane chain orientation becomes lower than that of a single layer and it is comparable with the chain orientation of PI-1 in a bilayer film made by the DML method.

Chapter 5. Summary

In this thesis, the effect of film thickness and processing conditions on the chain orientation of PI film was investigated using confocal Raman spectroscopy. In addition, the interdiffusional behavior between two different PIs was observed in bilayer PI film and how the two different drying methods affect the final width of interdiffusion and chain orientation.

Firstly, the effect of film thickness on the final chain orientation was examined. As the thickness of the BPDA-PDA PI film increased, the amount of residual solvent after drying was increased, and more solvent remained near the substrate side than near the air side leading to an inhomogeneous depth-wise distribution. This is because it takes longer for solvent molecules to diffuse out to a film surface as the film thickness increases, and the diffusional resistance increases near the film surface due to solvent evaporation. As a result, the tensile stress that induces an in-plane chain orientation was reduced for a thick PI film with an inhomogeneous depth-wise profile. In other words, the thicker film had a lower degree of in-plane chain orientation, especially near the substrate than near the surface. In addition, the beginning of imidization reaction in the curing process followed by drying was faster for thick PI as it retained more residual solvent inside. It is because the solvent molecules that were unbound to polymer chains could promote the imidization reaction by acting as a plasticizer. Once the chain rigidity of the polymer was enhanced by the imidization reaction, the chains were hardly packed densely to give a highly ordered structure in which the polymer chains were preferentially aligned to the in-plane direction. Therefore, both the degree and uniformity of the chain orientation of the dried PAA film in the thickness direction could considerably affect those of the PI film. The thick PI exhibited a lower average degree of in-plane orientation after curing than that of the

thin film and an inhomogeneous distribution with much lower degree of in-plane orientation near the substrate side than near the air side.

To see the effect of thermal history, BPDA-PDA PI films were manufactured by three different process protocols, and the degree of in-plane chain orientation of the fully imidized PI was investigated. The process path was defined according to the residual solvent concentration and DOI which were measured during the process of drying and curing. These variables explain the difference in chain orientation of the fully imidized PIs. For the protocol starting at higher temperature, the PAA was converted to PI with larger amount of solvent in the film. Because biaxial tensile stress caused by solvent evaporation makes PAA chains align to the in-plane direction, more residual solvent means less fraction of polymer chains orient to the in-plane direction. As a result, the protocol with a higher drying temperature made the PAA imidized to the stiffer PI at a more randomly oriented state. This feature was observed to lower the degree of in-plane chain orientation of the fully imidized PI. It could be due to an increase of chain rigidity which retards close packing of polymer chains during the subsequent solvent evaporation. The difference in chain orientation influenced the in-plane TEC. The TEC can be considered as an important parameter representing the dimensional stability of the film at high temperature processing. The TEC changed from 9 ppm/°C to more than 20 ppm/°C when manufactured by different protocols. In spite of the difference in TEC, the crystallinity and T_g did not change much, suggesting that the in-plane TEC was more significantly affected by the thermal history among the other film properties when manufacturing rod-shaped PI films.

Finally, the interdiffusion width and chain orientation of PI bilayer film was investigated when the film was made by both DML and LBL drying methods. The interdiffusion occurs during the drying process of PAA bilayer composed of BPDA-PDA and BPDA-ODA. The measurement of interdiffusion speed showed the broadening of interdiffusion width with a power law behavior with time and the exponent increased if there remained a larger amount of solvent in PAA solution. It means that the mobility of PAA chains which is most significantly affected by the solvent content, and the contact time of two layers can be crucial factors in determining the final interdiffusion width. As the bilayer film made by the DML method undergoes a longer contact time containing more solvent during the drying process, the interdiffusion width of the cured PI bilayer was observed larger than that made by the LBL method.

The chain orientation that directly affects the thermal expansivity of PI film is influenced by the variation of residual solvent content and imidization degree during the manufacturing process. The degree of in-plane orientation of the bottom layer which had a more rigid structure was observed to be vulnerable to the processing conditions. The degree of in-plane chain orientation of the bottom layer was smaller than that of a 20 μm -thick single layer film when the bilayer PI film consisting of two 20 μm -thick layers was made by the DML method. This was because the bilayer PI film made by DML drying experienced the same thermal history with a 40 μm -thick single layer, which generally lowers the degree of in-plane chain orientation. In case of LBL drying, the chain orientation of the bottom layer was mainly affected by the extent of solvent intrusion from the top layer. The solvent in the top layer diffused into the bottom layer easily when the bottom layer was dried at 100 $^{\circ}\text{C}$ and this made the

final degree of in-plane chain orientation of the bottom layer lower than that of a single layer. On the other hand, no significant difference in the degree of in-plane chain orientation was observed when the drying temperature of the bottom layer exceeded 130 °C. It was ascribed to the restrained solvent diffusion from the top layer as a larger fraction of PAA in the bottom layer was converted to PI at such a high drying temperature, becoming less soluble to the solvent.

References

1. G. Zhao, T. Ishizaka, H. Kasai, M. Hasegawa, T. Furukawa, H. Nakanishi, H. Oikawa, Ultralow-dielectric-constant films prepared from hollow polyimide nanoparticles possessing controllable core sizes, *Chem. Mater.* **2009**, 21, 419-424.
2. T. Kurosawa, T. Higashihara, M. Ueda, Polyimide memory: a pithy guideline for future applications, *Polym. Chem.* **2013**, 4, 16-30.
3. K. Xi, Z. Meng, L. Heng, R. Ge, H. He, X. Yu, X. Jia, Polyimide-polydimethylsiloxane copolymers for low dielectric constant and moisture resistance applications, *J. of Appl. Polym. Sci.* **2009**, 113, 1633-1641.
4. J.-S. Park, T.-W. Kim, D. Stryakhilev, J.-S. Lee, S.-G. An, Y.-S. Pyo, D.-B. Lee, Y. G. Mo, D.-U. Jin, H. K. Chung, Flexible full color organic light-emitting diode display on polyimide plastic substrate driven by amorphous indium gallium zinc oxide thin-film transistors, *Appl. Phys. Lett.* **2009**, 95, 013503.
5. B.-S. Park, W. Y. Kim, K.-B. Yoon, Luminous polyimide bearing the coumarin 6 chromophore in the side group: synthesis and fluorescence image patterning, *Korean J. Chem. Eng.* **2014**, 31, 172-177.
6. I.-H. Tseng, M.-H. Tsai, C.-W. Chung, Flexible and transparent polyimide films containing two-dimensional alumina nanosheets templated by graphene oxide for improved barrier property, *Appl. Mater. Interfaces* **2014**, 6, 13098-13105.
7. Y. Momoi, O. Sato, T. Koda, A. Nishioka, O. Haba, K. Yonetake, Surface rheology of rubbed polyimide film in liquid crystal display, *Optical Material Express* **2014**, 4, 1057-1066.

8. Y. Tsuda, Y. Matsuda, T. Matsuda, Soluble polyimides bearing long-chain alkyl groups on their side chain via polymer reaction, *Int. J. of Polym. Sci.* **2012**, 1-10.
9. Y. Mansoori, S. S. Sanael, M.-R. Zamanloo, G. Imanzadeh, S. V. Atghia, Synthesis and properties of new polyimide/clay nanocomposite films, *Bull. Mater. Sci.* **2013**, 36, 789-798.
10. E. Hamciuc, C. Hamciuc, V. E. Musteata, Y. Kalvachev, A. Wolinska-Grabczyk, Preparation and characterization of new polyimide films containing zeolite L and/or silica, *High Performance Polymers*, **2013**, 1-13.
11. M. Hasegawa, T. Matano, Y. Shindo, T. Sugimura, Spontaneous molecular orientation of polyimides induced by thermal imidization. 2. In-plane orientation, *Macromolecules* **1996**, 29, 7897-7909.
12. H. M. Tong, K. D. Hsuen, K. L. Saenger, G. W. Su, Thickness-direction coefficient of thermal expansion measurement of thin polymer films, *Rev. Sci. Instrum.* **1991**, 62, 422-430.
13. W. M. Prest, D. J. Luca, The origin of the optical anisotropy of solvent cast polymeric films, *J. Appl. Phys.* **1979**, 50, 6067-6071.
14. W. M. Prest, D. J. Luca, The alignment of polymers during the solvent-coating process, *J. Appl. Phys.* **1980**, 51, 5170-5174.
15. F. Li, K.-H. Kim, E. P. Savitski, J.-C. Chen, F. W. Harris, S. Z. D. Cheng, Molecular weight and film thickness effects on linear optical anisotropy of 6FDA-PFMB polyimides, *Polymer* **1997**, 38, 3223-3227.

16. H.-C. Liou, P. S. Ho, R. Stierman, Thickness dependence of the anisotropy in thermal expansion of PMDA-ODA and BPDA-PDA thin films, *Thin Solid films* **1999**, 339, 68-73.
17. J.-S. King, W. Lee, Li, Chang, W. Whang, Structural effect on stretch-induced birefringence in polyimide films *Jpn., J. Appl. Phys.* **2007**, 46, 6801-6806.
18. S. C. Noe, J. Y. Pan, S. D. Senturia, Optical waveguide as a method for characterizing the effect of extended cure and moisture on polyimide films, *Polym. Eng. Sci.* **1992**, 32, 1015-1020.
19. H. Nomura, M. Asano, *Jpn. J. Appl. Phys. Part1* **1993**, 32, 3933-3937.
20. H. Nomura, M. Asano, *Jpn. J. Appl. Phys. Part1* **1996**, 11, 5825-5830.
21. Y. Terui, S.-I. Matsuda, S. Ando, Molecular structure and thickness dependence of chain orientation in aromatic polyimide films, *J. Polym. Sci., Part B: Polym. Phys.* **2005**, 43, 2109-2120.
22. S.-I. Matsuda, S. Ando, Molecular orientation of rigid-rod polyimide films characterized by polarized attenuated total reflection/Fourier transform infrared spectroscopy, *J. Polym. Sci., Part B: Polym. Phys.* **2003**, 41, 418-428.
23. J. C. Coburn, M. T. Pottiger, S. C. Noe, S. D. Senturia, Stress in polyimide coatings, *J. Polym. Sci., Part B: Polym. Phys.* **1994**, 32, 1271-1283.
24. T. Miwa, Y. Okabe, M. Ishida, Effects of precursor structure and imidization process on thermal expansion coefficient of polyimide (BPDA/PDA), *Polymer* **1997**, 38, 4945-4949.
25. H.-C. Liou, R. Willecke, P. S. Ho, Study of out-of-plane elastic properties of PMDA-ODA and BPDA-PDA polyimide thin films, *Thin Solid Films* **1998**, 323, 203-208.

26. J.-H. Jou, P.-T. Huang, H.-C. Chen, C.-N. Liao, Coating thickness effect on the orientation and thermal expansion coefficient of polyimide films, *Polymer* **1992**, 33, 967-974.
27. M. Dabral, S. Xia, W. W. Gerberich, L. F. Francis, L. E. Scriven, Near-surface structure formation in chemically imidized polyimide films, *J. Polym. Sci., Part B: Polym. Phys.* **2001**, 39, 1824-1838.
28. C. Johnson, S. L. Wunder, FT-Raman investigation of the thermal curing of PMDA/ODA polyamic acids, *J. Polym. Sci., Part B: Polym. Phys.* **1993**, 31, 677-682.
29. N. Takahashi, D. Y. Yoon, W. Parrish, molecular order in condensed states of semiflexible poly(amic acid) and polyimide, *Macromolecules* **1984**, 17, 2583-2588.
30. Y. Zhai, Q. Yang, R. Zhu, Y. Gu, The study on imidization degree of polyamic acid in solution and ordering degree of its polyimide film, *J. Mater. Sci.* **2008**, 43, 338-344.
31. L. Leger, C. Creton, Adhesion mechanisms at soft polymer interfaces, *Phil. Trans. R. Soc.* **2008**, 366, 1425-1442.
32. P. G. de Gennes, Reptation of a polymer chain in the presence of fixed obstacles, *J. Chem. Phys.* **1971**, 55, 572.
33. S. F. Tead, E. J. Kramer, T. P. Russell, W. Volksen, Interdiffusion at polyimide interfaces, *Polymer* **1992**, 33, 3382-3387.
34. H. R. Brown, A. C. M. Yang, T. P. Russell, W. Volksen, Diffusion and self-adhesion of the polyimide PMDA-ODA, *Polymer* **1988**, 29, 1807-1811.

35. N. C. Stoffel, E. J. Kramer, W. Volksen, T. P. Russell, Imidization and interdiffusion of poly(amic ethyl ester) precursors of PMDA/3,4'-ODA, *J. Polym. Sci., Part B: Polym. Phys.* **1998**, 36, 2247-2258.
36. S. F. Tead, E. J. Kramer, T. P. Russell, W. Volksen, Solvent and curing effects on diffusion at polyimide interfaces, *W. Mater. Res. Soc. Symp. Proc.* **1989**, 154.
37. D. Wilson, H. D. Stenzenberger, P. M. Hergenrother, *Polyimides*, Blackie & Son Ltd, **1990**, Chapter 1.
38. N. C. Stoffel, E. J. Kramer, W. Volksen, T. P. Russell, Solvent and isomer effects on the imidization of pyromellitic dianhydride-oxydianiline-based poly(amic ethyl ester)s, *Polymer* **1993**, 34, 4524-4530.
39. S. I. Kim, S. M. Pyo, M. Ree, Investigation of glass transition behaviors in poly(amic acid) precursors of semiflexible polyimides by oscillating differential scanning calorimetry, *Macromolecules* **1997**, 30, 7890-7897.
40. Y. Terui, S. Ando, Coefficient of molecular packing and intrinsic birefringence of aromatic polyimides estimated using refractive indices and molecular polarizabilities, *J. Polym. Sci., Part B: Polym. Phys.* **2004**, 42, 2354-2366.
41. M. Hasegawa, N. Sensui, Y. Shindo, R. Yokota, Structure and properties of novel asymmetric biphenyl type polyimides. Homo- and copolymers and blends, *Macromolecules* **1999**, 32, 387-396.
42. L. Lin, S. A. Bidstrup, Effect of molecular orientation on the dielectric properties of spin-coated polyimide films, *J. Appl. Polym. Sci.* **1994**, 54, 553-560.

43. S. C. Noe, J. Y. Pan, S. D. Senturia, Optical waveguiding as a method for characterizing the effect of extended cure and moisture on polyimide films, *Polym. Eng. Sci.* **1992**, 32, 1015-1020.
44. H.-C. Liou, P. S. Ho, R. Stierman, Thickness dependence of the anisotropy in thermal expansion of PMDA-ODA and BPDA-PDA thin films, *Thin Solid Films* **1999**, 339, 68-73.
45. K. Sekiguchi, K. Takizawa, S. Ando, Thermal expansion behavior of the ordered domain in polyimide films investigated by variable temperature WAXD measurements, *J. Photopolym. Sci. Tech.* **2013**, 26, 327-332.
46. P. S. Ho, T. W. Poon, J. Leu, Molecular structure and thermal /mechanical properties of polymer thin films, *J. Phys. Chem. Solids* **1994**, 55, 1115-1124.
47. Y.-K. Xu, M.-S. Zhan, K. Wang, Structure and properties of polyimide films during a far-infrared-induced imidization process, *J. Polym. Sci., Part B: Polym. Phys.* **2004**, 42, 2490-2501.
48. H. Chung, Y. Joe, H. Han, The effect of curing history on the residual stress behavior of polyimide thin films, *J. Appl. Polym. Sci.* **1999**, 74, 3287-3298.
49. H. Chung, J. Lee, W. Jang, Stress behaviors and thermal properties of polyimide thin films depending on the different curing process, *J. Polym. Sci., Part B: Polym. Phys.* **2000**, 38, 2879-2890.
50. M. Ree, T. J. Shin, Y.-H. Park, S. I. Kim, S. H. Woo, C. K. Cho, C. E. Park, Residual stress and optical properties of fully rod-like poly(p-phenylene pyromellitimide) in thin films: Effects of soft-bake and thermal imidization history, *J. Polym. Sci., Part B: Polym. Phys.* **1998**, 36, 1261-1273.

51. S. H. Lee, Y. C. Bae, Thermal stress analysis for polyimide thin films and a substrate layer system, *Macromol. Chem. Phys.* **2000**, 201, 1286-1291.
52. T. Nishino, M. Kotera, N. Inayoshi, N. Miki, K. Nakamae, Residual stress and microstructures of aromatic polyimide with different imidization processes, *Polymer* **2000**, 41, 6913-6918.
53. H. Chung, C. Lee, H. Han, Moisture-induced stress relaxation of polyimide thin films, *Polymer* **2001**, 42, 319-328.
54. H. Lei, J. A. Payne, A. V. McCormick, L. F. Francis, W. W. Gerberich, L. E. Scriven, Stress development in drying coatings, *J. Appl. Polym. Sci.* **2001**, 81, 1000-1013.
55. J. A. Payne, A. V. McCormick, L. F. Francis, In situ stress measurement apparatus for liquid applied coatings, *Rev. Sci. Instrum.* **1997**, 68, 4564-4568.
56. S.-Y. Tam, Stress effects in drying coating, Thesis, **1997**, 58-05, 2564.
57. R. A. Cairncross, The fate of residual solvent in drying coatings: Can it get trapped and how?, Proceedings of the Pressure Sensitive Tape Council Tech XXV meeting **2002**.
58. E. B. Gutoff, Fundamentals of drying coatings, Proceedings of Tech XXVIII Technical Seminar **2005**.
59. B. Cuerrier, C. Bouchard, C. Allain, C. Bernard, Drying kinetics of polymer films, *AIChE* **1998**, 44, 791-798.
60. A. K. Ghosh, Fundamentals of paper drying – theory and application from industrial perspective, *Intech* **2011**, 25, 535-582.
61. U. W. Gedde, Polymer physics, Kluwer Academic Publishers **2001**, Chapter 9.

62. H.-M. Liem, P. Etchegoin, K. S. Whitehead, D. D. C. Bradley, Raman anisotropy measurement: An effective probe of molecular orientation in conjugated polymer thin films, *Adv. Funct. Mater.* **2003**, 13, 66-72.
63. H.-M. Liem, P. Etchegoin, K. S. Whitehead, D. D. C. Bradley, Raman scattering as a probe of morphology in conjugated polymer thin films, *J. Appl. Phys.* **2002**, 92, 1154-1161.
64. H.-M. Liem, P. Etchegoin, D. D. C. Bradley, Anomalous Raman scattering from the surface of conjugated polymer melts, *Physical Review B* **2001**, 64, 144209.
65. R. G. Snyder, Raman scattering activities for partially oriented molecules, *J. Mol. Spectroscopy* **1971**, 37, 353-365.
66. L. Margulies, M. Stockburger, Polarized resonance Raman spectra of an oriented diphenylpolyene, *J. Raman Spectroscopy* **1979**, 8, 26-31.
67. B. Jasse, J. L. Koenig, Orientational measurements in polymer using vibrational spectroscopy, *J. Macromol. Sci., Part C* **1979**, 17, 61-135.
68. M. Tanaka, R. J. Young, Review: Polarised Raman spectroscopy for the study of molecular orientation distributions in polymers, *J. Mater. Sci.* **2006**, 41, 963-991.
69. R. D. B. Fraser, The interpretation of infrared dichroism in fibrous protein structures, *J. Chem. Phys.* 1953, 21, 1511-1515.
70. W. Yu, Interfacial structure of bilayer compensation films prepared by direct coating process, Thesis **2012**.
71. E. Jabbari, N. A. Peppas, Polymer-polymer interdiffusion and adhesion, *Rev. Macromol. Chem. Phys.* **1994**, C34, 205-241.

72. E. Helfand, Y. Tagami, Theory of the interface between immiscible polymers, *J. Polym. Sci., Part B: Polym. Lett.* **1971**, 9, 741-746.
73. W. C. Kim, H. Pak, Interdiffusion at interfaces of binary polymer mixtures with different molecular weights, *Bull. Korean Chem. Soc.* **1999**, 20, 1323-1328.
74. W. C. Kim, C. J. Lee, H. G. Sim, H. Pak, Interdiffusion at interfaces of polymers with similar physical properties, *Bull. Korean Chem. Soc.* **2000**, 21, 577-582.
75. J.-M. Jung, H. Pak, Interdiffusion at interfaces of polymers with dissimilar physical properties, *Bull. Korean Chem. Soc.* **1997**, 18, 720-729.
76. U. Steiner, g. Krausch, G. Schatz, J. Klein, Dynamics of mixing between partially miscible polymers, *Phy. Rev. Lett.* **1990**, 64, 1119-1121.
77. H. Kim, Interdiffusion at polymer-polymer interfaces, Durham Thesis **2005**.
78. A. Karim, G. P. Felcher, T. P. Russell, Interdiffusion of polymers at short times, *Macromolecules* **1994**, 27, 6973-6979.
79. R. J. Composto, E. J. Kramer, D. M. White, Mutual diffusion in the miscible polymer blend polystyrene/poly(xylynyl ether), *Macromolecules* **1988**, 21, 2580-2588.
80. J. Vyorykka, Confocal Raman microscopy in chemical and physical characterization of coated and printed papers, Thesis, Helsinki university of Tech. **2004**.
81. N. Everall, Depth profiling with confocal Raman microscopy, part 1,2, *Spectroscopy* 2004, 19.

82. W. Schabel, I. Ludwig, M. Kind, Measurements of concentration profiles in polymeric solvent coatings by means of an inverse confocal micro Raman spectrometer-initial results, *Drying Tech.* **2004**, 22, 285-294
83. R. K. Arya, Non-Fickian drying of polymeric coatings, *Int. J. Sci. Tech. Res.* **2012**, 1,
84. I. Ludwig, W. Schabel, M. Kind, J.-C. Castaing, P. Ferlin, Drying and film formation of industrial waterborne latices, *AIChE* **2007**, 53, 549-560.
85. J. Krenn, P. Scharfer, M. Kind, W. Schabel, Drying of solvent-borne coatings with pre-loaded drying gas, *Eur. Phys. J. Special Topics* **2009**, 166, 45-48.
86. M. Vinjamur, R. A. Cairncross, Experimental investigations of trapping skinning, *J. Appl. Polym. Sci.* **2002**, 83, 2269-2273.
87. R. Saure, G. R. Wagner, E.-U. Schlunder, Drying of solvent-borne polymeric coatings: 1. Modeling the drying process, *Surf. Coat. Technol.* **1998**, 99, 253-256.
88. R. Saure, G. R. Wagner, E.-U. Schlunder, Drying of solvent-borne polymeric coatings: 2. Experimental results using FTIR spectroscopy, *Surf. Coat. Technol.* **1998**, 99, 257-265.
89. F. Adar, E. Lee, S. Mamedov, A. Whiteley, Experimental evaluation of the depth resolution of a Raman microscope, *Microsc. Microanal.* **2010**, 16, 360-361.
90. K. L. Saenger, H. M. Tong, Improved polyimide/polyimide adhesion via swelling agent enhanced interdiffusion, *J. Polym. Sci., Part C: Polym. Lett.* **1989**, 27, 235-237.

국문 초록

본 연구에서는 공정조건에 따라 변화하는 폴리이미드 사슬의 배향과 상호확산 현상에 대해 관찰하였다. 이를 통해 폴리이미드 필름 내에 잔류하는 용매량과 이미드화도의 두 가지 인자가 최종 사슬 배향과 상호확산 정도를 결정하는 데 있어 핵심적인 역할을 하게 됨을 알 수 있었다.

먼저, 폴리이미드 필름의 두께가 사슬 배향에 미치는 영향을 확인하기 위해 폴리이미드의 전구체인 폴리아믹산 용액을 이용하여 서로 다른 두께를 갖는 필름을 제조하였다. 그리고 건조와 경화 과정에서 필름 두께 방향으로의 잔류용매량 및 이미드화도 분포를 측정하였다. 필름이 두꺼워질수록 고분자 사슬은 더 낮은 in-plane 배향도를 갖게 되는데 특히 필름 표면보다 기재 쪽의 in-plane 배향도가 더 낮음을 알 수 있었다. 이러한 불균일한 배향 분포는 건조가 끝난 상태에서의 폴리아믹산 배향 분포와 유사하였다. 이는 필름이 두꺼워질 경우, 잔류 용매량이 많은 상태에서 더 빨리 강직한 구조를 갖는 폴리이미드로 변해 충분히 조밀한 구조를 갖지 못하기 때문인 것으로 설명이 가능하였다. 이러한 폴리이미드 사슬의 배향은 열이력 차이에 의해서도 달라질 수 있다. 초기 건조 온도가 높을수록 폴리아믹산 필름은 잔류 용매를 많이 함유한 상태에서 더 빨리 이미드화 반응을 진행하게 된다. 결과적으로 가장 높은 온도에서 건조한 경우에 최종적으로 경화된 폴리이미드 사슬의 in-plane 배향도가 가장 낮음을 알 수 있었다. 이 같은 배향 차이는 폴리이미드 필름의 결정화도나 유리전이온도에는 큰 변화를 주지 못한 반면 필름의 열팽창률을 크게 변화시킬 수 있음을 확인하였다.

다층 구조의 폴리이미드 필름을 제조하는데 있어 고분자 사슬의 배향과 상호확산 정도를 제어하는 것은 층간 접착특성을 확보하는 데 있어서 매우 중요한 인자이다. 본 연구에서는 2 층 구조의 폴리이미드 필름을 제조하는데 있어 direct multi-layer (DML) 건조 방식과 layer-by-layer (LBL) 건조 방식을 적용해 보았다. 두 폴리아미산 사이에서 발생하는 상호확산의 정도는 함유하고 있는 용매의 양과 두 층이 접촉하는 시간에 영향을 받는다. 이로부터 LBL 건조 방식에 비해 DML 건조 방식으로 제조된 폴리이미드가 더 큰 상호확산 폭을 갖게 됨을 설명할 수 있었다. 사슬 배향에 있어서는 상대적으로 강직한 분자 구조를 갖는 아래층이 건조 방식에 따라 큰 배향 변화를 보였다. 특히 LBL 건조 방식에서는 아래층의 건조 온도가 낮은 경우 이를 단일층으로 제조했을 때보다 더 낮은 in-plane 배향도를 갖는다는 것을 확인하였는데, 이는 건조 온도가 낮을 경우 위층의 용매가 아래층으로 쉽게 확산되는 현상과 밀접한 관련이 있음을 알 수 있었다.

주요어: 폴리이미드, 잔류용매, 이미드화도, 사슬 배향, 상호확산, 라만 분광법

학 번: 2011-30281